UNIVERSIDADE DE SÃO PAULO
ESCOLA DE ENGENHARIA DE SÃO CARLOS

MAURICIO FRANCISCO CALIRI JUNIOR

Contribuição para teoria de placas: análises estruturais de compósitos laminados e estruturas sanduíches via formulações unificadas

São Carlos
2015

MAURICIO FRANCISCO CALIRI JUNIOR

Contribuição para teoria de placas: análises estruturais de compósitos laminados e estruturas sanduíches via formulações unificadas

Tese apresentada à Escola de Engenharia de São Carlos da Universidade de São Paulo para obtenção do Título de Doutor em Engenharia Mecânica.

Área de concentração: Aeronaves.

Orientador: Prof. Assoc. Volnei Tita

São Carlos

2015

Caliri Junior, Mauricio Francisco
C153c Contribuição para teoria de placas: análises estruturais de compósitos laminados e estruturas sanduíches via formulações unificadas / Mauricio Francisco Caliri Junior; orientador Volnei Tita. São Carlos, 2015.

Tese (Doutorado) - Programa de Pós-Graduação em Engenharia Mecânica e Área de Concentração em Aeronaves -- Escola de Engenharia de São Carlos da Universidade de São Paulo, 2015.

1. Teorias Unificadas de Placa. 2. Método dos Elementos Finitos. 3. Continuidade C-1. 4. Estruturas Sanduíches. 5. Compósitos Laminados. 6. Anisotropia. 7. Análise Estrutural. 8. Métodos de Soluções Aproximadas. I. Título.

.

FOLHA DE JULGAMENTO

Candidato: Engenheiro **MAURICIO FRANCISCO CALIRI JUNIOR.**

Título da tese: "Contribuição para teoria de placas: análises estruturais de compósitos laminados e estruturas sanduíches via formulações unificadas".

Data da defesa: 17/04/2015

Comissão Julgadora:	**Resultado:**
Prof. Associado Volnei Tita **(Orientador)** (Escola de Engenharia de São Carlos/EESC)	Aprovado
Prof. Dr. **Marcelo Leite Ribeiro** (Escola de Engenharia de São Carlos/EESC)	Aprovado
Prof. Titular **Humberto Breves Coda** (Escola de Engenharia de São Carlos/EESC)	Aprovado
Prof. Dr. **António Joaquim Mendes Ferreira** (Universidade do Porto)	Aprovado
Prof. Dr. **Antonio Marcos Gonçalves de Lima** (Universidade Federal de Uberlândia/UFU)	Aprovada

Coordenador do Programa de Pós-Graduação em Engenheira Mecânica:
Prof. Associado **Marcelo Areias Trindade**

Presidente da Comissão de Pós-Graduação:
Prof. Associado **Paulo César Lima Segantine**

To my parents

Mauricio and Maria

and my fiancée

Izabel

Acknowledgements

I would like to thank all those who supported me from 2010 to 2015 in the conclusion of this Doctor Thesis. In special:

To the Conselho Nacional de Desenvolvimento e Tecnológico (CNPq) for the financial support (149908/2010-5).

To my friend and tutor, the Associated Professor Volnei Tita, for his guidance and knowledge which made possible the execution and conclusion of this work.

To my parents, whom always encouraged me to pursue the highest goals.

To the Associated Professor Reginaldo Teixeira Coelho for the use of the license of the commercial software Abaqus.

To the aeronautical structures group (GEA), for the discussions on this work.

“Only those who attempt the absurd will achieve the impossible”

M. C. Escher

“The (atomic) bomb will never go off.
I speak as an expert in explosives.”

Admiral William Leahy

Resumo

CALIRI JUNIOR, MAURICIO FRANCISCO. **Contribuição para teoria de placas: análises estruturais de compósitos laminados e estruturas sanduíches via formulações unificadas**. 2015. 246 f. Tese (Doutorado) – Escola de Engenharia de São Carlos, Universidade de São Paulo, São Paulo, 2015.

Em engenharia, a quantidade de problemas geométricos complexos que precisam ser resolvidos empregando teorias de placas ou cascas é notável. Esta é a razão por que há tantas teorias que buscam simplificar os problemas tridimensionais em outros menos custosos computacionalmente. Além disso, o aumento atual do uso de estruturas sanduíche requer que as formulações bidimensionais sejam mais precisas. Esta tese, num primeiro momento, compila a maioria das teorias de placa, comentando as principais diferenças, vantagens e desvantagens de cada uma. As formulações bidimensionais de placas laminadas são classificadas principalmente de acordo com o tratamento da coordenada na direção normal a superfície da mesma: Camada Única Equivalente (ESL), ESL refinada (teorias Zig-Zag) e Teorias Discretas ou de Camada (LW). Cada uma destas teorias é revista juntamente com as hipóteses de placas que são feitas para cada uma das camadas ou para o laminado como um todo. Para resolver tais problemas estruturais em engenharia, métodos numéricos são normalmente utilizados. Portanto, num segundo momento, alguns métodos de solução são citados e revisados, mas o foco é dado ao Método dos Elementos Finitos (MEF). A contribuição deste trabalho consiste na implementação de um novo método de solução de compósitos laminados e estruturas sanduíche com base em um sistema unificado de Formulação Generalizada (GUF) via MEF. Um elemento quadrilátero de 4 nós foi desenvolvido e avaliado com um código de Elementos Finitos desenvolvido pelo presente autor. Os requisitos para continuidade do tipo C-1 são respeitados para a variável de deflexão da placa. Esse método é nomeado de Formulação Generalizada do Caliri (CGF). Resultados para placas isotrópicas, placas de laminado compósito e estruturas sanduíche consideradas finas ou espessas são comparados com dados da literatura e soluções via Abaqus. Os resultados obtidos ao longo da espessura reforçam a necessidade de soluções de placa não-lineares para placas espessas (laminadas ou não). Mostrou-se que as soluções estáticas e dinâmicas empregando o método proposto fornecem resultados coerentes quando comparados com outros métodos de solução. Dentre os diversos estudos de caso investigados, verificou-se que é possível se obter resultados com alta

concordância. Para uma estrutura sanduíche com núcleo macio, o resultado de deslocamento previsto para um carregamento estático chega a 99.8% de concordância e o resultado de uma análise modal da mesma estrutura mostra uma concordância de 99.5% com os resultados de um modelo feito com elementos 3D em um programa comercial de elementos finitos.

Palavras-chave: Teorias Unificadas de Placa. Método dos Elementos Finitos. Continuidade C-1. Estruturas Sanduíches. Compósitos Laminados. Anisotropia. Análise Estrutural. Métodos de Soluções Aproximadas.

Abstract

CALIRI JUNIOR, MAURICIO FRANCISCO. **Contribution to theory of plates: structural analyses of laminated composites and sandwich structures via unified formulations**. 2015. 242 p. Thesis (PhD) – School of Engineering of São Carlos, University of São Paulo, São Paulo, 2015.

In engineering, the amount of complex geometrical problems, which need to be solved by using plates and shells theories, is remarkable. This is the reason why there are so many plate and shell theories which attempt to simplify three dimensional problems into ones with low computational cost. Additionally, the current increasing use of sandwich structures requires that the two dimensional formulations be accurate enough. First, this thesis compiles most of the plate theories from the literature and quotes the main differences, advantages and weaknesses of each one. The bi-dimensional laminated plate formulations are mainly classified according to the treatment of the variable in the normal direction of the plate surface: Equivalent Single Layer (ESL), Refined ESL (Zig-Zag theories) and Layer-Wise (LW) theories. Each one of these theories is reviewed along with the plate hypotheses which are made for each ply and/or laminate. To solve such complex structural engineering problems, numerical methods are normally used. Second, few solution methods are reviewed and quoted, but focus is given to the Finite Element Method (FEM). The contribution of this work is the implementation of a new solution method for laminated composites and sandwich structures based on a Generalized Unified Formulation (GUF) via FEM. A quadrilateral 4-node element was developed and evaluated using in-house Finite Element program. The C-1 continuity requirements is fulfilled for the transversal displacement field variable. This method is tagged as Caliri's Generalized Formulation (CGF). Results for isotropic plates, laminated composite plates and sandwich structures for thin and thick laminates are compared with literature data and solutions via Abaqus. The through-the-thickness profile results reinforce the need for non-linear plate (laminated or not) solutions. It was shown that the static and dynamic solutions employing the proposed solution method yield coherent results when compared with other solution methods. Among the different case studies investigated, it was verified that it is possible to obtain results with high agreement. For a soft-core sandwich structure, the displacement result for a static loading is reported as high as 99.8% and the result of a modal analysis of the same structure

shows an accuracy of 99.5%, comparing to the results from a 3D finite element model built with a commercial software.

Keywords: Unified Plate Theories. Finite Element Method. Continuity C-1. Sandwich Structures. Laminated Composites. Anisotropy. Structural Analysis. Approximate solution Methods.

Figures

Tables

Acronyms

0D	Zero-Dimensional
1D	One-Dimensional
2D	Two-Dimensional
3D	Three-Dimensional
6D	Six-Dimensional
AWRD	Ambartsumian–Whitney–Rath-Das theory
CAE	Computer Aided Engineering
CFD	Computational Fluid Dynamics
CLT	Classical Lamination Theory
CS	Coordinate System
DLM	Discrete Layer Model
DOF	Degree of Freedom
DPSE	Degenerated/continuum Plate/Shell Element
ESL(M)	Equivalent Single Layer (Models)
FCSR	Face to Core Stiffness Ratio
FE	Finite Element
FEM	Finite Element Method
FESA	Finite Element Structural Analyses
FSDT	First Shear Deformation Theory
FSI	Fluid Structure Interaction
GCS	Global Coordinate System
GFEM	Generalized Finite Element Method
GPVW	Generalized Principle of Virtual Work
GQ	Gauss Quadrature
HSDT	Higher Order Shear Deformation Theory
HSAPT	High order SAndwich Plate Theory
IC	Inter-laminar Continuity
IP	Integration Points
KR	Koiter's Recommendation
LCS	Local Coordinate System
LR	Lekhnitskii–Ren theory

LFAT	Love First Approximation Theory
LSAT	Love Second Approximation Theory
LW(M)	Layer-Wise (Models)
MAC	Modal Assurance Criterion
MQ	Multiquadric
MITC	Mixed Interpolation of Tensorial Components
MWR	Method of Weighted Residuals
MZZF	Murakami's Zig-Zag Function
PE	Plate Element
PVD	Principle of Virtual Displacements
PVW	Principle of Virtual Work
RBF	Radial Base Functions
RESL	Refined Equivalent Single Layer
RMC	Reissner–Murakami-Carrera theory.
RMVT	Reissner's Mixed Variational Theorem
SCF	Shear Correction Factor
SCT	Static Condensation Technique
TE	Theory of Elasticity
TI	Transversely Isotropic
VRT	Vlasov-Reddy Theory
WFHL	Weak Form of Hooke's Law
XFEM	Extended Finite Element Method
ZZ	Zig-Zag

Contents

Chapter 1 - Introduction

1.1 Scope

To perform an accurate structural simulation, there are innumerous variables which need to be handled. Depending on the loading, geometry or constitutive complexity of the problem, very particular approaches might be required. Sandwich structure plates, which are the scope of this work, present an outstanding complexity regarding its microscopic and macroscopic behavior (GIBSON; ASHBY, 1985). These complex laminated structures were devised in order to fulfill different application criteria such as thermal/sound insulation or damping purposes. In addition, such structures are usually applied to reduce weight or increase the energy absorption capacity of a structure.

Intelligent structures may be considered as a class of sandwich structures. These materials most commonly comprise a patch or a layer of piezoelectric material. Such structures are usually applied as monitors or actuators, depending whether the structure was scaled to read (passive) or cause deformation (active) in the structure. The use of intelligent structures in the aeronautical field is very appealing in both active and passive ways. From structural health monitoring to flight control, the applications are countless. Nevertheless, the success of these structures depends on accurate modeling of both mechanical and electrical responses of these, intelligent sandwiches (PIEFORT, 2001, MARINKOVIC; KOPPE; GABBERT, 2006, MORENO; TITA; MARQUES, 2010).

The commercial use of intelligent structures is narrowed due to its complexity and naturally the costs associated, but the use of "regular" sandwich structures is already common in the field. Some aircraft structures and hulls of boats use sandwich structures to reduce weight and therefore increase the payload. However, the application of these materials on primary structures is rare. Mainly because it is hard to model its tri-dimensional behavior with bi-dimensional assumptions.

Recently, the application of sandwich structures on wind turbines is becoming popular too (THOMSEN, 2009). In the last 25 years or more, the development and improvement of

wind blades has drawn much attention because they harvest clean energy (NATIONAL RENEWABLE ENERGY LABORATORY, 2006).

A regular blade diameter of wind turbine generators is 50 m long and they harvest approximately 1.5 MW for wind speeds higher than 12 m/s. However, nowadays, one can find wind turbine blades whose diameters is 120 m long, which can generate around 5 MW. Moreover, there are projects for wind turbines with blades with 200 m long in diameters (NATIONAL RENEWABLE ENERGY LABORATORY, 2006). This is the option to the lack/depletion of good locations for wind farms. In most countries the best or the only locations are already taken, and the solution found is to increase the farms performance by increasing the size wind turbine blades. This is a formidable structural and aeroelastic problem. The use of sandwich structures helps to reduce the weight of this structure but, naturally, it complicates the designing of such structures (IVANELL, 2005, HANSEN et al., 2006).

The aeroelastic problem may be regarded as a type of Fluid Structure Interaction (FSI). The *aeroelasticity* studies the interaction between body fields, aerodynamic forces and the structural reaction of the structure (BISPLINGHOFF; ASHLEY; HALFMAN, 1996).

In many aeronautical projects, the deformation related to the deflections of the structure cannot be neglected and the typical rigid body approach may not be sufficient. Aircraft fuselages, wings and wind turbine blades possess large spans which results in strong aeroelastic effects (BISPLINGHOFF; ASHLEY; HALFMAN, 1996).

Recognizing the fact that the aeroelastic solution can get very complex for sandwich structures depending on the loading case, this thesis is devoted to the structural solution only. The fluid solution, which is the loading part of the interaction, needs to be studied separately because the dynamics and magnitude of the fluid solution may range from cruise flight loads to maneuvers loads. This is left as a topic for future works because it involves specific solution methods, including Computational Fluid Dynamics (FERZIGER; PERIC, 2002, VOS et al., 2002). The coupling of both structural and fluid solution is also a field for much research (BHARDWAJ, 1997, ZWAAN; PRANANTA, 2002).

This thesis will contribute for the development of a computational solution method in order to predict the structural response of laminated composites and sandwich structures. More specifically, the Finite Element Method (FEM) along with unified plate theories will be used to investigate the response of such appealing structures.

1.2 Objectives

The main objective of the present work consists on the implementation of a new solution method for laminated composites and sandwich structures based on a Generalized Unified Formulation (GUF) via FEM. A quadrilateral 4-node element will be developed and evaluated using in-house Finite Element program. The C-1 continuity requirements will be fulfilled for the transversal displacement field variable.

In order to comply with the reasons and motivations of this work, this thesis set the following specific goals:

- To review and quote as many as possible the derived plate formulations up to date.
- To review and quote as many as possible the solutions methods for plate problems.
- To derive a new structural solution method for sandwich structures via FE.
- To derive a FE with partial C-1 continuity.
- To implement the formulated element into an in-house FE code.
- To evaluate the accuracy of the code and the element.
- To evaluate the formulation for different plate structures.
- To evaluate the proposed solution method using sandwich structures.
- To conclude about the limitations and potentialities of the proposed solution method.

1.3 Organization

Apart from this chapter, this thesis comprises six other chapters.

Chapter 2 was written to provide a review on the principles of structural mechanics. Since many different structural concepts will be handled in this work, the need for this chapter is clear. Different strain and stress tensors are reviewed and quoted throughout this thesis and a review on the types of these tensor is given. Also, the main constitutive behaviors are briefly quoted as well, mainly because sandwich structures with soft cores demand attention regarding both micro and macroscopic material response.

Chapter 3 is a review on plate theories. Sandwich structures are normally plate or shell structures. Hence the third dimension is usually simplified as the theory to solve the problem

becomes 2D. Different ways to derive these 2D plate formulations are presented. Then, the formulations are explained and reviewed according to the thickness of the plate. The thicker the plate is, the more complex (or non-linear) the formulation gets. But besides the thickness factor, the complexity of the theory also increases when the plate is a laminated composite structural material. Sandwich structures fall into this category. Laminated plate theories usually required an integration process in the thickness direction prior to solving the 2D equilibrium equations. Also, the material continuity between plies presents further complications. Finally, the recent Unified Formations for plates and shells are reviewed and their potentially explained.

Chapter 4 elucidates how the accuracy of the laminated plate solution may change according to the solution method. Differential equations are reviewed and the main solution method used in structural analysis are quoted. Global and local solution methods are discussed. However, focus is given to the Finite Element Method (FEM) because it is one of the most common commercial solution methods due to its flexibility in solving different engineering problems. In this chapter it is shown how the elementary equations are derived and whether the governing equations are solved with mixed variables or not for usual plate formulations. Next, the solution of unified plate theories via FEM is discussed for the references quoted. At the end of the chapter, few numerical techniques are explained to clarify the possible errors and issues one may face when solving static or dynamic structural solutions. It is an important chapter to show how Finite Element (FE) formulations may get cumbersome.

Chapter 5 is devoted to the contribution of this thesis. It presents a new solution method for the laminated plate problem. Through FE implementation of a plate element, a generalized unified plate formulation is solved in a more physically consistent way. A four node plate element is derived. An in-house code is developed to test the element. A brief explanation of the code is provided along with explanation on how the thickness integration is carried out.

Chapter 6 provides several evaluations of both theory and solution method accuracies. The chapter is divided in convergence, theory, thickness, dynamics, performance and sandwich structure evaluations. Analytical results from the theory of elasticity and from closed form solution are used to assess the accuracy of the proposed formulation. Moreover, the commercial software Abaqus is used to provide both 2D and 3D solutions for comparison of the variables behavior through-the-thickness of the plates. The “convergence section” exemplifies the rate of convergence of the proposed solution method for two case problems. Both “theory and thickness sections” evaluate the accuracy of the implemented solution method. The accuracy in the time domain is explored using vibration modes in the “dynamic sections”. Then before testing the formulation with highly anisotropic sandwich structures, a performance assessment

of the increase in processing time from one theory to another is given. The results show that the proposed formulation converges to the 3D solutions, and for some cases, outperforms the closed form solutions of the GUF.

Chapter 7 shows the conclusions of this thesis. The main findings are summarized in the "conclusion and recommendation sections". Then, the topics suggested throughout the text and further applications of plate solutions are suggest in the "future works sections".

Chapter 2 - Principles of Structural Mechanics

2.1 Strains

In structural mechanics, most of the constitutive laws are derived for the current state of deformation of a material body. However, it is cumbersome to derive the equations of motion for the current state of deformation. Therefore, these equations are normally written in the Lagrangian (or material) configuration, which describes the material body's position and its deformation in terms of its initial position. When deriving the equations of the body in terms of its current position, the approach is known as Eulerian (or spatial). Eulerian formulations are more common in fluid mechanics (CHEN; HAN, 1988, CRISFIELD, 1991, ZIENKIEWICZ; TAYLOR, 2000a, 2000b, MENDONÇA, 2005).

Before linking the states of deformation to the corresponding stresses and constitutive laws, the displacement vector and the deformation gradient are derived for a generic material element (Figure 1).

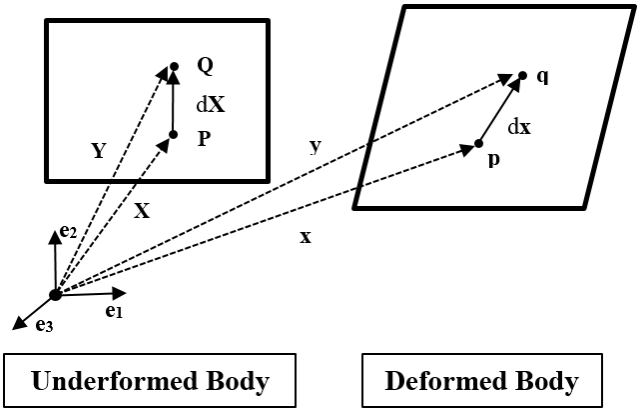

Figure 1. Undeformed and deformed configurations of a material body at time "t"

The position of a material element in a 3D space is defined by its position vector "X" and its displacement vector "u(X)" according to equation (2.1). The current position of the material element "x" at a particular instant "t" is in equation (2.1) too.

$$\boldsymbol{X} = X_i \boldsymbol{e}_i \tag{2.1}$$
$$\boldsymbol{u}(\boldsymbol{X}) = u_i(\boldsymbol{X})\boldsymbol{e}_i$$
$$\boldsymbol{x}(\boldsymbol{X}, t) = \boldsymbol{X} + \boldsymbol{u}(\boldsymbol{X}, t)$$
$$\boldsymbol{x}(\boldsymbol{X}, 0) = \boldsymbol{X}$$

In equation (2.1), the time variable can carry physical significance or not. This variable might only indicate a pseudo instant at which that specific deformation occurs. Nonetheless, in actual dynamic situations, this Degree of Freedom (DOF) cannot be handled so loosely.

To derive general non-linear strain relations, the current position is differentiated in respect to the current configuration. Ignoring the time variable, it is possible to have:

$$d\boldsymbol{x} = \frac{\partial \boldsymbol{x}}{\partial \boldsymbol{X}} d\boldsymbol{X} = \boldsymbol{F} d\boldsymbol{X} = \frac{\partial (\boldsymbol{X} + \boldsymbol{u})}{\partial \boldsymbol{X}} d\boldsymbol{X} \tag{2.2}$$

The partial derivative “F” is the deformation gradient, which can be expanded as:

$$\boldsymbol{F} = \begin{bmatrix} \frac{\partial \boldsymbol{x_1}}{\partial \boldsymbol{X_1}} & \frac{\partial \boldsymbol{x_1}}{\partial \boldsymbol{X_2}} & \frac{\partial \boldsymbol{x_1}}{\partial \boldsymbol{X_3}} \\ \frac{\partial \boldsymbol{x_2}}{\partial \boldsymbol{X_1}} & \frac{\partial \boldsymbol{x_2}}{\partial \boldsymbol{X_2}} & \frac{\partial \boldsymbol{x_2}}{\partial \boldsymbol{X_3}} \\ \frac{\partial \boldsymbol{x_3}}{\partial \boldsymbol{X_1}} & \frac{\partial \boldsymbol{x_3}}{\partial \boldsymbol{X_2}} & \frac{\partial \boldsymbol{x_3}}{\partial \boldsymbol{X_3}} \end{bmatrix} = \begin{bmatrix} 1 + \frac{\partial \boldsymbol{u_1}}{\partial \boldsymbol{X_1}} & \frac{\partial \boldsymbol{u_1}}{\partial \boldsymbol{X_2}} & \frac{\partial \boldsymbol{u_1}}{\partial \boldsymbol{X_3}} \\ \frac{\partial \boldsymbol{u_2}}{\partial \boldsymbol{X_1}} & 1 + \frac{\partial \boldsymbol{u_2}}{\partial \boldsymbol{X_2}} & \frac{\partial \boldsymbol{u_2}}{\partial \boldsymbol{X_3}} \\ \frac{\partial \boldsymbol{u_3}}{\partial \boldsymbol{X_1}} & \frac{\partial \boldsymbol{u_3}}{\partial \boldsymbol{X_2}} & 1 + \frac{\partial \boldsymbol{u_3}}{\partial \boldsymbol{X_3}} \end{bmatrix} = [\boldsymbol{I} + \boldsymbol{\nabla u}(\boldsymbol{X})] \tag{2.3}$$

For a tridimensional deformation along a line of current length “dx” and initial length “dX”, Green’s strain tensor “E_G” is obtained from the equation (2.4):

$$|d\boldsymbol{x}|^2 - |d\boldsymbol{X}|^2 = d\boldsymbol{x} \cdot d\boldsymbol{x} - d\boldsymbol{X} \cdot d\boldsymbol{X} = 2 d\boldsymbol{X}^{\boldsymbol{T}} \boldsymbol{\varepsilon_G} d\boldsymbol{X} \tag{2.4}$$

Note that the strain tensors are written in vector form. Appling equation (2.2) in (2.4):

$$2\boldsymbol{\varepsilon_G}(\boldsymbol{X}) = \boldsymbol{F}^T \boldsymbol{F} - \boldsymbol{I} \tag{2.5}$$
$$\boldsymbol{\varepsilon_G}(\boldsymbol{X}) = \frac{1}{2}[\boldsymbol{F}^T \boldsymbol{F} - \boldsymbol{I}] = \frac{1}{2}[\boldsymbol{\nabla u} + \boldsymbol{\nabla u}^T + \boldsymbol{\nabla u}^T \cdot \boldsymbol{\nabla u}]$$

The second term ($\boldsymbol{\nabla u}^T \cdot \boldsymbol{\nabla u}$) in equation (2.5) is responsible for the geometrical non-linearity effects. However, it is only significant when the gradient of the displacement field is large. Slender and thin structures usually fit into this description. When one neglects these terms, the geometrically linear theory is recovered.

For thin plates under moderately large deflections, von Kármán's description of Green's strain tensor in equation (2.6) is obtained by keeping only the terms with the $\partial u_3/\partial X_1$ and $\partial u_3/\partial X_2$ (CRISFIELD, 1991) derivatives.

$$\varepsilon_{11} = \frac{\partial u_1}{dX_1} + \frac{1}{2}\left(\frac{\partial u_3}{dX_1}\right)^2 \qquad 2\varepsilon_{23} = \frac{\partial u_3}{dX_2} + \frac{\partial u_2}{dX_3} \tag{2.6}$$

$$\varepsilon_{22} = \frac{\partial u_2}{dX_2} + \frac{1}{2}\left(\frac{\partial u_3}{dX_2}\right)^2 \qquad 2\varepsilon_{13} = \frac{\partial u_3}{dX_1} + \frac{\partial u_1}{dX_3}$$

$$2\varepsilon_{12} = \frac{\partial u_2}{dX_1} + \frac{\partial u_1}{dX_2} + \frac{\partial u_3}{dX_1}\frac{\partial u_3}{dX_2} \qquad \varepsilon_{33} = \frac{\partial u_3}{dX_3}$$

If moderately thick plates are considered, shear deformation assumptions (such as Mindlin/Reissner's) must be considered (ZIENKIEWICZ; TAYLOR, 2000b). Even the transverse normal strain and its non-linearity may be of significance. Other strain expressions are available in the literature according to the problem at hands. Almansi's strain formulation, which arises in the context of the Eulerian configuration, can be mentioned for instance. Similarly to Green's strain, Almansi's "E_A" is derived from:

$$|d\boldsymbol{x}|^2 - |d\boldsymbol{X}|^2 = d\boldsymbol{x} \cdot d\boldsymbol{x} - d\boldsymbol{X} \cdot d\boldsymbol{X} = 2d\boldsymbol{x}^T \boldsymbol{\varepsilon_A} d\boldsymbol{x} \tag{2.7}$$

$$\boldsymbol{\varepsilon_A}(\boldsymbol{x}) = \frac{1}{2}[\boldsymbol{I} - \boldsymbol{F}^{-T}\boldsymbol{F}^{-1}] = \frac{1}{2}[\boldsymbol{\nabla u} + \boldsymbol{\nabla u}^T - \boldsymbol{\nabla u}^T \cdot \boldsymbol{\nabla u}]$$

In equation (2.7), as opposed to equation (2.5), the displacement gradients are taken in respect to the current configuration "x" and not the initial "X" one.

Attention is advised when working with Almansi's strain in the spatial-Eulerian configuration. For each type of strain tensor, there is a physically consistent stress conjugate pair. If such conjugate stress and strain tensors are multiplied, the work calculated remains invariant to the type of the tensors chosen.

Almansi's strain is not the work conjugated to the Cauchy's (true) stress. It depends of the magnitude of the deformations. If the deformation level is not small, it is the logarithmic strain tensor which is the work conjugate of Cauchy's stress (CRISFIELD, 1991).

Since Cauchy's stress is given in the current configuration, the deformation must also be given in this configuration. For an initial length "ΔX" and a final length "Δx", the logarithmic strain "E_L" is calculated as:

$$\boldsymbol{\varepsilon_L}(\boldsymbol{x}) = \int_{\Delta X}^{\Delta x} \frac{d\boldsymbol{x}}{\boldsymbol{x}} = \frac{1}{2} ln[1 + 2\boldsymbol{\varepsilon_G}(\boldsymbol{X})] \tag{2.8}$$

The Eulerian characteristic is indicated with the differential assumption of the current strain as "dx/x". In the linear strain range, all strain tensors coincide. Even so, attention is required when either geometrical or material non-linearity are considered.

2.2 Stresses

Loadings can be classified either as force or couple (moment) excitations on a material body. The balance and equilibrium of these loadings yield the equations of motion. At a section in or on the material body whose area is "ΔA_n" and normal versor "n", the resultant force "ΔF_n" and couple "ΔM_n", produce stresses (Figure 2).

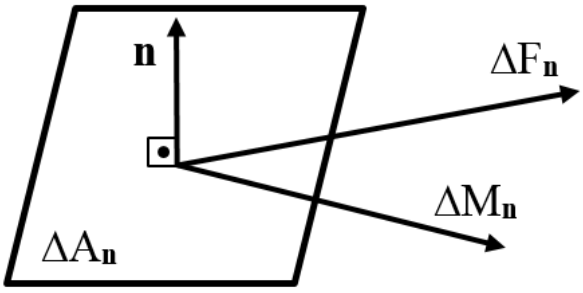

Figure 2. Traction and couple stress vectors on a deformable body

As the section area become infinitesimally small, along with its associated force and moment, the respective traction stress vector "t_n" and the couple stress "c_n" are obtained (see

equation (2.9)). Due to the infinitesimal size of these herein called material elements, it is usual to refer to these elements as material points (CHEN; HAN, 1988, ZIENKIEWICZ; TAYLOR, 2000a, 2000b, MENDONÇA, 2005).

$$\lim_{\Delta A_n \to 0} \frac{\Delta \boldsymbol{F}_n}{\Delta A_n} = \frac{d\boldsymbol{F}_n}{dA_n} = \boldsymbol{t}_n \qquad (2.9)$$
$$\lim_{\Delta A_n \to 0} \frac{\Delta \boldsymbol{M}_n}{\Delta A_n} = \frac{d\boldsymbol{M}_n}{dA_n} = \boldsymbol{c}_n$$

According to the limits in equation (2.9), each material element has its own traction and couple stress vector. The classical continuum mechanics does not describe the deformation and movement of a continuum body considering the contribution of couple stresses ($c_n = 0$). Nonetheless, there are in the literature, elaborated approaches which develop the concept of couple stresses in an attempt to describe complex material behaviors. A frequently quoted theory of continuum of this class is known by the name of Cosserat (GREEN; NAGHDI; WAINWRIGHT, 1965). One of the main advantages of this theory is the fact that both translational and rotational DOFs are taken as independent variables. From a phenomenological perspective, each material element is similar to a rigid body with six DOFs. Nevertheless, such increase in the DOFs of the theory also increases the complexity of the derivation processes. Constitutive relations in this framework are normally intricate to develop (SANSOUR; BEDNARCZYK, 1995, YANG et al., 2000, BIRSAN, 2007; NEFF; CHELMINSKI, 2007, ALTENBACH; EREMEYEV, 2010, SKATULLA; SANSOUR, 2013).

Staying in the field of the classical mechanics of continuum and dropping the term “traction” in “traction stress vector”, the current (or final) configuration will be assumed in the following. At the current configuration, Cauchy’s Lemma states that the stress vector in the interior of the body as a function of the outward directed normal (“n”) is balanced with the stress vector of the inward directed normal (“-n”). This theorem implies that a tensor field “σ” appears to equilibrate the external stress vector “t_n”.

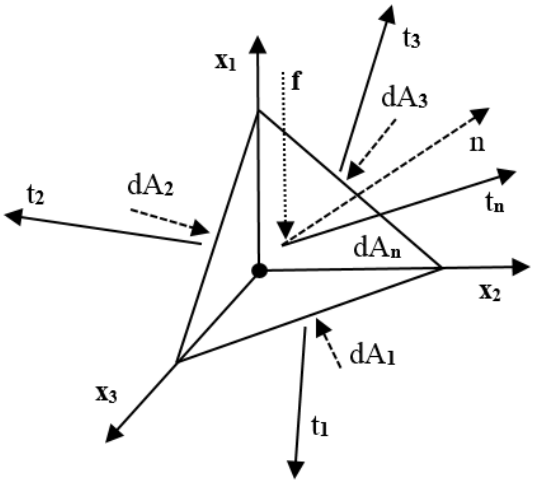

Figure 3. Equilibrium of traction stresses at a material point

To see this, a general Cartesian stress vector "t_i" is obtained by projection of the stress field tensor "σ" in the three Cartesian directions "e_i". Then, with the graphical aid of a general tetrahedron (Figure 3), one can see that the components of this general stress vector "t_i" are used to compute the stress vector "t_n" at a random section with normal direction "n".

Taking the limit as the volume of the tetrahedron tends to zero, the Cauchy's Theorem is finally obtained:

$$\boldsymbol{t}_i = \boldsymbol{\sigma}_{i1}e_1 + \boldsymbol{\sigma}_{i2}e_2 + \boldsymbol{\sigma}_{i3}e_3 = \sigma_{ij}\boldsymbol{e}_j \tag{2.10}$$

$$\boldsymbol{t}_n = t_i\boldsymbol{e}_i = \boldsymbol{t}_i n_i = \sigma_{ij}\boldsymbol{e}_j n_i \rightarrow t_i = \sigma_{ji}n_j$$

$$\sigma_{ji} = \begin{bmatrix} \sigma_{11} & \sigma_{12} & \sigma_{13} \\ \sigma_{21} & \sigma_{22} & \sigma_{23} \\ \sigma_{31} & \sigma_{32} & \sigma_{33} \end{bmatrix}$$

Cauchy's stress vector "σ_{ij}" is a symmetric second order tensor. The normal component of Cauchy's stress tensor "σ_{nn}", which is parallel to the normal direction ("n") and the tangential, or shear, stress component "σ_{ns}", which is parallel to the tangential direction ("s") are calculated as:

$$\sigma_{nn} = \boldsymbol{t}_n \cdot \mathbf{n} = \sigma_{ij}n_i\boldsymbol{e}_j \cdot n_k\boldsymbol{e}_k = \sigma_{ij}n_i n_j \tag{2.11}$$

$$\sigma_{ns} = \boldsymbol{t}_n \cdot \mathbf{s} = \sigma_{ij}n_i\boldsymbol{e}_j \cdot s_k\boldsymbol{e}_k = \sigma_{ij}n_i s_j$$

$$\boldsymbol{n} \cdot \mathbf{s} = 0$$

With current stress tensor σ defined, the equations of motion of a material point can be defined too.

Still in the current configuration, consider the material point represented by a cube of density "ρ" and edges "dx_i" moving with acceleration "ü" and submitted to a force field "b" as in Figure 4. The forces at this material element can be classified as field forces, external forces or internal reaction forces

Field forces are the forces produced on a body due to a source potential field on which this body is immersed. The magnitude of this force is normally proportional to the gradient of this potential field, the properties of the material and the geometry of the body.

External forces are loads directly applied to external points, edges or surfaces of the body.

Internal reaction forces are associated with the element's state of stress which arises from the material response to the above described field and external loads (Cauchy's Theorem).

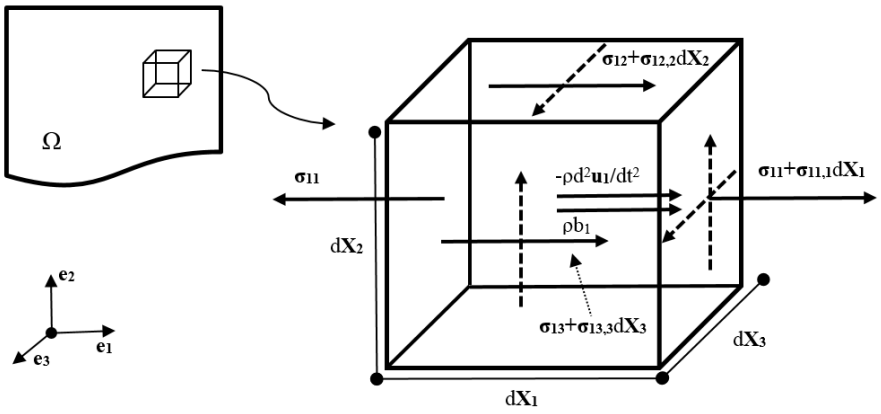

Figure 4. Momentum balance of a differential volume element

Ignoring microscopic dissipation effects, one can equate the internal stresses and the forces of the material point in Figure 4 as:

$$\rho\ddot{u}_1 = \frac{\partial\sigma_{11}}{\partial x_{11}} + \frac{\partial\sigma_{12}}{\partial x_{22}} + \frac{\partial\sigma_{13}}{\partial x_{33}} + \rho b_1 = \sigma_{11,1} + \sigma_{12,2} + \sigma_{13,3} + \rho b_1 \tag{2.12}$$

$$\rho\ddot{u}_2 = \frac{\partial\sigma_{21}}{\partial x_{11}} + \frac{\partial\sigma_{22}}{\partial x_{22}} + \frac{\partial\sigma_{23}}{\partial x_{33}} + \rho b_2 = \sigma_{21,1} + \sigma_{22,2} + \sigma_{23,3} + \rho b_2$$

$$\rho\ddot{u}_3 = \frac{\partial\sigma_{31}}{\partial x_{11}} + \frac{\partial\sigma_{32}}{\partial x_{22}} + \frac{\partial\sigma_{33}}{\partial x_{33}} + \rho b_3 = \sigma_{31,1} + \sigma_{32,2} + \sigma_{33,3} + \rho b_3$$

Compacting the component terms:

$$\nabla \cdot \boldsymbol{\sigma} = \rho(\ddot{\boldsymbol{u}} - \boldsymbol{b}) \tag{2.13}$$

The above equilibrium equation of motion was derived for the current configuration where "σ" is the Cauchy's stress. This equation is valid for any interior point of the domain "Ω" (Figure 4).

To properly couple the geometrical non-linearities of Green's strain tensor (2.5), its work conjugate, which is the second Piola-Kirchhoff's stress tensor "S", must replace Cauchy's stress in (2.13). Cauchy's stress is related to "S" by:

$$\boldsymbol{S} = \det(\boldsymbol{F})\boldsymbol{F}^{-1}\boldsymbol{\sigma}\boldsymbol{F}^{-T} \tag{2.14}$$

However, if equation (2.13) is written in the initial configuration, the stress measure, which will appear in this equation, is the first Piola-Kirchhoff stress tensor "T" and its conjugate is the displacement gradient "D" (CRISFIELD, 1991, MENDONÇA, 2005):

$$\boldsymbol{T} = \det(\boldsymbol{F})\boldsymbol{\sigma}\boldsymbol{F}^{-T} \tag{2.15}$$
$$\boldsymbol{D} = \nabla \boldsymbol{u}(\boldsymbol{X})$$

Finally, the equation of motion can be re-written in terms of the work conjugate "S-E_G" inserting equation (2.14) into equation (2.13):

$$\nabla \cdot \boldsymbol{\sigma}(\boldsymbol{x}) = \rho\ddot{\boldsymbol{u}} - \rho\boldsymbol{b} = \frac{1}{det(\boldsymbol{F})}[\nabla(\boldsymbol{x}) \cdot (\boldsymbol{F}\boldsymbol{S}(\boldsymbol{X})\boldsymbol{F}^{\boldsymbol{T}})] = \nabla \cdot [\boldsymbol{S}: (2\boldsymbol{\varepsilon}_{\boldsymbol{G}} + \boldsymbol{I})] \tag{2.16}$$

When kinematics of large displacements and rotations are considered, additional attention is advised when solving the equations of motion. As mentioned above, the material models are generally derived for the current state of deformation and adding the complexity of the non-linear terms, a modified scheme for solving Lagrangian equations is usually used. It is called the Updated Lagrangian Scheme (ULS). As opposed to the Total Lagrangian Scheme (TLS). The ULS is more complex than the TLS but it simplifies the stress-strain non-linear relations. In ULS, an update of the variables from the initial to the current state is required so that the increments of displacement are linear.

If the ULS is chosen for small strain situations, the strain couple of Cauchy's stress tensor can be the Almansi's strain tensor. It may ease the computational implementation. But if large strains are considered, the Logarithmic strain tensor should be coupled with Cauchy's stress (CRISFIELD, 1991).

There is a third kinematic scheme named Corotational (CRS). It simplifies the Lagrangian formulation of large displacements and small strains by splitting the rigid body motions and deformations. In this formulation only the deformation is considered in the calculation of internal forces and the tangent stiffness matrix (POLAT, 2010). Hence, when solving plate problems with the CRS and the Finite Element Method (FEM), an element independence can be achieved (FELIPPA; HAUGEN, 2005).

After defining the equations of motion for the interior material points, it now remains to establish the equations of motion on the boundary "Γ" of the respective domain "Ω". Boundary conditions (BC) can be separated into two classes. The first is known as *geometrical, essential* or *Dirichlet* boundary condition. For this type, the magnitudes of the irreducible(s) variable(s) of the problem on the boundary "Γ" are prescribed (HUEBNER; THORNTON, 1982, ZIENKIEWICZ; TAYLOR, 2000a, 2000b). In case of structural problems, the respective essential boundary condition is the prescription of the displacements on the boundaries:

$$\forall \mathbf{X} \in \Gamma^{u} : \boldsymbol{u}(\boldsymbol{X}, t) = \overline{\boldsymbol{u}}\,(\boldsymbol{X}, t) \tag{2.17}$$

The second type is the classified as *static, natural* or *Neumann* boundary conditions. This type is related to a flux of energy in and out of the domain "Ω" through the boundary "Γ" (HUEBNER; THORNTON, 1982, ZIENKIEWICZ; TAYLOR, 2000a, 2000b). Assuming the material point of Figure 3 to lie on the boundary "Γ" and that the boundary's face normal direction at this point is "n":

$$\forall \mathbf{X} \in \Gamma^{\sigma} : \boldsymbol{\sigma}(\boldsymbol{X}, t) \cdot \boldsymbol{n} = \overline{\boldsymbol{\sigma}}\,(\boldsymbol{X}, t) \tag{2.18}$$

Generically, both BCs can co-exist in the problem. Thus, the boundary "Γ" may be written as:

$$\Gamma = \Gamma^{u} \cup \Gamma^{\sigma} \tag{2.19}$$

All the equations from (2.17) to (2.19) are written as functions of time. This is because, for initial value problems (or transient problems), the values on the boundaries vary with time as well.

2.3 Material Behavior

2.3.1 Constitutive Equations

Material behavior and strain energy of a material point are related through Constitutive Equations. These relations provide the stress magnitude as a function of the strain "E", the strain rate "Ė" and the current plastic or damage history "α". As previously mentioned, the constitutive equations are generally written in the current configuration:

$$\boldsymbol{\sigma} = \boldsymbol{\sigma}(\boldsymbol{\varepsilon_L}, \dot{\boldsymbol{\varepsilon}}_{\boldsymbol{L}}, \boldsymbol{\alpha}) \tag{2.20}$$

Details on hardening, flow rules, dissipation and damage can be found in text books and works dedicated to material models (CHEN; HAN, 1988, CRISFIELD, 1991, 1997, ZIENKIEWICZ; TAYLOR, 2000b, CALIRI JR, 2010). Even so, whenever appropriated, a few comments and derivations will be provided throughout the text.

This section reviews only the linear elastic constitutive relations. Elasticity ensures that the stress is a state variable and can be derived from an elastic potential "W". As a state variable, the work required to change a material point from two different stress states is path independent in the strain space:

$$\int_{\varepsilon_a}^{\varepsilon_b} \boldsymbol{\sigma}(\varepsilon) d\varepsilon = \int_{\varepsilon_a}^{\varepsilon_b} \frac{\partial W}{\partial \varepsilon} d\varepsilon = W(\varepsilon_b) - W(\varepsilon_a) \tag{2.21}$$

Since constitutive laws may be non-linear and to account for multi-axial loading cases, the derivative of the stress tensor with respect to the strain tensor can be adopted as a method to build the constitutive tensor "C", thus:

$$\frac{\partial \boldsymbol{\sigma}}{\partial \varepsilon} = \frac{\partial W}{\partial \varepsilon \otimes \partial \varepsilon} = C_{ijkl} e_i \otimes e_j \otimes e_k \otimes e_l \tag{2.22}$$
$$\boldsymbol{\sigma} = \boldsymbol{C}\colon \varepsilon = C_{ijkl}\varepsilon_{ij} e_i \otimes e_j \quad with \quad C_{ijkl} = C_{jikl} = C_{jilk} = C_{ijlk}$$

The purpose of choosing the current configuration to define constitutive laws is now made clear. In experimental tests, the stresses and strains are always in the current deformed configuration. To track the rate of change of Piola-Kirchhoff's second stress tensor is very difficult, because the material will inexorably deform. Nonetheless, this Lagrangian tensor is required to derive geometrically non-linear equations (CRISFIELD, 1991).

Back to equation (2.22), if the constitutive tensor "C" is independent of the current strain, the constitutive law provides a linear link between stress and strain. Instead, if the constitutive tensor varies with the strain level, the material yields a non-linear stress-strain link regarding the current strain level.

For linear constitutive relations, Hooke's law for an isotropic material is well known. From the elastic potential function "W" as function of the strain level "ε", the constitutive law is postulated as:

$$W(\varepsilon) = \mu\varepsilon\colon \varepsilon + \frac{1}{2}\lambda(\varepsilon\colon 1)^2 \tag{2.23}$$
$$\lambda = \frac{\nu E}{(1+\nu)(1-2\nu)};\ \mu = \frac{E}{2(1+G)};\ (Lame's\ constants)$$

After differentiations of equation (2.22-2.23), the isotropic constitutive tensor is found:

$$\boldsymbol{C} = 2\mu \mathrm{I} + \lambda \mathbf{1} \otimes \mathbf{1} \tag{2.24}$$

It is usual, for isotropic materials, to encounter the above tensor explicitly written as:

$$\boldsymbol{\sigma} = \boldsymbol{C}\varepsilon = \begin{bmatrix}\sigma_n \\ \sigma_s\end{bmatrix} = \frac{E}{(1+\upsilon)(1-2\upsilon)} \begin{bmatrix} C_n & C_{ns} \\ C_{ns} & C_s \end{bmatrix} \begin{bmatrix}\varepsilon_n \\ \varepsilon_s\end{bmatrix} \tag{2.25a}$$

$$\sigma_n = [\sigma_{11} \quad \sigma_{22} \quad \sigma_{33}]^T;\ \ \sigma_s = [\sigma_{23} \quad \sigma_{13} \quad \sigma_{12}]^T$$
$$\varepsilon_n = [\varepsilon_{11} \quad \varepsilon_{22} \quad \varepsilon_{33}]^T;\ \ \varepsilon_s = [2\varepsilon_{23} \quad 2\varepsilon_{13} \quad 2\varepsilon_{12}]^T$$

$$C_n = \begin{bmatrix} (1-\upsilon) & \upsilon & \upsilon \\ & (1-\upsilon) & \upsilon \\ sym & & (1-\upsilon) \end{bmatrix} \tag{2.25b}$$

$$C_s = \begin{bmatrix} \frac{(1-2\upsilon)}{2} & 0 & 0 \\ & \frac{(1-2\upsilon)}{2} & 0 \\ sym & & \frac{(1-2\upsilon)}{2} \end{bmatrix};\ C_{ns} = 0$$

When anisotropic materials are considered, as the case of composite materials, the isotropic stress tensor may be replaced by an orthotropic constitutive tensor (mainly for fiber reinforced polymers). Orthotropic materials have different materials properties in three orthonormal directions (LEKHNITSKII, 1968). At this point, only mechanical properties are being considered.

The orthotropic constitutive tensor with its orthotropic directions 1-2-3 is written in Equation (2.26).

$$C_n = \begin{bmatrix} C_{11} & C_{12} & C_{13} \\ & C_{22} & C_{23} \\ sym & & C_{33} \end{bmatrix};\ C_s = \begin{bmatrix} C_{44} & 0 & 0 \\ & C_{55} & 0 \\ sym & & C_{66} \end{bmatrix};\ C_{ns} = 0 \tag{2.26}$$

$$C_{11} = \frac{1-\nu_{23}\nu_{32}}{\Delta} E_{11};\ C_{22} = \frac{1-\nu_{13}\nu_{31}}{\Delta} E_{22}; C_{33} = \frac{1-\nu_{12}\nu_{21}}{\Delta} E_{33}$$

$$C_{12} = \frac{\nu_{21}+\nu_{31}\nu_{23}}{\Delta} E_{11}; C_{13} = \frac{\nu_{31}+\nu_{21}\nu_{32}}{\Delta} E_{11};\ C_{23} = \frac{\nu_{32}+\nu_{12}\nu_{31}}{\Delta} E_{22}$$

$$C_{44} = G_{23}; C_{55} = G_{13}; C_{66} = G_{12}$$

$$\Delta = 1-\nu_{12}\nu_{21}-\nu_{23}\nu_{32}-\nu_{13}\nu_{31}-2\nu_{21}\nu_{32}\nu_{13}$$

For laminated composite materials, the reinforcements usually require that the stresses, strains and the constitutive tensor to be derived locally following the axes of orthotropy in each ply. The local material directions are usually referenced with indexes 1-2-3. In aerospace applications, the reinforcements are often made in one or two co-planar directions, because, normally, the structures designed are mostly panels. Hence, it is conventional to assign the index 1 to the material direction with the highest stiffness and strength (longitudinal in-plane direction or reinforcement direction). The in-plane direction perpendicular to direction 1 is tagged with the index 2 (transverse in-plane direction). The out-of-plane direction is indicated with index 3. See Figure 5.

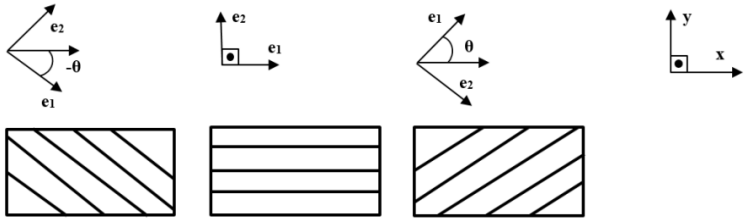

Figure 5. In-plane local material directions 1-2 and the global x-y orientation for a reinforced ply

These laminated composite materials can comprise a stacking sequence with several plies, each possessing its own local coordinate system. However, when the macroscopic forces and constraints are applied on the laminated structure, the equations of motion are derived in the global coordinate system. To transform the constitutive tensor of each ply "C^L" to the global coordinate system "C^G", equation (2.26) is rotated for each ply keeping the local out-of-plane direction parallel with the global normal direction.

$$\sigma_{ji}^{L} = \theta_{ik}\theta_{jl}\sigma_{kl}^{G} = R_{\theta}\sigma_{kl}^{G} \tag{2.27}$$
$$\boldsymbol{C}^{G} = \boldsymbol{R}_{\theta}^{T}\boldsymbol{C}^{L}\boldsymbol{R}_{\theta}^{-T}$$

Explicitly, for a local angle θ (henceforth tagged lamination angle) between the global axis "e_{G1}" and the local axis "e_{L1}":

$$C_n^G = \begin{bmatrix} \bar{C}_{11} & \bar{C}_{12} & \bar{C}_{13} \\ & \bar{C}_{22} & \bar{C}_{23} \\ sym & & \bar{C}_{33} \end{bmatrix};\ C_s^G = \begin{bmatrix} \bar{C}_{44} & \bar{C}_{45} & 0 \\ & \bar{C}_{55} & 0 \\ sym & & \bar{C}_{66} \end{bmatrix};\ C_{ns}^G = \begin{bmatrix} 0 & 0 & \bar{C}_{16} \\ 0 & 0 & \bar{C}_{26} \\ 0 & 0 & \bar{C}_{36} \end{bmatrix} \tag{2.28}$$

$$\bar{C}_{11} = C_{11}c^4 + 2(C_{12} + 2C_{66})s^2c^2 + C_{22}s^4$$
$$\bar{C}_{22} = C_{11}s^4 + 2(C_{12} + 2C_{66})s^2c^2 + C_{22}c^4$$
$$\bar{C}_{12} = (C_{11} + C_{22} - 4C_{66})s^2c^2 + C_{12}(s^4 + c^4)$$
$$\bar{C}_{16} = (C_{11} - C_{12} - 2C_{66})sc^3 + (C_{12} - C_{22} + 2C_{66})cs^3$$
$$\bar{C}_{26} = (C_{11} - C_{12} - 2C_{66})cs^3 + (C_{12} - C_{22} + 2C_{66})sc^3$$
$$\bar{C}_{66} = (C_{11} + C_{22} - 2C_{12} - 2C_{66})s^2c^2 + C_{66}(s^4 + c^4)$$
$$\bar{C}_{13} = C_{13}c^2 + C_{23}s^2;\ \bar{C}_{23} = C_{13}s^2 + C_{23}c^2;\ \bar{C}_{33} = C_{33};\ \bar{C}_{36} = (C_{13} - C_{23})sc$$
$$\bar{C}_{44} = C_{44}c^2 + C_{55}s^2;\ \ \bar{C}_{45} = (C_{55} - C_{44})sc;\ \ \bar{C}_{55} = C_{44}s^2 + C_{55}c^2$$
$$s = sin\,\theta;\ c\ =\ cos\,\theta$$

Figure 5 gives a clear picture of the directions involved in the derivation of the global constitutive tensor.

2.3.2 Strain Energy

The strain energy "U_P" will be referenced more than once and is briefly explained in this section. It can be calculated as (CHEN; HAN, 1988, HUEBNER; THORNTON, 1982, ZIENKIEWICZ; TAYLOR, 2000a, 2000b):

$$U_P = \frac{1}{2}\int_V \boldsymbol{\varepsilon}^T \boldsymbol{\sigma}\, dV = \frac{1}{2}\int_V \boldsymbol{\varepsilon}^T \boldsymbol{C}\boldsymbol{\varepsilon}\, dV \tag{2.29}$$

For an elastic body deformed by external forces, the internal strain energy "U_P" is the potential strain energy stored within the respective volume "V". The strain energy is sometimes tagged according to the main deformation (loading) of the structure, e. g. shear strain energy, bending strain energy, membrane strain energy, and so on. One can see that non-linear and/or anisotropic material constitutive tensors (somehow dependent of the current strain level "ε" and other factors) complicate the integral in equation (2.29). Figure 6 gives a graphical representation of possible constitutive scenarios. Three material behaviors can be seen: the linear elastic behavior (Elasticity); the non-linear elastic behavior (Viscous-Elasticity) and; the inelastic behavior (Plasticity) (CHEN; HAN, 1988).

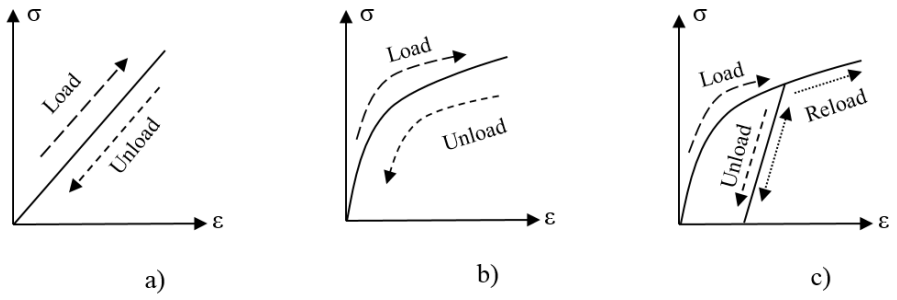

Figure 6. Uniaxial constitutive relations

The third constitutive example shows that after unloading a structure past the elastic regime, a parcel of the strain energy is converted into permanent deformation. It is clear that

for this case the modeling of non-linear and/or dissipative effects in a 3D general formulation is a delicate and necessary task.

So far the term “constitutive (material) model” was applied in a broad sense, but in the context of sandwich structures, which motivates the present work, a very particular class of constitutive behavior is observed. These materials are known as *cellular materials* (GIBSON; ASGBY, 1988). The name is due to the fact that these materials cannot be classified as porous materials, because the volume that the voids occupy is so big (porosity>70%) that the form of these voids directly impact on the macroscopic response of these material. Thus, the phenomenological mechanical response of cellular materials is a blend of the response of the bulk material and the structure its microstructure (CHEN; HAN, 1988, GIBSON; ASGBY, 1988, CALIRI JR, M. F., 2010). Therefore, a careful evaluation of structures built with cellular structures is advised.

Not only the constitutive tensor can increase the complexity of the integral (2.29), but also geometrical non-linearity of the strain tensors can be as hard as or harder than material non-linearity to integrate. Many convergence issues can arise when any non-linearity is addressed numerically. Such problems are usually due to use of non-physical implementation of material models and/or ill-formulated theories combined with a poor simplification of the domain (e.g.: the discretization/mesh used in FEM) and/or a poor solution method (CRISFIELD, 1991, 1997, ZIENKIEWICZ; TAYLOR, 2000b).

These issues discussed above will be later addressed in this work with plate and/or shell structures, mainly for laminated composite plates and sandwich structures. A good estimative of the strain energy and its distribution within these structures is crucial to obtain accurate static and dynamic results.

Chapter 3 - Plate Theories

3.1 The 2D Problem

Plate theories comprise a set of simplifications, which lessen the mathematical efforts in solving the 3D differential equations of motion for nearly 2D structures such as plates, shells, panels and sheets (TIMOSHENKO; KRIEGER, 1959, LEKHNITSKII, 1968).

Analytical solutions of a randomly shaped 3D body under different loadings and boundary conditions through the TE (Theory of Elasticity) are usually not possible for some cases.

Normally, the solutions for such complex cases are obtained numerically. However, numerical approaches are not always needed, if a major simplification in the TE equations is made. For plate structures, the common major simplification is the assumption that the thickness ("H=h") of the plate is much smaller than the other two dimensions, length ("a=L") and width ("b") (Figure 7). Hence, the out-of-plane direction variable is usually eliminated prior to solving the main equations.

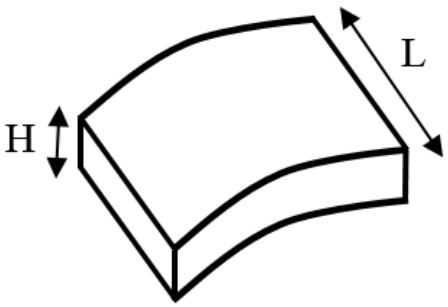

Figure 7. Generic 3D structure which can be approximated to a 2D structure (L, b >> H)

With this assumption, several other differential equations can be solved analytically. Still, there are cases where the numerical approach is the only possible solution method.

The analytical problem of reducing the three-dimensional equations of the Theory of Elasticity down to two-dimensional shell formulations was considered by Gol'denveizer (1968). In that paper, the author grouped these approaches into three categories: 1) the method of hypotheses; 2) the method of expansion with respect to thickness; and 3) the asymptotic

method. For each of these methods, the author wrote on the advantages and disadvantages of each regarding accuracy of the expected results of thin and thick shells. Gol'denveizer discussed the most important property of the state of stress of thin shells. It comprises the fact that the stresses can separated into an internal state of stress distributed throughout the shell and a boundary layer state of stress near the edge of the shells. This boundary layer effect is also known as Saint-Venant's effect (BIRSAN, 2007).

Therefore, before trying to solve the plate equations, the commonly found approaches in the literature used to derive 2D plate theories with the elimination of the out-of-plane coordinate are briefly discussed. They are: Axiomatic, Asymptotic and Continuum Based derivations (CARRERA, 2002).

3.1.1 Axiomatic Derivations

This approach is by far the most common one in the literature. Such derivations stem from postulated expressions for the displacement variables in classical continuum mechanics. Stress variables can be also approximated this way. This derivation assumes that such variables can be defined as polynomials expansions of the thickness coordinate. The respective coefficients are functions of the in-plane coordinates. Based on the most quoted axiomatic formulations, one can write the dependent (stress, strains) or independent (displacement) variables respectively as:

$$\sigma_i(x,y,z) = \sigma_i^0(x,y) + \left\{\sum_{j=1}^{N_\sigma} \sigma_j(x,y)z^j\right\}_i ; i = 1 \dots 6 \tag{3.1}$$

$$\varepsilon_i(x,y,z) = \varepsilon_i^0(x,y) + \left\{\sum_{j=1}^{N_\varepsilon} \varepsilon_j(x,y)z^j\right\}_i ; i = 1 \dots 6$$

$$u_i(x,y,z) = u_i^0(x,y) + \left\{\sum_{j=1}^{N_u} u_j(x,y)z^j\right\}_i ; i = 1 \dots 3$$

This axiomatic formulations can be taken as complete polynomials or not. Some particular theories begin from a complete polynomial of order "n" and applies physical

boundary conditions to eliminate or relate the coefficients of the expansion. Some postulates add sine or co-sine functions to the summations in equation (3.1), which are, respectively, the sum of the odd or even terms of the infinite expansion of the thickness coordinate with proper coefficients.

Putting aside this rough characteristic of finding a solution, the axiomatic derivation is very popular, because it allows for intuitive and/or optimal postulates. Therefore, the equations of motion tend to be as simple as desired, and most of classical plate theories are of this type.

3.1.2 Asymptotic Derivations

To derive plate theories with asymptotic methods, one chooses a physically consistent way to reduce the 3D elasticity problem to a 2D plate theory.

The approximate solutions are usually formulated by using a polynomial of small parameters somehow related to the plate's thickness "h". In the references (BERDICHEVSKII, 1979), two small ratios are frequently quoted:

$$h_* \approx \frac{h}{R} \qquad (3.2)$$
$$h_{**} \approx \frac{h}{l}$$

The first one, for the case of shell structures, is the ratio of a shell's thickness to its curvature. The second one is a term, which scales the thickness of the plate or shell with the current problem. Such term is usually the well-known aspect ratio "h/l". This term can indicate how deep the boundary layer effects are "felt" towards the plate's center. Along with the ratios in equation (3.2), the asymptotic solutions can use other small parameters such as the current strain level "ε". Asymptotic methods usually couple the "internal" and the "boundary layer" solutions iteratively. Axiomatic methods have the same continuous functions for both regions and, because of this the solutions are usually more complex.

A variational-asymptotic method was proposed by Berdichevskii (1979) to derive a non-linear theory of shells. From the three dimensional elasticity theory, the author proposed a solution for the displacement approximate functions whose terms are weighted according to the

problem and the desired accuracy. The thickness of the shell, "h", and the deformation level "ε", were chosen as accuracy thresholds in the asymptotic method. Different asymptotic theories were investigated: classical theory; fundamental refined theory; refined theory with geometric correction and considering transverse shear stress. These theories were classified according to whether they include or discard the terms of equation (3.2) along with their combinations and their powers. Depending on the problem, different combinations of the parameters may be used according to the accuracy desired. Comparing the following small ratios to unit, it is possible to write:

$$1 > h_{**} > h_{*} > h_{**}^{2} > h_{*}h_{**} > h_{*}^{2} > \varepsilon > \cdots \tag{3.3}$$

Classical plate theories can be set as a reference and its accuracy level associated to the unit value in equation (3.3). Refined theories demand the inclusion of smaller ratios. From left to right in equation (3.3), the first small term is associated to refined fundamental theories. The second can be seen as a geometric correction. The use of the third term enables the resolution of the transverse shear effects. If further refinements are demanded, the next small term, which is the product of ratios, can be explored, and so on.

Berdichevskii (1979) also pointed that the problem is usually split into an internal and a boundary layer problem. Among the hurdles in deriving the plate the theory, it is important to note the difficulty in handling the edge solution, i. e. the boundary layer problem. The author stated that the accuracy of the theories including transverse shear stress are much subordinated to the problem's boundary conditions.

Hence, a general format of the asymptotic solutions can be taken as:

$$\sigma_i(x,y,z) = \sigma_i^0(x,y) + \left\{ \sum_{j=1}^{N_\sigma} [\sigma(x,y,h_{*},h_{**},h_{*}^{2},h_{*}h_{**},h_{**}^{2},\varepsilon)]_j \right\}_i ; i = 1 \dots 6 \tag{3.4}$$

$$\varepsilon_i(x,y,z) = \varepsilon_i^0(x,y) + \left\{ \sum_{j=1}^{N_\varepsilon} [\varepsilon(x,y,h_{*},h_{**},h_{*}^{2},h_{*}h_{**},h_{**}^{2},\varepsilon)]_j \right\}_i ; i = 1 \dots 6$$

$$u_i(x,y,z) = u_i^0(x,y) + \left\{ \sum_{j=1}^{N_u} [u(x,y,h_{*},h_{**},h_{*}^{2},h_{*}h_{**},h_{**}^{2},\varepsilon)]_j \right\}_i ; i = 1 \dots 3$$

For isotropic plates and shells, the small ratios defined up until this point in this section suffice to achieve the asymptotic solutions. On the other hand, if multilayered plates and shells are considered, other perturbation ratios might need further investigation. The ratio of the longitudinal to the transverse in-plane local moduli of Young (E_L/E_T) is a clear example. Depending on the stacking sequence, the lamination angle can be treated indirectly as a perturbation variable too.

3.1.3 Continuum Based Derivations

These formulations receive this designation because they make use of non-usual more complex continuum theories. Plate and shell formulation can be described by choosing the appropriate DOFs to work on.

As already mentioned in Chapter 2, the Cosserat (after the Cosserat brothers, who studied this topic more than a hundred years ago) or Micropolar Continuum theory is a 6D continuum theory because the rotational DOFs are set as independent variables (GREEN; NAGHDI; WAINWRIGHT, 1965, SANSOUR; BEDNARCZYK, 1995, YANG et al., 2000, DIEBELS; STEEB, 2002, NEFF; CHELMINSKI, 2007, ALTENBACH; EREMEYEV (2010)).

For non-classical continua such as the Cosserat surface, the constitutive relations are also unique, because the rotational DOFs are uncoupled from the translational ones. They are usually more complex and numerous. Theories with six to eight elastic material properties can be found in the literature. Usually, the Cosserat parameters are obtained with differentiation of the strain energy.

Using thermodynamic principles and the Helmholtz free energy function, Green, Naghdi and Wainwright (1965) developed a constitutive elastic rule for these surfaces. Also, under specific assumptions, the classical shell theory derived according to Kirchhoff-Love hypothesis was obtained for comparison.

To clarify the usual derivation of Cosserat shells, a position vector “r” for an arbitrary point in the shell can be achieved with a sum of the current position “x” and the position along the thickness coordinate “ζ” parallel to the surface normal “n”:

$$\boldsymbol{r}(q_1, q_2, \zeta) = \boldsymbol{x}(q_1, q_2) + \zeta \boldsymbol{n}(q_1, q_2) \tag{3.5}$$

Where "q_1" and "q_2" are the in plane coordinates. This is a usual representation of a surface. However, the difference lies in the definition of strains.

From Neff and Chelminski (2007), the deformation of Cosserat (micropolar) models are obtained by coupling a displacement field "u" to an independent field of micro rotations "A_c". This micro rotations are related with the director vectors "d" which are linked with the microscopic properties of the material. Thus, the micropolar (or first Cosserat) strain tensor "ε_c" is:

$$\varepsilon_c = \boldsymbol{\nabla} u - \boldsymbol{A}_c\,(\boldsymbol{d}) \tag{3.6}$$

The tensor "ε_c" might not be symmetric as in the classical decomposition of the strain tensors into symmetric and skew-symmetric parts of the displacement gradient. Also, if one applies specifics constraints on these directors, different shell theories can be recovered such as the Kirchhoff–Love's and Mindlin-Reissner's.

Due to the presence of the rotations DOFs, the respective moments need to be equated in the equilibrium equations. This demands additional boundary conditions and material properties to be defined. For the sake of brevity and to avoid a wave of symbols definitions, more details of the equilibrium and kinematics are omitted. More details can be seen in the references of this section.

A comprehensive review of Cosserat plate and shell theories can be seen in Altenbach and Eremeyev (2010). Over 300 articles are cited. The basic kinematic assumptions assumed for this approach are explained. From very simple to complex structures, several Cosserat theories are shown by Altenbach and Eremeyev. Applications of this theory can be found in all areas. Solid mechanics applications comprise areas like plasticity, soil mechanics, composite structures and nanostructures. Also, the particularities in deriving constitutive equations and deformable structures are covered. Fluid mechanics applications are found as well with notes to magnetic liquids, polymer suspensions and liquid crystals.

More recently, Skatulla and Sansour (2013) worked on a Cosserat type of formulation, which considers multiple scale effects and is able to handle even inelastic material behavior with minor care. Different test cases solved with mesh-less methods showed good qualitative macro results and the accuracy of the method to consider micro-structure characteristics of the shell material.

Regarding sandwich structures, Diebels and Steeb (2002) attempted to account for the micro structure (cells) of foams using a Cosserat formulation through its microscopic derivation. During the derivation of the strain energy, two additional moduli (Cosserat parameters) emerged. The authors managed to relate one of them with the average size of cell in the foam. The results showed that this is a promising alternative to the microscopic lattice material models, which are considerably complex, and the phenomenological ones, which may be too robust. This is fertile area for future investigations.

In terms of the position and the director vectors, the general form for stretch "σ" and couple "M" stresses, the corresponding stretch "ε" and distortion "κ" variables and the displacement "u" and rotation "ϑ" fields, are summarized in equation (3.7).

$$\begin{aligned} &\sigma_i = f_i^{\sigma}(\boldsymbol{r},\boldsymbol{d});\ M_i = f_i^{M}(\boldsymbol{r},\boldsymbol{d}) \\ &\varepsilon_i = f_i^{\varepsilon}(\boldsymbol{r},\boldsymbol{d});\ \kappa_i = f_i^{\kappa}(\boldsymbol{r},\boldsymbol{d}) \\ &u_i = f_i^{u}(\boldsymbol{r},\boldsymbol{d});\ \vartheta_i = f_i^{\vartheta}(\boldsymbol{r},\boldsymbol{d}); i = 1 \dots 3 \end{aligned} \tag{3.7}$$

In sum, the difference among equations (3.1), (3.4) and (3.7) consists on:

- **Equation (3.1)**: The solution for each variable (u, σ, and ε) is attained by postulating the field variables as polynomials expanded in powers of the thickness direction (z). The associated coefficients are written in terms of the in-plane components (x, y).
- **Equation (3.4)**: The solution is obtained by physical consistent perturbation of the governing equations derived in terms of "u", "σ", or "ε". These equations are polynomials expanded in terms of small parameters. These parameters are usually small ratios of geometrical characteristics or material properties of the plate.
- **Equation (3.7)**: The rotational behavior is obtained from the independent rotational DOFs of the micropolar formulation. Each solved variable ("u", "ϑ", "σ", "M", "ε" and "κ") is function of a position vector and a direction. Constitutive relations and the link between translational and rotational DOFs are not straightforwardly derived.

From Section 3.1, it is clear that depending on the material properties, shape and size of the plate or shell, a particular derivation process might not suffice or be too cumbersome. Among several sources of error, the most common one is that to misjudge the thickness of the

plate. Thick, moderately thick and thin plates demand different approximations, as it will be seen at the next section.

3.2 Thick and Thin Plates

In order to better understand the limitations of each plate theory, the mechanics of thin and thick plates are reviewed in this part of the manuscript based on the literature (TIMOSHENKO; KRIEGER, 1959, LEKHNITSKII, 1968, MENDONÇA, 2005).

Historically, the classical kinematics assumptions adopted for plates lead to physically inconsistent formulations when compared to the differential equations of motion (2.12) derived by using the Theory of Elasticity. However, there are formulations, which are accurate enough for the most common of plate problems. If the plate is very thin, it approaches a membrane structure, which possesses no transversal stiffness and responds only to normal forces. On the other hand, if the plate is thick, the transversal reactions might interfere in the traction and bending results to a magnitude, which cannot be neglected.

To formulate specific theories, the hypothesis of a thin or a thick plate is normally adopted prior to derivation of the equations. Hence, in the present work, a plate can be taken as thin, moderately thick or thick plate, when:

- $l/h < 20 \rightarrow$ Thick plate
- $20 \leq l/h \leq 100 \rightarrow$ Moderately Thick/Thin plate
- $l/h > 100 \rightarrow$ Thin plate

It is important to mention that moderately thick/thin plates are usually modeled as thick plates. But regardless of the thickness assumption, the plate formulations usually share some or all of the following base hypotheses:

- The smallest dimension is the thickness coordinate ($h \ll l$).
- Deflections of the plate are small when compared to the thickness of the plate ($w \ll h$).
- Transversal extensions and stresses are usually neglected.

- Cutting sections, through the thickness of the plate, may or may not present linear or non-linear warping effects depending on material properties and thickness of the plate.
- For some formulations of thin plates, it is possible to assume "$w_{,x} - u_{,z} = 0$".

It should be mentioned that two different plate theories might give similar results in static analyses, but in dynamic cases, the same is not necessarily true. A particular theory may perform well in static analyses, but may fail in transient/dynamic cases.

Dynamic solutions are more difficult to obtain, because the theory must be well formulated for both spatial and time excitations. When transient kinematic effects are considered, mass and damping properties are needed in addition to the stiffness properties defined in section 2.3. The mass variable is always present in dynamic solutions, but the damping properties may not. There are different definitions for damping. Generally, it is related to the dissipation process of energy from a system under excitation (BEARDS, 1996; EWINS, 1985).

In complex systems, it is difficult to assert the exact origin of the dissipated energy and associate it with a specific phenomenon such as friction, viscosity and hysteresis (BEARDS, 1996). To exemplify the different sources of dissipation, Romberg et al. (2007) lists some of the possible sources of passive or induced structural damping for sandwich panels.

Johnson and Kienholz (1982) identified the need to solve the dynamic problems of structures in the field of frequency, instead of time. The solution in the time domain is easier and faster, but its accuracy depends on the choice of the natural modes. Usually only few natural modes are chosen. For this, complex material properties are usually devised.

In 2010, Salam and Bondok (2010) showed an analytical model to calculate the equivalent stiffness and damping properties of a sandwich beam. Comparison with numerical models in ANSYS endorsed the approach. Pervez and Zabaras (1992) worked with laminated composite materials to test an analytical formulation with parabolic distribution of the shear stresses. The damping influence was observed to change with the lamination parameters.

Li (2006) studied the damping properties in sandwich structures, but for acoustic purposes. The author investigated the properties of a sandwich structures made of a paper honeycomb core filled with a polyurethane foam and reinforced with carbon fiber skins (Figure 8). A method to assess the damping of these structures was proposed by the author. The author noticed that this particular sandwich structure does not present any advantage regarding the sound transmission loss behavior throughout the whole structure in comparison with a sandwich

with a pure aluminum panel. However, this foam filled paper honeycomb sandwich structure increases the damping properties of the structure

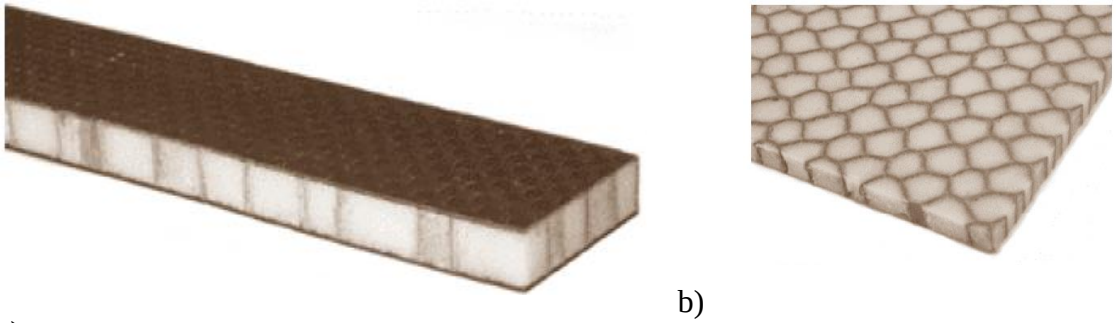

a) b)

Figure 8. a) Polyurethane foam-filled paper honeycomb core. b) foam-filled paper honeycomb core – adapted from Li (2006)

Liu (2008) also showed an extensive work on how to determine the damping in sandwich composite beams and plates. Metal or fiber reinforced skins with polymeric or honeycomb bores were studied with the addition of a damping layer. The author covered the main experimental methods to determine the damping constants: 1) free-decay (time domain); 2) curve fitting (frequency domain) and; 3) the power input method. Analytical models were also reviewed. Analytical results, experimental results and FE solutions using NASTRAN solver were compared and the need to properly model the energy dissipation was reminded.

Lima, Faria and Rade (2010) proposed a FE formulation to study the sensitivity of viscoelastic parameters of laminated structures made of materials, which are frequency and temperature dependent. The derivatives of the Frequency Response Functions (FRF) obtained by the current method were compared to that calculated by finite-difference method. A high order theory plate was used with a quadratic expansion for the transversal displacement and cubic ones for the in-plane fields. More high-order plate formulations can be seen in Rastgaar et al. (2004). In that work, a triangular C-1 element was implemented with a third order plate theory. Different natural modes of vibration for angle-ply and cross-ply laminated were studied and the results for different boundary conditions, aspect ratios were compared to FSDT and CLT plate theories.

Mendonça (2005) showed the influence of few different plate theories on the first natural frequency of a particular laminate. Carrera (2003) did the same, but with a unified plate formulation. Both references indicate that, even discarding the dissipation effects of the structure, the errors can miss the reference value by a factor of 2 or more (error > 100%).

The references pointed above are just a few which represent the need to properly choose the plate formulation for a particular engineering problem. The spatial resolution of the internal stress field according to a specific plate theory determines how the mass and damping effects affect the spatial and time results.

Therefore, a review on plate theories is required. Next section brings some classical plate formulations for thin, moderately thick and thick plates. It shows the effect of the hypotheses assumed during the derivation process on each plate theory. They serve as a reference for other more complicated formulations.

3.2.1 Moderately Thick Plate Formulations

Reissner-Mindlin's or just Mindlin's plate theory is the most common First Order Shear Deformation Theory (FSDT) (REDDY, 1990). It is a plate theory for moderately thick plates because transversal shear strains (warping) are treated linearly.

For moderately thick plates, the field variables used in the FSDT can be seen in Figure 9.

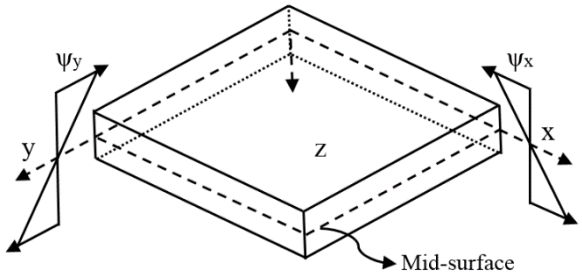

Figure 9. Isotropic plate representation

Mindlin's plate theory is of the asymptotic type. Therefore, the displacement functions are polynomials of the thickness coordinate "z". Specifically:

$$u(x,y,z) = u^0(x,y) + z\psi_x(x,y) \tag{3.8}$$
$$v(x,y,z) = v^0(x,y) + z\psi_y(x,y)$$
$$w(x,y,z) = w(x,y)$$

Considering the linear part of von Kármán's strain tensor in equation (2.6), the displacement field in equation (3.8) yields:

$$\varepsilon_x(x,y,z) = u^0_{,x}(x,y) + z\psi_{x,x}(x,y) \tag{3.9}$$
$$\varepsilon_y(x,y,z) = v^0_{,y}(x,y) + z\psi_{y,y}(x,y)$$
$$\varepsilon_z(x,y,z) = 0$$
$$2\varepsilon_{xy}(x,y,z) = \left[\psi_{x,y}(x,y) + \psi_{y,x}(x,y)\right]z \tag{3.9}$$
$$2\varepsilon_{yz}(x,y,z) = \left[\psi_y(x,y) + w_{,y}(x,y)\right]$$
$$2\varepsilon_{xz}(x,y,z) = \left[\psi_x(x,y) + w_{,x}(x,y)\right]$$

To get the respective stresses, the moments and forces for the representative element in the Figure 10 are equated to yield the differential equations of movement in (3.10):

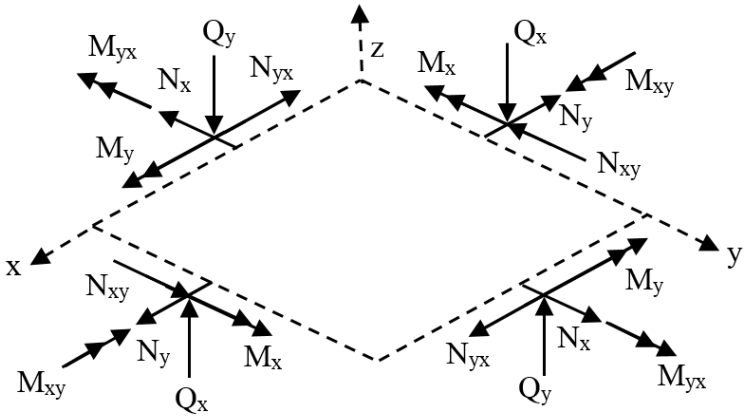

Figure 10. Equilibrated forces and moments on a plate element

$$M_{x,x} + M_{yx,y} - Q_x + z\tau_{xz}|^{H/2}_{-H/2} - \rho_1\ddot{u}^0 - \rho_2\ddot{\psi}_x = 0 \tag{3.10.}$$
$$M_{xy,x} + M_{y,y} - Q_y + z\tau_{yz}|^{H/2}_{-H/2} - \rho_1\ddot{v}^0 - \rho_2\ddot{\psi}_y = 0$$
$$N_{x,x} + N_{yx,y} + \tau_{xz}|^{H/2}_{-H/2} - \rho_0\ddot{u}^0 - \rho_1\ddot{\psi}_x = 0$$
$$N_{xy,x} + N_{y,y} + \tau_{yz}|^{H/2}_{-H/2} - \rho_0\ddot{v}^0 - \rho_1\ddot{\psi}_y = 0$$
$$Q_{x,x} + Q_{y,y} + N_x w_{,xx} + 2N_{xy}w_{,xy} + N_y w_{,yy} + w_{,x}\left[\rho_0\ddot{u}^0 + \rho_1\ddot{\psi}_x - \tau_{xz}|^{H/2}_{-H/2}\right]$$
$$+ w_{,y}\left[\rho_0\ddot{v}^0 + \rho_1\ddot{\psi}_y - \tau_{yz}|^{H/2}_{-H/2}\right] - q(x,y) - \rho_0\ddot{w} = 0$$
$$\rho_n(x,y) = \int_{-H/2}^{H/2} \rho\, z^n dz$$

Once the displacement fields are solved for, the normal and shear stresses in equation (2.12) can be integrated through the thickness of the plate to retrieve the moments and forces in equation (3.9):

$$\begin{aligned}\left(N_x; N_{xy}; M_x; M_{xy}; Q_x\right) &= \int_{-H/2}^{H/2}\left(\sigma_x; \tau_{xy}; \sigma_x z; \tau_{xy} z; \tau_{xz}\right)dz \\ \left(N_y; N_{yx}; M_y; M_{yx}; Q_y\right) &= \int_{-H/2}^{H/2}\left(\sigma_y; \tau_{yx}; \sigma_y z; \tau_{yx} z; \tau_{yz}\right)dz\end{aligned} \tag{3.11}$$

This thick plate formulation is an attempt to describe the transverse shear effects, which may be significant if the plate is considerably thick and/or soft. However, the FSDT is incapable of yielding a physically consistent result due to the kinematics adopted. This inconsistency is the fact that a constant value is assumed for both transverse shear strains and stresses. Originally, the formulation underestimates the macroscopic results and a correction is usually applied. This correction is the so-called "shear correction factor". This parameter depends on the material properties of the plate and the loading conditions. Moreover, a physically consistent value must be available to provide the basis for the shear correction factor calculation. The method developed by Reissner's to derive a shear correction factor κ for an isotropic plate is shown next.

Firstly, a physical result for the transverse shear stresses as a function of the thickness direction must be obtained. The procedure begins by using integrations of the differential equilibrium equations containing the transverse shear stresses and the in-plane normal stresses up to a section "z":

$$\begin{aligned}\tau_{xz}(x,y,z) + \left\{\int_{-H/2}^{z}\sigma_x(x,y,z)dz\right\}_{,x} + \left\{\int_{-H/2}^{z}\tau_{yx}(x,y,z)dz\right\}_{,y} &= 0 \\ \tau_{yz}(x,y,z) + \left\{\int_{-H/2}^{z}\sigma_y(x,y,z)dz\right\}_{,x} + \left\{\int_{-H/2}^{z}\tau_{xy}(x,y,z)dz\right\}_{,y} &= 0\end{aligned} \tag{3.12}$$

For a homogeneous isotropic plate in bending, the integration above becomes:

$$\tau_{xz}(x,y,z) = \frac{3}{2H}\left(1-\frac{4z}{H^2}\right)\left[M_{x,x}+M_{xy,y}\right] = \left(1-\frac{4z}{H^2}\right)\frac{3Q_x}{2H} \tag{3.13}$$
$$\tau_{yz}(x,y,z) = \frac{3}{2H}\left(1-\frac{4z}{H^2}\right)\left[M_{xy,x}+M_{y,y}\right] = \left(1-\frac{4z}{H^2}\right)\frac{3Q_y}{2H}$$

The results in equation (3.13) indicate that the transverse shear distributions are parabolic functions of the thickness "z" coordinate.

Reissner's procedure requires the equivalence of the shear strain energies calculated via the FSDT and the parabolic distributions in (3.13). The transverse shear strain energy via the FSDT is:

$$U_s^{FSDT} = \frac{1}{2}\int_\Omega \int_{-H/2}^{H/2}(\tau_{xz}\gamma_{xz}+\tau_{yz}\gamma_{yz})dz\,d\Omega = \frac{1}{2H\kappa}\int_\Omega \left(\frac{Q_x^2}{C_{55}}+\frac{Q_y^2}{C_{44}}\right)d\Omega \tag{3.14}$$

On the other hand, using the physical parabolic distributions in equation (3.13) and Hooke's constitutive tensor, the following expression for the transversal shear strain energy is:

$$U_s^{Parabolic} = \frac{1}{2}\int_\Omega \int_{-H/2}^{H/2}\left(\frac{\tau_{xz}^2}{C_{55}}+\frac{\tau_{yz}^2}{C_{44}}\right)dz\,d\Omega = \frac{3}{5H}\int_\Omega \left(\frac{Q_x^2}{C_{55}}+\frac{Q_y^2}{C_{44}}\right)d\Omega \tag{3.15}$$

Establishing an equivalent relation between (3.14) and (3.15), it is possible to calculate Reissner's shear correction factor κ:

$$U_s^{FSDT} = U_s^{Parabolic} \rightarrow \kappa = 5/6 \tag{3.16}$$

Other approaches are available in the literature. For the same problem, Timoshenko chooses the transversal strain level at the mid-plane section, which is maximum, to assess the value of the shear correction factor. Using equation (3.13) the maximum strain level is obtained and compared with the constant value obtained with Mindlin's plate theory and Hooke's law. This procedure yields a shear correction factor of 2/3.

3.2.2 Thin Plate Formulations

When thin plates are considered, the transversal shear strains are usually neglected and thereby all of the plate hypothesis made in the beginning of this chapter hold, yielding:

$$2\varepsilon_{yz}(x,y,z) = \left[\psi_y(x,y) + w_{,y}(x,y)\right] = 0 \qquad (3.17)$$
$$2\varepsilon_{xz}(x,y,z) = \left[\psi_x(x,y) + w_{,x}(x,y)\right] = 0$$

Now, to reach the membrane and bending differential equations of movement of isotropic thin plates, the shear forces are eliminated from equations (3.10) by re-arranging the equations in (3.10) and then applying equation (3.17) to obtain:

$$D\left[w_{,xxxx} + 2w_{,xxyy} + w_{,yyyy}\right] = q(x,y) - \rho H\ddot{w} \qquad (3.18)$$
$$u^0_{,xx} + A_1 v^0_{,xy} + A_2 u^0_{,yy} = A_3 \ddot{u}^0$$
$$v^0_{,yy} + A_1 u^0_{,xy} + A_2 v^0_{,xx} = A_3 \ddot{v}^0$$
$$D = EH^3/[12(1-v^2)]\,;A_1 = (1+v)/2\,;A_2 = (1-v)/2\,;A_3 = (1-v^2)\rho/E$$

The equations in (3.18) are recognized as Kirchhoff's thin plate theory.

At this point, thin and moderately thick plates have been covered. For these, linear models may suffice for most applications. However, if the plate is thick, the non-linear effects through the thickness and near boundaries (boundary layer effects) of the plate cannot be neglected since the plate is now actually a 3D structure.

3.2.3 Non-linear Thick Plate Formulations

Instead of struggling with the limitations of the FSDT for thick plates, other authors have proposed more robust solutions for the non-linear plate problem. This was accomplished by using non-linear terms of the thickness coordinate in the displacement fields. Plate theories with these non-linear terms are generically known as High order Shear Deformation Theories (HSDT). They allow for a physically consistent transverse shear stress distribution across the

thickness as well as the fulfillment of zero shear stress at the top and bottom surfaces of the plate. In some cases, the shear correction factor is not required or may be neglected in these formulations because the transversal strain energy can be better accommodated with the non-linear formulations, especially those with parabolic profiles, which approximate the real solution.

Among several widespread non-linear displacements axiomatic approaches, a pattern of HSDTs can be found in the literature as:

$$u_i(x,y,z) = u_i^0(x,y) - zu_{3,i}^0 + F(z)G_i(x,y,z);\ i = 1,2 \tag{3.19}$$
$$u_3(x,y,z) = u_3^0(x,y)$$

Some of the consulted theories, which fall in this pattern, are plotted in Figure 11. The respective equations can be found in the manuscript.

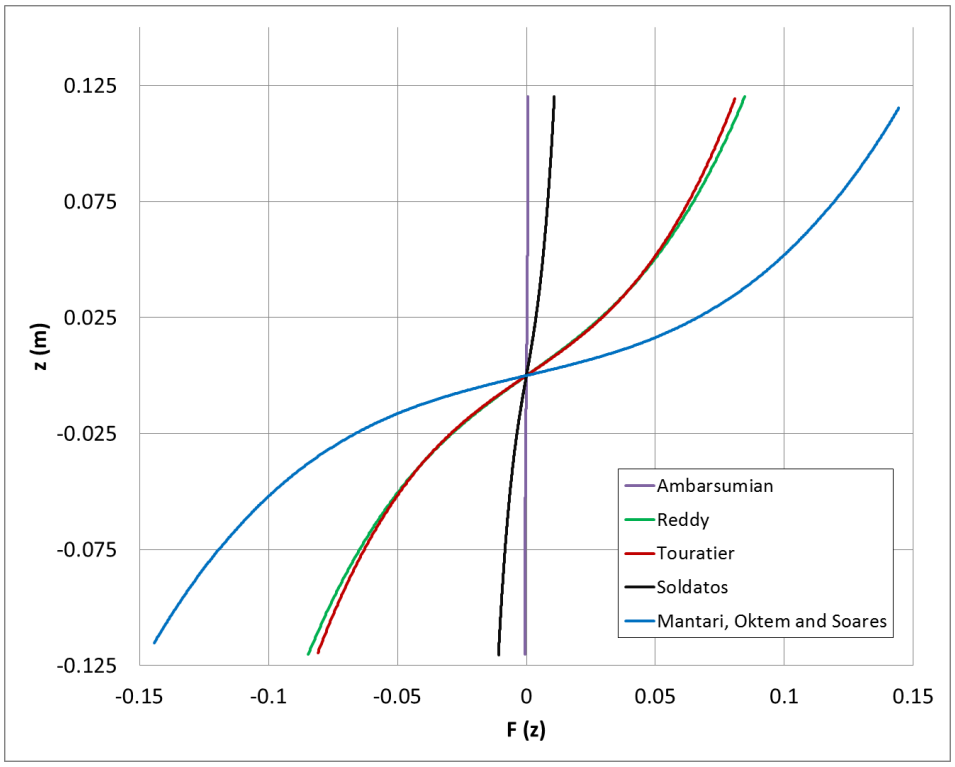

Figure 11. Shear functions behavior along the thickness coordinate (z)

(AMBARTISUMIAN, 1958) (3.20)

$$F(z) = \frac{z}{2}\left[\frac{h^2}{4} - \frac{z^2}{3}\right]$$
$$G_i(x,y,z) = \theta_i(x,y)$$

(REDDY, 1990) (3.21)

$$F(z) = z\left[1 - \frac{4}{3}\left(\frac{z}{h}\right)^2\right]$$

$$G_i(x, y, z) = \theta_i(x, y) + zu^0_{3,i} = \gamma^0_{3,i}$$

(TOURATIER, 1991) (3.22)

$$F(z) = \frac{h}{\pi} sin\left(\frac{z\pi}{h}\right)$$

$$G_i(x, y, z) = \theta_i(x, y) + zu^0_{3,i} = \gamma^0_{3,i}$$

(SOLDATOS, 1992) (3.23)

$$F(z) = zcosh\left(\frac{1}{2}\right) - hsinh\left(\frac{z}{h}\right)$$

$$G_i(x, y, z) = \theta_i(x, y)$$

(MANTARI; OKTEM; SOARES, 2012) (3.24)

$$F(z) = sin\left(\frac{z\pi}{h}\right) \exp\left\{m\left[cos\left(\frac{z\pi}{h}\right)\right]\right\} + m\frac{\pi}{h}$$

$$G_i(x, y, z) = \theta_i(x, y)$$

In figure 10, Mantari, Oktem and Soares' shear function "F" is weighted by a factor of "h/π" and the coefficient "m" is set to 0.5. Many other theories can be found in the literature. Some of these theories assume that the displacements in the thickness coordinate for equations on the pattern (3.19) present a constant value across the thickness. However, there are other formulations where the deflection is dependent on the thickness coordinate:

(KANT; OWEN; ZIENKIEWICZ, 1982, PANDYA; KANT, 1988) (3.25)

$$u_i(x, y, z) = u^0_i(x, y) + z\theta_i(x, y) + z^3\theta_{i3}(x, y);\ i = 1, 2$$

$$w(x, y, z) = w^0(x, y) + z^2 w_2(x, y)$$

(FERREIRA et at., 2011) (3.26)

$$u_i(x, y, z) = u^0_i(x, y) + zu_{1i} + \sin\left(\frac{z\pi}{h}\right) u_{3i}\ ;\ i = 1 \ldots 3$$

These latter theories better attend Koiter's recommendation (KR), which states that improvements on Kirchhoff-Love's thin plate theory is usually meaningless, unless the effects of transverse shear and normal stresses are taken into account at the same time (CARRERA, 1999). Thus, this recommendation is better suited for plates, where transversal shear effects cannot be neglected.

A note of caution is worthy taken at this point. Both the plate's rotation angle "θ_i" and the corresponding transverse shear deformation $\gamma_{3,i}$, in the above non-linear theories, must be carefully handled. Due a large variety of derivations founded in the references, these two variables might get mixed up, because of a misunderstanding by using a wrong sign convention or coincident symbol assignments.

To close this section, Navier's technique, which is used to achieve some analytical solutions, i.e. exact solutions, is reviewed (TIMOSHENKO; KRIEGER, 1959). It is often used as a benchmark for numerical solutions for a particular non-linear theory. With this method, the solutions are obtained by assuming double Fourier series for the unknown field variables. For this method to work, the loads applied are also given as a double Fourier series. In dynamic problems, the series are weighted by a decaying exponential function of time. Hence, as an example, the generic form of the displacement fields ("u") and the surface loading ("q") can be:

$$u_j(x,y,z) = F(z)\left\{\sum_{m,n}^{\infty,\infty} A_j^{mn} \sin\left(a_j^m x\right) \sin\left(b_j^n y\right) e^{i\omega_{mn}t}\right\}; j = 1 \dots 3 \tag{3.27}$$

$$q(x,y) = \left\{\sum_{m,n}^{\infty,\infty} Q_j^{mn} \sin\left(a_j^m x\right) \sin\left(b_j^n y\right) e^{i\omega_{mn}t}\right\} \tag{3.28}$$

It is nearly impossible to assert by mere inspection of the equations in this section (3.2), which formulation is the best one. Naturally, for analytical solvable problems with periodic (sine and or co-sine) behaviors throughout the plate structure, Navier's solution is certainly one candidate. Nevertheless, the actual engineering problems offer challenging boundary value problems, which are seldom solved by analytical solutions. Usually, a numerical method is chosen, which best suits the problem and tools at hand.

Navier's approach is not the best choice to be solved numerically, because the value of sum of sine and co-sine may be too high to be solved numerically or too low to give accurate results.

Thin plate formulations usually present very close results, because the thickness of the structure is too small to render too large errors. However, caution is required, if the material of the plate is too soft or if the plate is not thin enough, because thin plate problems are usually submitted to large displacements, which may enhance the formulation errors. Thus, a good choice could be a shear deformation theory, i.e. a moderately thick or non-linear formulation.

Reddy's approach in equation (3.21) is quoted as one of the most successful theory, because even though it stems from an axiomatic approach. The author used a physical condition of free shear stress at the top and bottom of the plate and removed the quadratic terms of the thickness expansion from the in-plane displacement fields. However, and unfortunately, only geometrically simple structures can be easily solved by using this formulation, because it demands continuity of the derivatives of deflection displacement field across sub-domains (elements) when solved numerically. This poses a considerably hurdle for its application.

An accurate choice of non-linear plate formulation is any theory, which allows for physical consistence, meaning that the displacement fields should resemble polynomials of the thickness direction with all terms up to, at least, the cubic term. Depending on the solution method, the coefficients of these expansions can be analytically or numerically determined and some eliminated to lessen the complexity of the problem.

Up to date and to the knowledge of the present author, if the plate problem is properly approached, especially, if the problem is divided into sub-domains/elements, the FSDTs with shear correction factors should offer good enough results. However, if the structure or its sub-domains end up too thick for whichever reason, HSDTs should represent a better option. Not only the HSDT give more accurate transversal results, but in plane results, as well. Therefore, the whole plate problem is better handled.

It is important to have the issues pointed above in mind, because the plate problem gets a bit more complicated when laminated composite and sandwich structures are analyzed. Therefore, this shows that new formulations and/or approaches should be proposed.

3.3 Laminated Plate Theories

The Classical Lamination Theory (CLT) is the most quoted theory for laminated plates perhaps because it is the simplest one. It is quickly explained in this section as a reference and

a foundation for more accurate and complex theories (LEKHNITSKII, 1968, MENDONÇA, 2005).

The CLT can be considered as a stacking of perfectly bounded thin plies. By perfectly bounded, the geometrical and elastic properties of the interfaces layers are disregarded in the derivation of the governing equations. To arrive at the well-known ABBD stiffness matrix, the traction, moments are equated with the respective stretches and rotations along with the orthotropic rotated properties from equation (2.28). The equation to be solved is:

$$\left(N_x; N_{xy}; N_y; M_x; M_{xy}; M_y\right) = \sum_{k=1}^{N} \int_{z_{k-1}}^{z_k} \left(\sigma_x; \tau_{xy}; \sigma_y; \sigma_x z; \tau_{xy} z; \sigma_y z\right)^k dz \tag{3.29}$$

with $\{\sigma_i\}^k = \left[\bar{Q}_{ij}\right]^k \{[\varepsilon^0] + z[\kappa]\}$

This previous integration lead to the 2D ABBD matricial system of equations:

$$\begin{Bmatrix} \boldsymbol{N} \\ \boldsymbol{M} \end{Bmatrix} = \begin{bmatrix} \boldsymbol{A} & \boldsymbol{B} \\ \boldsymbol{B} & \boldsymbol{D} \end{bmatrix} \begin{Bmatrix} \boldsymbol{\varepsilon^0} \\ \boldsymbol{\kappa} \end{Bmatrix} \tag{3.30}$$

Each of the ABBD components is a 6x6 matrix. The A matrix is the extensional behavior. The matrix D gives the bending and/or torsion behavior. And lastly, the B matrix is responsible for coupling the matrices A and D. These terms are:

$$A_{ij} = \sum_{k=1}^{N} \bar{Q}_{ij}^k \, h_k \tag{3.31}$$

$$B_{ij} = \sum_{k=1}^{N} \bar{Q}_{ij}^k \, h_k \bar{z}_k$$

$$D_{ij} = \sum_{k=1}^{N} \bar{Q}_{ij}^k \left(h_k \bar{z}_k^2 + \frac{h_k^3}{12} \right)$$

$\bar{z}_k = (z_k + z_{k-1})/2$ and $h_k = z_k - z_{k-1}$

Such simplified theory works fine for thin plates only. However, if one of the plies or the laminate is a moderate thick or thick plate, then a refined theory is needed.

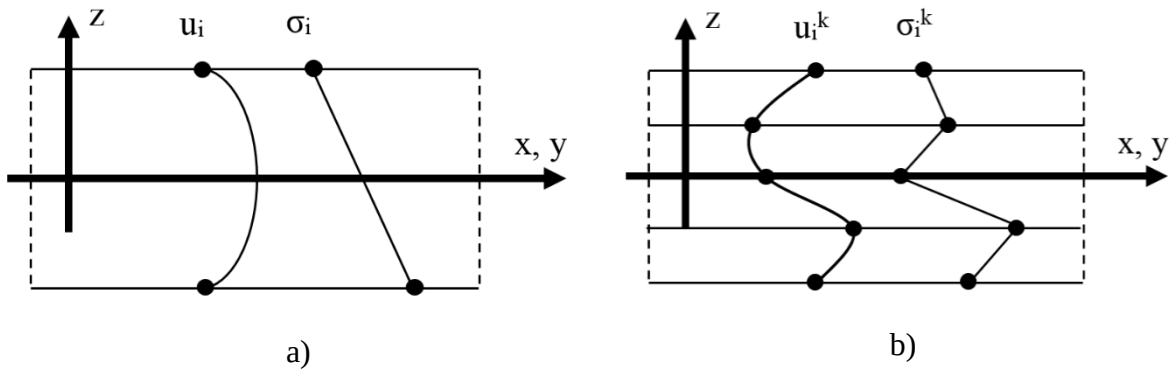

Figure 12. Displacement and stress fields in a) monocoque plates and b) multilayred plates

Refined laminated plate theories can be derived by using shear deformation theories or inserting extra DOFs at each ply interface to better simulate the inter-laminar continuity (IC) requirements and Zig-Zag (ZZ) effects of laminated structures. The physical behavior of the displacement and stress fields in laminated plates is exemplified in Figure 12.

Inter-laminar continuity refers to the physical integrity requirement that regardless of each ply's material property, the transverse normal and shear stresses must be represented by continuous functions throughout the thickness coordinate. Continuity is verified for the bottom ("b") face of an upper ply and the top ("t") face for a lower ply. Figure 13 illustrates this indexing.

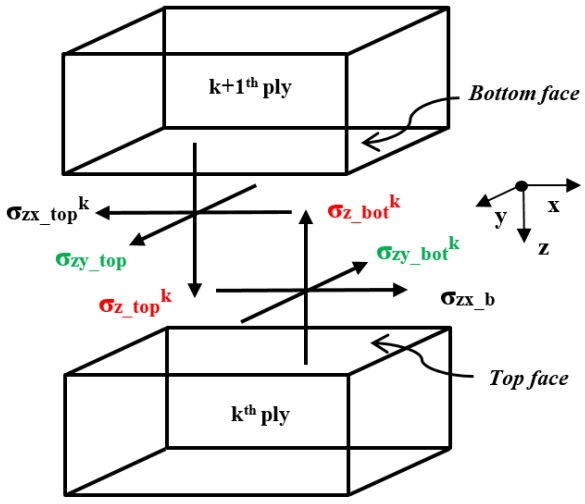

Figure 13. Top and bottom faces of consecutive plies

Deeper insights into the Theory of Elasticity show that the normal stress must remain a continuous function for any order of the in-plane derivatives. These and other assertions can be checked by writing the differential equilibrium equation for the top face a generic ply "k".

Based on the inter-laminar continuity IC of the normal stress "σ_{zz}", it is possible to write:

$$\sigma^k_{zz,z}|^t = -\left(\sigma^k_{zx,x} + \sigma^k_{zy,y}\right)|^t \tag{3.32}$$

Equation (3.32) is always true, disregarding the properties that the two consecutive plies possess. This asserts that IC of the normal transverse stress should always be present. On the other side, for the transverse shear stress "σ_{zx}", it is possible to write:

$$\begin{aligned}\sigma^k_{zx,z}|^t = -\{&C^k_{11}u^k_{,xx} + C^k_{12}v^k_{,xy} + C^k_{16}\left(u^k_{,xy} + v^k_{,xx}\right) + C^k_{13}\sigma^k_{zz,x} + C^k_{16}u^k_{,xy} + C^k_{26}v^k_{,yy} \\ &+ C^k_{66}\left(u^k_{,yy} + v^k_{,xy}\right) + C^k_{36}\sigma^k_{zz,y}\}|^t\end{aligned} \tag{3.33}$$

Now, the dependence on the material properties is observed. Therefore, the derivatives in the thickness directions are discontinuous, unless the plies are equal. A similar conclusion can be achieved for the transverse shear stress "σ_{zy}":

In the sequence, the ZZ effects are studied by using the equivalence of the transverse shear stresses:

$$\begin{aligned}&\sigma^k_{zx}|^t = \sigma^{(k+1)}_{zx}|_b \\ &\left(\bar{C}^{k+1}_{45}\bar{C}^{k+1}_{45} - \bar{C}^{k+1}_{55}\bar{C}^{k+1}_{44} - \bar{C}^{k+1}_{55}\bar{C}^{k}_{44} - \bar{C}^{k+1}_{45}\bar{C}^{k}_{45}\right)w^k_{,y}|^t \\ &\quad + \left(\bar{C}^{k+1}_{45}\bar{C}^{k+1}_{45} - \bar{C}^{k+1}_{55}\bar{C}^{k+1}_{44}\right)v^{(k+1)}_{,z}|_b + \left(\bar{C}^{k+1}_{55}\bar{C}^{k}_{44} - \bar{C}^{k+1}_{45}\bar{C}^{k}_{45}\right)v^k_{,z}|^t \\ &\quad + \left(\bar{C}^{k+1}_{55}\bar{C}^{k}_{45} - \bar{C}^{k+1}_{45}\bar{C}^{k}_{55}\right)\left[w^k_{,x} + u^k_{,z}\right]|^t = 0\end{aligned} \tag{3.34}$$

Continuity of the derivative of "v" in the thickness direction is possible, only if the consecutive plies are equal. The same can be found for the "u" variable.

Lastly, the transverse displacement "w" is investigated. The equilibrium of the transverse normal stress renders:

$$\begin{aligned}&\sigma^k_{zz}|^t = \sigma^{(k+1)}_{zz}|_b \\ &[\bar{C}^k_{13} - \bar{C}^{k+1}_{13}]u^k_{,x}|^t + [\bar{C}^k_{23} - \bar{C}^{k+1}_{23}]v^k_{,y}|^t + \bar{C}^k_{33}w^k_{,z}|^t - \bar{C}^{k+1}_{33}w^{(k+1)}_{,z}|_b \\ &\quad + [\bar{C}^k_{36} - \bar{C}^{k+1}_{36}]\left(u^k_{,y} + v^k_{,x}\right)|^t = 0\end{aligned} \tag{3.35}$$

Clearly, "w" does not have a continuous first derivative in thickness coordinate function, unless the consecutive plies are equal.

In summary, continuity in the thickness direction for two consecutive plies of different material properties yields:

- u, v and w are continuous functions, but $u_{,z}$, $v_{,z}$ and $w_{,z}$ are discontinuous
- σ_{xz} and σ_{yz} are continuous functions, but $\sigma_{xz,z}$ and $\sigma_{yz,z}$ are discontinuous
- σ_{zz} and all its derivatives in the thickness direction are continuous.

Not all laminated plate theories fulfill the above IC and ZZ effects. This occurs, because most of the formulations assume the same displacement field for all plies. This approach is named Equivalent Single Layer Theory (ESL). The mechanical contributions of every ply are summed up to provide an equivalent constitutive relation for the laminate. For example, the CLT fits in this type of laminated plate theories. In order to fulfill all the continuity requirements, an approach with distinct displacement fields for each ply is required. These theories are known as Layer-Wise Theories (LW). However, the number of DOFs of these formulations proportionally increases in function of the number of plies.

Finally, there is a third way to model a laminated plate and it is often quoted as a Zig-Zag theory. For these theories, an ESL approach is developed based on the IC and ZZ concepts. By doing this, the number of variables, although larger than the original ESL theory, is still less than the respective LW theory. In addition, the DOFs are made independent of the number of plies in the laminate.

3.3.1 Equivalent Single Layer (ESL) and Layer Wise (LW) Theories

Both classical thick and thin formulations for a plate as well as the CLT assume only one physical layer of thickness "H" to which the governing equations are derived. The lamination is incorporated in the classical plate formulations through constitutive relations and via integration in the thickness direction. This approach was already mentioned as Equivalent Single Layer (ESL) theory. The same displacement, strain and stress fields are assumed for the whole laminate.

In the Layer Wise (also known as discrete) class of theories, each of the variables (u, σ or ε) is handled locally. This means that, independently of the derivation method, N-layers laminate will have N-sets of variables. IC and ZZ compatibility requirements are used for linking two consecutive sets of variables. On the other hand, as an example, the set of equations for the "u" variable through the axiomatic approach becomes:

$$u_i^k(x,y,z) = u_i^{k0}(x,y) + \left\{ \sum_{j=1}^{N_u} \left[u_j(x,y) z^j \right]^k \right\}_i ; i = 1 \dots 3; k = 1 \dots N_l \tag{3.36}$$

$$u_i^k|^t = u_i^{(k+1)}|_b$$

Figure 14 depicts how a displacement field, for instance, is interpreted when seen through the ESL and LW perspectives.

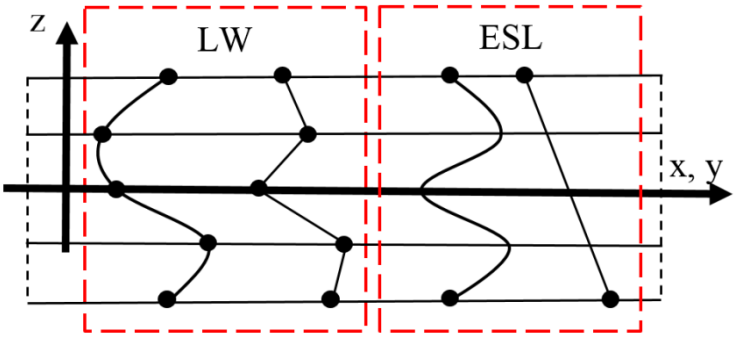

Figure 14. Linear and quadratic displacement field for ESL and LW descriptions

Next, trade-off questions naturally arise. Effectiveness of each approach is subordinated to the loading applied, geometrical ratios and material properties. Lamination parameters such as ratio of reinforcement/matrix Young's modulus, lamination angle and stacking sequence are of importance as well. The LW approach will always be better. However, the ESL one can be accurately used too, if the plate is thin, because both theories converge as the thickness of the plate tends to zero. Much of the discussion takes place when the stresses must be calculated for laminated plates of composite materials. High accuracy of stresses is advised when applying failure criteria, because there are several failure modes. Each type is more or less sensitive to a particular stress measure. Delamination is usually the trickiest criterion, since it is very sensitive to the transverse deformations, normally neglected in classical plate theories.

In attempt to avoid LW formulations, refined ESL formulations have been developed by different authors throughout the years. Since the references are numerous, the next section is devoted to this topic.

3.3.2 Refined Equivalent Single Layer (RESL)

A not so expansive class of plate formulations, yet more accurate than the ESL, is the Refined Equivalent Single Layer (RESL) class. Most of the representatives of this class are quoted in the literature as Zig-Zag (ZZ) theories. However, due to a practically insurmountable and confusing variety of ZZ theories, these are herein generally referred as RESL. When necessary, the ZZ tag is used to maintain the link with the original references.

The "hot" point of this class of theories is to somehow exploit the IC and ZZ effects to reduce a layer-wise/discrete problem to a one-layer problem with a constant number of unknown field variables and their coefficients. Consequently, confusion may emerge regarding the variables and DOFs being solved. For instance, instead of reducing the number of layers down to one, there are theories where the number of layers is actually increased for different reasons. This is quoted as (virtual) sub-lamination. The resulting theory is then one of the LW type, but with the number of DOFs depending on the number of sub-laminates and not the number of actual plies.

Based on the studied articles, ESL theories are always written in an axiomatic fashion. In most of the references, the refinements are made to the expressions of the displacement variables, and then stresses are obtained either by constitutive relations or by through-the-thickness integration. Nonetheless there are other approaches where the IC for stresses is assumed and the displacement variables are obtained by the same through-the-thickness integration of equilibrium equations.

Therefore, the derivation of ESL theories begins with one or both generic expressions:

$$\sigma_i^k(x,y,z) = \left\{ \sum_{j=1}^{N_{\sigma G}} [\sigma_G(x,y)\varrho_G(z)]_j + \sum_{j=1}^{N_{\sigma L}} \left[\sigma_L^k(x,y)\varrho_L^k(z)\right]_j \right\}_i ; i = 4,5 \tag{3.37}$$

$$u_i^k(x,y,z) = \left\{ \sum_{j=1}^{N_{uG}} [u_G(x,y)\chi_G(z)]_j + \sum_{j=1}^{N_{uL}} \left[u_L^k(x,y)\chi_L^k(z)\right]_j \right\}_i ; i = 1 \dots 3$$

The subscript "G" refers to global functions and coefficients valid throughout the thickness of the laminate. To fulfill the IC and ZZ requirements, local terms, indicated by the subscript "L", are added to complement or replace the global functions. After postulating the equations, the IC and ZZ conditions are used to find the relations between the local and global parameters of the global and/or local functions.

Simplified reproductions of displacement fields of RESL/ZZ theories are given next. These formulations were derived for beams and/or plates. However, for application of any of the following theories, the author recommends the use of the respective original reference.

(LEKHNITSKII, 1968) (3.38)

$$u^k = u_0^k + u_1^k x + u_2^k y + u_3^k xy + u_4^k x^2 + u_5^k z^2 + u_6^k z x^2 + u_7^k z^3$$
$$w^k = w_0^k + w_1^k x + w_2^k z + w_3^k xz + w_4^k x^2 + w_5^k z^2 + w_6^k x z^2 + w_7^k x^3$$

(WHITNEY, 1969) (3.39)

$$u^k = u_0(x,y)z + u_1(x,y)\chi_{u1}(z) + u_1^k(x,y)\chi_{u1}^k(z) + u_2^k(x,y)\chi_{u2}^k(z)$$
$$v^k = v_0(x,y)z + v_1(x,y)\chi_{v1}(z) + v_1^k(x,y)\chi_{u1}^k(z) + v_2^k(x,y)\chi_{u2}^k(z)$$
$$w^k = w_0(x,y)$$

(MURAKAMI, 1986) (3.40)

$$u^k = u_0(x,y) + u_1(x,y)z + [-1]^k u_1^k(x,y) z_L$$
$$v^k = v_0(x,y) + v_1(x,y)z + [-1]^k v_1^k(x,y) z_L$$
$$w^k = w_0(x,y)$$

(LI; LIU, 1997) (3.41)

$$u^k = u_0(x,y) + u_1(x,y)z + u_2(x,y)z^2 + u_3(x,y)z^3 + u_1^k(x,y)z_L + u_2^k(x,y)z_L^2 + u_3^k(x,y)z_L^3$$
$$v^k = v_0(x,y) + v(x,y)z + v_2(x,y)z^2 + v_3(x,y)z^3 + v_1^k(x,y)z_L + v_2^k(x,y)z_L^2 + v_3^k(x,y)z_L^3$$
$$w^k = w_0(x,y)$$

(ICARDI, 2001) (3.42)

$$u^k = u_0(x) + u_1(x)z + u_2(x)z^2 + u_3(x)z^3 + \bar{u}^k(x)\bar{\chi}^k(z)$$
$$w^k = w_0(x) + w_1^k(x)z + w_2^k(x)z^2 + w_3^k(x)z^3 + w_4^k(x)z^4 + \bar{u}_1^k(x)\bar{\chi}_1^k(z) + \bar{u}_2^k(x)\bar{\chi}_2^k(z)$$

(TESSLER; DI SCIUVA; GHERLONE, 2009) (3.43)

$$u^k = u_0(x) + u_1(x)z + \bar{u}^k(x)\bar{\chi}^k(z)$$
$$w^k = w_0(x)$$

Refined ESL theories are usually clumsy due to the lengthy derivation procedure. The results on the other hand are quickly and more accurately when compared to the pure ESL ones.

However, in order to answer which of the quoted theories would perform best, the formulation should be check for the least number of DOFs and algebraic operations to reach the desired accuracy of the variable under focus. Some ZZ theories model the stresses directly while other apply ZZ effects to each ply than solve the problem and still required post-processing steps to get the desired results.

Due to its increased accuracy, the RESL and LW plate theories are also much discussed for sandwich structure applications. Mainly because the sandwich is usually a moderately thick/thin to thick plate and the thickness of the core component is much greater than the skins'. Also, the core is usually lighter and softer. Due to these considerations, sandwich structures are reviewed in the next section.

3.3.3 Sandwich Structures

Sandwich structures are laminated plates with specific design criteria. They are designed either to: decrease weight, provide thermal and/or acoustic insulation, damp dynamic loadings or increase the transverse shear and normal strain for impact absorption purposes. A typical sandwich structure and its components are shown in Figure 15.

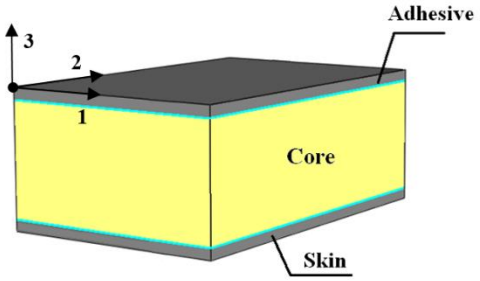

Figure 15. Components of sandwich structures

These particular improvements in a laminated structure are usually due to the core, which is normally made of a cellular material. This component can be an orthotropic metallic honeycomb, an isotropic viscous layer, a polymeric foam or metallic foam (GIBSON; ASHBY, 1988, MENDONÇA, 2005).

In addition to the core, there are also the skins and the adhesive layers. The skins are plate structures, which can be isotropic layers (aluminum skins, for instance) or anisotropic laminated composites. They are responsible for withstanding the bending and in-plane normal loadings. The adhesive layers are thin isotropic components whose thermo-mechanical influence on the structure is sometimes overlooked. However, for a particular loading case and depending on the associated geometrical and material characteristics of the core and the skins, the adhesive interfaces can strongly contribute to the overall behavior of the sandwich structure.

For commonly applied sandwich structures, the geometrical and material characteristics are:

$$\begin{aligned} &\textit{Thickness} && H_{core} >> h_{skins} \\ &\textit{Normal Elastic Modulus (in direction 3)} && E_{core} << E_{skins} \\ &\textit{Shear Elastic Modulus} && G_{core} << G_{skins} \\ &\textit{Density} && \rho_{core} << \rho_{skins} \\ &\textit{Loss Factor} && \eta_{core} >> \eta_{skins} \\ &\textit{Wave Speed} && c_{core} << c_{skin} \\ &\textit{Thermal Conductivity} && k_{core} << k_{skins} \end{aligned} \tag{3.44}$$

On this ground, a straightforward conclusion about which laminated plate theory best models the actual behavior of a particular sandwich composite material is the use of LW theories. However, if speed and storage requirements must be optimized, a mix of LW and RESL theories (usually non-linear) can be used. These approaches were tagged in the literature

as High order SAndwich Plate Theory (HSAPT) (FROSTIG, 1997, ELMALICH; RABINOVITCH, 2012).

In the present PhD Thesis, the numerical simulation of such structures is the motivation of this work. Due to the characteristics of this highly heterogeneous laminated plate configuration, it is not so rare to run into numerical issues and errors when even the simplest static analysis is simulated. Hence, it is a requirement to fully understand the characteristics of sandwich structures and laminated plate theories to later distinguish errors, which stem from numerical solution algorithms and those from simplification assumptions of implemented theories.

However, to really understand what each formulation is capable of providing the actual structure behavior, one can turn to the study Unified Plate Formulations. These formulations are capable of grouping most of the plate theories known. Not only insights of the simplifications that each theory carries out, but also this is a valuable tool to better answer the question of which formulation is the best for a particular case. In the present work, two unified approaches are reviewed.

3.3.4 Unified Formulations (UF)

Carrera's Unified Formulation (CUF) (CARRERA, 2002, CARRERA; DEMASI, 2002a, 200b, CARRERA, 2003b) is able to group axiomatic multi-layered C-0 plate formulations in a compact form. This compact form is known as *fundamental nuclei* or *kernel* matrix of the formulation. The theory is referenced according to the maximum order of expansion of the thickness coordinate, the integration in the thickness direction, the derivation procedure and whether the formulation accounts a Zig-Zag or Inter-laminar Continuity requirements.

To introduce the acronyms used in CUF, during the generalization of each theory type, the corresponding acronym letter is introduced. Since this is an axiomatic unification, the number of terms for a selected theory is related to the highest order of the thickness coordinate in the respective formulation (*acronym "N", which is a number correspondent to the highest order of the polynomial expansion of the thickness coordinate*).

It must be said that the kernel of CUF does not only yield a plate formulation but the respective governing equations of motion. Carrera chose the Principle of Virtual Displacements (PVD) to derive the kernel for the case of displacement variables only. For the theories developed in this way the acronym *"D"* is used to indicate the PVD method. The axiomatic displacement fields are compacted as:

$$\boldsymbol{u}(x,y,z) = F_0(z)\boldsymbol{u}_0(x,y) + F_1(z)\boldsymbol{u}_1(x,y) + \cdots + F_N(z)\boldsymbol{u}_N(x,y) = F_\tau \boldsymbol{u}_\tau \qquad (3.45)$$
$$F_0(z) = 1;\ \ F_1(z) = z;\ \ F_N(z) = z^N$$
$$\tau = 0 \ldots N_\tau$$

Next, the nature of the integration process across the thickness is approached. If the generic kinematics in (3.45) is valid for the whole stack of plies, then the formulation is of the ESL type (*acronym "E", for Equivalent*). To provide the Layer-Wise (*acronym "L", for Layer-Wise*) version of (3.45), the compatibility requirement of the displacement fields (3.46) demands that, at least, two linear transversal functions "$F_b(z)$" and "$F_t(z)$" exist.

$$\boldsymbol{u}_b^k = \boldsymbol{u}_t^{k-1} \qquad (3.46)$$

Hence, the displacement fields are compacted as:

$$\boldsymbol{u}^k(x,y,z) = F_b^k \boldsymbol{u}_b^k + F_\tau^k \boldsymbol{u}_\tau^k + F_t^k \boldsymbol{u}_t^k \qquad (3.47)$$
$$k = 1 \ldots N_l\ ;\ \tau = 2 \ldots N_\tau$$

In equation (3.47), the transversal functions are necessarily normalized for each ply, because of the LW compatibility requirements. In order to achieve a LW unified formulation, the transversal functions "F" must be generated automatically. This is accomplished by writing the functions "F" in terms of Legendre polynomials "L" (ARFKEN; WEBER 2005). These functions have a recurrence relation from which all transversal functions can be generated based on two base functions "L_0" and "L_1". Legendre polynomials are then given in terms of the local thickness variable "ζ^k":

$$F_b^k = \frac{L_0^k - L_1^k}{2};\ F_t^k = \frac{L_0^k + L_1^k}{2};\ F_\tau^k = L_r^k - L_{r-2}^k;\ L_0^k = 1;\ L_1^k = \zeta^k \tag{3.48}$$
$$L_{r+1}^k(\zeta^k) = \frac{(2r+1)\zeta^k L_r - rL_{r-1}}{r+1}$$
$$\zeta^k = \frac{2z - (z_t^k + z_b^k)}{h^k};\ -1 \le \zeta^k \le 1$$

With equation (3.48), the LW unification is complete.

For the case of the RESL or ZZ theories, the expression (3.45) is refined with Murakami's Zig-Zag Function (MZZF) (*acronym "Z", for Zig-Zag*). This refinement is attractive because it improves the ESL theories with the straightforward addition of a term. Such function is also written in terms of the local transverse coordinate "ζ^k", hence:

$$\boldsymbol{u}(x,y,z) = \boldsymbol{F}_\tau^k \boldsymbol{u}_\tau^k + \boldsymbol{F}_z^k \boldsymbol{u}_z^k;\ \tau = 0 \dots N_\tau \tag{3.49}$$
$$\boldsymbol{F}_z^k(\zeta^k) = (-1)^k \zeta^k$$

The assumptions from equation (3.45) to (3.49) can be applied to non-classical mixed formulations (*acronym "M", for Mixed formulations*). For instance, if stresses are also approximated in the axiomatic fashion along with the displacements, the kernel matrix is enlarged and the solution becomes more complicated. Since the transverse stresses depend on the local constitutive equations and, physically, the stresses are continuous functions across the thickness of the laminate, a LW description is always needed along with Legendre polynomials for the unification process of stresses variable in mixed theories.

For the ESL, RESL and LW approaches with the mixed formulation, only the compact form of the stress variables is shown in equation (3.50) since the condensation of the displacement fields is the same as that of the PVD.

$$\boldsymbol{\sigma}_n^k(x,y,z) = F_b^k \boldsymbol{\sigma}_{nb}^k + F_\tau^k \boldsymbol{\sigma}_{n\tau}^k + F_t^k \boldsymbol{\sigma}_{nt}^k \tag{3.50}$$
$$k = 1 \dots N_l\ ;\ \tau = 2 \dots N_\tau$$

Although equation (3.50) is a LW formulation, its solution at the top and bottom surfaces of the laminate are open. These values can be left free (*acronym "ni", for Free homogenous conditions at the Top and Bottom surface of the laminate*). Also, if the interlaminar continuity requirements is enforced, the acronym "*C*" is used. They are:

$$\boldsymbol{\sigma}_{nb}^{k} = \boldsymbol{\sigma}_{nt}^{k-1} \tag{3.51}$$
$$\boldsymbol{\sigma}_{nb}^{1} = \boldsymbol{\sigma}_{0}^{1};\ \ \boldsymbol{\sigma}_{nt}^{N_l} = \boldsymbol{\sigma}_{0}^{N_l}$$

Lastly, for the theories disregarding the influence of the transversal normal stress, the acronym "*d*" can be used. The full LW equations of mixed theories are:

$$\boldsymbol{\sigma}_{n}^{k}(x,y,z) = F_b^k \boldsymbol{\sigma}_{nb}^{k} + F_\tau^k \boldsymbol{\sigma}_{n\tau}^{k} + F_t^k \boldsymbol{\sigma}_{nt}^{k} \tag{3.52}$$
$$\boldsymbol{u}^{k}(x,y,z) = F_b^k \boldsymbol{u}_b^{k} + F_\tau^k \boldsymbol{u}_\tau^{k} + F_t^k \boldsymbol{u}_t^{k}$$
$$k = 1 \ldots N_l\ ;\ \tau = 2 \ldots N_\tau$$

In summary, the main acronyms used to tag a theory developed from CUF are grouped in Figure 16.

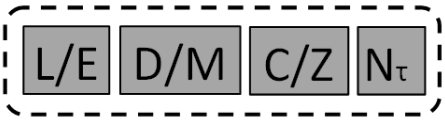

Figure 16. CUF acronyms

For both ESL and LW theories all kernels are firstly written for each layer "k". Then, to define whether the formulation will be of the ESL or LW type, the assemblage procedure (or integration through the thickness) must be specified. Figure 17 shows the concept for both theories. Using ESL theories, the contributions of each ply are summed up to give the overall structure constitutive behavior. On the other hand, the LW approach makes use of compatibility conditions at the top and bottom surfaces of each ply.

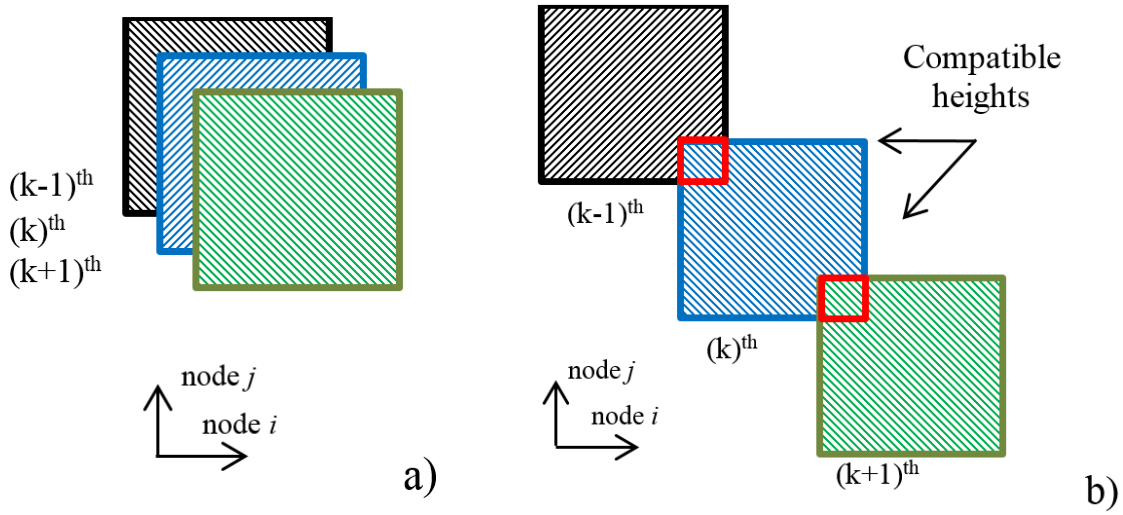

Figure 17. ESL (a) and LW (b) thickness assemblages of the stress, strain and/or displacement variables into the global matrix Kij

The ESL assemblage is straightfoward. The size of the kernel matrix is obtained from:

$$\begin{Bmatrix} P_x \\ P_y \\ P_z \end{Bmatrix}^T = \sum_{k=1}^{k=N_l} \begin{bmatrix} K_{uu}^{k\tau s} & K_{uv}^{k\tau s} & K_{uw}^{k\tau s} \\ & K_{vv}^{k\tau s} & K_{vw}^{k\tau s} \\ sym & & K_{ww}^{k\tau s} \end{bmatrix} \begin{Bmatrix} u \\ v \\ w \end{Bmatrix} = [\boldsymbol{K}] \begin{Bmatrix} u \\ v \\ w \end{Bmatrix} \tag{3.53}$$

$$K_{uu}^{\tau s} = \sum_{k=1}^{k=N_l} K_{uu}^{k\tau s}$$

$$size_{ESL}^{PVD}(K) = 3N_\tau \times 3N_\tau;$$

For the LW case, compatibility makes the formulation more intricate:

$$\begin{Bmatrix} P_x^{tk_1} \\ \vdots \\ P_x^{tk_1} = P_x^{tk_2} \\ \vdots \\ P_x^{bk_{(Nl-1)}} = P_x^{tk_{Nl}} \\ \vdots \\ P_x^{bk_{Nl}} \end{Bmatrix}_{m\times 1}^T = [\boldsymbol{K}_{uu}^{\tau s}]_{m\times m} \times \begin{Bmatrix} u^{tk_1} \\ \vdots \\ u^{bk_1} = u^{tk_2} \\ \vdots \\ u^{bk_{(Nl-1)}} = u^{tk_{Nl}} \\ \vdots \\ u^{bk_{Nl}} \end{Bmatrix}_{m\times 1} \tag{3.54a}$$

$$[\boldsymbol{K}_{uu}^{\tau s}]_{m\times m} \tag{3.54b}$$

$$= \begin{bmatrix} \begin{pmatrix} \kappa^{ttk_1} & \cdots & \kappa^{tbk_1} \\ \vdots & \ddots & \vdots \\ \kappa^{btk_1} & \cdots & \kappa^{bbk_1}+\kappa^{ttk_2} \end{pmatrix}_{\tau\times s} & \cdots & 0 \\ \vdots & \ddots & \vdots \\ 0 & \cdots & \begin{pmatrix} \kappa^{bbk_{(Nl-1)}}+\kappa^{ttk_{Nl}} & \cdots & \kappa^{tbk_{Nl}} \\ \vdots & \ddots & \vdots \\ \kappa^{btk_{Nl}} & \cdots & \kappa^{bbk_{Nl}} \end{pmatrix}_{\tau\times s} \end{bmatrix}_{m}$$

$$m = (N_l - 1)(N_\tau - 1) + N_\tau$$

$$size_{LW}^{PVD}(K) = 3m \times 3m;$$

In case of an ESL-RMVT formulation, a special assembly procedure for equation (3.52) is needed. When Reissner's Mixed Variational Theorem (RMVT) is considered, not only the displacement variables are calculated but the transversal stress values are calculated as well. RMVT is better detailed in Chapter 4. The ESL-RMVT formulation demands a LW assemblage of the stress variables. Basically, the pure displacement kernel is assembled as (3.53) and the pure transversal stress kernel as (3.54).

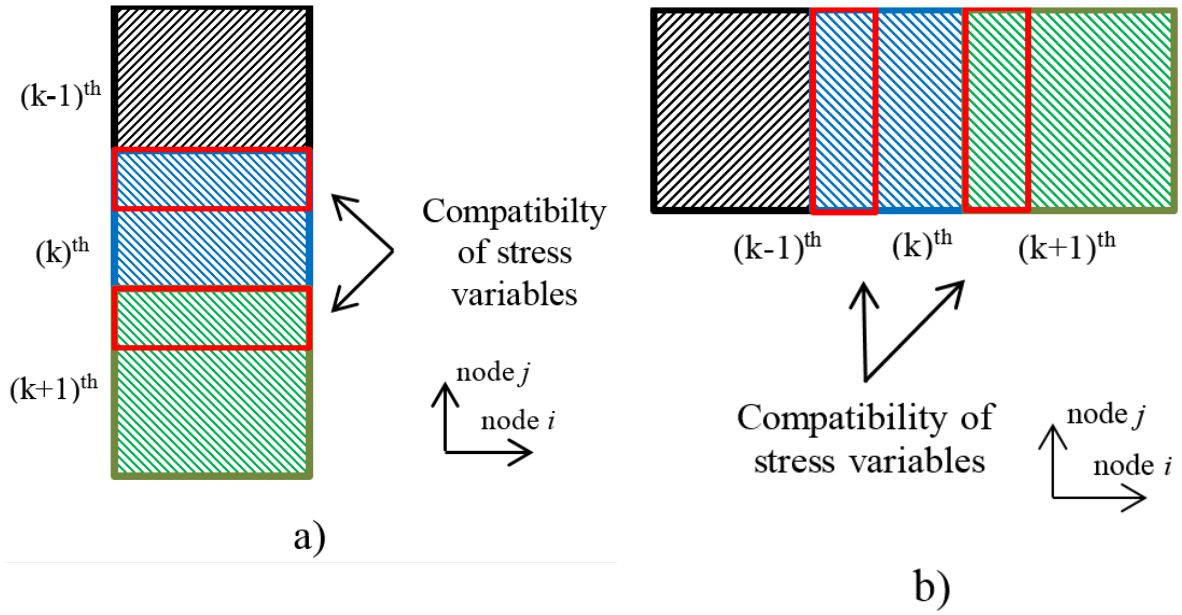

Figure 18. Assemblage of matrices (a) Kσ-u and (b) Ku-σ for ESL with RMVT into the global matrix Kij

For the other two coupling kernels, the top and bottom displacement rows or columns of consecutive plies are summed. Figure 18 depicts this case. Briefly, the sizes of the pure displacement, pure stress and coupling matrices associated to the ESL-RMVT are:

$$[\boldsymbol{K}_{u\sigma}^{\tau s}]_{\tau\times m} \tag{3.55}$$
$$= \left[\begin{pmatrix} \kappa^{ttk_1} & \cdots & \kappa^{tbk_1}+\kappa^{tbk_2} \\ \vdots & \ddots & \vdots \\ \kappa^{btk_1} & \cdots & \kappa^{bbk_1}+\kappa^{bbk_2} \end{pmatrix}_{\tau\times s} \quad \cdots \quad \begin{pmatrix} \kappa^{ttk_{(Nl-1)}}+\kappa^{ttk_{Nl}} & \cdots & \kappa^{tbk_{Nl}} \\ \vdots & \ddots & \vdots \\ \kappa^{btk_{(Nl-1)}}+\kappa^{btk_{Nl}} & \cdots & \kappa^{bbk_{Nl}} \end{pmatrix}_{\tau\times s} \right]_{\tau\times}$$

$$[\boldsymbol{K}_{\sigma u}^{\tau s}]_{m\times s} = \begin{bmatrix} \begin{pmatrix} \kappa^{ttk_1} & \cdots & \kappa^{tbk_1} \\ \vdots & \ddots & \vdots \\ \kappa^{btk_1}+\kappa^{btk_2} & \cdots & \kappa^{bbk_1}+\kappa^{bbk_2} \end{pmatrix}_{\tau\times s} \\ \vdots \\ \begin{pmatrix} \kappa^{ttk_{(Nl-1)}}+\kappa^{ttk_{Nl}} & \cdots & \kappa^{tbk_{(Nl-1)}}+\kappa^{tbk_{Nl}}+ \\ \vdots & \ddots & \vdots \\ \kappa^{btk_{Nl}} & \cdots & \kappa^{bbk_{Nl}} \end{pmatrix}_{\tau\times s} \end{bmatrix}_{m\times s}$$

$$size_{ESL}^{RMVT}(K_{u\sigma}) = 3N_\tau \times 3m;\ size_{ESL}^{RMVT}(K_{\sigma u}) = 3m \times 3N_s$$
$$size_{ESL}^{RMVT}(K_{\sigma\sigma}) = 3m \times 3m;\ size_{ESL}^{RMVT}(K_{uu}) = 3N_\tau \times 3N_\tau$$

Grouping the size and DOFs of all formulation, one gets:

$$size_{ESL}^{PVD}(K) = 3N_\tau \times 3N_\tau \tag{3.56}$$
$$size_{LW}^{PVD}(K) = 3m \times 3m$$
$$size_{ESL}^{RMVT}(K) = 3(N_\tau + m) \times 3(N_\tau + m)$$
$$size_{LW}^{RMVT}(K) = 6m \times 6m$$

Even though CUF groups any plate theory according to the axiomatic assumptions, the expanded expressions always comprise all terms up to the Nth order when derived automatically from the kernel matrices. Moreover, the same expansion is obtained for all vector components of the field variable (or scalar field variable). However, there are theories, such as Mindlin's, where each displacement component may have different maximum expansion orders. Therefore, CUF, despite powerful and fast, does not allow for straightforward extraction of all possible theories devised by this method.

To increase the DOFs of CUF, and thereby achieve a unification, which generates stiffness matrices more similar to those cited in this text, Demasi (DEMASI, 2008, DEMASI, 2009a, 2009b, 2009c, 2009d, 2009e, 2009f, DEMASI, 2012) uncoupled the order of expansion "N_τ" of each field variable and proposed a *Generalized Unified Formulation (GUF)*. Even with this generalization, the expansions comprise all terms, but, at least, each field variable can be approximated independently.

To make each displacement component expression independent, the transverse coefficients "F(z)" must carry an additional tag. Demasi (DEMASI, 2008, DEMASI, 2009a) proposed an indexing scheme for these coefficients, and it is explained in Figure 19.

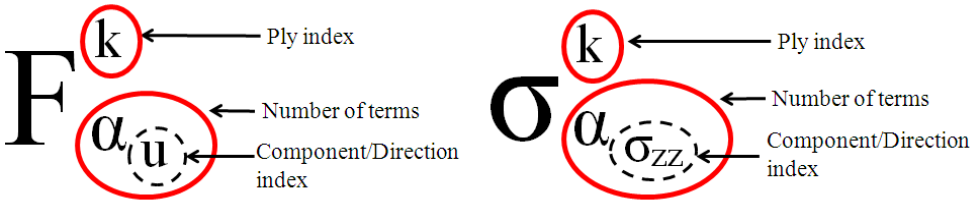

Figure 19. Indexing of the transverse function in GUF

It is easy to see that the only difference from CUF is the fact that now three expansion criteria (α_u, α_v and α_w) or six ($\alpha_{\sigma zx}$, $\alpha_{\sigma zy}$ and $\alpha_{\sigma zz}$) have to be chosen, such that:

$$\begin{aligned} u^k &= F^k_{\alpha_u} u^k_{\alpha_u}; \alpha_u = t, b, z \dots N_{\alpha_u} \qquad & \sigma^k_{zx} &= \mathcal{F}^k_{\alpha_{\sigma_{zx}}} \sigma^k_{\alpha_{\sigma_{zx}}}; \alpha_{\sigma_{zx}} = t, b \dots N_{\alpha_{\sigma_{zx}}} \\ v^k &= F^k_{\alpha_v} v^k_{\alpha_v}; \alpha_v = t, b, z \dots N_{\alpha_v} & \sigma^k_{zy} &= \mathcal{F}^k_{\alpha_{\sigma_{zy}}} \sigma^k_{\alpha_{\sigma_{zy}}}; \alpha_{\sigma_{zy}} = t, b \dots N_{\alpha_{\sigma_{zy}}} \\ w^k &= F^k_{\alpha_w} w^k_{\alpha_w}; \alpha_w = t, b, z \dots N_{\alpha_w} & \sigma^k_{zz} &= \mathcal{F}^k_{\alpha_{\sigma_{zz}}} \sigma^k_{\alpha_{\sigma_{zz}}}; \alpha_{\sigma_{zz}} = t, b \dots N_{\alpha_{\sigma_{zz}}} \\ t &= top; b = bottom; z = zigzag \end{aligned} \tag{3.57}$$

The GUF kernel for the PVD is:

$$K^{k\tau s} = \begin{bmatrix} K^{k\tau s}_{u_{\alpha_u} u_{\alpha_u}} & K^{k\tau s}_{u_{\alpha_u} v_{\alpha_v}} & K^{k\tau s}_{u_{\alpha_u} w_{\alpha_w}} \\ & K^{k\tau s}_{v_{\alpha_v} v_{\alpha_v}} & K^{k\tau s}_{v_{\alpha_v} w_{\alpha_w}} \\ sym & & K^{k\tau s}_{w_{\alpha_w} w_{\alpha_w}} \end{bmatrix} \tag{3.58}$$

For the RMVT case, the system of equations and the GUF's kernel is explicitly given by:

$$\begin{Bmatrix} P_x \\ P_y \\ P_z \\ \sigma_{zx} \\ \sigma_{zy} \\ \sigma_{zz} \end{Bmatrix} = [\boldsymbol{K}^{k\tau s}] \times \begin{Bmatrix} u \\ v \\ w \\ 0 \\ 0 \\ 0 \end{Bmatrix} \tag{3.59a}$$

$$\left[\boldsymbol{K}^{k\tau s}\right] = \begin{bmatrix} K^{k\tau s}_{u_{\alpha_u}u_{\alpha_u}} & K^{k\tau s}_{u_{\alpha_u}v_{\alpha_v}} & 0 & K^{k\tau s}_{u_{\alpha_u}\sigma_{\alpha_{\sigma_{zx}}}} & 0 & K^{k\tau s}_{u_{\alpha_u}\sigma_{\alpha_{\sigma_{zz}}}} \\ & K^{k\tau s}_{v_{\alpha_v}v_{\alpha_v}} & 0 & 0 & K^{k\tau s}_{v_{\alpha_v}\sigma_{\alpha_{\sigma_{zy}}}} & K^{k\tau s}_{v_{\alpha_v}\sigma_{\alpha_{\sigma_{zz}}}} \\ & & 0 & K^{k\tau s}_{w_{\alpha_w}\sigma_{\alpha_{\sigma_{zx}}}} & K^{k\tau s}_{w_{\alpha_w}\sigma_{\alpha_{\sigma_{zy}}}} & K^{k\tau s}_{w_{\alpha_w}\sigma_{\alpha_{\sigma_{zz}}}} \\ & & & K^{k\tau s}_{\sigma_{\alpha_{\sigma_{zx}}}\sigma_{\alpha_{\sigma_{zx}}}} & 0 & 0 \\ & sym & & & K^{k\tau s}_{\sigma_{\alpha_{\sigma_{zy}}}\sigma_{\alpha_{\sigma_{zy}}}} & 0 \\ & & & & & K^{k\tau s}_{\sigma_{\alpha_{\sigma_{zz}}}\sigma_{\alpha_{\sigma_{zz}}}} \end{bmatrix} \tag{3.59b}$$

For all three ESL, ESL-RMVT and LW assemblages, the size of the elementary matrix must be re-calculated as:

$$\begin{aligned} size^{PVD}_{ESL}\left(K^{(e)}\right) &= \tilde{n} \times \tilde{n} \\ size^{PVD}_{LW}\left(K^{(e)}\right) &= \tilde{m} \times \tilde{m} \\ size^{RMVT}_{ESL}\left(K^{(e)}\right) &= (\tilde{n} + \tilde{m}) \times (\tilde{n} + \tilde{m}) \\ size^{RMVT}_{LW}\left(K^{(e)}\right) &= 2\tilde{m} \times 2\tilde{m} \end{aligned} \tag{3.60a}$$

$$\begin{aligned} \tilde{n} &= N_{\alpha_u} + N_{\alpha_v} + N_{\alpha_w} \\ \tilde{m} &= m_{\alpha_u} + m_{\alpha_v} + m_{\alpha_w} \\ m_{\alpha_u} &= (N_l - 1)\left(N_{\alpha_u} - 1\right) + N_{\alpha_u} \\ m_{\alpha_u} &= (N_l - 1)\left(N_{\alpha_v} - 1\right) + N_{\alpha_v} \\ m_{\alpha_w} &= (N_l - 1)\left(N_{\alpha_w} - 1\right) + N_{\alpha_w} \end{aligned} \tag{3.60b}$$

The acronyms used in CUF can be generalized for the GUF. Figure 20 assembles the acronyms from CUF and GUF.

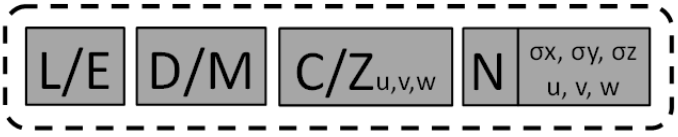

Figure 20. GUF acronyms

The first block refers to the LW or ESL integration across the thickness direction. Second block is the derivation of the governing equations. The subscript "c", if it is shown, indicates that the stress variables were eliminated with static condensation. Third block

accounts for IC and ZZ effects. The subscripts in acronym “Z” indicate which displacement fields are refined with MZZF. The forth block shows the orders of expansion in the thickness coordinate for each transversal stress or displacement variable.

This section on Unified Formulations ended the discussion on plate theories. Nevertheless, the present author is aware that the choice of plate formulation alone does not guarantee accurate solutions. Actually, it is a good plate formulation with an accurate solution method, which guarantees the accuracy of the approach. In this section several plate theories were discussed. In this scope, the unified formulations were judged as a good tool to investigate the precision of specific plate theories. Therefore, both CUF and GUF will be further discussed in order to explicitly write the kernel matrix for a particular solution method.

Before discussing solution methods and their influence on the plate solutions, the references used in this Chapter 3 will be shown and commented in the next section 3.4.

3.4 Review on Plate Theories and Solution Methods

Now that most of the acronyms have been introduced and the most common variables of the plate problem were described, a chronological review on plate theories is given in this manuscript, including comments on the respective solution methods. Once these formulations are normally devised for particular geometries, the effectiveness of the proposal is sometimes linked to the solution method due to the assumptions of the derived theory. Commonly, there are cases where the use of an analytical solution method is not possible. After this review, the next chapter will address the topic of approximate solution methods.

Damping of flexural waves of a beam was achieved by Kerwin (1959) by using a viscoelastic and a constraining layers. Analytical and experimental investigations were presented. The loss factor of this three-layer sandwich beam was retrieved based on geometrical and material influences. In that work, the loss factor is characterized by the imaginary contribution of the bending stiffness of the sandwich beam. All dissipation effects were assumed restricted to the damping layer. The thickness of the constraining layer and the excitation frequency were taken as accounted for in the loss factor expressions. Temperature effects were investigated too.

Srinivas and Rao (1970) worked on an exact solution for bending, vibration and buckling problems of thick orthotropic rectangular plates and laminates. The method for deriving exact solutions is based on double Fourier series, i.e. a sum of infinite trigonometric functions. Such an approach can represent any function, theoretically. Thin plate theory (Kirchhoff's) and Reissner-Mindlin's thick plate theories for small strains were investigated. Results showed a dependence of the laminate orthotropic properties and the assumption of thin or thick laminate. Similarly, Kulkarni and Pagano (1972), proposed an approach to solve the dynamics of composite laminates in cylindrical bending, also by using Mindlin's plate theory. In the displacement formulation, a time dependent exponential term multiplies the single Fourier series. Analytical dispersion results for symmetrical and unsymmetrical laminates were discussed with the aid of non-dimensionalized frequency and phase velocity values. For low anisotropy and symmetrical laminates, the proposed approach showed the best results.

Di Sciuva (1985) developed an equivalent single layer anisotropic plate element based on Ambartsumian's ZZ theory. Even though the author refers to his formulation as discrete, it is not a Layer-Wise theory, because the number of degrees of freedom of the element does not depend on the number of layers. It is a 4-node (with 8 DOFs per node) rectangular element, including bending, extension and transverse shear contributions. Since it treats the shear strains as nodal parameters, it is classified as a mixed approach with eight variables per node (three displacements, three rotations and two shear strains). Hermitian polynomials were used as interpolation functions for the transverse displacement fields and the remaining variables linearly. The idea was to preserve C-1 continuity requirements for the bending problem. A first order shear deformation theory was chosen to estimate the displacement fields. Cylindrical bending of cross-ply and angle-play laminates and bending of a square cross-ply laminate were studied via this element. Good agreement was observed in both low and high span-to-thickness ratios.

An improved plate formulation was derived by Toledano and Murakami (1987) based on the Reissner's mixed variational approach (REISSNER, 1986). The Zig-Zag approach using Legendre polynomials from the previous work of Murakami (MURAKAMI, 1986) was developed. However, higher order displacement functions were chosen, more specifically, they assumed displacements from Lo, Christensen and Wu (LO; CHRISTENSEN; WU, 1977). The resultant laminate formulation fitted in the equivalent single layer type of laminated plate theory. Once again, the cylindrical bending of symmetrical and non-symmetrical cross-ply laminates were investigated. Macroscopic responses of this formulation, such as central deflection, were accurately modeled when compared to a reference exact solution. The results

retained a high level of accuracy even at small span-to-thickness ratios. Comparison of Murakami's first order shear deformation Zig-Zag theory with the non-Zig-Zag high order formulation of Lo, Christensen and Wu indicated that the previous one is more accurate in modeling laminated plates.

Owen and Li (1987a, 1987b) presented a three dimensional first order shear deformation plate element in two companion papers. The solution method exploited a sub-structuring technique, which allows one to increase the actual number of layers in the laminate. However, the main advantage of this sub-structuring was the fact that only one set of layer equations needed to be solved. All the other layer equations could be solved by using the results of this one set of equations, which had been solved. This dramatically reduces the size of the problem. However, an increase in the total processing time is expected. For a better comparison to elasticity solutions, a smoothing technique was used to interpolate the results from the integration points to the boundaries of the element. This is particularly appealing for transverse stresses with selective or reduce integration. Thin and thick laminated composite plates in static, dynamic and stability problems were investigated. Since it is a Layer-Wise type of plate formulation, good accuracy was obtained for displacements and stresses across the thickness of the laminate with the linear approximation. Nonetheless, a comparison using a 27 node element with higher order variation of the in-plane displacement was performed. It did not show considerable improvement of the results in order to justify the increase of parameters.

A higher-order theory satisfying the zero transverse shear stress on the top and bottom layers of laminated plates was presented by Kant and Pandya (1988). A C-0 nine-node iso-parametric quadrilateral element is derived. The laminated theory was an equivalent single layer type. Seven degrees of freedom were determined per node. Three translations and two rotations plus other two special rotations were considered. These special rotation DOFs were used to model two transverse shear strains. Since continuity is not guaranteed when calculating the stress within each layer via constitutive relations, integration of equilibrium equations was chosen as a more accurate technique. It requires extra post-processing of results, but the level of accuracy is much greater. However, the presented results were still not exact according to the references consulted in the article. The model also performed well from the limit of thick plates ($L/h \geq 10$) without shear correction factors.

Pandya and Kant (1988) published more evaluation of results with their formulation. The same nine-node iso-parametric element with seven DOFs per node was used. The evaluations were performed on a symmetrical laminated plate and on a sandwich plate with a soft core. Both higher order theories discussed in the papers were studied. One fulfilled the

requirements of zero transverse shear stress at bottom and top faces of the laminate, but the other did not. From the results data set, one sees that the additional restrain of zero transverse stress worsened the results globally. Such finding was very interesting for helping engineers or scientists to choose a plate formulation to be implemented. Moreover, much better results than those calculated via Classical Laminated Theory were reported. However, the solution still lacks accuracy for the material sets chosen.

All current third-order plate theories were revised by Reddy (1990). Differences and similarities were pointed to identify the actual contributions. After compiling all of these third-order theories, Reddy proposed a general, consistent-strain plate theory from which any of the reviewed theories can be derived. He also accounted for non-linear strains by using von Kármán's assumptions. No validation or comparison was conducted because it might be due to the fact that this class of high-order theory was already investigated in the consulted references.

To determine static and dynamic characteristics of plates and shells, Noor, Burton and Peters (1990) investigated a two-step solution procedure. Based on a predictor first step, an overall gross response of the plate was obtained through a first order shear deformation theory by using the aid of shear correction factors. Then, in a second step, a correction of the predicted values was carried out by two different methods. The first one estimated the shear correction factor to calculate the stresses, while the second method used the dependence of the displacement components on the thickness coordinate. Based on the simulated tests, the two-step procedures were sensitive to the symmetry of the laminate as well as on the shear correction factors. One of the main advantages of the method is the easy and cheap implementation of the predictor phase. Hence, via post-processing (correction), better results can be achieved without the need of complicated element formulations.

At this point, considering the articles so far, several plate theories started to pile. Plate formulations with different approaches and purposes can be found in the literature. Gilewski and Radwanska (1991) conducted a survey of finite elements for moderately thick shells. They classified the shell formulations as 3D degenerated shell elements or 2D shell elements based on assumed functions. They also separated their reference according to: stability, dynamics, laminated and sandwich shells, geometrically non-linear problems, physically non-linear problems, heat transfer problems and other review papers. Regarding the performance of the proposed formulations, it was highlighted the fact that newer formulations tend to be more computationally expansive but are more accurate. Mixed or hybrid are examples of these earlier approaches.

Touratier (1991) proposed a new type of expansion of the thickness coordinate to derive a plate formulation. Instead of adding one more non-linear term to the expansion of the thickness coordinate in the in-plane displacement assumed functions (TOURATIER, 1988), a sine functions was chosen. This is endorsed with the fact that the derivative of the sine function is the cosine function, which is an even function, and therefore is capable of representing the zero shear stress at the bottom and top surfaces of the laminate. Also, no shear corrections factors were needed. The transverse displacement was taken as constant and equal to the membrane value. Benchmark cases were analytically solved with this formulation by using Navier type solutions. Comparisons to other references and 3D elasticity solutions showed an equivalence of the proposed theory with the other high order theories. The author also verified the dependence of the formulation in terms of the material anisotropy.

In the following year, Touratier (1992) presented and tested a sinusoidal function of the thickness coordinate, in the scope of shallow shell structures (the thickness of the shell is much smaller than the shell's radius h<<R). Good agreement was achieved and a C-1 finite element type indicated as a possible solution for the differential equations. The geometrical concept of shells was evaluated for R/L ratios from 5 up to 100, and finally for plate formulation. One clearly observed that a shell theory was required for heavily curved surfaces. If a plate theory is used, then a convergence studied is required, and more plate elements are expected to achieve the same accuracy with shells elements. However, depending on the theory and material anisotropy, the discrepancy in the number of elements might not be so high.

A discrete layer two node laminated beam element was formulated by Averill (1994). By discrete, Averill means that he applied a Zig-Zag type of formulation. It is still classified within the equivalent single layer (ESL) type of approach, but, some researches usually refer the proposed formulation as a refined theory. Linear interpolation was used for the in-plane displacement DOFs and a special quadratic interpolation for the out of plane deflection, because only two nodes are available. Also, the in-plane membrane rotation and a weighting factor were defined as DOFs at nodes. Therefore, this element has eight DOFs. The weighting parameter was chosen to provide a soft clamping option in the beam analyses. For instance, by setting only the rotation at the boundaries to zero and leaving the weighting factor as a free parameter, the shear stress magnitude at the clamped boundary would no longer be zero. Through bending and free vibration cases, the author shows the better accuracy of his formulation when compared to FSDTs.

Burton and Noor (1995) investigated nine different approaches for cylindrical and doubly-curved sandwich panels by using differential calculus. Geometric and material

variations of parameters were studied to assess the accuracy of the chosen approaches. Of the nine approaches used to model sandwich panels, two classify as equivalent single layer (ESL) theory, the other five as discrete layer theories (Zig-Zag refinement was applied to a laminate with three equivalent single layers corresponding to the core, lower and upper skin layers) and the last two were based on predictor-corrector algorithms. Sensitivity results of all nine approaches compared to three dimensional analyses showed that the most robust type of approach is the discrete one. More specifically, the one with cubic variation of in-plane displacements and quadratic variation of out-of-place displacement is the best formulation among all nine. However, it is the one with most parameters to be defined, 27 to be exact, 14 more than the second (discrete and mixed linear theory) and 15 more than the third (predictor-corrector technique with post-processing of results) most expansive approach. More detailed results, regarding strain energy sensitivity to geometric and material variations, can be found in the original paper.

Exploiting the concept of superposition, Li and Liu (1997) proposed a global-local refined multilayered plated theory. Such theory could be classified as an equivalent single layer (ESL) theory, because it is made independent of the number of layer through Zig-Zag refinements. To summarize, the displacement functions, “u”, “v” and “w” were composed of a global set of terms and a pair of locally calibrated terms. The local calibration was available for two terms only due to the continuity DOFs. The in-plane global displacement comprises expansion terms in the plate’s thickness direction up to the third order. On the other hand, the out-of-plane displacement was considered constant, regarding the thickness direction. The local terms could be paired according to the thickness direction expansion order of each term as 0-1, 0-2, 0-3, 1-2, 1-3 and 2-3. All six derivations gave different results. This occurred, because each local term had a distinct contribution to the laminate response. The zeroth-order refers to the mid-plane displacement of each composite layer. The first-order term is of rotational angle. The second-order term represents the curvature of the displacement distribution of the composite laminate. Finally, the third-order term can be linked to the curvature of the transverse stress. First, second and third order terms are equally important for complex laminate configurations. Only the zeroth-order term could be ignored due to the fulfillment of continuity conditions at the laminate interfaces. Thus, to account for all these mechanical contribution in their formulation, the authors proposed a double superposition by grouping the refined first (1), second (2) and third (3) order terms, such that one term was always left alone, and three configurations were obtained: 1,2-3; 1,3-2 and 2,3-1. The hyphen separates the groups. These possible combinations comprised the pair of DOFs locally available for calibration of the plate

formulation. These three formulations were implemented in a 13 DOFs four node quadrilateral element. The cylindrical bending results turned out to be equal and accurate for the [0/90/0] laminate simulated. Comparisons for odd and even number of plies were provided. Stacks of 2, 3, 6, 7, 14 and 15 plies were simulated and compared. Although all results were in good agreement to the elasticity solution, the even stacking was slightly better.

Another beam model was created by Karama et at. (1998). Deriving analytical solutions (Levy's technique), these researchers studied the potential of a discrete layer theory using trigonometric functions to represent the transverse shear stress. Once again, the "discrete" term refers to a Zig-Zag type of theory, which is an enhanced equivalent single layer (ESL) formulation. All results were compared to image problems solved in the commercial software Abaqus. However, no comments on how these problems were modeled in Abaqus. For thin beams (h/L =0.044), good agreement between the authors' and Abaqus' solutions was obtained. Difference was lower than 1% for linear problems. In non-linear problems, i.e. buckling, a difference lower than 5% was observed for the first five critical loads. For thick beams (h/L = 0.44), the difference could be higher than 35%. Further analyses are not possible because the numeric model in the Abaqus was not detailed.

An overview of modeling and stability of sandwich structures was shown by Librescu and Hause (2000). The paper presented issues related to the geometrically linear and non-linear curved and flat sandwich plate theories. Buckling and post-buckling strength were studied and few published results were selected for stability investigation purposes. The authors also highlighted the complexity of studying such structures due to lay-up asymmetries: 1) asymmetry with respect to the mid-surface of the sheets, which generates face bending-stretching coupling; 2) asymmetry with respect to the mid-surface of the core now responsible for global bending-stretching coupling; and 3) the presence of ply-angle plies between the principal orthotropic axes of the skins materials and the orientation of the panel, which induces a bending-shearing coupling. Selected results of buckling and post-buckling of uni-facings (1-ply skins) and multi-layered skins of flat and curved sandwich panels were exhibited. One of the main trends, which could be identified, was the fact the sandwich composite structures had a much larger load carrying capacity than the usual laminated composite structures. This was enhanced by the fact that shells panels do not exhibit the snap-through buckling and they were robust regarding imperfections. Only in extreme situations of combined loads, the snap-through buckling could be seen.

Most of the terms involved in derivation shell theories were discussed by Yang et al. (2000). These ideas were highlighted: 1) the degenerated shell approach, 2) stress-resultant-

based formulations and Cosserat surface approach, 3) reduced integration techniques with stabilization (hourglass control), 4) incompatible modes approach, 5) enhanced strain formulations (mixed and hybrid formulations), 6) elements based on the 3-D elasticity theory, 7) drilling degrees-of-freedom elements, 8) co-rotational approaches and 9) higher-order theories for composites. The authors went over each topic explaining briefly each of these terms. Also, it is highlighted the papers, which can be viewed for further insights and explanations.

Icardi (2001) developed a laminated beam theory via Zig-Zag refinements. Third-order and fourth-order expansions in thickness direction were assumed for in-plane and transverse displacement, respectively. Closed form and 3D elasticity solutions from the literature were used to assess the accuracy of the formulation. A C-0 two-node beam element with 8 DOFs was derived to be free of shear locking effects. By setting the shear strain as one of the DOFs, the approach could be referred to as of mixed type. The FEM solutions of the current equivalent single layer (ESL) model, and the FEM solutions from stacking of sub-laminates (plies) were also obtained. Sub-lamination increased the current number of DOFs to $2N_{sl}+1$ DOFs. Where "N_{sl}" is the number of sub-laminates. This method was proposed as an alternative to integration of constitutive equation due to inconsistency of the displacement fields. Some examples solved in the literature were used to endorse the accuracy of the proposal.

Meunir and Shenoi (2001) investigated a fiber reinforced plastic (FRP) sandwich material by using Reddy's high-order shear deformation theory. An equivalent single layer (ESL) theory with complex material properties was used in the analytical solution of the first free vibration frequency. The authors experimentally characterized the elastic-viscoelastic properties (damping) of the PVC closed-cell foam named HEREX C70.130 from 30 to 90 degrees Celsius and from 0 to 500 Hz. As for the material properties of the skins, a reinforcement named Eglass/DX-210 found in the literature was chosen. Careful studied of results showed that the dynamic response of the sandwich structure was temperature and frequency dependent in the investigated ranges. Moreover, the dynamic properties seemed to be insensitive to the stacking sequence of the skin. On the other hand, the results changed considerably, if as the plate approached a square (a=b) and as the core-to-skin thickness ratio increased.

A refined first order shear deformation multilayered plate element was evaluated in linear and non-linear analyses by Polit and Touratier (2002). The triangular element preserved C-1 requirements for the transverse deflection and comprised a co-sine transverse shear strain distribution. For the non-linear contributions, von Kármán's assumptions were developed. The

transverse normal stress was obtained via integration of equilibrium equations, and the displacement field preserved inter-laminar continuity. Through integration of constitutive relations, a Zig-Zag refined displacement field was attained. Accurate results with good convergence patterns could be observed. Among the findings, it was worth highlighting the fact that simpler approaches of multilayered structures might overestimate the stability of the structure.

Also published in 2002, Yu, Hodges and Volovoi (2002) carried out an asymptotic three-dimensional (3D) study of anisotropic elasticity theory with the purpose of modeling laminated shells. The method splits the 3D problem into a linear one-dimensional (1D), through-the-thickness analysis, and a non-linear, two-dimensional (2D), shell analysis. The derivation process uses small shell parameters ratios such as deformation/radius, deformation/thickness, thickness/radius and thickness/length. In order to provide a practical solution, this formulation was changed to look similar to Reissner-Mindlin's shell/plate theory. Even though the proposed theory was of the form of an Equivalent Single-Layer first-order shear deformation theory, the results were comparable to Layer-Wise formulations. Cylindrical bending test cases were investigated for the proposed approach along with a CLT, FSDT and exact 3D solutions. The numerical results showed excellent agreement and validated the fidelity of the approach.

Ghugal and Shimpi (2002) reviewed over 412 papers on shear deformation theories for laminated plates. Equivalent and refined single layer theories as well as layer-wise theories were reviewed and many references could be found on each topic. Based on the references contained in the paper, the authors concluded that there was a lack of critical evaluation works on unsymmetrical laminated plates. For such cases, even formulations with more than five displacement variables might be insufficient to properly model these laminates.

More than a hundred references regarding Zig-Zag axiomatic theories for multi-layered shell and plate structures were consulted by Carrera (2003a). Focus was given to those which present a continuous displacement field and inter-laminar continuity of transverse stresses. Three lines of research were found. According to Carrera (2003a), Lekhnitskii was the first to point a Zig-Zag methodology (Lekhnitskii Multilayered Theory - LMT). Then, Ambartsumian showed a similar approach (AMT), which is more often encountered in the literature. One last methodology was proposed by Reissner, who proposed a mixed approach (RMVT) to achieve inter-laminar continuity of transverse stresses. Carrera (2003a) introduced his contribution within this latter approach by proposing the Weak Form of Hooke's Law (WFHL) in order to lessen the computation of mixed approaches. This WFHL reduces the mixed problem down to

the classical displacement formulation. The aftermath of all reviewed articles called for more benchmarks of the three studied formulation with elasticity solutions. Also, asymptotic, continuum based and other plate/shell theories should be compared as well.

By exploiting the concept of virtual sub-lamination, Icardi (2003) investigated the trade-off by using higher order displacement formulations with and without Zig-Zag considerations as oppose for increasing or decreasing the real number of layers of sandwich beams. Exact 3D solutions obtained via the theory of elasticity were used to assess the accuracy of the sub-lamination scheme. Overall results pointed a tendency of using Zig-Zag formulations to increase the accuracy of thick and very anisotropic plates. The applied virtual sub-lamination also allowed a local study of damage and failure of a composite layer by reducing the stiffness/strength a sub-layer.

Murakami Zig-Zag function (MZZF) was studied (CARRERA, 2004) in the modeling of multi-layered plates and shells. Linear and higher order displacement formulations (up to fourth order) were firstly studied. Then, advanced use of the MZZF was addressed via mixed formulations, where there are stress considerations in addition to the displacement field. Thermal, static and dynamic test cases results of orthotropic simply supported plates and shells were given for accuracy comparisons. Once again, the literature showed that the use of ZZ improvements were preferred to the use of higher order theories alone. Since the advance use of MZZF comprises a formulation of the mixed type, the results are usually better than those obtained through classical displacement formulation. Thus, the use of the mixed formulation is somewhat equivalent to the use of MZZF via classical displacement irreducible formulations. When MZZF is used along with mixed theories (advanced approach), the results improve only slightly when compared to the application of only either MZZF or stress-displacement theories.

Nayak, Shenoi, and Moy (2004) studied the dynamics of laminated sandwich composite by using the concept of ESL theories. The proposed formulation was based on Reddy's plate theory, and the equilibrium equations were solved by using Newmark's integration algorithm. Two different methods for defining the critical time steps were investigated. The finite element method was chosen to solve the equations. A C-0 four node and a C-0 nine node elements were implemented with seven displacement DOFs. An assumed strain method was adopted to minimize the effects of shear locking and spurious energy modes in the FE implementation. To keep the exact element mass, a consistent mass matrix was derived. Based on eight static or dynamic examples, different side/thickness and face/core thickness ratios, clamped and free boundary conditions, aluminum and PVC cores in different lamination patterns were

investigated. Overall results agreed well with the literature, regarding sandwiches with thick and soft cores.

Exact three dimensional solutions for isotropic thin and thick plates were addressed in Demasi (2007). Once again in the literature, a Navier-type solution by using Fourier series was elaborated. The Mixed Form of Hooke's Law (MFHL) was used and leads to the descriptions of the boundary conditions on the top and bottom surfaces in terms of transverse stresses. The related eigenvalue problem did not yield enough linearly independent eigenvectors. Hence a combination of eigenvectors multiplied by functions of the thickness direction was proposed to derive six distinct eigenvectors. For the sinusoidal pressure load on the top surface, the exact solution was obtained. Thin plate theory (TPT) and classical plate theory (CPT) were also derived from the exact solution. As a validation test, a 5^{th} and a 10^{th} order axiomatic formulations based on Reissner's Mixed Variational Theorem (RMVT) were implemented for comparison.

Demasi (2008a) presented the extension of a previous work on exact solutions for isotropic plates to multilayered plates. Following the steps of the previous paper, the exact static 3D solution was developed for the multilayered case. To assess the accuracy of the formulation, 23 different 2D axiomatic theories were reviewed and implemented. Mixed and classical displacement formulations were investigated by using Murakami's Zig-Zag refinements or not. Equivalent single layer and layer-wise theories were discussed too. Displacement fields with very high order expansion of the thickness coordinate (e.g. 7^{th}, 8^{th} and 9^{th} order, hence the tag "quasi 3D") were derived and verified for a 3 layer sandwich plate. Results for low order formulations were also provided. Different aspect and length to thickness ratios were investigated. After solving a sandwich plate with a soft core under sinusoidal pressure, the accuracy of the present formulation was demonstrated.

A numerical and experimental study of the Golla–Hughes Method (GHM) applied to viscoelastic sandwich beams was performed by Barbosa and Farage (2008). The approach proposal transformed the dynamic equilibrium equations written in Laplacian-domain into a time-domain. This process generates another degree of freedom, which was used to model the viscoelastic response. GMH method uses a complex Young Modulus expressed in the Laplacian-domain with a dissipation function. For this approach, four dynamic parameters had to be calibrated with fitting of experimental tests. Three beams (1.0 m, 0.8 m and 0.5 m long) made of three aluminum layers were studied and the first three natural frequencies and loss factors were obtained and compared to theoretical values. The maximum error reported was 13%. Other three similar sandwiches were built, but with a viscoelastic core composed by a

double-face adhesive and double adherent faces (3M Scotch©). Experimental results showed a clear larger dissipation with the viscoelastic layer. The proposed finite element was a combination of two elastic frame elements, one quadrilateral linear viscoelastic plate element and four rigid connection elements. Twenty four DOFs and five dissipation parameters resulted in a hereafter super element. Shear deformation was introduced in the quadrilateral element representing the core. Convergence tests using 12, 24 and 48 (super) elements showed that 24 elements were enough to model the sandwich beams. The small divergence in the results was explained based on the errors from the fitting of the experimental curves to determine the dissipation parameters.

Application of plate theories to sandwich structures was reviewed by Hu et al. (2008). Equivalent single layer (ESL) and layer-wise (LW) formulations were reviewed along with Zig-Zag (ZZ) refinements. Since the use is usually made of a viscoelastic mechanically weaker than the faces material, the approach attempted a layer-wise plate formulation. Such theory comprises two layers to model the skins and one to represent the core. To estimate the accuracy of the proposed formulation, seven other different plate theories and two problems were chosen. CLT, HSDT-Reddy's (with and without ZZ-IC), HSDT-Touratier's (with and without ZZ-IC) and two other models, which assigned the CLT plate theory to the faces and the FSDT one to the core. Firstly, the problem was a three-point bending test of a sandwich beam to evaluate stress and displacement fields. The second problem was the free vibration analysis of a simply supported viscoelastic sandwich beam. Solutions for both cases were derived analytically. A numeric solution was developed by using a bi-dimensional eight nodes plate element with 16 DOFs (2D-Q8), which was implemented in-house Matlab FE code. Dynamic and static tests showed the need to use higher order models for thick and soft core sandwich structures. Besides, inter-laminar continuity of transverse stresses was required to correctly determine the maximum shear stress in the laminate.

To offer a better modeling of laminated beams, Tessler, Di Sciuva and Gherlone (2009) developed a refined Zig-Zag beam theory. The work was based on Timoshenko's beam theory, and it was named as Di Sciuva's Zig-Zag Theory (DSZZT) and Averill's Zig-Zag Theory (AZZT). Both of these Zig-Zag theories suffer from deficiencies to correctly model the shear stress for clamped boundary conditions. These errors stemmed with the enforcement of constant shear stress through the thickness (DSZZT) and poorly defined penalty functions (AZZT). In addition, DSZZT demands C-1 continuity in FE implementations, and AZZT violates variational requirements. Both Zig-Zag theories lack a layer invariance, which means that different results may be achieved with the same formulation, depending on how the user

calibrates the models for the stacked layers. The proposed refined Zig-Zag theory was set to vanish at top and bottom layers, better accommodates clamped boundary conditions and it is still C-0 continuous, which is ease FE modeling. A simply supported beam subjected to sinusoidal transverse load and a cantilever beam subjected to point load at the free end were used to evaluate the refined Zig-Zag model. Results for the second case presented higher discrepancies when compared to a high-fidelity FEM/NASTRAN model. The comparisons among results showed the potential of the current theory to predict displacement, stresses and forces.

The 1-2-3 global-local approach proposed by Li and Liu (1997) was changed to provide a plate formulation, which demands only C-0 continuity in finite element implementations. By eliminating the first derivative of transversal displacement from the in-plane displacement functions, the Zhen and Wanji (2010) managed to rearrange the terms and derive a C-0 plate formulation. Two different laminate configuration and two more sandwich plate configurations were studied under static loading conditions. Up to moderately thick plates (l/h = 20), the C-0 formulation results nearly match those obtained via the C-1 requirements. Both theories could accurately represent the exact results. These results were obtained by using analytical formulations via Navier trigonometric series.

The C-0 plate element for laminated structures derived by Zhen and Wanji (2010) was applied to dynamic analysis (ZHEN, WANJI; XIAOHUI, 2010). The solution was obtained via analytical and numerical solution procedures. The first one used the dynamic version of Navier-type series, and the second one was implemented by using an eight node quadrilateral element. A consistent mass matrix was considered. Counting the displacement variables per node, the number DOFs of the element was equal to 13x8 = 104. This was considerably high for an equivalent single layer (ESL) theory implementation. Nonetheless, this number was independent of the number of plies in the laminate. A convergence studied indicated an adequate mesh density of 8x8. The comparison of the natural frequencies for two cross-ply laminates and a sandwich plate with a core 1000 times softer than the faces was shown. Qualitative results for geometric variations of the core to face thickness ratio, aspect ratio and span to thickness ratio equal to the exact results. The absolute values for each frequency exhibited a more accurate answer than the theories chosen for comparison.

Bending and vibration of laminated composite and sandwich plates were investigated by Tu, Thach and Quoc (2010) through an equivalent single layer (ESL) theory. Third order terms were assumed for the in-plane displacement and a transverse displacement field independent, which was a function of the in-plane variable. A FEM implementation of C-0 nine

nodes elements yields 81 DOFs for the current plate theory. The mass matrix was derived consistently. Few parametric studies were provided. Comparison with other approximate solutions from the literature for the free vibration test showed good agreement. Unfortunately, the base solution was not the exact solution. On the other hand, the static bending results agreed well with its exact solution.

Based on the harmonic response of sandwich plates, a characterization method of dynamic properties was proposed by Matter et al. (2011). A mixed-experimental technique was derived from the minimization of the differences between modal parameters evaluated numerically and experimentally. First, a layer-wise three layer shell formulation was proposed. The highest order term in the expansion through the thickness was left as a variable. The governing equations assumed the structural damping formulation with complex material properties, which were assumed to not vary with frequency. This is acceptable for low damping behavior. Then, the design of a double experimental setup was performed. A scanning laser vibrometer with a dynamic shaker setup was firstly used. The second approach comprised a loudspeaker, which emitted a contact-free excitation on the plate. In the correlation of results, the free boundary condition was adopted and the plates were hanged by using nylon wires. Such correlation was developed via the Modal Assurance Criterion (MAC). The criteria in the optimization process exploited the low core-to-skin stiffness ratio characteristics of the sandwich plate. This experimental-numerical identification process is verified for a honeycomb-glass/epoxy sandwich plate and a foam-carbon/epoxy one. Third order was chosen for the plate theory, and the mesh was a 12x12 with nine nodes per element. Results for the honeycomb core sandwich identified the loss and storage parameters with a precision of 0.001. On the other hand, the foam core sandwich provided not only good results, but also, some did match the references. Although the constitutive model was not a function of the frequency, this influence along with other temperature non-linear parameters can be implemented.

The work of Ghinet and Atalla (2011) presented the formulation of a discrete (layer-wise) laminate model (DLM) for thick sandwich composite plates and beams with linear viscoelastic layers. Structural damping was considered. The proposed layer-wise theory was based on Reissner–Mindlin's displacement field. However, upon realization of its ineffectiveness in capturing dilatational responses (symmetric modes of motion) in soft core sandwich structures, a complementary *ad hoc* study by using improved displacement functions was performed. The solution of the governing equations was obtained through the Rayleigh–Ritz technique with hierarchical trigonometric form functions. Bending and transversal shearing behavior were determined by using a cantilever beam and a free-free condition. Results

were compared to numerical spectral finite elements method (SFEM), 3D finite element method (FEM) using NASTRAN and experimental tests. Some parameters were computed for validation: structural damping loss factor, natural frequencies, wave numbers, mechanical impedance and input mobility. The orthotropy of the laminate influences the damping loss factor due to the dependence of the heading of the propagating solutions. Nevertheless, the developed DLM provided excellent agreement with the base methods and experimental data.

Santiuste, Thomsen and Frostig (2011) investigated the thermo-mechanical nonlinear response of an axi-symmetric circular sandwich plates with a compliant foam core. Based on previous works (FROSTIG, 1997, FROSTIG; THOMSEN, 2008), the plate formulations followed the same displacement assumptions. Such assumptions fitted in the High order SAndwich Plate class of Theories (HSAPT). This class of theories analyzes the faces and the core separately. Different displacement functions are assigned to each component. Santiuste, Thomsen and Frostig (2011) used CLT for the faces and integrated the equilibrium equations to find a displacement field for the core, which varies in a quadratic pattern in function of the thickness direction. Two FEA models were built in Abaqus to assess the accuracy of the proposed analytical formulation and its simplifications. One model was 2D and used axi-symmetric elements (CAX4R), and another model, which was 3D has and used solid elements (C3D8R). Despite being slightly stiffer, the analytical results showed good absolute and qualitative agreement with the numerical models. For the PVC core thermo-mechanical properties used in the models, it is clear that this material must be modeled with temperature dependent properties. In addition, this dependence, which softens the core and increases the beam's displacement results, generates new convergence issues in the Newton's solution algorithm. This directly impacts on the speed of the solution since finer spatial and time discretization are needed.

Mantari, Oktem and Soares (2012a) proposed a new equivalent single layer (ESL) theory for laminated plates. The out-of-plane displacement followed the usual independence of the thickness coordinate. On the contrary, the in plane displacements defined by the FSDT were improve by using two terms multiplying the rotation variable. The first term was essentially the parameter "m" to be calibrated. The second term was a sine function of the thickness coordinate weighted by an exponential function of the same "m" parameter multiplied by a co-sine function of the thickness coordinate. In order to obtain the best value for "m", several solutions for different length-to-thickness ratios were grouped and a value of 0.5 was suggested. The governing equations were solved via Navier-type solutions. Based on the references and the

selected examples, the proposed theory was equally accurate. By incorporating Zig-Zag functions, the authors believed that the results should lower the errors.

Another HSAPT theory was developed by Mantari, Oktem and Soares (2012b). A three layer formulation was derived by using an improvement of in-plane displacements via a tangential trigonometric function. The transverse displacement was assumed constant in the thickness direction for all three components. The upper and lower skins presented a linear shear deformation theory with Zig-Zag refinement. For the core, the tangential function was applied by using a FSDT. To reduce the DOFs per node down to seven, the compatibility of displacement at the top and bottom interfaces was exploited. A four node element was implemented for this formulation, yielding an element with 28 DOFs. To avoid shear locking of the linear interpolation, a reduced integration scheme was adopted. The results seemed very accurate up to a skin-to-core stiffness ratio of 15.

Demasi (2012) went over the concept and definitions of Zig-Zag effects of laminated structures. Then, a review of his generalized unified formulation was given. Next, the author proposed the partially inclusion of Marakami's Zig-Zag Function (MZZF). By partially, it means that, by exploiting the GUF, one is able to refine only one of the variable displacements considered by the MZZF. To assess the accuracy of the partially inclusion of the MZZF, a baseline model was chosen and compared to the exact results for the test case chosen. The baseline solution was an advanced high order theory (AHSDT) of fourth order (ED444) for all three displacement variables. Without ZZ refinements. The ZZ refinements consist of the straightforward inclusion of the MZZF to the selected DOF. The static results showed that for thin plates, the ZZ effects can be neglected. For thick laminates, the MZZF is more effective, when added to all displacements DOFs at the same time. Next best option was to apply the MZZF simultaneously on both in-plane displacement fields.

Neves et al. (2012b) studied a laminated composite structures with material properties varying gradually over the thickness (Functionally Graded Materials - FGM). However, the formulation accounted for a three layer laminate. Two configurations were studied. For the first one, both faces were isotropic and the core was a FGM layer. In the second one, the core was an isotropic material and the skins were FGM layers. Due to this discontinuity of material through the thickness of the laminate, MZZF was applied to both in-plane displacement functions of their previous formulation with a hyperbolic sine function of the thickness coordinate (NEVES et al., 2012a). Governing equations and the RBF solutions for the static examples were derived via the same drill. The results were given for p = 0.2, 0.5, 1, 2, 5, and

10 values for the exponential volumetric function. Results showed the same level of accuracy of the previous work.

By using a first order shear deformation theory, Asadi, Wang and Qatu (2012) developed a theory for deep shells. The main part of the approach lies on keeping the term "z/R" in the shell formulation. The equations of motion were solved exactly by assuming a product of trigonometric function for the five classical displacement variables. Regular shell theories derived with the FSDT and Qatu's formulation, including the term "z/R" (with a shear correction factor of 5/6), were compared to 3D results computed by using a solid elements in a finite element model built in Ansys. Qatu's shell formulation showed a small improvement over the regular FSDT.

Unfortunately, there are innumerous other papers on plate and shell theories that were not quoted in this work which can be of help for a particular issue. Those herein discussed can be checked for a cross-reference investigation. Mainly, the papers which comprise extensive reviews of the literature are advised (REDDY, 1990, GHUGAL AND SHIMPI, 2002, CARRERA, 2002, CARRERA; DEMASI, 2002a, 2002b, CARRERA, 2003a, 2003b, DEMASI, 2008a, ALTENBACH; EREMEYEV, 2010).

And the question of which plate theory presents the best results, especially in intricate cases such as those of Sandwich Structures, remains open. As more and more references are seen, it is possible to say that a linear plate theory can give better results than a sophisticated non-linear one if it is better solved, numerically and/or physically. This means that numerical errors will be minimized and/or the solution will not neglect/ignore the relevance of physical behaviors and dimensions of the problem. That is why next Chapter is devoted to a brief review on solution methods.

Chapter 4 - Approximate Solution Methods

4.1 Differential Equations

There are many alternative methods to solve linear or non-linear (initial) boundary value problems within a domain and on its boundaries (HUEBNER; THORNTON, 1982, ZIENKIEWICZ; TAYLOR, 2000a, 2000b). A differential problem is posed as:

$$L(\psi) - f = 0 \tag{4.1}$$

The differential operator "L" is applied to a field variable "(ψ)" and/or its derivatives, while "f" is a function of the independent variables. The equation (4.1) above can be solved either in an exact (e.g. Laplace's method, Fourier's method, separation of variables) or approximate solution (e.g. Ritz's method, Galerkin's method, Perturbation, Finite Elements, Finite Differences, Radial Base Functions (RBF)).

Depending on the complexity of the geometry and/or the physics of the problem, the approximate solutions may be the only resource for a solution based on the initial information of "N+1" points. Generally, the field variables "ψ" are approximate as:

$$\psi(\boldsymbol{x}) \cong \tilde{\psi}(\boldsymbol{x}) = \psi_o(\boldsymbol{x}) + \sum_{i=1}^{i=N} c_i \psi_i(\boldsymbol{x}) \tag{4.2}$$

To solve equation (4.1), an appropriate integration procedure must be chosen. Depending on how this integration procedure takes place, the solution can be further classified as *Strong* or *Weak formulation*. In sum, the strong solution method respects the continuity requirements of all field variables and their derivatives within "L(ψ)" along with the essential and natural BCs. On the other hand, the weak formulation can use integration by parts, for instance, to reduce the continuity requirements of the same differential problem and thereby lessen the overall solution cost. Nonetheless, the weak and strong formulations may coincide. When the numeric solution is an approximation, a residual "R" is expected:

$$L(\tilde{\psi}) - f = \mathcal{R} \tag{4.3}$$

Either formulation strong or weak is obtained by weighing the differential equation using a particular function test (trial, weighting) function "W". This integration is known as Method of Weighted Residuals (MWR):

$$\int_{\Omega} (L(\tilde{\psi}) - f) W \, dV = \int_{\Omega} \mathcal{R} W \, dV \tag{4.4}$$

Depending on the choice of "W", the method can be further classified as Galerkin's, Least Square, Sub-domain collocation or Point collocation. The weak formulation can also be obtained from *variational calculus*. This branch of mathematics can be used to link the differential problem (4.1) to a functional "Π" related to the physics of the problem. If such functional exists, the differential problem (4.1) is substituted by the minimization of this functional as:

$$\delta\Pi(\psi) = \sum_{i=1}^{i=N} \frac{\partial \Pi}{\partial x_j} \delta x_j = 0 \rightarrow \frac{\partial \Pi}{\partial x_j} = 0 \tag{4.5}$$

Ritz's method solves equation (4.1) by finding the stationary solution of the corresponding problem. In particular, Ritz's method uses trial functions, which are valid for the whole domain. On the other side, when the trial functions are applied to local sub-domains (elements), the method is known as the Finite Element Method (FEM).

To split the domain into a set of elementary sub-domains is usual procedure for boundary value problems with complex geometries, as the case of structural mechanics.

The problem of discretization goes beyond the initial boundary value problem. Fracture mechanics and plasticity boundary value problems are cases where the discretization can change abruptly and even discontinuities may emerge in the domain. Thus, regular discretizations may corrupt the solution algorithms due to geometrical complications, which appear as the phenomenon takes place. For instance, a crack or a void representation within the bulk material might need extremely complicated algorithms or very dense meshes to track morphological changes and accurately give a solution for this region.

The Generalized Finite Element Method (GFEM) and the Extended Finite Element Method (XFEM) are techniques, which can offer an interesting option to these problems

(BABUSKA; BANERJEE; OSBORN, 2003, BABUSKA; BANERJEE, 2012, KIM; DUARTE; PROENÇA, 2012). These methods can ease the solution of problems such as propagation of cracks and evolution of phase or domain boundaries. The core of these methods is the partition of unity method (PUM) concept for enriching finite elements or meshless approximations (MELENK; BABUSKA, 1996). A partition of unity comprises a sum of functions "φ" within a domain "Ω" such that:

$$\sum_{\forall i} \varphi_i(\boldsymbol{x}) = 1;\ \forall\, \boldsymbol{x}\ \in \Omega \tag{4.6}$$

Based on equation (4.6), the approximation for the field variable "ψ" can be re-casted in a generalized form as:

$$\psi(\boldsymbol{x})_{GFEM/XFEM} \cong \tilde{\psi}_{FEM}(\boldsymbol{x}) + \left\{ \sum_{i=1}^{i=N(h)} \varphi_i^h(\boldsymbol{x}) \tilde{\theta}_i^{h,p}(\boldsymbol{x}) \right\}_{GFEM/XFEM} \tag{4.7}$$

The partition functions "φ" have the property to enhance the response the approximating function "θ". This product is tagged as *enrichment function* and can be applied locally or globally. This couple is normally chosen according to the problem at hands. For instance, a particular GFEM/XFEMs can choose "ψ"="θ" and/or "φ"="N". Depending on how such enrichments are chosen, the problem may improve or ease the solution in a way which it is still subordinated to how the mesh wraps the boundaries of the problem. Nonetheless the equation (4.7) can be written to be completely mesh-free as well. Since GFEM/XFEMs are meant for domains with a critical region, the common partition function is a "hat-shaped" function. The tip of the hat is built to coincide with the critical region. Figure 21 exhibits how a hat function enhances the approximate solution for a function "ψ".

The indexes "h" and "p" refer to the type of further refinements within GFEM/XFEM functions. The first is related to refinement of the current mesh, i.e. to the increase of the number of elements (grid points). The second parameter "p" refers to the choice of the enrichment functions, which can be non-linear and non-polynomial.

These partition functions can be derived with or without previous knowledge of the problem, e.g. where the crack is located. Some of these functions are derived via perturbation methods, since singularities are usually handled.

Once singularities and discontinuity are often present, the numerical integration is normally an issue in these methods. Some techniques can be used to overcome these illnesses: Higher order Gauss quadrature, adaptive quadrature for singular functions, sub-domain quadrature and conversion of 2D (3D) surface (volume) integrals to line (surface) integrals.

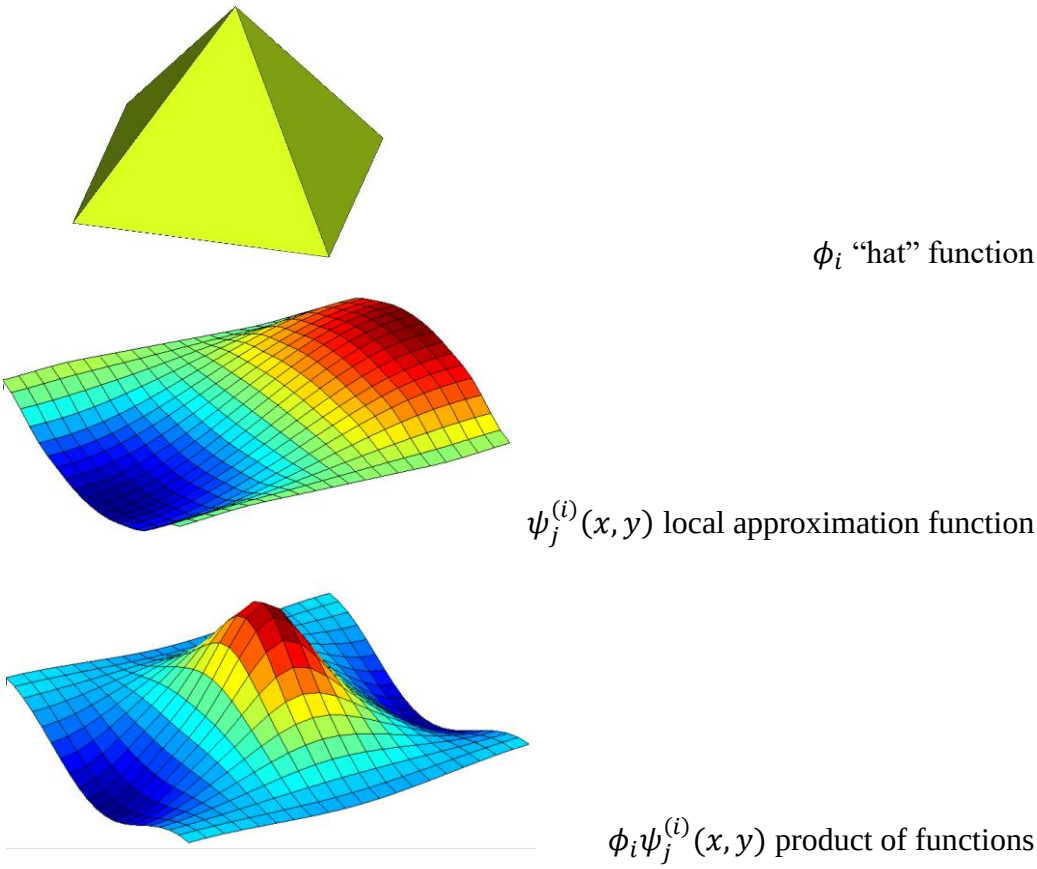

Figure 21. GFEM/XFEM approximation with hat functions

.

4.2 Finite Element Method

FEM is the most common numerical solution method in Computational Structural Dynamics (CSD), because the boundaries (limits) of a structure must be accurately represented and tracked as the structure moves and deforms in a 3D space. Thus, the problems are usually of the kinematics type, rather than a constitutive/flux problem, as in Computational Fluid Dynamics (CFD).

It is then clear that the domain will be studied as a set of elements, which conform to the boundaries of the structure. Figure 22 depicts an element sharing a portion "Γ_e" of the external boundary "Γ" of the domain "Ω".

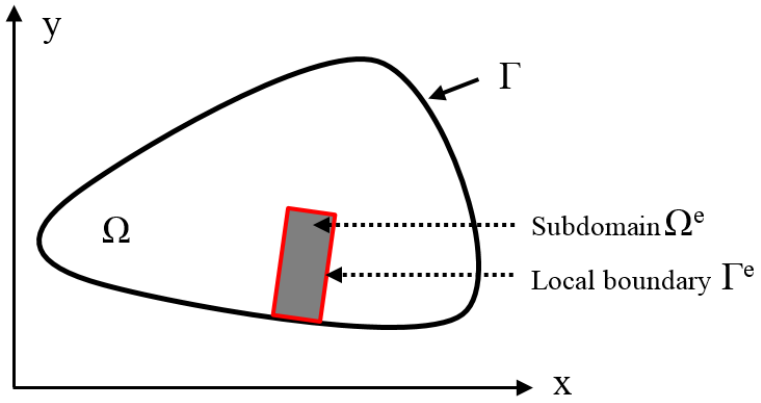

Figure 22. Elementary sub-domain

More specifically, the differential problem for all points within the domain "Ω" (Figure 22) is:

$$m\ddot{\psi} + c\dot{\psi} + k\psi = F(t) \tag{4.8}$$

The variable "ψ" to be solved in equation (4.8) can be a vector or a scalar field. For a material point, i.e., at the microscopic level in which equation (4.8) was written, the coefficients "m", "c" and "k" contain the point's mass, damping and stiffness constitutive data. For a real structure, i.e., for a boundary value problem, the same coefficients are matrices comprising the structure's geometrical and constitutive macroscopic (or phenomenological) information of mass, damping and stiffness. Mathematically, the field variable "ψ" is then a vector containing the magnitudes of the respective field at specified points inside the domain and on its boundaries.

$$[M]\{\ddot{\psi}\} + [C]\{\dot{\psi}\} + [K]\{\psi\} = \{F\} \tag{4.9}$$

Function "F" is the external excitation applied to the material point or over a region of the structure.

To derive the structure's equations of motion, it is important that the microscopic and macroscopic concepts are well understood. For instance, it is possible that for a particular

boundary value problem, there are no dissipative effects at the microscopic level of the investigated media. However due to the geometry of structure, a dissipative effect may appear. Geometry also influences the specific mass, creating a geometrical inertia for structures referenced as *moment of inertia*.

In the next solution step, the choice of a strong or weak formulation must follow. As explained earlier, it is a matter of continuity of the approximate expression for the field variable being solved. First, the approximate field variable of the domain can be split into "N_e" local fields related to their respective sub-domains called "finite elements":

$$\psi \cong \tilde{\psi} = \sum_{i=1}^{i=N_e} N_i{}^{(e)} \psi_i^e \tag{4.10}$$

These "N^e" functions (henceforth called *interpolation functions*) may or may not fulfill the physical requirements of *compatibility* and/or *completeness*.

A function is said to be C-R continuous when it will remain a Continuous function, even if it is derived up to the R^{th} order. Assuming that the highest derivative in the elementary equation of (4.4) or (4.5) is of order (R+1), then the compatibility and completeness requirements are:

- *Compatibility*: At the element interfaces, "ψ" must be C-R continuous
- *Completeness*: Within the element, "ψ" must be C-(R+1) continuous

The mathematical requirements of compatibility and completeness ensure physical consistence of the discretization with the physical behavior of the structure. They guarantee that the approximate solution converges to the exact solution as the number of elements tends to infinity (or their size to zero).

Unfortunately, to find elementary functions, which adhere to these constraints, is a very difficult task but for few particular cases. Since finding these interpolation functions is a problem dependent task, it will be addressed at a separated section for the case of plate-like structures. Defining these interpolation functions is often referenced as *choosing* or *creating* a finite element.

This manuscript adopts the Principle of Virtual Work to derive the FEM equations of motion, because it is a conservative method capable of generating both weak and strong formulations. Likewise, the MWR can yield the same governing equations.

For physical problems, the derivation process may begin from a more general principle, in this case, the Extended Hamilton's Principle (EHP). It accounts for dissipative effects and internal forces and may be regarded as Generalized Principle of Virtual Work (GPVW):

$$\delta\mathcal{H} = \delta\int_{t_0}^{t_1}[M - \Pi + W_d]dt = \int_{t_0}^{t_1}[\delta M - \delta\Pi + \delta W_d]dt = \int_{t_0}^{t_1}[\delta M - \delta(\Pi_i - \Pi_e) + \delta W_d]dt = 0 \tag{4.11}$$

The equation (4.11) above is consistently applied at the element level if the compatibility and completeness requirements for the elementary interpolation functions are fulfilled. "Π_i" is the internal potential energy, "Π_e" comprise the external loads, including body forces, "M" is the kinematic energy and "W_d" is the work of dissipative forces. Thus, for a domain with N_d discrete values of ψ and an element with N_r discrete values of ψ, the element equations are obtained with:

$$\frac{\partial\mathcal{H}}{\partial\tilde{\psi}_i} = 0, for\ i = 1 \dots N_d \rightarrow \frac{\partial\mathcal{H}^e}{\partial\tilde{\psi}_i} = 0, for\ i = 1 \dots N_r \tag{4.12}$$

Equation (4.12) can be written in terms of one or more inter-related field variables. If more than one field variable is kept in the governing equations, the formulation is then said to be *reducible* or *mixed*, as previously mentioned. However, if the formulation is written in terms of a field variable, which is a function of the problem's independent variables only, the problem is said to be *irreducible.*

Weak formulations are very common, because they are easy to develop and implement. On the other side, inexorably, errors due to the weakness of the formulation itself and numerical issues often emerge. Low convergence rates, instability, spurious modes, locking and overall inaccurate micro and macroscopic results can be mentioned.

4.2.1 Principle of Virtual Displacements and Reissner's Mixed Variational Theorem

Applying the GPVW from (4.11) on a conservative structural problem of an initially undeformed body, its terms are calculated for the respective forces applied along a virtual displacement "δu":

$$\int_{t_0}^{t_1} \delta M \, dt = -\int_{t_0}^{t_1} \int_{\Omega} \rho \ddot{\boldsymbol{u}} \cdot \delta \boldsymbol{u} \, d\Omega \, dt + \int_{\Omega} \rho [\dot{\boldsymbol{u}} \cdot \boldsymbol{u}]|_{t_0}^{t_1} \, d\Omega \tag{4.13}$$

$$\int_{t_0}^{t_1} \delta \Pi_i \, dt = \int_{t_0}^{t_1} \int_{\Omega} [\nabla \cdot \boldsymbol{\sigma}] \cdot \delta \boldsymbol{u} \, d\Omega \, dt = \int_{t_0}^{t_1} \int_{\Omega} \delta \boldsymbol{\varepsilon}^T : \boldsymbol{\sigma} \, d\Omega \, dt$$

$$\int_{t_0}^{t_1} \delta \Pi_e \, dt = \int_{t_0}^{t_1} \left\{ \int_{\Omega} \boldsymbol{b} \cdot \delta \boldsymbol{u} \, d\Omega + \int_{\Gamma} \boldsymbol{T} \cdot \delta \boldsymbol{u} \, d\Gamma \right\} dt$$

For stationary problems, after re-arranging equation (4.13), one gets:

$$\delta M - \delta(\Pi_i - \Pi_e) = 0 \tag{4.14}$$

$$-\int_{\Omega} \rho \ddot{\boldsymbol{u}} \cdot \delta \boldsymbol{u} \, d\Omega - \int_{\Omega} \delta \boldsymbol{\varepsilon}^T : \boldsymbol{\sigma} \, d\Omega + \int_{\Omega} \boldsymbol{b} \cdot \delta \boldsymbol{u} \, d\Omega + \int_{\Gamma} \boldsymbol{T} \cdot \delta \boldsymbol{u} \, d\Gamma = 0$$

If equation (4.14) is carefully analyzed, one can see that it is written as a mixed formulation, because all field variables ("u", "ε" and "σ") appear explicitly. When a constitutive relation and a geometric compatibly condition, such as (2.6), are applied into the internal forces term:

$$\int_{\Omega} \delta \boldsymbol{\varepsilon}^T : \boldsymbol{\sigma} \, d\Omega = \int_{\Omega} \delta \boldsymbol{\nabla u}^T : \boldsymbol{C} : \boldsymbol{\nabla u} \, d\Omega \tag{4.15}$$

Hence, the irreducible form obtained is:

$$\int_{\Omega} \rho \ddot{\boldsymbol{u}} \cdot \delta \boldsymbol{u} \, d\Omega + \int_{\Omega} \delta \boldsymbol{\nabla u}^T : \boldsymbol{C} : \boldsymbol{\nabla u} \, d\Omega = \int_{\Omega} \boldsymbol{b} \cdot \delta \boldsymbol{u} \, d\Omega + \int_{\Gamma} \boldsymbol{T} \cdot \delta \boldsymbol{u} \, d\Gamma \tag{4.16}$$

But equation (4.16) is already the classical PVD equation of motion. It is an irreducible formulation based on the displacement fields.

As an alternative to irreducible formulations, mixed formulations may reduce the continuity requirements of (4.16). On the one hand, the continuity requirements are lessen, but on the other hand, the size of the governing equations increases.

Reissner's Mixed Variational Theorem (RMVT) can be interpreted as a constrained variational principle (ZIENKIEWICZ; TAYLOR, 2000a). Taking such constrain as "Q(u)=0" is imposed on (4.14) in "Ω" or "Γ":

$$\delta M - \delta(\Pi_i - \Pi_e) + \delta\Pi_\lambda = 0 \tag{4.17}$$

$$\delta\Pi_e - \delta K = \int_\Omega \{[\delta\boldsymbol{\nabla u}^T : \boldsymbol{C} : \boldsymbol{\nabla u}] + \boldsymbol{\lambda}^T \delta\boldsymbol{Q}(\boldsymbol{u}) + \delta\boldsymbol{\lambda}^T \boldsymbol{Q}(\boldsymbol{u})\}\, d\Omega$$

$$\boldsymbol{Q}(\boldsymbol{u}) = 0;\ in\ \Omega \text{ or } \Gamma$$

Letter "λ" is known as Lagrange multiplier. It physically constrains the initial equation (4.16). Reissner's Mixed Variational Theorem attempts to create C-0 continuity of the transversal stresses (σ_z, σ_{xz} and σ_{yz}) in equation (4.17) without explicitly link to the displacement fields. First of all, the stresses are split into in-plane and out-of-plane stresses with indexes "s" and "n", respectively. Then, the constrain function "Q" is assigned to the normal stresses:

$$\int_\Omega [\delta\boldsymbol{\nabla u}^T : \boldsymbol{C} : \boldsymbol{\nabla u}]\, d\Omega = \int_\Omega \{[\delta\boldsymbol{\nabla u}^T : \boldsymbol{C} : \boldsymbol{\nabla u}]_s + [\delta\boldsymbol{\nabla u}^T : \boldsymbol{Q}(\boldsymbol{u})]_n + \boldsymbol{\lambda}^T \delta\boldsymbol{Q}(\boldsymbol{u})\}\, d\Omega \tag{4.18}$$

Next, the Lagrange multiplier is supposed to take the following form:

$$\boldsymbol{\lambda} = (\boldsymbol{\nabla u})_n^G - (\boldsymbol{\nabla u})_n^H \tag{4.19}$$

Superscripts "G" and "H" stand for Geometrical relations and Hooke's constitutive relation. The constrain function "Q" is taken as an assumed stress "σ_A" field. Hence, RMVT is given by:

$$\delta\Pi_e - \delta M = \int_\Omega \left\{[\delta\boldsymbol{\nabla u}^T : \boldsymbol{\sigma}_H]_s + [\delta\boldsymbol{\nabla u}^T : \boldsymbol{\sigma}_A]_n + \delta\boldsymbol{\sigma}_A\{(\boldsymbol{\nabla u})_n^G - (\boldsymbol{\nabla u})_n^H\}\right\} d\Omega \tag{4.20}$$

Depending on the continuity characteristics of the approximate variable fields used, RMVT may render weak or strong formulations. Just like the irreducible formulation, the mixed formulations also have limitations and requirements to achieve a stable and convergent solution. For instance, the number of unknown variables of the reducible type "N_{ru}" must be greater than the number of unknown variables of the irreducible type "N_{iu}". For the structural case (ZIENKIEWICZ; TAYLOR, 2000a):

$$N_\sigma \geq N_u \tag{4.21}$$

Also, the elements formulated in this way do not always pass the single patch test, but a mesh with two or more elements might. Therefore, the reduced-selective integration of these elements is more intricate.

4.2.2 Finite Element Formulation: Plates and Shells

In FEM, the discretized problem has a phenomenological response, which is dependent on the microscopic behavior of the material in which the domain is built. This macroscopic response is given by the structural inertial, dissipative and stiffness matrices. These matrices are an outcome of the method used to derive the elementary governing equations. If the virtual displacement "δu" in virtual work formulation or the weighting function "W" in the generalized MWR respect the mathematical continuity requirements of the respective integrals and the essential and natural BCs of the problem, the resulting structural matrices and boundary equations yield a strong formulation. This is true, even if the system is being solved without discretization (e.g. via Ritz's, RBF). If any of these requirements is not fulfilled, the resulting discretized (or not) structural problem is simpler to implement and integrate, but render weak solutions with inherent pathologies.

The FEM provides weak solutions, because the interpolation functions do not always fulfill the continuity requirements and, besides, Neumann's BCs are usually disregarded. That is because the elements are formulated without previous knowledge of the boundary value problem and it should still fit general purpose problems. On the other hand, Dirichlet's BCs are properly described in the FEM formulation through PVD. Hence, the *FEM is a weak solution*

method. Nonetheless, FEM is also capable of yielding exact results (HUEBNER; THORNTON, 1982, ZIENKIEWICZ; TAYLOR, 2000a, 2000b).

Regardless of the method through which the governing equations are derived, when the domain is split into "N_e" elementary sub-domains, the local approximate functions must be chosen according to the global and local problem. In FEM, each formulation is referenced as a different element. These elements may differ according to the physics of the problem, geometric considerations and dimensionality and numeric corrections.

Plate elements comprises a class of 2D elements with their main simplification being the elimination of the thickness coordinate. This kinematic simplification is usually performed according to one of techniques listed in section 3.1. The geometric or shape simplification, on the other hand, may or may not be required. If the plate is assumed to be a square flat plate with sides parallel with the coordinate direction, then the spatial independent variables of the global coordinates can be used to the local solution with straightforward translation of the global coordinate system variables. Unfortunately, this is not the usual case. Figure 23 depicts two surfaces discretized as an assembly of flat square or triangular plate elements.

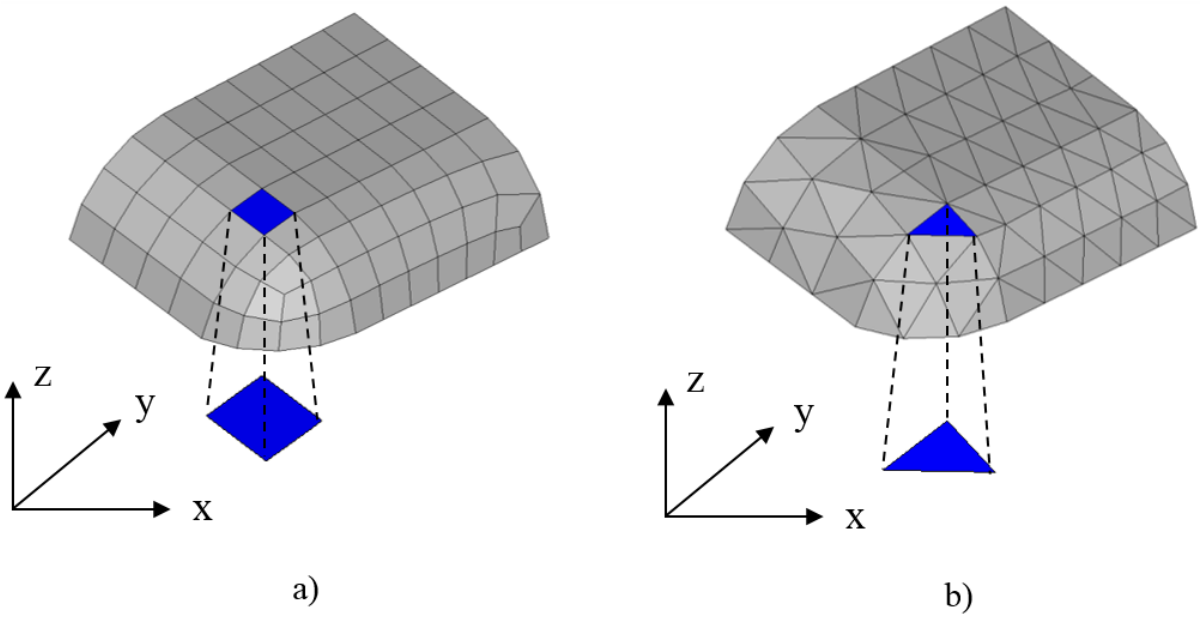

Figure 23. Discretized generic surface: a) square elements; b) triangular elements

Regarding the shape of the original surface, due to the lack of computational resources in the past, plate-like structures were split into *plate* and *shell* categories. The first was developed to discretize plan thin structures whereas the second should discretize thin curved structures.

To account for surface curvatures, the kinematics of shell elements is commonly derived in spherical coordinates ("r", "α", "β"). However, the mathematics is always more delicate than the case of plate elements. Mainly, because instead of a rotated or a translated CS, the equations must handle two angles as independent variables. Fortunately, nowadays, the computers are powerful enough to allow the representation of curved structures as assembly of small flat elements. However, even then, shell formulations are sometimes required in engineering cases with millions of DOFs or a highly non-linear material and/or geometrical behavior.

Once most of the real plate-like structures are 3D surfaces exhibiting some curvature, the word *shell* is used in the literature to reference a generic surface, despite the fact this local curvature tends to zero as the element size is reduced. Since shell structures are always 3D, the corresponding *shell formulations* are always derived in a 3D fashion or in an axis-symmetric way. On the other hand, flat plate structures can be formulated disregarding one of the independent spatial variables from the start, and hence the entire problem is 2D.

The shell structure can be split into a 2D kinematic plate problem and a 3D shape problem. When plate/shell elements are derived this way, they are tagged as *3D degenerated/continuum plate/shell element (DPSE)*. The interpolation functions used to solve the 3D geometric problem are also referenced as *shape functions*. It is interesting at this point to introduce the concepts of *sub-parametric*, *iso-parametric* and *super-parametric* element. To explain the concept, it is supposed that the interpolation functions are polynomial-like functions of the independent spatial variables. If the order of the polynomial used to interpolate, the dependent field variable (e. g. "$\psi(x, y, x)$") is greater than the order of the polynomial used to interpolate the spatial coordinates (e.g. "x", "y" and "z") into a local problem (e.g. "ξ", "η" and "ζ"), the DPSE is classified as *sub-parametric*. The reverse situation classifies the DPSE as *super-parametric*. If the orders of the interpolations coincide, then the formulation is *iso-parametric*.

The FEM needs the development of the structural inertial, dissipative and stiffness matrices, which account for a particular kinematics and physical behavior. In this process, there are shape interpolations and field interpolations to be considered. For shells elements, both interpolations are needed. Hence, a Local Coordinate System (LCS) is usually established based on the Global coordinate system (GCS). Governing equations are normally written in the GCS.

Shape interpolations are exemplified in equation (4.22) in natural coordinates (LCS) and the field interpolations are shown in equation (4.14) in the GCS.

$$\boldsymbol{x}(\xi,\eta,\zeta) = \sum_{k=1}^{N_r} N_i(\xi,\eta,\zeta)\boldsymbol{x}_i \tag{4.22}$$

$$\boldsymbol{\psi}(x,y,z) = \sum_{i=1}^{N_r} H_i(x,y,z)\boldsymbol{\psi}_i \tag{4.23}$$

Since the governing equations can be written at the element level, and, to ease the integration procedure, the governing equations are integrated in the natural coordinate system. This demands a coordinate transformation. To move the interpolation functions from the GCS to the LCS, a chain rule is applied and the derivatives are given by:

$$\begin{Bmatrix} \frac{\partial N_i}{\partial \xi} \\ \frac{\partial N_i}{\partial \eta} \\ \frac{\partial N_i}{\partial \zeta} \end{Bmatrix} = \begin{bmatrix} \frac{\partial x}{\partial \xi} & \frac{\partial y}{\partial \xi} & \frac{\partial z}{\partial \xi} \\ \frac{\partial x}{\partial \eta} & \frac{\partial y}{\partial \eta} & \frac{\partial z}{\partial \eta} \\ \frac{\partial x}{\partial \zeta} & \frac{\partial y}{\partial \zeta} & \frac{\partial z}{\partial \zeta} \end{bmatrix} \begin{Bmatrix} \frac{\partial N_i}{\partial x} \\ \frac{\partial N_i}{\partial y} \\ \frac{\partial N_i}{\partial z} \end{Bmatrix} = \boldsymbol{J} \begin{Bmatrix} \frac{\partial N_i}{\partial x} \\ \frac{\partial N_i}{\partial y} \\ \frac{\partial N_i}{\partial z} \end{Bmatrix} \tag{4.24}$$

The matrix "J" is the *Jacobian Matrix*. For an element with "N_r" nodes, if (4.22) is inserted into "J":

$$\boldsymbol{J} = \begin{bmatrix} \sum_{i=1}^{N_r} \frac{\partial N_i(\xi,\eta,\zeta)}{\partial \xi} x_i & \sum_{i=1}^{N_r} \frac{\partial N_i(\xi,\eta,\zeta)}{\partial \xi} y_i & \sum_{i=1}^{N_r} \frac{\partial N_i(\xi,\eta,\zeta)}{\partial \xi} z_i \\ \sum_{i=1}^{N_r} \frac{\partial N_i(\xi,\eta,\zeta)}{\partial \eta} x_i & \sum_{i=1}^{N_r} \frac{\partial N_i(\xi,\eta,\zeta)}{\partial \eta} y_i & \sum_{i=1}^{N_r} \frac{\partial N_i(\xi,\eta,\zeta)}{\partial \eta} z_i \\ \sum_{i=1}^{N_r} \frac{\partial N_i(\xi,\eta,\zeta)}{\partial \zeta} x_i & \sum_{i=1}^{N_r} \frac{\partial N_i(\xi,\eta,\zeta)}{\partial \zeta} y_i & \sum_{i=1}^{N_r} \frac{\partial N_i(\xi,\eta,\zeta)}{\partial \zeta} z_i \end{bmatrix} \tag{4.25}$$

Applying equation (4.22) into equation (4.16) and ignoring the "time" variable in this moment:

$$\int_{\Omega} \{\rho\ddot{\boldsymbol{u}}(\xi,\eta,\zeta)\cdot\delta\boldsymbol{u}(\xi,\eta,\zeta)+\delta\boldsymbol{\nabla u}^{T}(\xi,\eta,\zeta)\colon\boldsymbol{C}\colon\boldsymbol{\nabla u}(\xi,\eta,\zeta)-\boldsymbol{b}(\xi,\eta,\zeta)\cdot\delta\boldsymbol{u}(\xi,\eta,\zeta)\}\,|\boldsymbol{J}(\xi,\eta,\zeta)|d\xi d\eta d\zeta = \int_{\Gamma}\boldsymbol{T}^{*}(\xi,\eta,\zeta)\cdot\delta\boldsymbol{u}(\xi,\eta,\zeta)\,d\Gamma_{(\xi,\eta,\zeta)} \tag{4.26}$$

After interpolation, the structural matrices can be identified from equation (4.26). They are isolated in equation (4.27).

In equation (4.27), the sub-scripts “i”, “j”, “k” and “l” are related to nodal number. “Nr” is the number of nodes in the structure. To derive the element equations, one must insert the kinematics of each displacement field into (4.27) and perform the integrations.

$$[\boldsymbol{M}] = \int_{\Omega}\rho H_i H_j\,|\boldsymbol{J}|d\Omega_{(\xi,\eta,\zeta)} \tag{4.27}$$

$$[\boldsymbol{K}] = \int_{\Omega}\partial H_i C_{ijkl}\partial H_l\,|\boldsymbol{J}|d\Omega_{(\xi,\eta,\zeta)}$$

$$[\boldsymbol{F}] = \int_{\Omega}\boldsymbol{\rho}H_i\,|\boldsymbol{J}|\Omega_{(\xi,\eta,\zeta)}$$

$$[\boldsymbol{\Pi}] = \int_{\Omega}\boldsymbol{T}^{*}H_i\,|\boldsymbol{J}|d\Gamma_{(\xi,\eta,\zeta)}$$

$$\{i,j,k,l\}\,\epsilon\,N_r$$

It can be noted that, if equation (4.27) is being evaluated at element level, the construction of the structural global matrices requires a further connectivity step. This connectivity matrix “A” is composed of zeros and ones to indicate uncoupling and coupling of local and global nodes in non-structured meshes, respectively. For an elementary structural matrix “$K^{(e)}$”, there will be “N_r” nodes to be mapped onto “N” global nodes:

$$\{\boldsymbol{K}\}^{G}_{Nx1} = [\boldsymbol{A}]_{NxNr}\{\boldsymbol{K}\}^{(e)}_{Nrx1} \tag{4.28}$$

It is clear that when solving (4.28), there will be many zeros in the global structural matrices. If the non-zero values are grouped close to the trace of the matrix, the matrix is said to be sparse or a band matrix (Figure 24).

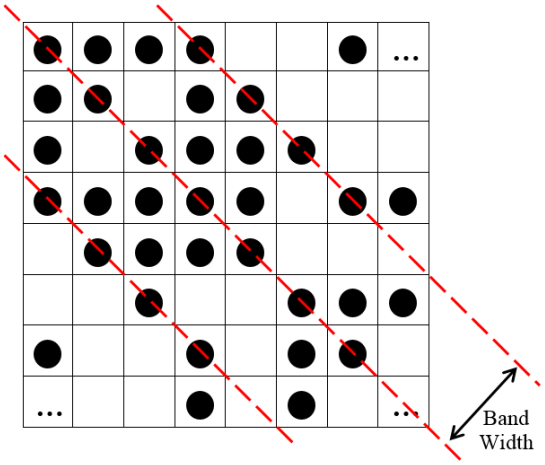

Figure 24. Sparse matrix "K"

The main advantage of this sparseness is the possibility to exchange a global matrix problem to small vector problems. This can severely reduce the amount of computation loops and memory requirements.

Back at the element level, each choice of kinematics for (4.27) yields a different set of continuity requirements, which is linked to the number of nodes of the element. Thus, infinite structural matrices can be devised. Based on the multi-layered plate formulations found in the literature, it is very appealing that all multi-layered plate formulations be grouped into a single one. The already mentioned Unified Formulations. If such theories are implemented in a FEM code, the possibilities are endless. Both CUF and GUF kernels will be derived next in the frame of FE and weak solutions.

4.2.3 Finite Element Kernels

When deriving the structural matrices via CUF, the outcome are FE *kernel* matrices from which infinity plate formulations can be derived and solved via FEM. This provides a way to properly compare different plate formulations because the only changing variables are the maximum order of expansion of the thickness coordinate. Therefore, the differences in the results can be directly related to the change of the plate formulation.

The full derivation process of CUF's kernel is herein shortened for both PVD and RMVT derivations. The GCS ("x-y-z") is adopted to derive CUF without loss of generality.

Carrera (2003b) assumed an iso-parametric element description for the displacement and transversal stress variables. Then, the shape functions and the vectors of nodal displacement variables “q” and transversal shear stresses “g” are:

$$\begin{aligned}
&\boldsymbol{u}_t^k = N_i \boldsymbol{q}_{\tau i}^k \\
&\boldsymbol{q}_{\tau i}^k = \left\{ \boldsymbol{u}_{\tau i}^k \; \boldsymbol{v}_{\tau i}^k \; \boldsymbol{w}_{\tau i}^k \right\}^T \\
&\boldsymbol{\sigma}_{nt}^k = N_i \boldsymbol{g}_{\tau i}^k \\
&\boldsymbol{g}_{\tau i}^k = \left\{ \boldsymbol{\sigma}_{xz\tau i}^k \; \boldsymbol{\sigma}_{yz\tau i}^k \; \boldsymbol{\sigma}_{zz\tau i}^k \right\}^T
\end{aligned} \tag{4.29}$$

Assuming linear small strains and putting the displacement equations from (4.29) into (4.16), the PVD FE kernel is single 3x3 symmetric matrix in equation (4.30). Else, by putting the displacements and the stresses from equation (4.29) into equation (4.20), the RMVT FE kernel are the four 3x3 matrices in equation (4.31).

$$\begin{aligned}
&\delta^{PVD}\Pi_i^k = \delta \boldsymbol{q}_{\tau i}^{kT} \boldsymbol{K}^{k\tau sij} \boldsymbol{q}_{sj}^k \\
&\boldsymbol{P}_{\tau i}^k = \boldsymbol{K}^{k\tau sij} \boldsymbol{q}_{sj}^k \\
&\boldsymbol{K}^{k\tau sij} = \langle \nabla_p^T (N_i \boldsymbol{I}) Z_{pp}^{k\tau s} \nabla_p \left(N_j \boldsymbol{I} \right) + N_i Z_{nn}^{k\tau, zs, z} N_j + \nabla_p^T (N_i \boldsymbol{I}) Z_{pn}^{k\tau s} \nabla_n \left(N_j \boldsymbol{I} \right) \\
&\qquad + \nabla_n^T (N_i \boldsymbol{I}) Z_{np}^{k\tau s} \nabla_p \left(N_j \boldsymbol{I} \right) + \nabla_n^T (N_i \boldsymbol{I}) Z_{nn}^{k\tau s} \nabla_n \left(N_j \boldsymbol{I} \right) + \nabla_p^T (N_i \boldsymbol{I}) Z_{pn}^{k\tau s, z} N_j \\
&\qquad + \nabla_n^T (N_i \boldsymbol{I}) Z_{nn}^{k\tau s, z} N_j + N_i Z_{np}^{k\tau, zs} \nabla_p \left(N_j \boldsymbol{I} \right) + N_i Z_{nn}^{k\tau, zs} \nabla_n (N_j \boldsymbol{I}) \rangle_\Sigma
\end{aligned} \tag{4.30}$$

$$\begin{aligned}
&\delta^{RMVT}\Pi_i^k = \begin{Bmatrix} \delta \boldsymbol{q}_{\tau i}^k \\ \delta \boldsymbol{g}_{\tau i}^k \end{Bmatrix}^T \begin{bmatrix} \boldsymbol{K}_{uu}^{k\tau sij} & \boldsymbol{K}_{u\sigma}^{k\tau sij} \\ \boldsymbol{K}_{\sigma u}^{k\tau sij} & \boldsymbol{K}_{\sigma\sigma}^{k\tau sij} \end{bmatrix} \begin{Bmatrix} \delta \boldsymbol{q}_{sj}^k \\ \delta \boldsymbol{g}_{sj}^k \end{Bmatrix} \\
&\begin{Bmatrix} \boldsymbol{P}_{\tau i}^k \\ 0 \end{Bmatrix}^T = \begin{bmatrix} \boldsymbol{K}_{uu}^{k\tau sij} & \boldsymbol{K}_{u\sigma}^{k\tau sij} \\ \boldsymbol{K}_{\sigma u}^{k\tau sij} & \boldsymbol{K}_{\sigma\sigma}^{k\tau sij} \end{bmatrix} \begin{Bmatrix} \boldsymbol{q}_{sj}^k \\ \boldsymbol{g}_{sj}^k \end{Bmatrix}
\end{aligned} \tag{4.31}$$

$$\begin{aligned}
&\boldsymbol{K}_{uu}^{k\tau sij} = \langle \nabla_p^T (N_i \boldsymbol{I}) Z_{pp}^{k\tau s} \nabla_p \left(N_j \boldsymbol{I} \right) \rangle_\Sigma \\
&\boldsymbol{K}_{u\sigma}^{k\tau sij} = \langle \nabla_p^T (N_i \boldsymbol{I}) Z_{pn}^{k\tau s} N_j + \nabla_n^T (N_i \boldsymbol{I}) E^{\tau s} N_j + N_i E^{\tau, zs} \left(N_j \boldsymbol{I} \right) \rangle_\Sigma \\
&\boldsymbol{K}_{\sigma u}^{k\tau sij} = \langle -N_i Z_{np}^{k\tau s} \nabla_p \left(N_j \boldsymbol{I} \right) + N_i E^{\tau s} \nabla_n \left(N_j \boldsymbol{I} \right) + N_i E^{\tau s, z} \left(N_j \boldsymbol{I} \right) \rangle_\Sigma \\
&\boldsymbol{K}_{\sigma\sigma}^{k\tau sij} = -\langle N_i Z_{nn}^{k\tau s} N_j \rangle_\Sigma
\end{aligned}$$

Where the following acronyms were used:

$$E^{\tau s}; E^{\tau,zs}; E^{\tau s,z} = \langle F_\tau F_s; F_{\tau,z} F_s; F_\tau F_{s,z} \rangle_z \tag{4.32}$$

$$Z_{pp}^{k\tau s}; Z_{pn}^{k\tau s}; Z_{np}^{k\tau s}; Z_{nn}^{k\tau s} = \langle \bar{C}_{pp}^k F_\tau F_s; \bar{C}_{pn}^k F_\tau F_s; \bar{C}_{np}^k F_\tau F_s; \bar{C}_{nn}^k F_\tau F_s \rangle_z$$

$$Z_{nn}^{k\tau,zs,z}; Z_{pn}^{k\tau s,z}; Z_{nn}^{k\tau s,z}; Z_{np}^{k\tau,zs}; Z_{nn}^{k\tau,zs}$$

$$= \langle \bar{C}_{nn}^k F_{\tau,z} F_{s,z}; \bar{C}_{pn}^k F_\tau F_{s,z}; \bar{C}_{nn}^k F_\tau F_{s,z}; \bar{C}_{np}^k F_{\tau,z} F_s; \bar{C}_{nn}^k F_{\tau,z} F_s \rangle_z$$

$$\langle \mathcal{B} \rangle_\Sigma = \int \mathcal{B} d\Sigma \,; \langle \mathcal{F} \rangle_z = \int \mathcal{F} dz \,; \;\; \Sigma \cup z = \Omega$$

$$n = normal\ direction; \; p = in - plane\ directions$$

Applying the same procedure above to the inertial term, the consistent inertial kernel matrix, valid for both PVD and RMVT is:

$$\delta \boldsymbol{M}^k = \ddot{\boldsymbol{q}}_{\tau i}^{kT} \boldsymbol{M}^{k\tau sij} \delta \boldsymbol{q}_{sj}^k \tag{4.33}$$

$$\boldsymbol{M}^{k\tau sij} = \langle N_i \rho_{ij}^{k\tau s} N_j \rangle_\Sigma$$

Of great importance in dynamic problems, although not detailed in this work, is the need of a dissipative structural matrix. Using CUF, a consistent dissipative kernel can be attained analogously as:

$$\delta \boldsymbol{C}^k = \dot{\boldsymbol{q}}_{\tau i}^{kT} \boldsymbol{C}^{k\tau sij} \delta \boldsymbol{q}_{sj}^k \tag{4.34}$$

$$\boldsymbol{C}^{k\tau sij} = \langle N_i c_{ij}^{k\tau s} N_j \rangle_\Sigma$$

However, equation (4.34) is based on the microscopic dissipative characteristics of the continuum material. This microscopic behavior is usually overlooked for stiff materials and the macroscopic damping behavior is achieved through experimental analyses. Such phenomenological response is frequency ("ω") (or mode) dependent. It is normally approached with further introduction and work of a complex constitutive tensor "C":

$$\boldsymbol{C} = \boldsymbol{C}(\omega) = \boldsymbol{C}_s + i\boldsymbol{C}_l(\omega) = \boldsymbol{C}_s[1 + i\eta(\omega)] \tag{4.35}$$

The ratio of loss "C_l" and storage "C_s" and loss moduli gives the loss factor "η" (TITA, 1999, TITA; CARVALHO; LIRANI, 2001, TITA; CARVALHO; LIRANI, 2003).

After integration through the thickness, the elementary matrices are written at the ply level. Analogously to equations (3.53), (3.54) and (3.55), the ESL, LW and RMVT-ESL FE asseambleges can be seen in equations (4.36), (4.37) and (4.38), respectevely.

$$\begin{Bmatrix} P_x \\ P_y \\ P_z \end{Bmatrix}_i^T = \sum_{k=1}^{k=N_l} \begin{bmatrix} K_{uu}^{k\tau sij} & K_{uv}^{k\tau sij} & K_{uw}^{k\tau sij} \\ & K_{vv}^{k\tau sij} & K_{vw}^{k\tau sij} \\ sym & & K_{ww}^{k\tau sij} \end{bmatrix} \begin{Bmatrix} u \\ v \\ w \end{Bmatrix}_j = \left[\boldsymbol{K}^{(e)}\right] \begin{Bmatrix} u \\ v \\ w \end{Bmatrix}_j \tag{4.36}$$

$$K_{uu}^{\tau sij} = \sum_{k=1}^{k=N_l} K_{uu}^{k\tau sij}$$

$$size_{ESL}^{PVD}\left(K^{(e)}\right) = 3N_\tau \times 3N_\tau; DOF_{ESL}^{PVD}\left(K^{(e)}\right) = 3N_\tau N_r$$

$$\begin{Bmatrix} P_x^{tk_1} \\ \vdots \\ P_x^{tk_1} = P_x^{tk_2} \\ \vdots \\ P_x^{bk_{(Nl-1)}} = P_x^{tk_{Nl}} \\ \vdots \\ P_x^{bk_{Nl}} \end{Bmatrix}_{m\times 1}^T = \left[\boldsymbol{K}_{uu}^{\tau sij}\right]_{m\times m} \times \begin{Bmatrix} u^{tk_1} \\ \vdots \\ u^{bk_1} = u^{tk_2} \\ \vdots \\ u^{bk_{(Nl-1)}} = u^{tk_{Nl}} \\ \vdots \\ u^{bk_{Nl}} \end{Bmatrix}_{m\times 1} \tag{4.37}$$

$$\left[\boldsymbol{K}_{uu}^{\tau sij}\right]_{m\times m} =$$

$$\begin{bmatrix} \begin{pmatrix} \kappa^{ttk_1} & \cdots & \kappa^{tbk_1} \\ \vdots & \ddots & \vdots \\ \kappa^{btk_1} & \cdots & \kappa^{bbk_1} + \kappa^{ttk_2} \end{pmatrix}_{\tau\times s} & \cdots & 0 \\ \vdots & \ddots & \vdots \\ 0 & \cdots & \begin{pmatrix} \kappa^{bbk_{(Nl-1)}} + \kappa^{ttk_{Nl}} & \cdots & \kappa^{tbk_{Nl}} \\ \vdots & \ddots & \vdots \\ \kappa^{btk_{Nl}} & \cdots & \kappa^{bbk_{Nl}} \end{pmatrix}_{\tau\times s} \end{bmatrix}_{m\times m}$$

$$m = (N_l - 1)(N_\tau - 1) + N_\tau$$

$$size_{LW}^{PVD}\left(K^{(e)}\right) = 3m \times 3m;\ DOF_{LW}^{PVD}\left(K^{(e)}\right) = 3mN_r$$

$$\left[\boldsymbol{K}_{u\sigma}^{\tau sij}\right]_{\tau\times m} \tag{4.38a}$$

$$= \left[\begin{pmatrix} \kappa^{ttk_1} & \cdots & \kappa^{tbk_1} + \kappa^{tbk_2} \\ \vdots & \ddots & \vdots \\ \kappa^{btk_1} & \cdots & \kappa^{bbk_1} + \kappa^{bbk_2} \end{pmatrix}_{\tau\times s} \quad \cdots \quad \begin{pmatrix} \kappa^{ttk_{(Nl-1)}} + \kappa^{ttk_{Nl}} & \cdots & \kappa^{tbk_{Nl}} \\ \vdots & \ddots & \vdots \\ \kappa^{btk_{(Nl-1)}} + \kappa^{btk_{Nl}} & \cdots & \kappa^{bbk_{Nl}} \end{pmatrix}_{\tau\times s} \right]_{\tau\times}$$

$$\left[\boldsymbol{K}_{\sigma u}^{\tau sij}\right]_{m\times s}=\begin{bmatrix}\begin{pmatrix}\kappa^{ttk_1} & \cdots & \kappa^{tbk_1}\\ \vdots & \ddots & \vdots\\ \kappa^{btk_1}+\kappa^{btk_2} & \cdots & \kappa^{bbk_1}+\kappa^{bbk_2}\end{pmatrix}_{\tau\times s}\\ \vdots\\ \begin{pmatrix}\kappa^{ttk_{(Nl-1)}}+\kappa^{ttk_{Nl}} & \cdots & \kappa^{tbk_{(Nl-1)}}+\kappa^{tbk_{Nl}}+\\ \vdots & \ddots & \vdots\\ \kappa^{btk_{Nl}} & \cdots & \kappa^{bbk_{Nl}}\end{pmatrix}_{\tau\times s}\end{bmatrix}_{m\times s} \tag{4.38b}$$

$$size_{ESL}^{RMVT}(K_{u\sigma})=3N_\tau\times 3m;\ size_{ESL}^{RMVT}(K_{\sigma u})=3m\times 3N_s$$
$$size_{ESL}^{RMVT}(K_{\sigma\sigma})=3m\times 3m;\ size_{ESL}^{RMVT}(K_{uu})=3N_\tau\times 3N_\tau$$

Grouping the size and DOFs of all FE kernels for an element of N_r nodes:

$$\begin{aligned}
&size_{ESL}^{PVD}\left(K^{(e)}\right)=3N_\tau\times 3N_\tau && DOF_{ESL}^{PVD}\left(K^{(e)}\right)=3N_\tau N_r\\
&size_{LW}^{PVD}\left(K^{(e)}\right)=3m\times 3m && DOF_{LW}^{PVD}\left(K^{(e)}\right)=3mN_r\\
&size_{ESL}^{RMVT}\left(K^{(e)}\right)=3(N_\tau+m)\times 3(N_\tau+m) && DOF_{ESL}^{RMVT}\left(K^{(e)}\right)=3(N_\tau+m)N_r\\
&size_{LW}^{RMVT}\left(K^{(e)}\right)=6m\times 6m && DOF_{LW}^{RMVT}\left(K^{(e)}\right)=6mN_r
\end{aligned} \tag{4.39}$$

For Demasi (DEMASI, 2008, DEMASI, 2009a, 2009b, 2009c, 2009d, 2009e, 2009f, DEMASI, 2012), the PVD FE stiffness kernel becomes:

$$K^{k\tau sij}=\begin{bmatrix}K_{u_{\alpha_u}u_{\alpha_u}}^{k\tau sij} & K_{u_{\alpha_u}v_{\alpha_v}}^{k\tau sij} & K_{u_{\alpha_u}w_{\alpha_w}}^{k\tau sij}\\ & K_{v_{\alpha_v}v_{\alpha_v}}^{k\tau sij} & K_{v_{\alpha_v}w_{\alpha_w}}^{k\tau sij}\\ sym & & K_{w_{\alpha_w}w_{\alpha_w}}^{k\tau sij}\end{bmatrix} \tag{4.41}$$

For the RMVT case, the GUF's kernel is explicitly given by:

$$\left[\boldsymbol{K}^{k\tau sij}\right]=\begin{bmatrix}K_{u_{\alpha_u}u_{\alpha_u}}^{k\tau sij} & K_{u_{\alpha_u}v_{\alpha_v}}^{k\tau sij} & 0 & K_{u_{\alpha_u}\sigma_{\alpha_{\sigma_{zx}}}}^{k\tau sij} & 0 & K_{u_{\alpha_u}\sigma_{\alpha_{\sigma_{zz}}}}^{k\tau sij}\\ & K_{v_{\alpha_v}v_{\alpha_v}}^{k\tau sij} & 0 & 0 & K_{v_{\alpha_v}\sigma_{\alpha_{\sigma_{zy}}}}^{k\tau sij} & K_{v_{\alpha_v}\sigma_{\alpha_{\sigma_{zz}}}}^{k\tau sij}\\ & & 0 & K_{w_{\alpha_w}\sigma_{\alpha_{\sigma_{zx}}}}^{k\tau sij} & K_{w_{\alpha_w}\sigma_{\alpha_{\sigma_{zy}}}}^{k\tau sij} & K_{w_{\alpha_w}\sigma_{\alpha_{\sigma_{zz}}}}^{k\tau sij}\\ & & & K_{\sigma_{\alpha_{\sigma_{zx}}}\sigma_{\alpha_{\sigma_{zx}}}}^{k\tau sij} & 0 & 0\\ & sym & & & K_{\sigma_{\alpha_{\sigma_{zy}}}\sigma_{\alpha_{\sigma_{zy}}}}^{k\tau sij} & 0\\ & & & & & K_{\sigma_{\alpha_{\sigma_{zz}}}\sigma_{\alpha_{\sigma_{zz}}}}^{k\tau sij}\end{bmatrix} \tag{4.42}$$

For all three ESL, ESL-RMVT and LW assemblages, the amount of DOFs of the elementary matrix must be re-calculated:

$$
\begin{aligned}
&size_{ESL}^{PVD}\left(K^{(e)}\right) = \tilde{n} \times \tilde{n} && DOF_{ESL}^{PVD}\left(K^{(e)}\right) = \tilde{n}N_r \\
&size_{LW}^{PVD}\left(K^{(e)}\right) = \tilde{m} \times \tilde{m} && DOF_{LW}^{PVD}\left(K^{(e)}\right) = \tilde{m}N_r \\
&size_{ESL}^{RMVT}\left(K^{(e)}\right) = (\tilde{n} + \tilde{m}) \times (\tilde{n} + \tilde{m}) && DOF_{ESL}^{RMVT}\left(K^{(e)}\right) = (\tilde{n} + \tilde{m})N_r \\
&size_{LW}^{RMVT}\left(K^{(e)}\right) = 2\tilde{m} \times 2\tilde{m} && DOF_{LW}^{RMVT}\left(K^{(e)}\right) = 2\tilde{m}N_r \\
&\tilde{n} = N_{\alpha_u} + N_{\alpha_v} + N_{\alpha_w} \\
&\tilde{m} = m_{\alpha_u} + m_{\alpha_v} + m_{\alpha_w} \\
&m_{\alpha_u} = (N_l - 1)\left(N_{\alpha_u} - 1\right) + N_{\alpha_u} \\
&m_{\alpha_u} = (N_l - 1)\left(N_{\alpha_v} - 1\right) + N_{\alpha_v} \\
&m_{\alpha_w} = (N_l - 1)\left(N_{\alpha_w} - 1\right) + N_{\alpha_w}
\end{aligned}
\tag{4.43}
$$

To decrease the DOFs of the RMVT, both CUF and GUC can be solved with Static Condensation Techniques (SCT) (HUEBNER; THORNTON, 1982, CRISFIELD, 1991, ZIENKIEWICZ; TAYLOR, 2000a). By this means, the mixed system can be reduced to a single corresponding PVD one. Static condensation, also known as Guyan's static condensation technique (MOULIN; KARPEL, 1998), appears more often in the context of coupling problems where two systems are excited by one common source. Fluid Structure Interactions (FSI) is an example. Hence, the two systems are coupled to yield a single system, which is normally faster and easier to solve.

In the case of CUF and GUF, depending on the solution procedure, such elimination can be performed at element, ply or structure level. If it is applied at structure level, then the solutions with and without SCT are the same. However, at ply and element level, some differences are seen. This technique is commonly used in 2D analyses to remove the DOFs related to internal nodes of heavy element, because these nodes do not have a direct coupling with the neighboring elements. The procedure is very simple, it stems from the system of equations in (4.31). A change of variables at element level (after integration of the stiffness matrices across the thickness) yields the elementary stiffness matrices containing only displacement variables:

$$\begin{Bmatrix} \boldsymbol{P} \\ 0 \end{Bmatrix}^T = \boldsymbol{P};\ \begin{Bmatrix} \boldsymbol{q} \\ \boldsymbol{g} \end{Bmatrix} = \boldsymbol{q}_{SCT}$$
$$\boldsymbol{K}_{SCT} = \boldsymbol{K}_{uu} - \boldsymbol{K}_{u\sigma}(\boldsymbol{K}_{\sigma\sigma})^{-1}\boldsymbol{K}_{\sigma u} \tag{4.44}$$
$$\boldsymbol{K}_{SCT}\boldsymbol{q}_{SCT} = \boldsymbol{P}$$

Condensation techniques is one of many numerical techniques and issues found in the scope FE solutions. The next section cover some of the main numeric issues, which are commonly encountered.

4.3 Numerical techniques

A revision on the thin and thick plate concepts is advised in FEM. Specially in dynamics analyses. Besides the span-to-thickness ratio threshold between theories, the boundary conditions of the problem and its time scale should be considered too.

The boundary conditions will define if the shell limits comprise a thin or a thick plate. Perhaps different approaches are needed for a shell with a constant thickness throughout the whole domain if supports, welds, junctions, contacts, etc, are assigned in the model.

Second, if a dynamic simulation is performed, the time scale, also represent by wave number, is another parameter to be monitored. Depending on the time scale of the problem, the mesh may need refinement to properly resolve the structure response. Also, this can be accentuated by the boundary conditions mentioned above.

Thus, to expose the accuracy, stability, convergence, speed and size aspects of the corresponding differential plate problems, few numerical techniques and issues, which arise when FEM is used in structural plate problems, are reviewed.

4.3.1 Gauss Quadrature (GQ)

Integration of the element formulations are normally performed numerically. Gauss quadrature is the most often quote method, because it can integrate polynomial functions

exactly in a unit cubic domain (HUEBNER; THORNTON, 1982, ZIENKIEWICZ; TAYLOR, 2000a). The analytical integration is performed by using NG (Number of Gauss Points) and numerically according to:

$$F(x,y,z) = \int_{-1}^{1}\int_{-1}^{1}\int_{-1}^{1} f(x,y,z \dots x^a, y^b, z^c)\, dV = \sum_{m=1}^{NG}\sum_{n=1}^{NG}\sum_{0=1}^{NG} W_m W_n W_o f(x_m, y_n, z_o) + R \tag{4.45}$$

Hence, the analytical evaluation is traded for a triple sum of the integrand evaluated at the local coordinates ("x_m", "y_n", "z_o") multiplied by the weighting factors calculated at the respective integration points ("x_m", "y_n", "z_o"). These weighting factors are tabulated values according to the order of polynomial integrand. The Residual "R" can be brought to zero, if it is calculated for "NG^3" integration points:

$$NG \geq \frac{a+b+c+1}{2} \tag{4.46}$$

A table with weighting factors for a polynomial function up to the 8th order can be found in Huebner and Thornton (1982).

One notices that the number of integration points, within the unit cubic domain, required for exact (full) integration, grows with the dimension of the problem and with the non-linearity of the integrand. Sometimes, this requirement is too strong or too expensive for a particular formulation. This is also an incentive for pure 2D formulations, because the number of integration points greatly decreases. However, as an alternative, the number of integration points is lowered and a "*reduced*" integration is thereby performed.

In the context of plate formulations, this measure is usually adopted when the phenomenon of *shear-bending locking* arises. Despite the fact that reduced integration can overcome this pathology, the solution itself yields a new one. This new problem is the appearance of more of the so-called *spurious energy modes*. These modes are related to an unreal uncontrolled displacement of the internal nodes of the mesh due to the relaxation provided by the reduced integration. This should be avoided in structural analysis because the problem's strain energy will either diverge the solution or deform wrong regions of the domain.

4.3.2 Shear-Bending Locking

Shear-bending locking, or shear locking or just locking, are term arose in the literature of shear-bending problems, because due to the use of a thick plate formulation on a thin shell.

Since the coupling terms are somewhat hidden in the PVD and RMVT statements, the shear-bending coupling of an isotropic material will be exposed for study. For a linear small strain theory, the equilibrium equations of the shear-bending problem only, with displacements "w" and rotation's "θ" gives the system (ZIENKIEWICZ; TAYLOR, 2000a, 2000b):

$$\begin{Bmatrix} \boldsymbol{f}_w \\ \boldsymbol{f}_\theta \end{Bmatrix} = [\boldsymbol{K}_b + \boldsymbol{K}_s] \begin{Bmatrix} \boldsymbol{w} \\ \boldsymbol{\theta} \end{Bmatrix} \tag{4.47}$$

$$[\boldsymbol{K}_b + \boldsymbol{K}_s] = \begin{bmatrix} 0 & 0 \\ 0 & \boldsymbol{K}^b_{\theta\theta} \end{bmatrix} + \begin{bmatrix} \boldsymbol{K}^s_{ww} & \boldsymbol{K}^s_{w\theta} \\ \boldsymbol{K}^s_{\theta w} & \boldsymbol{K}^s_{\theta\theta} \end{bmatrix}$$

$$\boldsymbol{K}^s_{ww} = \int_\Sigma (\nabla \boldsymbol{N}_w)^{\mathrm{T}} \alpha \nabla \boldsymbol{N}_w d\Sigma;$$

$$\boldsymbol{K}^s_{w\theta} = \boldsymbol{K}^{sT}_{\theta w} = \int_\Sigma \boldsymbol{N}_\theta{}^{\mathrm{T}} \alpha \nabla \boldsymbol{N}_w d\Sigma$$

$$\boldsymbol{K}^s_{\theta\theta=} \int_\Sigma \boldsymbol{N}_\theta{}^{\mathrm{T}} \alpha \boldsymbol{N}_\theta d\Sigma;$$

$$\boldsymbol{K}^b_{\theta\theta} = \int_\Sigma (\boldsymbol{\partial N}_\theta)^{\mathrm{T}} \boldsymbol{D} \boldsymbol{\partial N}_\theta d\Sigma$$

$$\alpha = Gh$$

From the system of equations (4.47) above, the shear-bending coupling is represented by the sum of the pure bending "K^b" and the shear induced bending "K^s" sttifnesses (the two last integrals in (4.47)). To better analyse this coupling, the inspection of these two last integrals suggests the creation of the folling ratio "$R^{s\text{-}b}$":

$$R^{s-b} = \frac{\alpha}{D/l^2} = 12(1-\upsilon^2)\frac{G}{E}\left(\frac{l}{h}\right)^2 \propto \left(\frac{l}{h}\right)^2 \tag{4.48}$$

To aid the investigation even further, main differences between thin and thick theories and their common purposes are grouped in Table 1.

Table 1 - Comparison of thin and thick plate classical theories

Thin Theory	Thick Theory
Large displacements Continuity C-1	Small Displacements Continuity C-0
Near zero transversal strains $\nabla w - \theta \approx 0$	Non-zero transversal strains $\nabla w - \theta \neq 0$

So, in shear-bending coupled problems, if a thick theory is applied to a thin element, the expected large displacement of the thin structure will be hampered by the thick formulation, because part of the energy applied to the structure is being numerically converted to transversal shear strain according to Table 1. Equation (4.47) poses a constraint so strong that the element eventually "stops moving" prematurely, i.e. "it locks". This virtual shear strain energy is also referred as *parasitic or spurious shear strain*.

Mathematically, this can be seen through equation (4.48). The pure bending stiffness matrix is inversely proportional to R^{s-b} while the bending shear induced stiffness matrix is proportional to R^{s-b}. So, if the element is sufficiently thin (usually "l/h">100) the induced bending stiffness will tend to infinity, which leads to locking of the element. On the other hand, if a thin theory is applied to a thick structure, the displacement results will be under-estimated, because the transversal displacement due to transversal shear strain is neglected.

This locking is a pathology of the plate formulation and should not be mistaken with *machine locking* (BRIASSOULIS, 1993). The latter is due to the computer's round-off (related to the machine precision), which may be reached before or regardless of the formulation locking.

Nevertheless, sometimes due to meshing difficulties or lack of better formulations, this pathology has to be overcome. The most common technique is the *reduced* or *selective* integration. The integration formula in (4.47) does not need to have the same amount of integration points in all directions. Also, the shear, bending and membrane equations can be integrated with different number of integration points as well. Naturally, inaccurate results are expected. But, this integration error may be smaller than the locking induced error, what makes the approach attractive.

If the integrations of all terms are reduced, the integration is tagged as *reduced*. If only the problematic terms (those scaled by "R^{s-b}"), or any other set of integrands are handled this

way, then integration is said *selective*. Else, if the integration is performed exactly, the procedure is termed *full* integration.

4.3.3 Spurious Energy Modes

Though straightforward and easy to implement, reduced and selective integrations give birth to additional *spurious* or *zero energy modes* (ZIENKIEWICZ; TAYLOR, 2000a, 2000b). These are due to singularities in the system of equilibrium equations integrated via reduced or selective methods. This occurs, because the number unrestrained nodal DOFs is larger than the number of independent relations (strain relations) at the integration points. Such pathology must be avoided in Computational Structural Dynamics (CSD), because it can jeopardize the solution locally or globally. This phenomenon is more common during integration of linear interpolation functions, because more spurious modes can be formed. As non-linearity increases with the order/complexity of the integrand, the modes are shifted to higher frequencies, because more elements need to be excited.

Figure 26 depicts how the nodes of a mesh can move and yield a virtual displacement of nodes whose strain energy is zero.

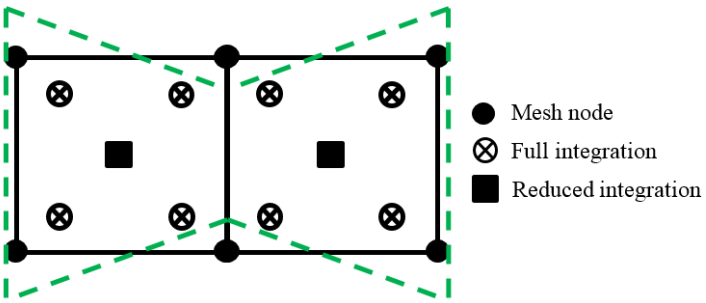

Figure 25 .Propagation of hour-glass modes through a mesh

For higher-order interpolations, the “Escher” modes (ZIENKIEWICZ; TAYLOR, 2000a) appear for a larger number of elements when reduced integration is used (Figure 26).

Therefore reduced or selective integration is not recommended. However, unfortunately, sometimes, the reduced integration is needed and these spurious modes must be controlled somehow. The methods to achieve such control are known as hour-glass control due

to the most common shape of the spurious energy modes (Figure 25). For details see Belytschko et al. (1984), Schulz (1987), Koh and Kikuchi (1987) and Zienkiewicz and Taylor (2000a).

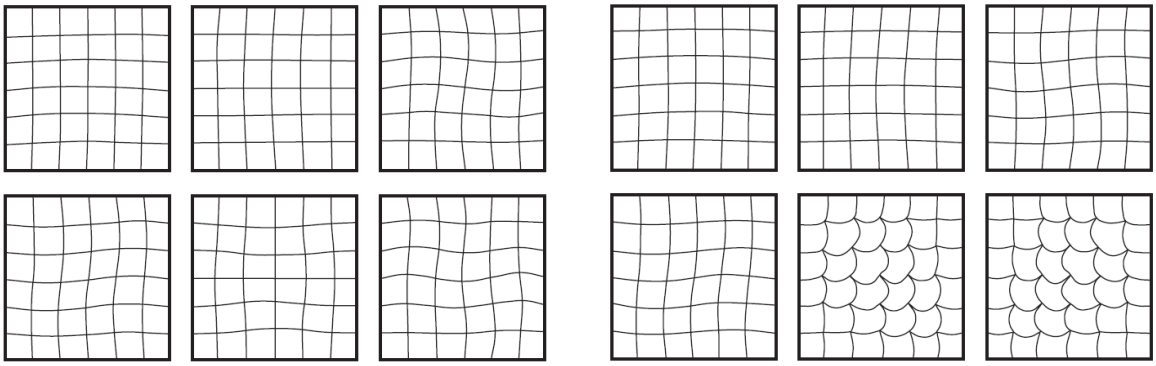

a) b)

Figure 26. First six modes of a mesh with (a) full integration and (b) reduced integration (ZIENKIEWICZ; TAYLOR, 2000a)

4.3.4 Drilling

Shell elements, in comparison with the pure 2D plate formulations, present a pathology, which is known as *drilling* (ZIENKIEWICZ; TAYLOR 2000b). This term makes reference to the shell's rotational DOF "θ_ζ" around its plane's normal direction.

This situation occurs when all elements meeting at a common node are co-planar in the solution's CS. Nodes of flat (folded) segment of elements or nodes at the straight boundaries of developable surfaces like cones (Figure 27) can be pointed as examples.

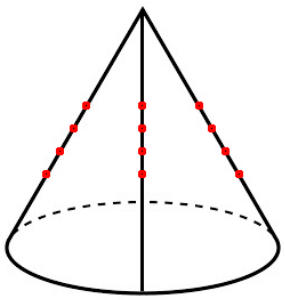

Figure 27. Cone with highlighted drilling nodes

Locally, the shell elements only have five out of six physical DOFs, because the drilling rotational stiffness is null. This gives the local singularity:

$$k_{\theta_\zeta} = 0 \rightarrow 0\theta_\zeta = 0 \tag{4.49}$$

This problem is always present for shells with 5 physical DOFs (i. e. shells without azimuthal stiffness), but when the system is solved at the GCS, this illness can be masked by the transformation of coordinates. Depending on the computer round-off error (precision) and the solution algorithm, such singularity may render an ill-posed problem with errors of different magnitudes. Therefore this pathology is usually difficult to detect.

To circumvent this debility, few techniques are available in the literature and they may be grouped into three categories (IURA; ATLURI, 1992) which:

I. Derives a displacement function where drilling is an independent DOF, which induces in-plane deformations (introduction of a fictitious drilling stiffness).
II. Derives a functional in which the drilling DOF does not induce in-plane deformation.
III. Uses higher-order theories.

As an example of the second group, which is assumed to be a better option to the use of non-physical stiffness, a variational approach from Iura and Atluri (1992) is given. For the in-plane problem, the elastic potential is modified as:

$$\overline{\Pi}_i = \Pi_i - \int_\Sigma \frac{1}{\alpha_\tau E h} \tau^2 d\Sigma \tag{4.50}$$

where "α_τ" is a penalty number and "τ" is the in-plane skew-symmetric component of the stress tensor [N/m].

4.3.5 Lumping

Lumping is the engineering term for matrix diagonalization (ZIENKIEWICZ; TAYLOR 2000a). Like STCs, it is also commonly used in FSI and CSD analyses (ARGYRIS; TENEK, 1994a, ARGYRIS; TENEK, 1994b, ARGYRIS; TENEK, 1994c, KOLMAN, et al., 2007, SHANEL; KOLMAN; PLESEK, 2012). Mathematically, to deal with diagonal matrix always reduces the size of the problem. This is strategic, since the matrix problem is converted

into a vector problem. Also, when the equation (4.9) needs to be integrated in the time domain, the marching algorithms would have uncoupled mass and damping equation. To see this, for time independent constitutive properties, let one assume the following approximate time equation:

$$[M]\left\{\ddot{\tilde{\psi}}(t)\right\} + [C]\left\{\dot{\tilde{\psi}}(t)\right\} + [K]\{\tilde{\psi}(t)\} = \{F(t)\} \tag{4.51}$$

After that, for the usual second-order equations in structural dynamics, the central difference approximation for the derivatives in time can be applied:

$$\left\{\dot{\tilde{\psi}}\right\}_t = \frac{\{\tilde{\psi}\}_{t+\Delta t} - \{\tilde{\psi}\}_{t-\Delta t}}{\Delta t + \Delta t} \tag{4.52}$$

$$\left\{\ddot{\tilde{\psi}}\right\}_t = \frac{\{\tilde{\psi}\}_{t+\Delta t} - 2\{\tilde{\psi}\}_t + \{\tilde{\psi}\}_{t-\Delta t}}{\Delta t \Delta t}$$

Equating (4.51) in (4.52) yield the following set of implicit linear algebraic equations:

$$[\bar{K}]\{\tilde{\psi}\}_{t+\Delta t} = \{\bar{F}\}_t \tag{4.53}$$

$$[\bar{K}] = \frac{1}{\Delta t^2}[M] + \frac{1}{2\Delta t}[C]$$

$$\{\bar{F}\}_t = \{F(t)\} - \left[[K] - \frac{2}{\Delta t^2}[M]\right]\{\tilde{\psi}\}_t - \left[\frac{1}{\Delta t^2}[M] - \frac{1}{2\Delta t}[C]\right]\{\tilde{\psi}\}_{t-\Delta t}$$

If the mass and damping matrices are somehow lumped, these matrices can be simply added, yielding a compact and explicit system. This equation becomes explicit; because the non-diagonal stiffness matrix only contributes to the solution at current time “t” on the RHS of (4.53), i.e. the variables calculated in the step “t” require only the variables calculated in the step “t-1”. On the other hand, for the implicit form, the variables calculated in the step “t” require not only the variables calculated in the step “t-1”, but also at the same step “t”. Moreover, the contributions of mass and damping can be summed in a vector fashion whereas the response of the stiffness matrix “K” still retains its matrix aspect.

$$\{\tilde{\psi}\}_{t+\Delta t} = [\bar{K}]^{-1}\left\{\left[\{F(t)\} + \frac{2\{\tilde{\psi}\}_t - \{\tilde{\psi}\}_{t-\Delta t}}{\Delta t^2}[M] + \frac{1}{2\Delta t}[C]\{\tilde{\psi}\}_{t-\Delta t}\right]_{lumped} - [K]\{\tilde{\psi}\}_t\right\} \tag{4.54}$$

Therefore, the store requirements for (4.54) are lower than the ones for (4.53). The same is not always true for the overall speed solution. Explicit algorithms inherent the criterion that the time interval (step) "Δt" must be smaller than a critical value "Δt_{crit}". This way, equation (4.54) is classified as *conditionally stable.* The evaluation of the maximum value for the critical time to minimize the overall solution time is naturally problem and algorithm dependent. A brief discussion on stability is given hereafter for Newmark's algorithm for completeness. Further and detailed discussions can be seen in Zienkiewicz and Taylor (2000a).

Newmark's algorithm (or implicit solution) assumes that the average acceleration over an integration time step is constant:

$$\left\{\ddot{\tilde{\psi}}\right\}_{av} = \left(\left\{\ddot{\tilde{\psi}}\right\}_{t+\Delta} + \left\{\ddot{\tilde{\psi}}\right\}_t\right)/2 \tag{4.55}$$

And, therefore, equation (4.53) changes to:

$$[\bar{K}] = \frac{4}{\Delta t^2}[M] + \frac{2}{\Delta t}[C] + [K] \tag{4.56}$$

$$\{\bar{F}\}_{t+\Delta t} = \{F(t+\Delta t)\} + [C]\left(\frac{2}{\Delta t}\{\tilde{\psi}\}_t + \left\{\dot{\tilde{\psi}}\right\}_t\right) + [M]\left(\frac{4}{\Delta t^2}\{\tilde{\psi}\}_t + \frac{4}{\Delta t}\left\{\dot{\tilde{\psi}}\right\}_t + \left\{\ddot{\tilde{\psi}}\right\}_t\right)$$

This is an implicit algorithm, which is unconditionally stable. It cannot be lumped, because the system's effective "stiffness matrix" comprises the stiffness matrix [K], which is cannot be diagonalized. Actually, this algorithm can be derived from the Newmark-β algorithm by setting with "β" equal to 0.25 and "γ" equal to 0.5 in the respective recurrence formulas:

$$\{\tilde{\psi}\}_{t+\Delta t} = \{\tilde{\psi}\}_t + \Delta t\left\{\dot{\tilde{\psi}}\right\}_t + \Delta t^2\left[\left(\frac{1}{2} - \beta\right)\left\{\ddot{\tilde{\psi}}\right\}_t + \beta\left\{\ddot{\tilde{\psi}}\right\}_{t+\Delta t}\right] \tag{4.57}$$

$$\left\{\dot{\tilde{\psi}}\right\}_{t+\Delta t} = \left\{\dot{\tilde{\psi}}\right\}_t + \Delta t\left[(1-\gamma)\left\{\ddot{\tilde{\psi}}\right\}_t + \gamma\left\{\ddot{\tilde{\psi}}\right\}_{t+\Delta t}\right]$$

To analyze the stability of the generic Newmark-β algorithm, the recurrence relations (4.57) are inserted in the equilibrium equation (4.53):

$$[\bar{K}]\{\tilde{\psi}\}_{t+\Delta t} = \{\bar{F}\}_{t+1} \tag{4.58}$$

$$[\bar{K}] = \frac{1}{\beta\Delta t^2}[M] + \frac{\gamma}{2\beta\Delta t}[C]$$

$$\{\bar{F}\}_{t+\Delta t} = \{F(t+\Delta t)\}$$
$$+ [C]\left[\left(\frac{\gamma}{\beta\Delta t}\{\tilde{\psi}\}_t + \frac{\gamma}{\beta}\left\{\dot{\tilde{\psi}}\right\}_t + \gamma\Delta t\left(\frac{1}{2\beta}-1\right)\left\{\ddot{\tilde{\psi}}\right\}_t\right)\right.$$
$$\left. - \left(\left\{\dot{\tilde{\psi}}\right\} + (1-\gamma)\Delta t\left\{\ddot{\tilde{\psi}}\right\}_t\right)\right]$$
$$+ [M]\left(\frac{1}{\beta\Delta t^2}\{\tilde{\psi}\}_t + \frac{1}{\beta\Delta t}\left\{\dot{\tilde{\psi}}\right\}_t + \left(\frac{1}{2\beta}-1\right)\left\{\ddot{\tilde{\psi}}\right\}_t\right)$$

After that, applying the Routh-Hurwitz requirements (ZIENKIEWICZ; TAYLOR, 2000a) to the system of equations above, the stability criteria can be finally defined:

$$\gamma \geq 2\beta \geq \frac{1}{2} \tag{4.59}$$

Explicit integration algorithms can be obtained by setting "β" equal to 0 back in equation (4.58). For different values of "γ", different well-known explicit time integration algorithms can be obtained:

$$\gamma = 0 \rightarrow Euler \tag{4.60}$$
$$\gamma = \frac{1}{2} \rightarrow Crank - Nicholson$$
$$\gamma = \frac{2}{3} \rightarrow Galerkin$$
$$\gamma = 1 \rightarrow Backward\ Difference$$

For explicit algorithms, the stability requirements of (4.59) are re-calculated. Taking the most critical term in the explicit form of the resulting matrix (4.58):

$$\Delta t_{crit} \leq \sqrt{\frac{4\tilde{m}}{\tilde{k}}};\ \gamma \geq \frac{1}{2} \tag{4.61}$$

$$\Delta t_{crit} < \frac{2\gamma - 1}{\gamma}\frac{\tilde{c}}{\tilde{k}};\ \gamma < \frac{1}{2}$$

$$\tilde{m} \rightarrow micro + macro\ inertia$$

$$\tilde{c} \rightarrow micro + macro\ damping$$

$$\tilde{k} \rightarrow micro + macro\ stiffness$$

Above, the fact that the mass, dissipation and inertia coefficients comprise the microscopic and the macroscopic contributions of the structure was enhanced. As a reminder, the micro contribution is the constitutive contribution of the bulk material. The macro one, appears when such constitutive values are defined from the macroscopic response of assemblies. To complete the section, two estimates of critical time step for sandwich composite plates (NAYAK; SHENOI; MOY, 2004) can be mentioned:

$$\Delta t^{I}_{crit} \leq \frac{1}{2}\sqrt{\frac{3\rho(1-\upsilon^2)}{E_2 h^2}}\Delta x^2 \tag{4.62}$$

$$\Delta t^{II}_{crit} \leq \frac{1}{2}\sqrt{\frac{\rho(1-\upsilon^2)}{E_2\left[2 + \frac{\pi^2}{12}(1-\upsilon)\left(1 + \frac{3}{2}\left(\frac{\Delta x}{h}\right)^2\right)\right]}}\Delta x$$

From the formulas within this section, stability is related to the time that the information carried at a current velocity takes to cross the local distance "Δx". This distance is defined by the resolution of the domain, so it is usually a fixed parameter with a minimum size. If the time step "Δt" is too large, there will be an excess of information in the element. Actually, this is related to the elastic wave speed within the media. The information term should be read as the size of the band of the frequencies being carried. Higher frequencies are related to larger bands, and vice-versa. The fastest convection of information is the denser and softer must be the sub-domain (element) to handle the energy, which is proportional to the size of the band of frequencies. Low velocities imply in low frequencies and therefore low energy levels and the

time step can be maximized. On the contrary, high velocities imply in high frequencies and high energy levels. Thus, the time step must be reduced.

4.4 Review on Solution Methods and Plate Elements

After exposing and discussing the aspects of approximate solutions for boundary value problems of plate-like structures (shells), a complementary chronological review is provided with focus on solution methods using FEM.

Regarding shear strain and material anisotropy, Noor and Mathers (1975) studied convergence and accuracy of several finite elements. All elements were conforming and obeying the C-0 continuity requirements. The elements were based on shallow-shell theory, but they were modified to account for shear and rotary inertia. They focused on the effects of: 1) Changing the order of the approximating polynomials; 2) Including internal degree of freedom; 3) Using derivatives of displacements as nodal parameters. By analyzing static, dynamic and large displacement problems, the authors concluded that: 1) Higher order displacement models achieve a certain level of accuracy with fewer unknowns than a lower order model; 2) Higher order models are more robust regarding the limit of thin plates; 3) The use of derivatives as nodal parameters require special attention due to possible non-physical discontinuities; 4) Adding internal nodes is preferred for adding lattice ones when convergence is at stake. However, for free vibration and buckling, it is better to add nodes on the lattice to improve accuracy, except in the case of higher vibration modes where internal nodes are again advised; 5) Mixed models are insensitive to variations in shear strain and thickness. Higher orders interpolations are preferred in order to improve the performance of the element. On the other hand, mixed approaches require an extra pre-processing step regarding matrix storage of the variables; 6) Even though anisotropy has proven to highly influence the results, the bending-extensional coupling does not have any major effect on convergence or accuracy of the analyzed elements.

A non-flat shell element was developed by using a mixed interpolation approach by Bathe and Dvorkin (1984). Such technique interpolated the strain values calculated at the mid-side of the element edges. None specific shell theory was addressed and the element was meant to suit thick and thin shell analyses without shear locking. The formulation also accounts for

large displacements and rotations, but only for small strains. The second Piola-Kirchhoff stress tensor was used with the conjugate Green-Lagrange strain tensor in the Total Lagragian formulation of the finite element. In addition, for few patch tests, several other examples including linear buckling and perfect plasticity (material non-linearity) cases were compared to other analytical solutions and experimental tests. The formulation showed good predictive capability. All these findings can be found in details in the PhD thesis of Dvorkin (1984). In that thesis, the locking problem is better emphasized and explained. Among other issues, the author addressed the fact that this phenomenon was a property of the element geometry and could be eliminated, if the ratio thickness/length is large enough. It was also discussed how a reduced/selective integration can be performed without yielding spurious zero energy modes due to rank deficiency of the stiffness matrix.

Later, Bathe and Dvorkin (1985) derived a modified four node plate element, exploiting the continuum degenerate concepts. An iso-parametric element was developed based on the Kirchhoff's theory. Since the strains were solved as nodal parameters, the formulation was considered as a mixed type one. This was one of the main achievements of this formulation, the use of different interpolations for transverse displacements and transverse shear strains. The authors achieved a robust element free or independent of pathologies such as shear locking, zero energy modes and distorted elements

By using a displacement formulation previously developed (DI SCIUVA, 1985), Di Sciuva (1986) compared the accuracy and convergence of triangular and rectangular layered elements derived by the formulation (refined theory) and via the classical one. The latter possessed only five variables per node (3 translations and 2 rotations) and the Zig-Zag effects within the laminate were not represented. The benchmark problems comprised bending and free undamped vibration tests. Among the main findings, the elements formulated via the classical theory presented shear locking, while those formulated with the refined theory did not. The results from elements based on the refined theory also had a better accuracy. Another interesting finding was the fact that the accuracy of the models built within triangular elements was sensitive to their directions relative to the plate.

Fried, Johnson, and Tessler (1986) investigated the minimal amount of degrees of freedom of triangular elements to properly account for shear strains in bending of thin plates. They began from the theoretical number of degrees of freedom needed to have compatible elements for bending of thin plates and removed as many DOFs as possible. For a second order element, the minimal amount of DOFs found was 9, for fourth order elements, the minimal

amount of DOFs was 12. The next element was a sixth order element with 18 DOFs. This latter element was the most well-known C-1 compatible triangular element.

Kansa (1990a) reviewed the use of interpolation functions to treat spatially scattered data and how to obtain partial derivatives from this set of values. A review on interpolation function and methods showed that approximation functions could be grouped into global or local approaches. Of all the methods tested, Hardy's multiquadric (MQ) global scheme provided the best results. The method was based on the assumption that any function can be represented as a series of functions, which are dependent on the distance of a particular value in space to a reference point. Curiously, MQ approach was better suited to regions or set of points with a steep gradient of values. For flat regions/surfaces, the MQ methods did not perform so well due to ill-conditioning of the coefficient matrices. A hybrid method with local monotonic cubic spline functions and MQ was suggested. On the other hand, this technique was able to give accurate interpolations for regions with "track" data configuration or presenting very poor cell aspect ratios. Since MQ depends on all data points, large three dimensional problems become prohibitive and portioning of the domain is advised.

In a companion paper Kansa (1990b), the MQ technique was applied to parabolic, hyperbolic and elliptic differential equations. For a diffusion-advection problem with a given mesh, the MQ method showed superiority over the FD methods for large cell Peclet numbers ($Pe_{cell} = u\Delta x/D$). The von-Newmann blast wave was used to study hyperbolic equations. Better convergence rates were seen by using the MQ scheme. Lastly, Poisson's equation was solved. Essential and essential-natural boundary condition configurations were handled with the MQ scheme. A considerable improvement could be achieved by slightly increasing the number of interior nodes. Overall results for all three case studies rendered excellent results.

A 40 degree of freedom rectangular plate element (Q40) was proposed by Di Sciuva (1993) for solution of laminated plates. Inter-laminar continuity of transverse stresses was assumed to be fulfilled by the equivalent single layer approach. Of the ten degrees of freedom per node, one had 3 translations, 4 rotations, 2 curvatures and 1 twist. The DOFs ensured C-1 continuity for the transverse quantities of general shape quadrilaterals. Fifth order Hermite polynomials were used as interpolation functions to compel with the C-1 requirements. The shape functions were defined with linear Lagrange polynomials and, hence, in-plane variables had isoparametric treatment, while the transverse ones presented a sub-parametric approach. Non-linear strains were considered according to von Kármán's assumptions. Classical (CQ40), First (FQ40) and higher-order (HQ40) shear deformable plate theories were implemented for this element with (RFQ40 and RHQ40) and without Zig-Zag effects. The formulations

accounting for ZZ effects were referred to as “Refined” theories. Results with these elements were compared to closed form solutions for static, dynamic and non-linear problems concerning laminates. Inspecting the result tables, the refined elements showed the best agreement with the analytical solutions.

Briassoulis (1993) reformulated a shear-bending four-node C-0 element to eliminate both formulation and machine locking issues. Mindlin-Reissner plate theory was used to account for shear effects. Such formulation’s locking pathology takes place at the thin plate limit as commented earlier. To counter this locking, the author modified the shear-bending coupling term in the element’s stiffness matrix. The respective term was evaluated solely with the contribution of the tangential edge shear strain component. By doing so, the spurious functions, responsible for this locking mechanism were avoided. Moreover, the use of full integration ensured no zero-strain energy modes. After solving the formulation’s shear locking issue, the machine locking problem was addressed. If very thin plates (h/L < 1xE-3, this limit is dependent of external loads and boundary conditions) are not considered, the proposed formulation is insensitive to the machine’s precision. However, if thinner plates are considered, machine locking will take place. A solution for this problem was proposed by using the addition of a weighing factor on the shear correction factor of approximately the inverse of the thin plate limit. Then, multiplying the shear correction factor by 1xE6 rendered a first order shear deformation theory free of locking issues. This formulation was tested and the accuracy level was as good as the plate theory used, but with no locking.

To solve membrane and bending problems in shallow shells, the Ritz method was remembered as an alternative solution method by Qatu and Algothani (1994). This technique was compared to the well-known FEM procedure with non-compatible triangular (three or six nodes) and rectangular (four or eight nodes) elements. With much fewer degrees of freedom and slightly less accurate results, the Ritz method proved to be a valuable technique to study laminated shells in bending.

Kant and Kommineni (1994) developed a nine-node iso-parametric C-0 finite element based on a cubic higher order plate theory to simulate the dynamic and non-linear behavior (von Kármán assumptions) of laminated doubly curved shells. Bending, shear and membrane contributions were considered in the formulation. Symmetric and non-symmetric laminated shells were evaluated under dynamic loadings. The mass matrix was made diagonal to enable the use of an efficient time marching scheme. Selective integration was employed to minimize locking. No damping was considered. Sandwich plates were analyzed, and it was observed that the larger ratio skin-to-core elastic modulus increased the influence of the shear contribution.

First order (5 DOFs per node) shear deformation theories were compared to the cubic higher order (9 DOFs per node) and large differences in amplitude and phase responses were registered. Hence, the use of first order shear theories in the analyses of sandwich shells was not recommended.

An important fact was highlighted by Qatu (1994). Even though geometric non-linearity assumptions are important, it should only be considered for thin to moderately thick plates and shells (l/h > 20). On the other hand, if the structure is a thick plate or shell and the deflections are approximately equal to the thickness of the structure, material non-linearity should be considered instead. The author basically advocated that a formulation accounting for both shear deformation and geometric non-linearity did not have practical use in typical engineering problems with laminated structures.

In two studies (ARGYRIS; TENEK, 1994a, 1994b), a multi-layered triangular flat element named LACOT (LAminated Composite Triangle) was generalized within the range of linear, non-linear and thermal applications. Based on a Kirchhoff type of plate theory, the authors derived a finite element trying to avoid the classical pathologies such as membrane and shear locking, spurious and zero-energy modes and induced anisotropy. To do so, the Natural Mode Method was proposed. In summary, natural modes are the pure straining modes, which exclude rigid-body displacements. A new coordinate system, defined as Natural Coordinate System, was directed by in-plane total strain directions. In this new coordinate system, the 18 DOFs were reduced to 12 DOFs. Hence, the 12x12 element stiffness matrix accounted for dilatation, distortion and shearing effects. The shearing effect was uncoupled from the direct strains and was estimated from the anti-symmetrical bending contributions. The stiffness matrix was formulated and assembled by using the Intelligent Physical Lumping Method (ARGYRIS; TENEK, 1994a). Through equivalence of strain energy, the continuum media was lumped into a discrete one. The technique proposal was assumed to better assess and control the stiffness matrices of finite elements. Non-linear analyses of large displacements and small strains endorsed these assumptions with good result for different composite plates (ARGYRIS; TENEK, 1994a). Since it was used a first order shear deformation theory, shear correction factors were derived based on equivalence of transverse shear strain energy. Good agreement with the reference results were achieved via the formulation in static linear and non-linear examples. Integration of the elasticity differential equations of equilibrium allowed for a quadratic estimation of continuum transverse stresses. Best results were seen for thin plates (l/h = 100), because the laminate was analyzed by using an equivalent single layer theory.

Still using natural coordinates and the Intelligent Physical Lumping Method, Argyris and Tenek (1994c) developed a shallow shell theory named. In the proposed formulation, the triangular edges were represented by third order polynomials and, therefore, linear curvatures. Unlike the similar laminated flat elements also developed by the authors, the global stiffness matrices were full with different coupling terms. Similarly to these flat elements, the azimuthal degree of freedom was handled by using small (1E-6) weighting factor to avoid singularities in the global stiffness matrix. In the paper, the linear and non-linear examples of isotropic and composite shells evidenced the accuracy and robustness of the formulation. Better convergence results for the shell element were achieved in comparison to the equivalent flat element. Also, no locking effects, spurious modes, hourglass modes or the like were seen. Despite all positive results, no dynamic effects were discussed.

Two small-strain shell elements created by Dvorkin (1995) via the mixed interpolation of tensorial components (MITC) criterion were reviewed in order to apply such concept on elasto-plastic analyses. A four node element (MITC4) and an eight node one (MITC8) were detailed to point how the specific interpolation can avoid the shear locking pathology. The proposed elements were free of spurious energy modes, which are very common in reduced/selective integration techniques. The author stated that the success of the MITC approach in calculating the transverse strains relied on interpolating the values of the strains calculated at the mid-side nodes of the element. After bringing up the advantages and particularities of the MITC4 and MITC8 elements, the author derived an elasto-plastic formulation for finite strains, i.e., large strains, for the MITC4 element. The new element was named MITC4-TLH after the developed Total Lagrangian-Hencky formulation. Hencky's logarithmic strain tensor and its conjugate stress tensor were used. Due to the interest in metallic materials, isotropic hardening (by using associated flow rule) and von Mises (J_2) yield criterion were assumed. Even though two examples applying the elasto-plastic formulation were given, no comparison to experimental or other analytical-numerical approach was provided.

Sansour and Bednarczyk (1995) formulated and tested two finite shell elements (four and nine node) by using a new shell theory built on the concepts of the Cosserat continuum. A complete discussion of the derivation process was available for two configuration spaces (Killing or Euclidian metric). Displacement and rotation fields were explicitly introduced. Proper numerical treatment was conducted to avoid locking-phenomena and to allow the formulated element to proper model finite rotations. Drilling degrees of freedom were inherent in the theoretical formulation. The elements were developed on a partially mixed variational principle. Regarding regular discretization, the four and the nine node elements showed

equivalent accuracy. However, the nine node element was a better choice for large distortion behaviors. These conclusions were extracted from solved examples of snap through of a hinged cylinder, snap through of a spherical cap, pinched cylinder, pinched cylinder with rigid diaphragm and pinched hemispherical shell.

Using Sander's thin shell theory, a conforming ten node triangular element with 30 DOFs was developed by Farsakh and Qatu (1995). The constitutive relations of the element were derived for laminated composite shells in the scope of equivalent single layer theories. Negligible shear deformation was assumed. Sander's shell theory is a deep shell theory and hence, softer than the shallow shell theory. Because of this, the proposed element formulation exhibited better accuracy and convergence performance due to its conforming characteristics. This conclusion was obtained after inspection and comparison of the element and its shell theory to other theories and solution techniques (analytic, FEM, Ritz and experimental) in static and vibration problems of anisotropic laminated shells.

Taylor, Vasiliev and Dillard (1997) investigated first order shear deformation theory by splitting the solution into the potential of the displacement field and stream functions related to the rotational plane motion. By recognizing that the stream functions were related to boundary layer effects, a locking (as $h \rightarrow 0$, shear strain does not vanish, the so-called parasitic shear) free solution was derived, when the authors neglected the influence of the boundary effects (stream functions) on the transverse shear strains. Only in pure torsion or contact problems, for instance, such effects should not be discarded as affirmed by the authors. Thus, a 36 DOFs four node element with C-2 continuity requirements was developed (the element's edges were aligned with the global x-y axis). Excellent agreement with exact Navier type solutions and good convergence rate (1*x*1 meshes with symmetry conditions) were verified. Although the results were promising, the approach was only possible in transversely isotropic materials. For orthotropic and anisotropic materials the separation of the governing equations into independent equations was rarely possible.

By exploiting a sub-structuring technique, a six node Layer-Wise triangular plate/shell element was created by Botello, Oñate and Canet (1999) by using a mixed displacement-strain formulation. The mixed approach consisted on removing the excessive stiffness of the first order shear deformation theory used. Such sub-structuring technique allowed one to decrease the actual number of layer equations to be solved down to one set of layer equations. However, it also enabled one to increase the number of layer equations in order to increase accuracy, i.e. a three layer laminate can be turned into a nine layer virtual laminate. Although such technique did reduce the size of the system matrix, the extra algebraic calculations required more

processing time. Therefore one might now solve larger systems at slower speeds by using the same hardware. If storage is not an issue, perhaps the technique proposal is not that attractive. Thus, an extra investigation is required. Static and dynamic examples in the paper showed good behavior of the element for both thin and thick composite laminates compared to other literature results.

Carrera (1999) studied the influence of the transverse normal stress on the classical displacement or mixed (Reissner's Mixed Variational Theorem) plate and shells theories. The evaluated formulations were equivalent single layer theories by using improved displacements according to Murakami's Zig-Zag theory. Up to third order theories were implemented and compared to a fourth order mixed Layer-Wise theory, which yields nearly exact elasticity's results. Formulations of previous researches were also compared for simply supported static problems and free vibration analyses. Carrera (1999) concluded that the Koiter's recommendation should also be extended to laminated plates and shells, regarding interlaminar continuity. For highly anisotropic and thick shells, only a Layer-Wise description of the problem could provide very accurate dynamic results.

Touratier and Polit (2000) presented a C-1 six-node triangular plate element with 81 DOFs. It was a conforming element by using a refined (Zig-Zag) plate theory respecting the inter-laminar continuity between plies of the laminate; hence, it was an equivalent single layer approach. It comprised a cosine distribution of transverse shear strains and satisfied the top-bottom boundary conditions. Only five generalized displacements were used: Argyris's (1968, apud TOURATIER; POLIT 2000, p. 310) interpolation for the transverse normal displacement, and Ganev's (1980, apud TOURATIER; POLIT 2000, p. 310) interpolation for the membrane displacements and the transverse shear rotations. The transverse normal stress was deduced from the equilibrium equations. Some examples in linear statics, dynamics and statics for geometrically non-linear analysis were studied for sandwich plates. Comparisons of the current element (named C-1 GAG/SIN-C) were provided for 3D elasticity solutions. Other four elements (C-1 GAG/SIN: Sinus model without continuity, GAG/KL: Kirchhoff-Love model, GAG/RM: Reissner-Mindlin model and CL8: C-0 eight-node quadrilateral finite element) were implemented to investigate the accuracy of the proposed element. No spurious energy modes, very fast convergence and no shear locking were confirmed, and the results were accurate for a sandwich plate.

Carrera and Demasi (2002a, 2000b) published two companion papers with 4, 8 and 9 node plate elements formulated via PVD or RMVT methods. A nomenclature pattern according to the order of expansion, variational statement, variable description, inter-laminar continuity

and Zig-Zag displacement functions was proposed. This formulation could be regarded as a type of Unified Formulation. It means that any plate theory in the literature (actually most of them) can be described by using the proper choice of variables and constants in this work's formulation. In the first part of the work, the element formulations were presented and explained. Special attention should be paid to the elements developed via RMVT approach due to the extra stress DOFs involved. On the second part, 66 different elements were evaluated by using symmetrical and unsymmetrical laminated plates under four load cases: concentrated force, uniform pressure, sinusoidal and bi-sinusoidal loads. Shear locking was avoided by using selective/reduced integration. The authors found that the RMVT elements did not introduce additional numeric issues, when compared to those based on the classical PVD statement. The results also showed that mixed models with continuity of transverse normal stress were more attractive than those that violate the physical constraint. Layer-Wise solutions proved to be computationally expansive and could be compared to 3D elasticity solutions. Therefore this type of formulation should be used only in extreme cases of side-to-thickness, core-to-skin thickness/elastic modulus ratios. Anisotropic laminated composite materials with unsymmetrical layups may also need Layer-Wise approximations.

Still regard UFs, an extensive review of multilayered plate and shell structures was carried out by Carrera (2002). In the frame of axiomatic approaches, he proposed a Unified Formulation for shells and plates and named it CUF (Carrera's Unified Formulation). This formulation allows users to choose the order of expansion in the thickness direction for the variables at hand. The order of expansion was the same for all directions of the variable being solved. Zig-Zag refinements can also be implemented within CUF. This was accomplished through the definition of a fundamental nucleus of the stiffness matrix. In his research, different theories to represent the complicating effects arising from the material anisotropy along with the C-0z continuities requirements were discussed and grouped according to: 1) elimination of the thickness coordinate z; 2) choice of unknown variable; 3) definition of global displacement; and 4) solution through FE methods. The first group was divided in: I) Continuum or stress resultants based models; II) Asymptotic approaches; III) Axiomatic approaches. The second group comprised: I) Stress formulation; II) Displacement formulation; and III) Mixed formulation. The third group was formed by: I) Equivalent single layer models; II) Layer-wise models. Finally, as an option to the two dimensional plate and shell elements, the last category offers the possibility of solving the equations by: I) Developing degenerated finite elements; II) Using hybrid methods; III) Employing global/local approaches with "p" or "s" methods. Concerning the classical models applied to multilayered structures, Carrera (2002) pointed that

transverse shear strains, neglected in classical theories (Kirchhoff–Love, CLT) are insufficient to properly model thick laminates. Also, the classical thick plate formulations (Reissner–Mindlin, FSDT) did not neither describe Zig-Zag effects nor inter-laminar continuity, which was unsatisfactory for local failure analyses, for instance. For such problems, Koiter's recommendation should be followed, i.e. both transverse and normal stresses should be considered at the same time. It was seen that three Zig-Zag types of theory can be found in the literature (Lekhnitskii's, Ambartsumian's and Reissner's). Lekhnitskii's and Ambartsumian's theories are derived by equating the transverse stresses at the layer interfaces and integrating the strain relations via constitutive equations (Hooke's Law) to find the Zig-Zag displacement functions. Reissner used a mixed approach and decided for solving both displacement and stress variables which in turn yields better results. To reduce the number of variables in this latter approach, Carrera (2002) proposed the use of a Weak Form of Hooke's Law (WFHL) so that the final matrices comprised only stresses or displacements. To end, this review concluded that the use of Layer-Wise theories is mandatory to obtain nearly 3D displacement fields and transverse stresses directly from constitutive relations.

In order to evaluate the accuracy and robustness of the proposed unified compact formulation (CARRERA, 2002), he published a companion paper (CARRERA, 2003b) with a broad collection of other published plate and shell theories. Firstly, to assess the exact accuracy of each formulation, he used analytical solutions to bending and vibration of plates, Layer-Wise versus Equivalent Single Layer description, pre and post evaluations of transverse normal stresses, bending of shells, vibration of shells, and finally, the effect of transverse normal stress on bending and vibration of plates. Secondly, nine node finite element solutions were used to compare the different formulations. Shear locking effect was handled by Assumed Natural Shear Strain concept. Whenever available, closed form solutions were used to evaluate the errors of the FE method. After a detailed inspection of results, in summary, Carrera (2002) endorsed that:

- Mixed descriptions (RMVT) are more accurate than the classical displacement (PVD) formulation.
- Mixed analyses do not require any post-processing procedure.
- Layer-Wise descriptions are more accurate than Equivalent Single Layer ones, but they are computationally more expansive.
- As the number of layers increases, Layer-Wise theories become insensitive to the order of expansion or the variational approach used (displacement or mixed).

- Unsymmetrical laminates are sensitive to the order of expansion. Quadratic expansions seem to be more effective on these laminates.
- The accuracy of equivalent single layer theories developed on displacement variables only decreases in function of the increase of plies in the laminate.
- For thick laminates and sandwich structures, the transverse normal stress cannot be neglected.
- Comparison of equivalent single layer theories show that the mixed formulation (RMVT) needs both inter-laminar continuity and Zig-Zag effects, else using the mixed approach is pointless.
- The accuracy of the different formulations is still subordinate to the expected outputs. Better evaluations of in-plane stress with respect to transverse one are obtained by different modeling.

Based on Carrera's previous works above, Carrera and Ciuffreda (2005) provided an enlarged comparison of plate theories. Thirty seven theories were implemented. They considered bending problems of sandwich and cross-ply plates under harmonic, uniform, triangular and tent-like distributions of transverse pressure loads. Some of the loads were new in the literature. The theories were solved via Navier-type analytical solutions and via Finite Element Method. Equivalent single layer theories, Layer-Wise theories, classical displacement formulations and mixed formulations, all with different accuracy orders, were put to the tests. ZZ effects and inter-laminar continuity were also analyzed. The outcome of the tests can be summarized by stating that the best approximate plate solution was the Layer-Wise type of fourth order obtained through a mixed approach (LM4), and the least accurate is the classical laminate theory (CLT). The other thirty-five approaches lie in between, such that, in order or decreasing accuracy one has: LM > LD > EMZC > EDZ > EMC > ED > CLT. Other findings that should be highlighted are the fact that equivalent displacement theories can be completely wrong even for moderately thick plates and weak core laminates, which demands higher order or Layer-Wise descriptions of displacements.

Ferreira, Roque and Jorge (2005) used a shear deformation theory for modeling symmetric composite plates discretized by a meshless method based on global multiquadric radial basis functions (RBF). There are different RBFs such as:

$$g_i(\boldsymbol{r}_i) = (\boldsymbol{r}_i{}^2 + c^2)^{1/2} \quad \rightarrow Multiquadrics \tag{4.71}$$

$$g_i(\boldsymbol{r}_i) = (\boldsymbol{r}_i{}^2 + c^2)^{-1/2} \quad \rightarrow Inverse\ multiquadr \tag{4.72}$$

$$g_i(\boldsymbol{r}_i) = e^{-c^2 \boldsymbol{r}_i{}^2} \quad \rightarrow Gaussian \tag{4.73}$$

$$g_i(\boldsymbol{r}_i) = \boldsymbol{r}_i{}^2 log \boldsymbol{r}_i \quad \rightarrow Thin\ plate\ splines \tag{4.74}$$

$$g_i(\boldsymbol{r}_i) = \{1 - c\boldsymbol{r}_i\}^8 \{32(c\boldsymbol{r}_i)^3 + 25(c\boldsymbol{r}_i)^2 + 8c\boldsymbol{r}_i + 1\} \quad \rightarrow Wendland's \tag{4.75}$$

$$\boldsymbol{r}_i = \|\boldsymbol{x} - \boldsymbol{x}_i\|$$

"r" is the position vector and "c" is the reference to be calibrated. The paper was restricted to the multiquadric function applied on regular grids for different densities. By using trigonometric functions in the thickness direction, the criterion of null transverse shear stresses at the top and bottom surfaces of the plate was satisfied, since this is a strong solution form. The results of cross-ply and sandwich laminates for 11, 15 and 21 grid points were in much better agreement to the exact solution, when compared to the results obtained via CLT, FSDT and HSDT theories.

To avoid having to handle with C-1 and C-2 continuity requirements and by using of a refined plate theory (Zig-Zag behavior modeled via Heaviside function) to solve laminated plates by using Finite Elements, a post-processing method is developed and recommended by Icardi (2005). The core of the proposed formulation lies on the equivalence of strain energy values obtained by using the well-known FSDT theory with basic five DOFs (u, v, w, θ_x, θ_y) and a high order Zig-Zag plate theory. Such approach was motivated by the inaccuracy of the FSDT to properly capture the transverse stresses. Firstly an eight-node C-0 rectangular plate element was derived by using the second order serendipity shape functions for the FSDT. The element was used to obtain a first estimate of the basic five displacement values. Next, by interactively adding corrective terms, the FSDT solution was improved until the new strain energy obtained has achieved the value of the one, which was obtained via Zig-Zag theory. This was accomplished by minimizing the functional defined by the difference of strain energies computed via FSDT and Zig-Zag formulation. To compute the strains and stresses, the basic displacement values were interpolated by using spline functions, which are then differentiated. Transverse stresses were post-processed by using integration of local equilibrium equations and the procedure devised by Rolfes and Rohwer (1997, 1998a, 1998b). To quantify the accuracy of the method, Icardi (2005) compared the results of his refined (3D) formulation to exact solutions. Also, the author studied the failure of laminates under low velocity impact loads and chose eight composite failure criteria and checked the results of his formulation using

experiment results. The predicted impact-induced damage and delamination occurrences across the thickness showed good agreement to those detected by ultrasonic inspection.

Reissner-Mindlin plate theory was enhanced with the MITC (Mixed Interpolation of Tensorial Components - DVORKIN, 1995) technique by Moreira, Dias Rodrigues and Ferreira (2006), which calculated the strain values at the mid-side nodes of the element and, hence, prevented the bending shear lock phenomenon. Two elements were proposed. They were tagged as layw4c and layw4m. The first one did not carry the incompatible quadratic modes of deformation implemented in the second element to improve the membrane shear response. Drilling degrees of freedom were tackled by using fictitious drilling stiffness. The consistent mass matrix was lumped through a diagonal-scaling technique known as HRZ (after Hinton, Rock and Zienkiewicz, 1976), which better preserved the coupling terms in the original matrix. The elements passed the thin plate patch test, and the plate formulation was tested using particular static examples found in the literature (Morley's skew plate, pinched cylinder, Srinivas' orthotropic sandwich plate with soft core, etc) and the usual dynamic evaluations of natural frequencies. The static results reached the reference data for meshes as large as 32*x*32 elements. Dynamic results showed a faster convergence rate for the natural frequencies calculated via HRZ lumped mass matrix. As a layer-wise approach, all results were very close to the reference values, which were assumed exact.

Karger et al. (2006) improved the FSDT performance applied to sandwich structures, by using a three layer (Layer-Wise), eight-node element with nine DOFs per node. By using a pre-processing of the equilibrium equations, the transverse strain stiffness contribution was enhanced. To avoid second order shape functions, the strain derivatives were replaced by transverse shear forces, which only needed first derivatives of the shape function. This was accomplished by writing the strain derivatives in terms of moment derivatives. The transverse shear stresses were obtained by post integration of the equilibrium equations. A soft core sandwich structure under a sinusoidally distributed transverse load was used for benchmark. The exact solution by Pagano (1970 apud KARGER et al., 2006, p. 851) and few approximate others by Carrera and Demasi (2000a, 2000b) via other equivalent single layer theories were compared. Numerical results showed that the new element had good prediction capabilities in regarding displacements and stresses. For instance, the adopted post processing delivered very good transverse stresses.

The 81 DOFs triangular C-1 element, previously defined in Touratier and Polit (2000), was considered by Dau, Polit and Touratier (2006). This multi-layered element based on a refined ZZ theory was improved to account for geometrical non-linearity. A Total Lagrangian

configuration was considered, as well as von Kármán's approach for moderately large deflections and small rotations and strain constrains for non-linear behavior. Through consistent linearization, the tangent stiffness matrix was derived and, hence, solved via Newton's method. One layer orthotropic plate under uniform load was studied in the linear and non-linear range to evaluate the locking problem. The results indicated that the formulation was free of shear locking, when applied to plates. Length to thickness ratios from thick (ratio around 8.696) to very thin (ratio around 8695.652) plates were analyzed. Application of the proposed formulation to shell configurations did not share the same success due to inherent coupling of strains, because of the curvature of the structure. Also, the results for a plate sandwich with a honeycomb core and facings, both made of aluminum showed good agreement to the considered references. To assess influence of boundary conditions and the non-linear response, two and four layers cross-ply laminate were investigated as well as an orthotropic cylinder. To complete the non-linear evaluation of the proposed theory, the experimental tests of four different sandwich plates made from identical components were compared to the solution via finite elements. The sandwich plates were composed of an aluminum honeycomb core and epoxy-glass fiber composite faces. The critical load was determined showing good accuracy.

D'Ottavio et al. (2006) applied Carrera's Unified Formulation (CUF) to a selected case study in order to assess the precision of unified formulations. The case consisted of a three-ply laminate of graphite/epoxy with the stacking sequence [0/90/0]. All plies have the same thickness. The longitudinal elastic modulus was 25 times greater than the transversal one. Shear locking was found in some of the tests of formulations, and it was suppressed by using selective/reduced integration as usual. The authors did remind the fact that shear and membrane locking may be less pronounced, but still present, depending on the order of the formulation, plate and element geometry and material properties. Just as observed by Carrera (2003b), CUF results were robust and as accurate as the analyzed theories could be in the finite element implementation.

Demasi (2006) was mainly concerned with stress variables in Layer-Wise mixed formulations. The author implements Carrera's unified formulation and, then solves the equations via condensing or not the stress DOFs at element level to work with displacements only at the structure level instead of a linear system. The approach yielded two multi-layered elements: LMN and LMNF (L = layer-wise, M = mixed formulation, N = order of expansion of the variables in the z-direction, F = full case without condensation). When static-condensation was used, the continuity of transverse stresses was not guaranteed as opposed to the full case where it was. Static-condensation was sub-structuring technique usually applied in

dynamic analyses to lessen the computational costs due to DOFs that it needed to be solved via a FE model. A two layer beam and a four layer plate were analyzed. The first example was compared to a numeric solution obtained via a commercial FE package NASTRAN. Unfortunately, no details of the NASTRAN model explicitly were given. The second example was compared to analytical 3D solutions. Comparisons of the first example were given graphically and presented a satisfactory overall matching of results. The second case was compared to a table containing the results for the investigated two elements implemented up to the fourth order. It was seemed that the transverse stresses were greatly improved by using the LMNF element, but the transverse displacement was not. Also, no information on the in-plane results was provided to assess the full accuracy of the formulation with this example.

A previous work of Li and Liu (1997) was improved in the work of Zhen and Wanji (2007) to account for transverse normal strains. The new refined global-local higher-order theory was the extension of Li and Liu's 1,2–3 global-local higher-order theory with explicit contribution of transverse normal deformation through higher order terms in the transverse displacement equation (w). The expression "1,2-3 global-local" means that there were two local refinements. The first modification added first and second (1,2) order descriptions to the local displacements. The second local refinement was the inclusion of a third order term (3). Only two refinements were possible, because of the number of available continuity requirements. The approach was independent of the number of layers in the laminate. Such proposal was implemented via Finite Elements with C-1 continuity of transverse displacement. An eight node serendipity element was turn into a four node one by removing the mid-side nodes via Hermite functions. Based on this reduction, the element presented 4*x*19 DOFs. This element was name QLP19 and Li and Liu's QLP13. Despite the effort to find the meaning of this letter acronym, it was believed that QLP stands for "Quadrilateral Plate". However, the numbers were related to the DOFs of each node. The method of the discrete thin plate quadrilateral element DKQ (Batoz and Tahar, 1982) was used to circumvent the C-1 requirement in the work. C-0 displacement functions were derived to formulate the shear strain. Thermal strains were also accounted for the plate theory proposal. The results of three case studies with different length-to-thickness ratios and laminate configurations showed that the performance of the proposed element was very close to the exact analytical solutions and was better than Li and Liu's.

Demasi (2008b) proposed a further generalization of Carrera's Unified Formulation (CUF). This generalization was tagged as GUF (Generalized Unified Formulation). Exactly as in CUF, the theory revolved around a *fundamental nuclei* or *kernel* of the unified formulation. For CUF, this kernel is a 3*x*3 invariant stiffness matrix, which expands according to the

refinements included for the displacement fields (order of expansion and inclusion of Zig-Zag terms) and the type of approach (Equivalent Single Layer or Layer-Wise). For the current GUF, each displacement field was now uncoupled from the others regarding the refinements chosen. Now, each field can be refined independently from the other. The procedure now yields a kernel matrix with 6 components (due to symmetry) which are expanded differently one from the other. By these means, the author says that the formulation has 6 1*x*1 invariant matrices instead of on 3*x*3 invariant matrix as in CUF. The integration of the thickness direction terms is now more delicate, because of the complexity of the integrand. Since, for each displacement field "u", "v" and "w", one can now assign infinite refinement combinations, the author suggested the symbol ∞-3 for GUF and ∞-1 for CUF. To test the formulation, a Navier-type solution was used to obtain an analytical solution. Inspection of the results showed that the choice of maximum expansion order in the thickness direction could render poor or very accurate predictions. It depends on each refinement level the user chooses for each displacement field. The approach also is attractive for multi-field problems such as thermo-electric-mechanical problems, piezoelectric materials for instance.

The same theory published in the previous work (DEMASI, 2008) was reviewed in the next work (DEMASI, 2009a). However, a more comprehensive and detailed explanation and derivation all the GUF's kernels were presented. The formulation was based on displacement variables, only; hence it was tagged as classical approach. Despite mentioning FEM in the title, the article only pointed the potential of the formulation in the development of intelligent codes. They should use the minimum computational resources by automatically reducing the formulation's DOFs to the essentials. Several combinations of refinement for the three displacement fields were tested and compared to the exact solution to assess the influence of each refinement type and intensity.

Distributed among five companion articles is a new GUF based on a mixed approach derived by Demasi (2009b). The work followed the steps of the "∞-3" axiomatic classical displacement formulation, where infinite uncoupled refinements were made possible for each of the three displacement variables. Now, three other uncoupled refinements for stress variables were developed. Since there were three more stress variables, the new theory was hence tagged as "∞-6". In the article, it was raised all the existing type of plate theories and briefly explained the differences and performances. Based on the same logic of the GUF developed with displacements variables only via PVD, the governing equations for this mixed case, presented in part I, yielded 13 1*x*1 invariant kernel matrices. For comparison, Carrera's unified

formulation generates 4 3*x*3 invariant kernel matrices with 22 non-zero terms for the mixed formulation.

Mixed Layer-Wise approaches require the coupling of the displacement and stress kernel matrices. The second part (DEMASI, 2009c) detailed the advantages of the formulation and how the kernel matrices for each layer were assembled to form the global stiffness matrix. Due to the large amount of DOFs, a static condensation technique can be applied to reduce the computational cost. This possibility and its consequences were already studied by Demasi (DEMASI, 2006). The author also detailed how to obtain the in-plane and out-of-plane stresses through constitutive equations and through integration of equilibrium equations.

Part III (DEMASI, 2009d) deals by using high order equivalent single layer theories. What must be highlighted in the paper was the assemblage procedure from layer level to multilayer level to get the global stiffness matrix based on this mixed unified formulation. Three combinations were evaluated. When pure displacement kernel matrices were involved, the contributions were summed as usual. When the coupling kernel matrices were involved, only the terms corresponding to the transverse displacement and stress of the top and bottom layers of two consecutive plies were summed. Finally, when pure stress kernel matrices were assembled, the process follows the Layer-Wise drill. Considering the complexity of the assemblage, the author tagged the proposed formulations as “quasi-layerwise” approaches.

Zig-Zag considerations were made in the fourth paper (DEMASI, 2009e). The author briefly reviewed the main Zig-Zag theories and similarly to part III of his investigation, it was explained how an equivalent single layer formulation could be enhanced. Murakami’s Zig-Zag function was explained and chosen to refine the formulations due to its simplicity and effectiveness. Once again, care should be paid to the assemblage process, which renders a quasi-layer-wise global stiffness matrix.

The GUF based on a mixed approach is summarized in a flowchart in the last paper (DEMASI, 2009f). To test the infinite theories, the author analytically solved two test cases via Navier-type functions. Among the main findings, one can point the fact that the displacement and stress fields in the thickness direction may oscillate. Also, the use of Murakami’s refinement did not always improve the results. Other conclusions could be drawn from this last paper (part V), but due to the complexity of the combined refinements, it was wise to read them in the original paper.

Carrera, Cinefra and Nali (2010) incorporated the MITC technique in CUF by using the principal of virtual displacement (PVD). A bi-sinusoidal transversal load was considered for evaluation of the modification. Closed-form Analytical solutions (A) of this loading case are

compared to the current MITC4 approach, and the classical displacement formulations under some different numerical scheme: Full 2*x*2 Gauss points (N), Reduced 1*x*1 Gauss point (R) and Selective 1*x*1 gauss point for bending and 1*x*1 for transverse shear. Overall results pointed that, in order of decreasing accuracy, one has: A>R>S>MITC4>N (“>” means more accurate). However, all three approximate solutions (R, S and M) yielded spurious energy modes. It was stated that these ‘unphysical modes’ are case dependent on the material, geometries, mesh, loadings, etc. A convergence study of the natural frequencies of an isotropic aluminum beam, solved via the selective integration scheme, revealed that the number of spurious modes was reduced by the increase of mesh density. In this context, the MITC technique reduced even further the number of spurious energy modes and shifts the remaining mode to higher frequencies. Thus, despite the increase of complexity in deriving the modified CUF, the amount DOFs was the same of the original CUF.

Ferreira et al. (2011) addressed a solution to CUF through radial base functions (RBF). The fundamental nuclei were determined for the classical displacement approach (PVD) by using integration by parts of the equations of motion. The global matrix was assembled in an equivalent single layer fashion. The meshless radial base method was then reviewed. Based on the method, the solution for the static problem, the dynamic problem and the buckling one were derived. Two axiomatic plate theories were considered. Both Murakami’s Zig-Zag function and a full second order series expansion of the thickness coordinate for the transverse displacement were carried out. For in-plane displacements, the first theory added a cubic term to the FSPT formulation, and the second one added a sine function of the thickness coordinate. These refinements tried to accurately model the transverse shear stresses. The results showed slightly dependence of the grid densities tested (13 *x* 13, 17 *x* 17 and 21 *x* 21). Prediction of the exact results via the sine plate theory gave better results. This was probably due to the fact that the fist plate theory carried only the first two terms of the sine trigonometric function infinite series

Active and Passive damping in sandwich structures was the subject of MOITA et al.. (2011). A five layer sandwich plate was considered. Bottom and top layers were piezoelectric layers acting either as a sensor or an actuator. The core was made of a viscoelastic material to passively increase the damping of the structure. In-between these layers are the elastic composite laminated layers. For the elastic and piezoelectric layers, the CLT was considered and the viscous core was solved via FSPT. The dynamic equations, considering the mechanical deformation from the piezoelectric layers, were derived by using Hamilton’s principle. To get a solution, a non-conforming C-0 triangular plate element was developed with eight degrees of freedom per node. One of these DOFs was saved to control the singularities in the global

stiffness matrix when shell elements were coplanar. This was because the original theory did not have any stiffness related to the drilling DOF (rotation around the element's normal direction). Three test cases proved the effectiveness of the theoretical solution to model the passive and active damping of sandwich structures. For the tests of sandwich structures, the active damping was as effective as the as the passive one. However the study lacked information on the sensitivity of the electric parameters in the overall results. No experimental data was given either.

An improved C-0 three iso-parametric node beam element with high order displacement functions was proposed in Chakrabarti et al. (2011). The equivalent single layer theory was developed considering Zig-Zag assumptions. The in-plane displacement was a combination of a linear Zig-Zag function with different slopes at each layer and a cubically varying function over the thickness. On the other hand, the transverse displacement was given by using a linear interpolation of the mid-thickness displacement value of each component. This field was assumed to vary quadratically through the core thickness and constant over the face sheets. Transverse shear stress continuity conditions at the layer interfaces and the conditions of zero transverse shear stress at the top and bottom of the beam were fulfilled. This formulation presented seven DOFs per node; hence the current element had 21 DOFs. Static verification of the proposed theory showed good accuracy of the model to the consulted exact solution, and compared to FE models developed within Abaqus. Unfortunately, no details were given regarding this FE models obtained by Abaqus.

According to Carrera, Miglioretti and Petrolo (2011a), CUF approach was used to achieve a better understanding of each expansion term in each displacement variable. The ESL models obtained via classical displacement formulation were studied. Particularly, the fourth order equivalent single layer (ED4) was compared to Layer-Wise couple (LD4). This LD4 theory was used as a reference solution. Once again, an analytical closed form solution was used to solve the equations for a laminated plate under different transverse loads. Next, other different parameters were allowed to change: the length-to-thickness ratio, the orthotropic ratio, the ply orientation, symmetry of lamination and boundary conditions in addition to the loading. Each of these five parameters was evaluated one at the time. Then, the influence of each expansion term in the ED4 theory was assessed by its removal. The resulting theory was graphically compared to the LD4 solution for the in-plane normal stress and the out-of-plane shear stress. By inspecting these graphs, specific displacement functions were derived for each displacement and stress variable. The new results when compared to data from the literature showed that the formulation could reduce the errors to up three orders of magnitude. As to the

parametric study of the formulations, the influence of each term was also greatly influenced by the laminate configuration. All parameters exhibited a qualitative influence on the results and the inclusion or removal of terms may change with the parameter. The intensity of each term also varied in function of the parameters. The work endorsed explicitly the difficulty in formulation of accurate and robust plate theory.

Thin and thick shells were analyzed by Ferreira et al. (2011a) by using a radial basis method. Carrera's unified formulation was implemented for a particular set of displacement field functions. All three displacement variables presented the membrane contribution, a linear term in the thickness direction and a sine function for the thickness direction as well. Using the principle of virtual displacements (PVD), the fundamental nuclei for doubly curved shells were explicitly demonstrated. The collocated approach demanded the definition of the essential and natural boundary conditions, which form a second set of nuclei matrices. The dynamic and static results were obtained on a Chebyshev grid and an optimized form of Wendland's radial function. The meshless approach had the advantage of easy coding, absence of mesh and easy discretization of the equations of motion. The static displacements and the natural frequencies outputs from present method were in excellent agreement to the analytical solutions.

Carrera, Miglioretti and Petrolo (2011b) once more explored CUF to generate guidelines on choosing which expansion terms should be retained and those that should be removed to predict the response of plates in bending conditions. The authors developed several diagrams to evaluate the contributions as functions of the loading and boundaries conditions, geometry, material and anisotropy of the plate. All these diagrams were grouped to yield the Best Plate Curve. It was an exponential decay shaped curve, which bounded the theories with the lowest number of terms for a given accuracy. Although it was a very laborious task, it seems to be the best tool to choose a particular high order theory according to the desired accuracy and computational cost.

Once again, static and free vibration problems with cross-ply laminated plates and buckling cases were investigated by Ferreira et al. (2011b). They developed RBF solution by using an equivalent single layer theory improved via Murakami's Zig-Zag function for the linear in-plane displacement functions, and a quadratic expansion of the thickness coordinate for the transverse displacement. PVD was assumed. Just as their previous work, the numerical problems were solved by using an improved version of Wendland's radial function in a Chebyshev grid. Comparison to the approximate and exact results from the literature indicated a good resolution of the method. Direct comparison of the proposed formulation to the previous

sine one by the same authors was not possible due to the difference laminate configurations of the given examples.

Sartorato et al. (2011) presented a method to calculate the shear correction factors for laminated plates using FE simulations of a representative volume unit of unidirectional fibers. The importance of the shear correction factors in dynamic analyses was shown via direct and indirect comparisons due to the lack of references. Later, Sartorato and Tita (2012) developed a laminated beam element with a different calculation of the shear correction factor from Sartorato et al. (2011). Transversal shear strain energy assumptions were used in this case. The element was implemented in Abaqus through a FORTRAN sub-routine (UEL – User Element). The influence of the shear correction factor for different lamination parameters was investigated.

The paper developed by Bouayed and Hamdi (2012) brought a new Layer-Wise sandwich shell element for dynamic and vibration problems. The displacement functions vary linearly with the normal direction of the shell. The element had twelve DOFs per node and eight nodes with quadratic shape functions. No shear locking was seen in the results by using the approach proposal, and the element was considered to be locking free. The dynamic equations of motion were solved in the frequency domain to save computational time. A sandwich plate and a cylindrical sandwich shell academic test cases were solved by using the proposed element and via 3D finite element models created in two commercial software (Rayon-VTM and Nastran). Then, an experimental validation was carried out for two industrial windscreens with and without acoustics properties in the thin viscoelastic core layer made by polyvinyl butyral (PVB). The windscreens were hanged with light elastic strings and the frequency response was measured by using the Polytec Laser Vibrometer System PSV-400. Dynamic results confirmed the accuracy of the proposed approach for the sandwich

A four node dynamic finite element based on a HSAPT was developed by Elmalich and Rabinovitch (2012). FSPT was assigned to the displacement field in the skins. As for the core, the in-plane displacements were defined with full cubic order expansion series of the thickness coordinate. Second order was used for the transverse displacement. Through compatibility conditions at the two interfaces, the core's displacement functions were rearranged as a function of the top and bottom displacement DOFs. Thus, the FE approximation comprised 11 displacement DOFs. Therefore, the element had 44 DOFs, which were considerably low for laminated composite structure theories. The equations of motion were solved with Newmark's algorithm. No damping was considered. The first 20 vibration modes detected by the present model were compared to experimental and 2D FEA results from the same reference. Apart from

values for three natural frequencies, the formulation results were no more than 4% different from the references. To test the numeric aspects of the formulation, an “L-shaped” sandwich plate was studied. Some unique aspects of the sandwich structure such as localized effects, deformability of the core, boundary conditions effects and the evolution of the natural frequencies were evaluated.

Laminated composite structures with material properties varying gradually over the thickness (Functionally Graded Materials - FGM) were investigated in Neves et al. (2012a). In-plane displacements were improved via hyperbolic function of the thickness coordinate. The out-of-plane displacement was described by using a full second order polynomial of the thickness coordinate. An exponential function by using a parameter “p” was suggested to evaluate the volumetric fraction of ceramic at a given height. The law-of-mixtures was then suggested to obtain the average material properties at this given height. Dynamic equations of motion and boundary conditions of derived via PVD method through integration by parts. An aluminum (bottom face) to alumina (top face) composite plate was studied numerically by using the proposed formulation. To accurately solve the varying properties in the thickness direction, 91 mathematical layers were used to solve the equations via RBF method. Chebyshev grid was used and tested for three mesh densities. Results pointed to a quasi-3D solution of the chosen examples for p = 1, 5 and 10.

In the more recently work (CHALAK et al., 2012), the authors proposed an extension to a previous one (CHAKRABARTI et al. (2011). In the new paper, a C-0 nine node quadratic element was developed. The in-plane displacement functions were the same as those used for the beam element previously defined. It was a combination of a linear Zig-Zag function with different slopes at each layer and a cubically varying function over the thickness. The out-of-plane displacement was assumed to vary quadratically through the core thickness and constant over the face sheets. It was obtained via Lagrangian interpolation of the respective values in each layer. For the core, compatibility at the interfaces granted a total of 11 DOFs. Hence, the element possessed 99 DOFs. Several numerical problems were solved for different problems of laminated composite and sandwich plates. The results of the present FE model were accurate compared to many published results.

Neves et al. (2012b) studied a laminated composite structures with material properties varying gradually over the thickness (Functionally Graded Materials - FGM). However, the formulation now accounts for a three layer laminate. Two configurations were studied. For the first, both faces were isotropic and the core was a FGM layer. In the second one, the core was an isotropic material and the skins were FGM layers. Due to this discontinuity of material

through the thickness of the laminate, MZZF was applied to both in-plane displacement functions of their previous formulation by using a hyperbolic sine function of the thickness coordinate (NEVES et al. 2012a). Governing equations and the RBF solutions for the static examples were derived via the same drill. The results were given for p = 0.2, 0.5, 1, 2, 5, and 10 values for the exponential volumetric function. Results showed the same level of accuracy of the previous work.

Based on CUF, Ferreira et at. (2013) modified the mass and stiffness finite element matrices to model the viscoelastic behavior of the layers. Displacement functions were linear in respect to the thickness direction. To this purpose, complex engineering parameters were assumed. Next, Hamilton's principle was used to derive the equations of motion. A nine node element was implemented and the resulting eigenvalue problem was solved iteratively. Damped sandwich cases evaluations pointed an excellent agreement to the reference results.

Chinosi et al. (2013), in the frame of CUF, derived an equivalent single layer element based on the interpolation idea of Dvorkin (1995). Instead of interpolating the strains, the authors proposed a parabolic interpolation of the transverse stresses. On the other hand, the displacement degrees of freedom were described via FSPT. Under these assumptions, the formulation was named EM1-2, since it was derived from Reissner's theorem. Tests of the present formulation for sandwich plates showed equivalence between FSPT and the EM1-2 plate formulations. Nonetheless, the EM1-2 resulted respect inter-laminar continuity requirements. Moreover, the locking issue was successfully circumvented.

FGM were investigated once more by Neves et al. (2013). The authors considered the same expansion series of the thickness direction for all three displacement fields. It was the FSPT with a cubic term added. The same exponential function of volume fraction was considered and the results for few values of "p" were given. This work was focused on the normal strain level, which was up until now neglected in previous studies. Using RBF with Wendland's function, static, dynamic and buckling problems were evaluated. The results showed a partial improvement in comparison with the reference.

A global-local formulation considering FSPT for the global displacements and a linear single local refinement for both global in-plane displacements was published by Khalili, Shriayat and Rajabi (2014). Compatibility conditions at the interfaces rendered a nine-node element with eleven DOFs per node. It was a 99-DOFs element. The transverse stresses were calculated via integration of equilibrium equations. Overall results matched quite well the analytical one.

Lastly and very recently, a FE approach for geometrically non-linear problems of fiber reinforced plates and shells was presented by Sampaio, Paccola and Coda (2015). The motivation of this implementation was its ability to model a shell with short or long fibers without having to increase the number of DOFs of the element with the inclusion of the fibers. In this sense, the formulation can be tagged as of the ESL type. Also, the need for matching the fibers and shells nodes was avoided. They used a 70-DOF triangular element. The displacement results of the five test cases showed the good potential of the formulation. No microscopic results were given.

It was seen that many different derivation methods and assumptions can be used to solve a structural problem using a FE code. Other solution methods such as RBFs and Fourier series were quoted but they are not as flexible. It means that the FEM is able to solve a larger variety of geometrically complex problems. Accuracy of the solution methods usually increases with the number of DOFs of the formulation. However, solution time and effort increase too. In the end, it becomes hard to answer whether to choose from a “p” or “h” solution refinement. As comment earlier, the first increases the complexity of the interpolation functions. The second tries to improve accuracy by increasing the number of sub-domains which is usually achieved by reducing their initial size in an attempt to geometrically linearize the problem.

For the reasons pointed above, the present PhD thesis shows a new solution method based on the generalized CUF, which is more physically consistent with the “plate problem” as it accurately solves the first derivations of the transversal displacement using a C-1 implementation. Using this implementation, the performance and accuracy of different plate theories can be investigated for both in-plane and out-of-plane behaviors. The next Chapter details the proposal.

Chapter 5 - A New Generalized Plate Solution - CGF

5.1 From GUF to CGF

In this chapter, a new generalized solution method for the Generalized Unified Formulation of plates and shells proposed by Demasi (DEMASI, 2009a) is developed in this PhD thesis and is henceforth tagged as CGF (Caliri's Generalized Formulation).

The proposed formulation is to use the Finite Element Method to solve the analytical kernel of GUF in equation (3.58). Its respective FE kernel in equation (4.51) will be modified to account for an implementation with C-1 compatibility requirements of the deflection displacement field. The in-plane displacement fields will be implemented with C-0 fields. Di Sciuva (1985) did something similar, but for a particular ZZ theory, as reviewed earlier.

Therefore, using the irreducible form within the PVD, a more physically consistent solution method and a more accurate formulation via FE are expected. Also, this further generalizes the GUF by allowing more theories to be grouped into this solution method, such as Reddy's (1990). For starters, the author investigated the proposed formulation by using a four node quadrilateral plate element. Linear Serendipity interpolations are used for the in-plane displacement fields and Hermitian interpolations are used to achieve the C-1 behavior of the transversal displacement field.

Changing the linear interpolation of the in-plane displacements to quadratic fields should increase the accuracy of the solution. Nonetheless, four more nodes (Serenditipy quadratic element) are used in such formulation and because of this, the respective solution method might become high expansive computationally. Thus, firstly, the author will present the initially proposed formulation and assess its computational performance, accuracy and errors as well as its potentialities and limitations in Chapter 6.

5.1.1 C-1 Kinematic Assumptions

The derivation of the FE C-1 displacement kernel begins with the recognition that two rotations and a twist and the respective coupled moments will be equilibrated and solved for as well. This is a characteristic of CGF. The analytical kernel from GUF does not involve this additional degrees of freedom. They appear naturally in the solution method herein proposed due to the C-1 requirement of the FEM. So, the elementary equilibrium system for a static case using CGF is:

$$\begin{Bmatrix} \boldsymbol{P} \\ \boldsymbol{M} \end{Bmatrix}_i^{(e)} = \begin{bmatrix} K_{uu} & K_{uw} \\ K_{wu} & K_{ww} \end{bmatrix}_{ij}^{(e)} \begin{Bmatrix} \boldsymbol{u} \\ \boldsymbol{w}, \end{Bmatrix}_j^{(e)} - \begin{bmatrix} M_{uu} & 0 \\ 0 & M_{ww} \end{bmatrix}_{ij}^{(e)} \begin{Bmatrix} \ddot{\boldsymbol{u}} \\ \ddot{\boldsymbol{w}}, \end{Bmatrix}_j^{(e)} \tag{5.1}$$

The stiffness matrices of equation (5.1) are not in their unified form yet. Meaning that one cannot see the parameters of neither the unification nor the generalization. The total number of DOFs in the element is related to the number of terms in the displacement field assumed axiomatically. From GUF, the unified kinematics used in CGF are:

$$\begin{aligned} u^k(x,y,z) &= \wp_{\alpha_u}^k(z) u_{\alpha_u}^k(x,y); \alpha_u = t, b, z \dots N_{\alpha_u} \\ v^k(x,y,z) &= \wp_{\alpha_v}^k(z) v_{\alpha_v}^k(x,y); \alpha_v = t, b, z \dots N_{\alpha_v} \\ w^k(x,y,z) &= \wp_{\alpha_w}^k(z) w_{\alpha_w}^k(x,y); \alpha_w = t, b, z \dots N_{\alpha_w} \\ t &= top; b = bottom; z = zigzag \end{aligned} \tag{5.2}$$

To derive the proposed unified formulation, the linear part of equation (2.6) will be used to obtain the strain fields. From equation (5.2):

$$\begin{aligned} \varepsilon_{xx} &= u_{,x} & \varepsilon_{xz} &= \frac{1}{2}\left(w_{,x} + u_{,z}\right) \\ \varepsilon_{yy} &= v_{,y} & \varepsilon_{yz} &= \frac{1}{2}\left(w_{,y} + v_{,z}\right) \\ \varepsilon_{xy} &= \frac{1}{2}\left(u_{,y} + v_{,x}\right) & \varepsilon_{zz} &= w_{,z} \end{aligned} \tag{5.3}$$

However, if a kernel for geometrically non-linear cases is needed, e. g. post-buckling, the full version of (2.6) can be inserted in the derivation process instead. Naturally, the kernel is expected to be much larger and is left as a matter for future works.

5.1.2 CGF FE Kernel

In general, the C-1 approximating functions and their first derivative must be continuous across the element boundaries. To accomplish this, the interpolation functions for 2D elements must:

I. Contain at least some cubic terms because there are three nodal values "ψ", "$\psi_{,x}$" and "$\psi_{,y}$" assigned at each node.
II. Contain the remaining second order derivative terms "$\psi_{,xx}$", "$\psi_{,xy}$" and "$\psi_{,yy}$" as nodal variables if the element is non-rectangular.

For triangles, the second requirement is a must and cannot be skipped. Therefore the most common C-1 triangular element has 6 nodes and 18 DOFs. Actually it needs 21 variables to be C-1 continuous, but the last three DOFs are the normal derivatives at the mid-side nodes of the element, which are written in terms of the other nodal variables.

For quadrilaterals, with element sides are parallel to the GCS axis, only the cross derivative needs to be solved. This is the case for the current C-1 implementation, which coincides with the requirement of the solution for the bending of thin plates (HUEBNER; THORNTON, 1982). Enforcing full C-1 continuity might physically over-constraint the element, if the plate stiffness varies from element to element or there is a material change. In this case the continuity of moments normal to the interfaces cannot be achieved.

A survey on C-1 requirements for interpolation functions shows that C-1 problems are usually solved with Hermite polynomials (HUEBNER; THORNTON, 1982, ZIENKIEWICZ; TAYLOR, 2000b). The property that makes Hermitian polynomials suitable for C-1 problems is the fact that the polynomial itself and its derivatives up to the "n^{th}" order are either zero or unity at the end point of the closed interval [0, 1]. In a 1D case, for a node at "x_1"= 0 and for a second node one "x_2" = 1:

$$H_{mi}^{n}(x_i) = 1;\ m = 0 \qquad \frac{d^k H_{mi}^{n}(x_i)}{dx^k} = 0;\ m \neq k \qquad \frac{d^k H_{mi}^{n}(x_i)}{dx^k} = 1;\ m = k \tag{5.4}$$

where "m" is the order of the derivative and "i" makes reference to the node and "n" is the order of the Hermite polynomial.

For the 2D plate problems with C-1 continuity, the respective interpolation functions can be achieved by multiplying two 1D Hermite polynomials. For the plate bending problem (equation (3.18)), which requires C-1 continuity, the approximation function becomes:

$$w \cong \widetilde{w} = \sum_{i=1}^{i=N_e} H_j^1(x,y)^{(e)} w_i + H_j^2(x,y)^{(e)}\left(w_{,x}\right)_i + H_j^3(x,y)^{(e)}\left(w_{,y}\right)_i + H_j^4(x,y)^{(e)}\left(w_{,xy}\right)_i \tag{5.5}$$

$$H_j^1(x,y) = H_{0j}^{(1)}(x)H_{0j}^{(1)}(y) \qquad H_j^3(x,y) = H_{1j}^{(1)}(x)H_{0j}^{(1)}(y)$$

$$H_j^2(x,y) = H_{0j}^{(1)}(x)H_{1j}^{(1)}(y) \qquad H_j^4(x,y) = H_{1j}^{(1)}(x)H_{1j}^{(1)}(y)$$

The other displacement fields are approximated in a C-0 fashion and, therefore, are interpolated with the regular linear Serendipity functions. Since the chosen Hermite polynomials are cubic, the formulation can be classified as sub-parametric. Explicit expressions of the interpolation functions in natural coordinates can be found in Appendix A.

To achieve the generalized unified FE kernel of CGF, the generalization from equation (5.2) is added to the following PVD in equation (5.6). In this equation a laminate with "N_l" plies is assumed.

$$\sum_{k=1}^{N_l}\left\{\int_{\Gamma^k}\int_{z^k} \boldsymbol{\nabla}\{F_\alpha^{kr}\delta u_\alpha^k\}^T : \boldsymbol{C} : \boldsymbol{\nabla}\{F_\alpha^{ks}u_\alpha^k\}dzd\Gamma^k - \int_{\Gamma^k}\int_{z^k}\rho\{F_\alpha^{kr}\ddot{u}_\alpha^k\}\cdot\{F_\alpha^{ks}u_\alpha^k\}dzd\Gamma^k - \delta L_{ext}^k\right\} = 0 \tag{5.6}$$

The unification continues with the respective vector "$\{u_\tau\}_i$" of nodal variables:

$$\boldsymbol{u}_{\tau}^{k} = {}^{c0}N_i \boldsymbol{u}_{\tau i}^{k} \leftrightarrow \boldsymbol{u}_{\tau}^{k} = \left\{\boldsymbol{u}_{\alpha_u}^{k}, \boldsymbol{v}_{\alpha_v}^{k}\right\} \tag{5.7}$$

$$w_{\alpha_w}^{k} = {}^{c1}H_i w_{\alpha_w i}^{k}$$

$$\{u_{\tau}^{k}\}_i = \left\{u_{\alpha_u}^{k} \quad v_{\alpha_v}^{k} \quad \left[w^k \quad w_{,x}^{k} \quad w_{,y}^{k} \quad w_{,xy}^{k}\right]_{\alpha_w}\right\}_i$$

$$i = 1 \ldots 4$$

Then, inserting equation (5.7) in (5.6), the respective PVD with nodal variables becomes:

$$\int_{\Omega} \boldsymbol{\nabla}\{F_{\alpha}^{kr}[N_i]\{\delta u_{\alpha}^{k}\}_i\}^T : \boldsymbol{C} : \boldsymbol{\nabla}\left\{F_{\alpha}^{ks}\left[N_j\right]\{u_{\alpha}^{k}\}_j\right\} d\Omega \tag{5.8}$$

$$- \int_{\Omega} \rho\{F_{\alpha}^{kr}[N_i]\{\ddot{u}_{\alpha}^{k}\}_i\} \cdot \left\{F_{\alpha}^{ks}\left[N_j\right]\{\delta u_{\alpha}^{k}\}_j\right\} d\Omega - \delta L_{ext} = 0$$

where:

$$\boldsymbol{\nabla} F_{\alpha}^{kr}[N_i]\{\delta u_{\alpha}^{k}\}_i = \{\partial F_{\alpha}^{kr}[N_i] + F_{\alpha}^{kr}[\partial N_i]\}\{\delta u_{\alpha}^{k}\}_i \tag{5.9}$$

$$\partial F_{\alpha}^{rk} = \begin{pmatrix} 0 & 0 & 0 \\ 0 & 0 & 0 \\ 0 & 0 & F_{\alpha_w,z}^{kr_w} \\ 0 & 0 & 0 \\ F_{\alpha_u,z}^{kr_u} & 0 & 0 \\ 0 & F_{\alpha_v,z}^{kr_v} & 0 \end{pmatrix}$$

$$[\partial N_i] = \begin{pmatrix} \partial_x & 0 & 0 \\ 0 & \partial_y & 0 \\ 0 & 0 & \partial_z \\ \partial_y & \partial_x & 0 \\ \partial_z & 0 & \partial_x \\ 0 & \partial_z & \partial_y \end{pmatrix} \begin{Bmatrix} N_i & 0 & & 0 & & \\ 0 & N_i & & 0 & & \\ 0 & 0 & H_i^1 & H_i^2 & H_i^3 & H_i^4 \end{Bmatrix}$$

The “Ns” in equation (5.9) refer to the linear Serendipity interpolations and the “Hs” indicate the cubic Hermite polynomials. Lastly, the “C” is the regular constitutive matrix written in the global coordinate system for laminated plates. However, for this formulation, some terms are re-allocated:

$$C = \begin{Bmatrix} C_{11} & C_{12} \\ C_{21} & C_{22} \end{Bmatrix} \tag{5.10}$$

$$C_{11} = \begin{Bmatrix} \bar{C}_{11} & \bar{C}_{12} & \bar{C}_{13} \\ \bar{C}_{21} & \bar{C}_{22} & \bar{C}_{23} \\ \bar{C}_{31} & \bar{C}_{32} & \bar{C}_{33} \end{Bmatrix}; C_{22} = \begin{Bmatrix} \bar{C}_{66} & 0 & 0 \\ 0 & \bar{C}_{55} & \bar{C}_{54} \\ 0 & \bar{C}_{45} & \bar{C}_{44} \end{Bmatrix} \tag{5.11}$$

$$C_{12} = \begin{Bmatrix} \bar{C}_{16} & 0 & 0 \\ \bar{C}_{26} & 0 & 0 \\ \bar{C}_{36} & 0 & 0 \end{Bmatrix} = C_{21}^{T}$$

At last, evaluating the respective integrals, the elementary FE kernel of CGF is:

$$kernel_{CGF} \rightarrow \boldsymbol{K}_{CGF}^{krsij} = \begin{bmatrix} [\boldsymbol{K}_{uu}^{krs}] & [\boldsymbol{K}_{uw}^{krs}] \\ [\boldsymbol{K}_{wu}^{krs}] & [\boldsymbol{K}_{ww}^{krs}] \end{bmatrix}_{ij}^{(e)} = \tag{5.12}$$

$$\begin{bmatrix} \boldsymbol{K}_{uu}^{kr_u s_u} & \boldsymbol{K}_{uv}^{kr_u s_v} & \boldsymbol{K}_{uw}^{kr_u s_w} & \boldsymbol{K}_{uw,x}^{kr_u s_w} & \boldsymbol{K}_{uw,y}^{kr_u s_w} & \boldsymbol{K}_{uw,xy}^{kr_u s_w} \\ & \boldsymbol{k}_{vv}^{kr_v s_v} & \boldsymbol{K}_{vw}^{kr_v s_w} & \boldsymbol{K}_{vw,x}^{kr_v s_w} & \boldsymbol{K}_{vw,y}^{kr_v s_w} & \boldsymbol{K}_{vw,xy}^{kr_v s_w} \\ & & \boldsymbol{k}_{ww}^{kr_w s_w} & \boldsymbol{K}_{ww,x}^{kr_w s_w} & \boldsymbol{K}_{ww,y}^{kr_w s_w} & \boldsymbol{K}_{ww,xy}^{kr_w s_w} \\ & & & \boldsymbol{K}_{w,xw,x}^{kr_w s_w} & \boldsymbol{K}_{w,xw,y}^{kr_w s_w} & \boldsymbol{K}_{w,xw,xy}^{kr_w s_w} \\ & sym & & & \boldsymbol{K}_{w,yw,y}^{kr_w s_w} & \boldsymbol{K}_{w,yw,xy}^{kr_w s_w} \\ & & & & & \boldsymbol{K}_{w,xyw,xy}^{kr_w s_w} \end{bmatrix}_{ij}^{(e)}$$

Where, “r”, “s”, “i” and “j” are recursive indexes. The 21 explicit components of this elementary symmetrical kernel are given in equation (5.13-5.18):

$$\begin{aligned} K_{uu}^{krsij} &= \mathbb{Z}_{11}^{kr_u s_u}\langle N_{i,x}N_{j,x}\rangle + \mathbb{Z}_{61}^{kr_u s_u}\langle N_{i,y}N_{j,x}\rangle + \mathbb{Z}_{16}^{kr_u s_u}\langle N_{i,x}N_{j,y}\rangle + \mathbb{Z}_{66}^{kr_u s_u}\langle N_{i,y}N_{j,y}\rangle \\ &\quad + \mathbb{Z}_{55}^{kr_{u,z} s_{u,z}}\langle N_i N_j\rangle \end{aligned} \tag{5.13}$$

$$\begin{aligned} K_{uv}^{krsij} &= \mathbb{Z}_{12}^{kr_u s_v}\langle N_{i,x}N_{j,y}\rangle + \mathbb{Z}_{62}^{kr_u s_v}\langle N_{i,y}N_{j,y}\rangle + \mathbb{Z}_{16}^{kr_u s_v}\langle N_{i,x}N_{j,x}\rangle + \mathbb{Z}_{66}^{kr_u s_w}\langle N_{i,y}N_{j,x}\rangle \\ &\quad + \mathbb{Z}_{54}^{kr_{u,z} s_{w,z}}\langle N_i N_j\rangle \end{aligned}$$

$$K_{uw}^{krsij} = \mathbb{Z}_{13}^{kr_u s_{w,z}}\langle N_{i,x}H_j^1\rangle + \mathbb{Z}_{63}^{kr_u s_{w,z}}\langle N_{i,y}H_j^1\rangle + \mathbb{Z}_{55}^{kr_{u,z} s_w}\langle N_i H_{j,x}^1\rangle + \mathbb{Z}_{54}^{kr_{u,z} s_w}\langle N_i H_{j,y}^1\rangle$$

$$
\begin{aligned}
K_{uw,x}^{krsij} &= \mathbb{Z}_{13}^{kr_u s_{w,z}}\langle N_{i,x}H_j^2\rangle + \mathbb{Z}_{63}^{kr_u s_{w,z}}\langle N_{i,y}H_j^2\rangle + \mathbb{Z}_{55}^{kr_{u,z} s_w}\langle N_i H_{j,x}^2\rangle \\
&\quad + \mathbb{Z}_{54}^{kr_{u,z} s_w}\langle N_i H_{j,y}^2\rangle \\
K_{uw,y}^{krsij} &= \mathbb{Z}_{13}^{kr_u s_{w,z}}\langle N_{i,x}H_j^3\rangle + \mathbb{Z}_{63}^{kr_u s_{w,z}}\langle N_{i,y}H_j^3\rangle + \mathbb{Z}_{55}^{kr_{u,z} s_w}\langle N_i H_{j,x}^3\rangle \\
&\quad + \mathbb{Z}_{54}^{kr_{u,z} s_w}\langle N_i H_{j,y}^3\rangle \\
KK_{uw,xy}^{krsij} &= \mathbb{Z}_{13}^{kr_u s_{w,z}}\langle N_{i,x}H_j^4\rangle + \mathbb{Z}_{63}^{kr_u s_{w,z}}\langle N_{i,y}H_j^4\rangle + \mathbb{Z}_{55}^{kr_{u,z} s_w}\langle N_i H_{j,x}^4\rangle \\
&\quad + \mathbb{Z}_{54}^{kr_{u,z} s_w}\langle N_i H_{j,y}^4\rangle
\end{aligned}
\tag{5.13}
$$

$$
\begin{aligned}
K_{vu}^{krsij} &= K_{uv}^{krsij} \\
K_{vv}^{krsij} &= \mathbb{Z}_{22}^{kr_v s_v}\langle N_{i,y}N_{j,y}\rangle + \mathbb{Z}_{62}^{kr_v s_v}\langle N_{i,x}N_{j,y}\rangle + \mathbb{Z}_{26}^{kr_v s_v}\langle N_{i,y}N_{j,x}\rangle + \mathbb{Z}_{66}^{kr_v s_v}\langle N_{i,x}N_{j,x}\rangle \\
&\quad + \mathbb{Z}_{44}^{kr_{v,z} s_{v,z}}\langle N_i N_j\rangle \\
K_{vw}^{krsij} &= \mathbb{Z}_{23}^{kr_v s_{w,z}}\langle N_{i,y}H_j^1\rangle + \mathbb{Z}_{63}^{kr_v s_{w,z}}\langle N_{i,x}H_j^1\rangle + \mathbb{Z}_{45}^{kr_{v,z} s_w}\langle N_i H_{j,x}^1\rangle + \mathbb{Z}_{44}^{kr_{v,z} s_w}\langle N_i H_{j,y}^1\rangle \\
K_{vw,x}^{krsij} &= \mathbb{Z}_{23}^{kr_v s_{w,z}}\langle N_{i,y}H_j^2\rangle + \mathbb{Z}_{63}^{kr_v s_{w,z}}\langle N_{i,x}H_j^2\rangle + \mathbb{Z}_{45}^{kr_{v,z} s_w}\langle N_i H_{j,x}^2\rangle + \mathbb{Z}_{44}^{kr_{v,z} s_w}\langle N_i H_{j,y}^2\rangle \\
K_{vw,y}^{krsij} &= \mathbb{Z}_{23}^{kr_v s_{w,z}}\langle N_{i,y}H_j^3\rangle + \mathbb{Z}_{63}^{kr_v s_{w,z}}\langle N_{i,x}H_j^3\rangle + \mathbb{Z}_{45}^{kr_{v,z} s_w}\langle N_i H_{j,x}^3\rangle + \mathbb{Z}_{44}^{kr_{v,z} s_w}\langle N_i H_{j,y}^3\rangle \\
K_{vw,xy}^{krsij} &= \mathbb{Z}_{23}^{kr_v s_{w,z}}\langle N_{i,y}H_j^4\rangle + \mathbb{Z}_{63}^{kr_v s_{w,z}}\langle N_{i,x}H_j^4\rangle + \mathbb{Z}_{45}^{kr_{v,z} s_w}\langle N_i H_{j,x}^4\rangle + \mathbb{Z}_{44}^{kr_{v,z} s_w}\langle N_i H_{j,y}^4\rangle
\end{aligned}
\tag{5.14}
$$

$$
\begin{aligned}
K_{wu}^{krsij} &= K_{uw}^{krsij} \\
K_{wv}^{krsij} &= K_{vw}^{krsij} \\
K_{ww}^{krsij} &= \mathbb{Z}_{33}^{kr_{w,z} s_{w,z}}\langle H_i^1 H_j^1\rangle + \mathbb{Z}_{45}^{kr_w s_w}\langle H_{i,y}^1 H_{j,x}^1\rangle + \mathbb{Z}_{55}^{kr_w s_w}\langle H_{i,x}^1 H_{j,x}^1\rangle \\
&\quad + \mathbb{Z}_{44}^{kr_w s_w}\langle H_{i,y}^1 H_{j,y}^1\rangle + \mathbb{Z}z_{54}^{kr_w s_w}\langle H_{i,x}^1 H_{j,y}^1\rangle \\
K_{ww,x}^{krsij} &= \mathbb{Z}_{33}^{kr_{w,z} s_{w,z}}\langle H_i^1 H_j^2\rangle + \mathbb{Z}_{45}^{kr_w s_w}\langle H_{i,y}^1 H_{j,x}^2\rangle + \mathbb{Z}_{55}^{kr_w s_w}\langle H_{i,x}^1 H_{j,x}^2\rangle \\
&\quad + \mathbb{Z}_{44}^{kr_w s_w}\langle H_{i,y}^1 H_{j,y}^2\rangle + \mathbb{Z}_{54}^{kr_w s_w}\langle H_{i,x}^1 H_{j,y}^2\rangle \\
K_{ww,y}^{krsij} &= \mathbb{Z}_{33}^{kr_{w,z} s_{w,z}}\langle H_i^1 H_j^3\rangle + \mathbb{Z}_{45}^{kr_w s_w}\langle H_{i,y}^1 H_{j,x}^3\rangle + \mathbb{Z}_{55}^{kr_w s_w}\langle H_{i,x}^1 H_{j,x}^3\rangle \\
&\quad + \mathbb{Z}_{44}^{kr_w s_w}\langle H_{i,y}^1 H_{j,y}^3\rangle + \mathbb{Z}_{54}^{kr_w s_w}\langle H_{i,x}^1 H_{j,y}^3\rangle \\
K_{ww,xy}^{krsij} &= \mathbb{Z}_{33}^{kr_{w,z} s_{w,z}}\langle H_i^1 H_j^4\rangle + \mathbb{Z}_{45}^{kr_w s_w}\langle H_{i,y}^1 H_{j,x}^4\rangle + \mathbb{Z}_{55}^{kr_w s_w}\langle H_{i,x}^1 H_{j,x}^4\rangle \\
&\quad + \mathbb{Z}_{44}^{kr_w s_w}\langle H_{i,y}^1 H_{j,y}^4\rangle + \mathbb{Z}_{54}^{kr_w s_w}\langle H_{i,x}^1 H_{j,y}^4\rangle
\end{aligned}
\tag{5.15}
$$

$$K_{w,xu}^{krsij} = K_{uw,x}^{krsij} \tag{5.16}$$
$$K_{w,xv}^{krsij} = K_{vw,x}^{krsij}$$
$$K_{w,xw}^{krsij} = K_{ww,x}^{krsij}$$
$$K_{w,xw,x}^{krsij} = \mathbb{Z}_{33}^{kr_{w,z}s_{w,z}}\langle H_i^2 H_j^2\rangle + \mathbb{Z}_{45}^{kr_w s_w}\langle H_{i,y}^2 H_{j,x}^2\rangle + \mathbb{Z}_{55}^{kr_w s_w}\langle H_{i,x}^2 H_{j,x}^2\rangle + \mathbb{Z}_{44}^{kr_w s_w}\langle H_{i,y}^2 H_{j,y}^2\rangle + \mathbb{Z}_{54}^{kr_w s_w}\langle H_{i,x}^2 H_{j,y}^2\rangle$$
$$K_{w,xw,y}^{krsij} = \mathbb{Z}_{33}^{kr_{w,z}s_{w,z}}\langle H_i^2 H_j^3\rangle + \mathbb{Z}_{45}^{kr_w s_w}\langle H_{i,y}^2 H_{j,x}^3\rangle + \mathbb{Z}_{55}^{kr_w s_w}\langle H_{i,x}^2 H_{j,x}^3\rangle + \mathbb{Z}_{44}^{kr_w s_w}\langle H_{i,y}^2 H_{j,y}^3\rangle + \mathbb{Z}_{54}^{kr_w s_w}\langle H_{i,x}^2 H_{j,y}^3\rangle$$
$$K_{w,xw,xy}^{krsij} = \mathbb{Z}_{33}^{kr_{w,z}s_{w,z}}\langle H_i^2 H_j^4\rangle + \mathbb{Z}_{45}^{kr_w s_w}\langle H_{i,y}^2 H_{j,x}^4\rangle + \mathbb{Z}_{55}^{kr_w s_w}\langle H_{i,x}^2 H_{j,x}^4\rangle + \mathbb{Z}_{44}^{kr_w s_w}\langle H_{i,y}^2 H_{j,y}^4\rangle + \mathbb{Z}_{54}^{kr_w s_w}\langle H_{i,x}^2 H_{j,y}^4\rangle$$

$$K_{w,yu}^{krsij} = K_{uw,y}^{krsij} \tag{5.17}$$
$$K_{w,yv}^{krsij} = K_{vw,y}^{krsij}$$
$$K_{w,yw}^{krsij} = K_{ww,y}^{krsij}$$
$$K_{w,yw,x}^{krsij} = K_{w,xw,y}^{krsij}$$
$$K_{w,yw,y}^{krsij} = \mathbb{Z}_{33}^{kr_{w,z}s_{w,z}}\langle H_i^3 H_j^3\rangle + \mathbb{Z}_{45}^{kr_w s_w}\langle H_{i,y}^3 H_{j,x}^3\rangle + \mathbb{Z}_{55}^{kr_w s_w}\langle H_{i,x}^3 H_{j,x}^3\rangle + \mathbb{Z}_{44}^{kr_w s_w}\langle H_{i,y}^3 H_{j,y}^3\rangle + \mathbb{Z}_{54}^{kr_w s_w}\langle H_{i,x}^3 H_{j,y}^3\rangle$$
$$K_{w,yw,xy}^{krsij} = \mathbb{Z}_{33}^{kr_{w,z}s_{w,z}}\langle H_i^3 H_j^4\rangle + \mathbb{Z}_{45}^{kr_w s_w}\langle H_{i,y}^3 H_{j,x}^4\rangle + \mathbb{Z}_{55}^{kr_w s_w}\langle H_{i,x}^3 H_{j,x}^4\rangle + \mathbb{Z}_{44}^{kr_w s_w}\langle H_{i,y}^3 H_{j,y}^4\rangle + \mathbb{Z}_{54}^{kr_w s_w}\langle H_{i,x}^3 H_{j,y}^4\rangle$$

$$K_{w,xyu}^{krsij} = K_{uw,xy}^{krsij} \tag{5.18}$$
$$K_{w,xyv}^{krsij} = K_{vw,xy}^{krsij}$$
$$K_{w,xyw}^{krsij} = K_{ww,xy}^{krsij}$$
$$K_{w,xyw,x}^{krsij} = K_{w,xw,xy}^{krsij}$$
$$K_{w,xyw,y}^{krsij} = K_{w,yw,xy}^{krsij}$$
$$K_{w,xyw,xy}^{krsij} = \mathbb{Z}_{33}^{kr_{w,z}s_{w,z}}\langle H_i^4 H_j^4\rangle + \mathbb{Z}_{45}^{kr_w s_w}\langle H_{i,y}^4 H_{j,x}^4\rangle + \mathbb{Z}_{55}^{kr_w s_w}\langle H_{i,x}^4 H_{j,x}^4\rangle + \mathbb{Z}_{44}^{kr_w s_w}\langle H_{i,y}^4 H_{j,y}^4\rangle + \mathbb{Z}_{54}^{kr_w s_w}\langle H_{i,x}^4 H_{j,y}^4\rangle$$

---

with:

$$\langle \dots \rangle = \int_{\Sigma} (\dots) d\Sigma \tag{5.19}$$

and:

$$\mathbb{Z}_{33}^{kr_{w,z}s_{w,z}} = \bar{C}_{33}^{k} \int_{z_b^k}^{z_t^k} F_{r_{w,z}}(z) F_{s_{w,z}}(z) dz \tag{5.20}$$

During the calculation of the global stiffness matrix, the thickness integrations of equation (5.20) are performed separately from the in-plane integrations. This greatly speeds up the numerical integration process.

For dynamic problems, the mass kernel matrix is also required. It is obtained from:

$$\begin{aligned} &\delta \boldsymbol{M}^{k} = \ddot{\boldsymbol{u}}_{ri}^{kT} \bar{\boldsymbol{M}}^{krsij} \delta \boldsymbol{u}_{sj}^{k} \\ &\bar{\boldsymbol{M}}_{mn}^{krsij} = \boldsymbol{M}^{krsij} \delta_{mn} \;\; m,n = \{u, v, w, w_{,x}, w_{,x}, w_{,xy}\} \\ &\delta_{mn} = 1 \;\leftrightarrow\; m = n \\ &\delta_{mn} = 0 \;\leftrightarrow\; m \neq n \end{aligned} \tag{5.21}$$

Explicitly, the components of the diagonal mass kernel matrix are:

$$\begin{aligned} M_{uu}^{krsij} &= \Lambda^{kr_u s_u} \langle N_i N_j \rangle \\ M_{vv}^{krsij} &= \Lambda^{kr_v s_v} \langle N_i N_j \rangle \\ M_{ww}^{krsij} &= \Lambda^{kr_w s_w} \langle H_i^1 H_j^1 \rangle \\ M_{w,_x w,_x}^{krsij} &= \Lambda^{kr_w s_w} \langle H_i^2 H_j^2 \rangle \\ M_{w,_y w,_y}^{krsij} &= \Lambda^{kr_w s_w} \langle H_i^3 H_j^3 \rangle \\ M_{w,_{xy} w,_{xy}}^{krsij} &= \Lambda^{kr_w s_w} \langle H_i^4 H_j^4 \rangle \\ \Lambda^{kr_w s_w} &= \rho^k \int_{z_b^k}^{z_t^k} F_{r_w}(z) F_{s_w}(z) dz \end{aligned} \tag{5.22}$$

To be integrated numerically, equations from (5.9) to (5.22) are evaluated at the LCS (Local Coordinate System, also known as *natural coordinates*).

It must be said that the C-1 continuity of the deflection is not a requirement from the PVD derivation in this case. It is, however, when one wants to derive a FE solution for the relatively large curvatures of thin plates only (HUEBNER; THORNTON, 1982). The PVD derivation in the thesis demands only continuity of the displacement fields to ensure convergence. Thus, the interpolation of first derivatives and the cross derivative of the transversal displacement was a choice, not a requirement. Once again, the purpose was to achieve a more physically consistent formulation.

In order to evaluate the accuracy of the formulation, an in-house FE code was developed. This code solves linear static problems and eigenvalue extraction problems, e. g. modal and/or buckling analyses. Details are given in next section.

5.2 In-house FE Code

Most of the reviewed references develop a finite element (based on a plate or shell theory) to solve random problems in a specific FE code. This approach is very common due to the popularity and commercial diffusion of the FE codes, and their ability to read these so called *user-elements*.

However, it is not so easy to insert and odd element formulation into a commercial FE code. Most of the times, the main issue is the coupling of the DOFs from the user element into the commercial solver. Also, the increase of unusual DOFs, requires the (initial) boundary values for boundary conditions. Therefore, these implementations are not straightforward and additional errors are expected. That is why this work does not attempt such implementation at the moment. Nonetheless, this is a requirement for a rigorous evaluation of the processing time. An option is to implement other elements in this in-house code. However, the first option is much more attractive as it allows the user to practically test an element with different kinds of engineering problems. This remains as a matter for future works.

In an attempt to control most of the implementation errors, an in-house code was developed using Matlab™. Two versions were developed. Both versions share most of the code, but on average, the codes are 3000 lines long. One code solves the problem in the ESL fashion

whereas the second does almost the same, but for a LW implementation. Since the solution is linear, the solution is obtained without iterative algorithms. Thus, the main steps (or blocks) of both codes algorithms were simplified in Figure 28.

The first step of the FE program (i) collects the dimensions and the material properties of the plate or the laminated plate. If the plate is laminated, the thickness of each ply must be set along with its azimuthal rotation angle of the ply. In this step the global stiffness matrix of each ply is computed too.

i. **Problem size and material properties**
ii. **Formulation selection (N_u, N_v and N_w)**
iii. **Calculation of the thickness polynomials or Legendre polynomials (For LW)**
iv. **Meshing**
v. **Pre-calculation of interpolation functions at IPs**
vi. **Thickness integration and matrix assemblage (for ESL)**
vii. **ESL/LW stiffness and mass kernels calculation**
viii. **Case problem solver**
ix. **Post-processing: Displacements, strains, natural frequencies, modal shapes, etc**

Figure 28. FE code steps

Step (ii) reads the number of expansion terms for each of the three displacement fields independently. Note that the maximum order of the polynomial is N-1, because of the constant term in the complete polynomial expansion. Therefore, the minimum number of N is 1, which refers to a displacement which is independent of the thickness coordinate. For the LW case, due to compatibility requirements, the minimum number of terms is 2 and the polynomials are at least linear functions of the thickness coordinate.

Based on the highest number of terms set for the polynomial expansions, Step (iii) analytically calculates all of these terms "F_τ" (see equation 3.45). For the ESL code the terms are easily defined, but for the LW case, the Legendre polynomials must be used to calculate the functions of the thickness coordinate "F_τ" according to equation 3.48 (e. g.). These terms also need to be calculated analytically, because when integrated, different evaluations of the functions are required. A recurrence formula was implement so that the program automatically calculates all of the necessary terms, up to the highest number of expansion terms.

In the next step, step (iv), the plate is meshed in a structured way so that no mapping matrix is needed to build the global stiffness and mass matrices. Some nodes are also tagged for future boundary condition constraining.

After struggling with slow integration in Matlab to assemble the global matrices, the code was optimized with step (v). At this step, a previous calculation of all expected values of the interpolation functions at IPs was performed and the value stored. This was needed because the assemblage of the global matrices in step vii) contains 7 loops for the ESL code and 8 for the LW one. In addition, the most inner loops are the in-plane integration loops where Matlab needs to evaluate the analytical functions, so there is an issue. Matlab has a minimum processing time to evaluate an analytical function, which is already too long.

In step (vi), the thickness integration is performed. In case the code is the ESL version, the sum of the transversal stiffness of each ply takes place to obtain the laminate transversal stiffness.

In step (vii) the kernel components in equations (5.13) to (5.18) and in equation (5.22) are integrated and assembled to form the global stiffness and mass matrices, respectively.

Using the global matrices assembled, the boundary conditions are applied and the problem is solved directly in Matlab during step (viii).

Lastly, the post-processing phase in step (ix) brings the displacement fields, strains, stresses, modal frequencies, modal shapes, etc.

This summary of the code explains what each block does and a brief explanation of their purpose. Next, the details of the numeric in-plane and out-of-plane integrations are given to show that the integrations are in fact exact. Also, the post-processing assumptions used to calculate the strains and stresses with CGF are explained too.

5.2.1 In-plane Integration

Equations (5.13) to (5.18) need to be evaluated at the LCS. For the derived kernel with cubic Hermitian polynomials and Serendipity linear functions, the in-plane integration is performed separately from the thickness integration.

For every component of the kernel matrix, each term of the sum of this particular component demands a specific number of integration points. To clarify, a random component

of the kernel matrix is brought to equation (5.23). If one looks at equation (5.23), the component of the stiffness kernel comprises a sum of five terms.

$$K_{uu}^{krsij} = z_{11}^{kr_u s_u}\langle N_{i,x}N_{j,x}\rangle + z_{61}^{kr_u s_u}\langle N_{i,y}N_{j,x}\rangle + z_{16}^{kr_u s_u}\langle N_{i,x}N_{j,y}\rangle + z_{66}^{kr_u s_u}\langle N_{i,y}N_{j,y}\rangle + z_{55}^{kr_{u,z} s_{u,z}}\langle N_i N_j\rangle \quad (5.23)$$

All five terms are multiplications of a Serendipity linear functions with a Hermitian cubic ones. If the interpolation functions are inserted into the first term of the right side of equation (5.23) and considering the derivations, one gets:

$$\langle N_{i,x}N_{j,x}\rangle \propto 1.\eta.1.\eta \propto \xi^0.\eta^2 \quad (5.24)$$

To discover the minimum number of IPs (Integration Points) needed to achieve an exact integration, equation (4.55) can be used to get:

$$NG \geq \left(\frac{2+0+1}{2}\right) \cong 2 \quad (5.25)$$

Where NG is the Number of Gauss' points. Hence, based on equation (5.25) at least 4 (NG^2) IPs are needed. It is clear that each term of the sum in (5.23) may require a different minimum number of IPs to achieve exact integration. Some numbers of IPs may coincide. Therefore, to easy the implementation of the code, the most expansive term of each component of the kernel is considered to perform the in-plane integrations. In this case, the last term:

$$NG \geq \left(\frac{2+2+1}{2}\right) \cong 3 \quad (5.26)$$

Thus, to build the respective stiffness kernel component with the developed code, 9 evaluations of (5.23) are needed for a particular pair of nodes (i, j) and expansion terms (r, s) of an element. In case of LW formulation, this process repeats for every ply too.

With this logic, step (v) was built considering NG = (3, 4, and 7) and thus, three sets of (9, 16, and 49) IPs were calculated and stored for every interpolation function and its in-plane derivatives.

5.2.2 Thickness Integration

In ESL theories, the contributions in the thickness direction of all layers are simply summed at the mid-section of the plate ("z" = 0) in the assemblage process of the transversal stiffness. On the other hand, for LW theories, only the stiffness terms at the compatible nodes are summed. One may revisit Figure 17 for visualization of the difference between the assemblage of the integrated thickness terms in ESL and LW theories.

Using equation (5.20) as example, the matrix assemblage and integration procedures at ply level for ESL theories are performed according to:

$$\mathbb{Z}_{33}^{r_{w,z}s_{w,z}} = \sum_{k=1}^{k=N_l} \left\{ \bar{C}_{33}^{k} \int_{z_b^k}^{z_t^k} F_{r_{w,z}}(z) F_{s_{w,z}}(z) dz \right\} \tag{5.27}$$

where "N_l" is the number of layers. However, to perform the integration numerically, a coordinate transformation to the local coordinate system of the ply is needed. Thus:

$$z^k = z_m^k \zeta^k + z_p^k \tag{5.28}$$
$$z_m^k = \left(z_t^k - z_b^k\right)/2 \; ; z_p^k = \left(z_t^k + z_b^k\right)/2$$

and, for each ply, the integration becomes:

$$\int_{z_b^k}^{z_t^k} F_{r_{w,z}}(z) F_{s_{w,z}}(z) dz = \sum_{m=1;}^{NG} W_m F_{r_{w,z}}(\zeta_m) F_{s_{w,z}}(\zeta_m) \frac{h^k}{2} \tag{5.29}$$

The calculus of the number of IPs is similar to that of the in-plane integration. For equation (5.29) and for "$N_{\alpha w}$" number of terms, this integrand is proportional to:

$$F_{r_{w,z}}(\zeta_m) F_{s_{w,z}}(\zeta_m) \propto \zeta^{(N_{\alpha_w}-2)} . \zeta^{(N_{\alpha_w}-2)} \tag{5.30}$$

Then, the number of IPs is equal to NG, which in this case is:

$$NG \geq \frac{\left((N_{\alpha_w} - 2) + (N_{\alpha_w} - 2) + 1\right)}{2} \tag{5.31}$$

This logic is repeated for every possible combination of expansion terms in the integrand of the thickness integration. Nonetheless, only the critical combinations are chosen. This means that some integrations, though exact, are not optimized. In others, the derivatives in the integrands do not alleviate the integrations. This was adopted for the sake of simplicity, just like the in-plane integrations.

For the LW case, the thickness integration is also performed at ply level. The change in variables in (5.28) is also required, but the sum in (5.29) is skipped. However, since the Legendre polynomials are already written in the LCS, the change of variables is performed only at the post-processing stage and for Jacobians. CGF uses the recurrence formula in equation (3.48) to build all the expansion terms "F_τ^k" in the LCS automatically.

Chapter 6 - Evaluation via Literature Data and Abaqus

Three types of structures are chosen to evaluate the accuracy and performance of the proposed solution method: isotropic plates, orthotropic laminated composite plates and sandwich structures. For each of these cases, different thickness-to-length ("h/l") ratios are tested to evaluate the ability of the solution to predict both thin and thick responses of each chosen formulation. Five different sets of material properties and/or lamination angles are considered. In Table 2 below, these five cases are listed and related to the investigation performed.

Table 2 - Matrix test used in the evaluation of CGF for each structural case

Solution Method	**CGF (4-node quadrilateral plate element)**					**Abaqus**	
						2D	**3D**
Investigation/ Case	*Convergence*	*Theory*	*Thickness*	*Dynamic*	*Sandwich Structure*	*All*	*All*
I	ED/LD111 ED/LD333 l/h=20 b/a=1	n/a	n/a	n/a	n/a	Shell element S4 (linear)	Continuum element C3D20 (quadratic)
II/II*	ED/LD111 ED/LD333 l/h=20 b/a=1	ED/LD110-3 ED/LD220-3 ED/LD330-3 l/h=4 b/a=1**	ED/LD111 ED/LD332 l/h=4, 10, 20, 100, b/a=1	ED/LD111 ED/LD332 l/h=20, b/a=1	n/a		
III	n/a	n/a	n/a	ED/LD111 ED/LD332 l/h=20, b/a=1	n/a		
IV	n/a	n/a	n/a	n/a	ED/LD111 ED/LD333 l/h=10, FCSR=2, b/a=1		
V	n/a	n/a	n/a	n/a	ED/LD225 l/h=4, FCSR=10, 10000, b/a=3		

*Different boundary conditions are used in modal analyses; **Layer-wise formulations start with a minimum of two terms in the expansions

The investigations comprise the aspects of convergence rate, theory accuracy, thickness influence, dynamics (inertia) and sandwich structure behavior. The acronyms from the UFs in section 3.3.4 are used in this evaluation. As a reminder, the letter "D" stands for the PVD derivation process, the "L" or "E" letters stand for LW and ESL formulations. Finally, the three numbers at the end represent the highest order of the expansion terms in the three directions. A

formulation tagged as ED332 represents an equivalent single layer approach derived with the principal of virtual displacements with cubic in-plane expansions and quadratic transversal displacement.

Each of the following sections investigates the influence of a particular variable. Loading, constraining, material properties and dimensions of the problem are defined at the beginning of each section. They were chosen based on the available references. Both ESL and LW approaches are evaluated. To avoid reconstruction of the graphical results from the references, the FE commercial code Abaqus is used to complement the literature data so that a direct comparison of the current CGF results, through the thickness of the plate, is also possible. In addition, the influence of the singularities due to the boundary layer conditions can be better understood with the 3D models.

It must be said that the C-1 aspect of CGF regarding the rotations and moments are not herein discussed for the sake of brevity and the lack of experimental results. This is also left for future publications.

The 3D models in Abaqus do not need much explanation for the current study. The C3D20 continuum element is a hexahedron with 20 nodes and parabolic interpolation of displacements. However, the 2D models built for these comparisons have a rather fancy structural element, S4.

In Abaqus, there are thin (Kirchhoff's Theory), thick (Mindlin's FSDT) and general purpose shell elements available. The threshold from thin to thick shells is a thickness corresponding to $1/15^{th}$ of the characteristic length of the shell in this software. Both general purpose and thick elements in Abaqus exhibit transverse shear stress regardless of the settings. The S4 element is a general purpose shell element formulated for large-strains. It is fully integrated and hence no membrane/bending spurious modes are expected. No hourglass control is required either. Also, it is a finite-membrane-strain shell element and these membrane strains are derived based on the Koiter-Sander's shell theory. Nonetheless, drilling control is required. This formulation can be found in Abaqus' theory manual. The transverse stresses are found by assuming the strain values at the midpoint of the element edges and solving for these variables explicitly. It means that this element formulation is considered as of the *mixed* type. Therefore it does not suffer from shear-bending locking. According to Abaqus' theory manual, the procedure follows the work of Bathe and Dvorkin (1984), which was already reviewed in this PhD thesis. The constitutive relations incorporate a shear correction factor of 5/6.

When laminated sections are considered, the formulation falls within the ESL category. The shear correction factor is recalculated, because the transversal stresses vary throughout the

thickness. The actual shear correction factor is calculated after equating the shear strain energy through the thickness of the laminate with a particular shear distribution obtained from the equilibrium of bending and shearing forces throughout the plies. For the record, there is a LW solution in Abaqus based on Mindlin's theory. It is called continuum shell element. Since this is a mid-term solution in terms of accuracy (between S4 and C3D20 formulations), such approach was not evaluated in this work as it would merely assess the accuracy of this formulation in Abaqus. Thereby, it does not contribute much with this work.

Back at the threshold of thin to thick plates, the value adopted in Abaqus is higher than the one shown in this PhD thesis, which is 1/20. Therefore, one can say that the limit chosen in this thesis is more robust. The reasons for this assertion lie in the world of real engineering problems, as mentioned in the beginning of section 4.3 of this manuscript. Normally, the engineering models have many different types of continuum and/or structural elements. Also, welds, junctions and contact are very common. All of these elements can change the thin-thick threshold throughout the model of a shell with constant thickness. Therefore, robustness is good thing to be sought. This is something to be considered and another motivation for implementing higher order theories.

The comparisons are organized so that the influence of each parameter/variable of the formulation is isolated. Thus, each of the following sections shall discuss one particular type of investigation. These investigations consider both micro and macroscopic results. For CGF, the nodal stresses are calculated with the following steps:

i. **All 6 "displacement fields" were built for each node.**
ii. **These fields were evaluated throughout the thickness the of plate.**
iii. **The strains were calculated at the centroid ($\xi = \eta = \zeta = 0$) of the elements using compatibility relations with the pre-calculated displacement fields in "ii".**
iv. **For each node, the nodal strain values were obtained from the average values from the surrounding elements.**
v. **Finally, the nodal stresses were evaluated from constitutive relations applied on the calculated strain fields in "iv".**

The centroid value is expected to provide the best set of results for linear quadrilaterals plates. The same procedure (centroid values) is adopted within Abaqus 2D. In Abaqus 3D, the nodal values are obtained with extrapolated values from the integration points within the elements. This should provide the best results at the nodes (ABAQUS/CAE User's Manual).

It is worth saying that the recovery of stresses is a very delicate matter and the evaluation at the integration points is preferred to the nodal evaluation. These points, also called "*material points*", receive this name because, due to the better representation of experimental stress values, they are used to assess the microscopic limits of the material via plasticity and/or failure algorithms, for instance. The choice of how the stress/strain values are obtained is a very broad field and is actually a field of its own (ROGOVOY, 1997). Therefore, no specific post-processing techniques are handled in the present work. Moreover, the present author believes that a more complex formulation can avoid the need for additional complex post-processing steps. Nonetheless, every code needs a minimum of post-processing.

In this thesis, only a spline interpolation of the nodal output variables was performed over the extensions of the plate to smooth some of the selected plots. Thus, the figures obtained with CGF show meshes twice finer than the ones actually used in the calculations.

As a general reminder, this author highlights that the terms "error", "deviation", "precision", "accuracy" and the like, are taken as indicators of how close the results obtained with CGF are to the reference ones obtained with other solution methods. Meaning that the "errors" seen in this section may be actually larger or smaller when compared to experimental results.

6.1 Convergence Evaluations

Firstly, convergence tests are performed. This section is mainly concerned with the convergence rate aspects of CGF and that is why only the transversal displacement is studied. Two cases are used to assess the accuracy and convergence rate of CGF. The material properties used in these cases are in Table 3.

Case I is a clamped isotropic plate under a unit center load. The material properties are isotropic. The same dimensions and density were chosen for both cases, as it can be seen in Table 3.

Case II is a simply-supported laminated plate under a unit bi-sinusoidal pressure. The laminate is a symmetric four-ply composite structure whose material properties are those from Table 3. The stacking sequence is [0°/90°/90°/0°]. Generically, this bi-sinusoidal pressure is:

$$p(x,y) = P_0 \sin(\pi x/a)\sin(\pi x/b) \tag{6.1}$$

where P_0 is the magnitude of the pressure and "a" and "b" are the lengths of the plate sides. In both cases the plate is a square (a = b = l = l) and is considered a thick or moderately thick plate considering the dimensions of the problem.

From 4x4 (16 elements) up to 32x32 (1024 elements) mesh densities, the convergence trend of the transversal displacement obtained with CGF is shown. Two different formulations and both LW and ESL approach are studied.

Table 3 - Material properties and plate dimensions for static analyses evaluations

Case / Material	**l** (mm)	**h** (mm)	**E_1** (MPa)	**$E_2 = E_3$** (MPa)	**$G_{12} = G_{13}$** (MPa)	**G_{23}** (MPa)	**$\upsilon_{12} = \upsilon_{13} = \upsilon_{23}$**	**ρ** (ton/mm²)
I - Isotropic	1000	50	70000	E_1	$E_1/2.6$	$E_1/2.6$	0.3	7e-9
II - Orthotropic			$25E_2$	1000	$0.5E_2$	$0.2E_2$	0.25	

Table 4 shows the convergence studies performed for both cases using both ESL and LW approaches. The analytical baseline value for Case I was taken from Timoshenko and Krieger (1959). This is an exact value for thin plates under a center load. On the other hand, the analytical value taken from Pagano and Hatfield (1972) was obtained through the Theory of Elasticity (TE).

The point chosen for comparisons of the displacement fields is the center of the plate, meaning, for a global coordinate system located at mid-plane lower corner of the plate: x = y = l/2; z = 0.

Table 4 - Convergence study of the mid-plane center transversal displacement (μmm)

		Case I		Case II	
Theory	Mesh Size	ESL	LW	ESL	LW
111	4x4	-3.1321	-3.5796	-36.4491	-39.3890
	16x16	-5.2824	-6.0371	-38.1743	-41.5006
	32x32	-5.4531	-6.2321	-38.3010	-41.7364
333	4x4	-3.5456	-4.0375	-38.9561	-39.6221
	16x16	-6.3840	-7.2189	-40.8006	-41.7975
	32x32	-6.6426	-7.4392	-40.9320	-42.1204
Abaqus 2D	16x16	-7.6284		-41.2355	
Abaqus 3D	16x16x8	-7.5161		-41.6638	
Reference	Analytical	-6.9888*		-41.024**	

*Timoshenko and Krieger (1959); ** Pagano and Hatfield (1972)

To exemplify Case I, Figure 29 shows the transversal displacement of the top face of plate for the LD333 theory and the mesh with 16x16 elements.

Next, the profile of the nodal variables obtained by CGF and calculated at the top of the plate, for the same model of Figure 29, is provided from Figures 30 to 35. Since this is a C-1 implementation, the in-plane rotations and the twist are shown as well. To improve the magnitude of the plots, the results were normalized with the scale factor, *"sf_{displ}"*, which is the transversal displacement:

$$sf_{displ} = 100h^3 \, E_2 \, / P_0 \, l^4 \tag{6.2}$$

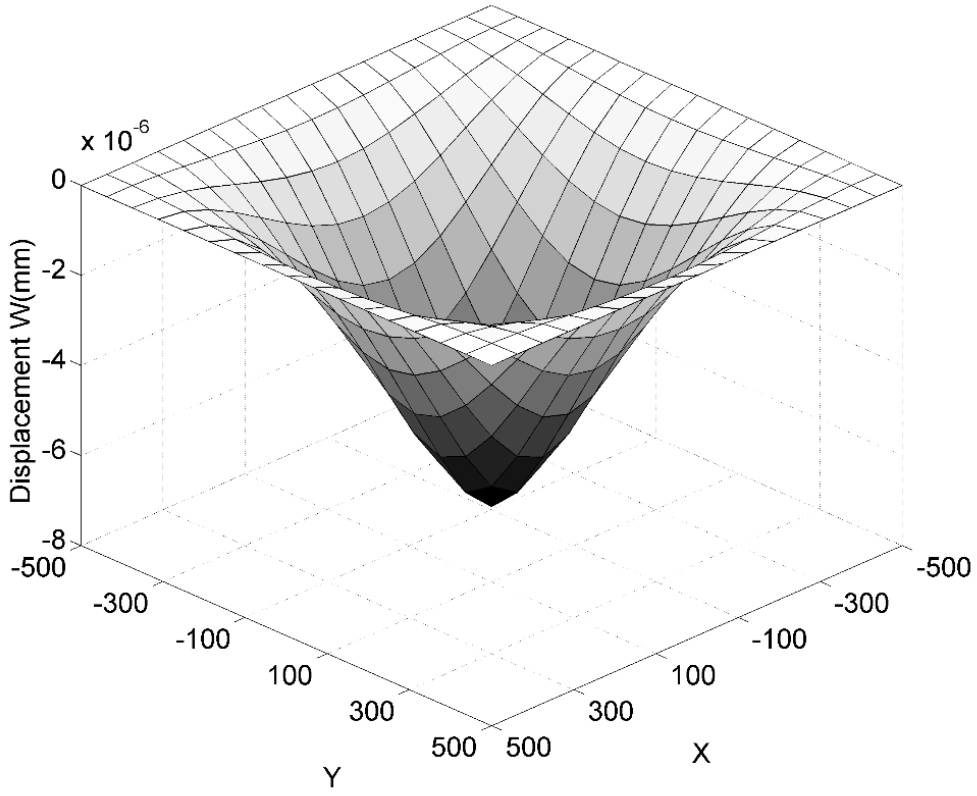

Figure 29. Transversal displacement field at the top of the plate (Case I-LD333-16x16)

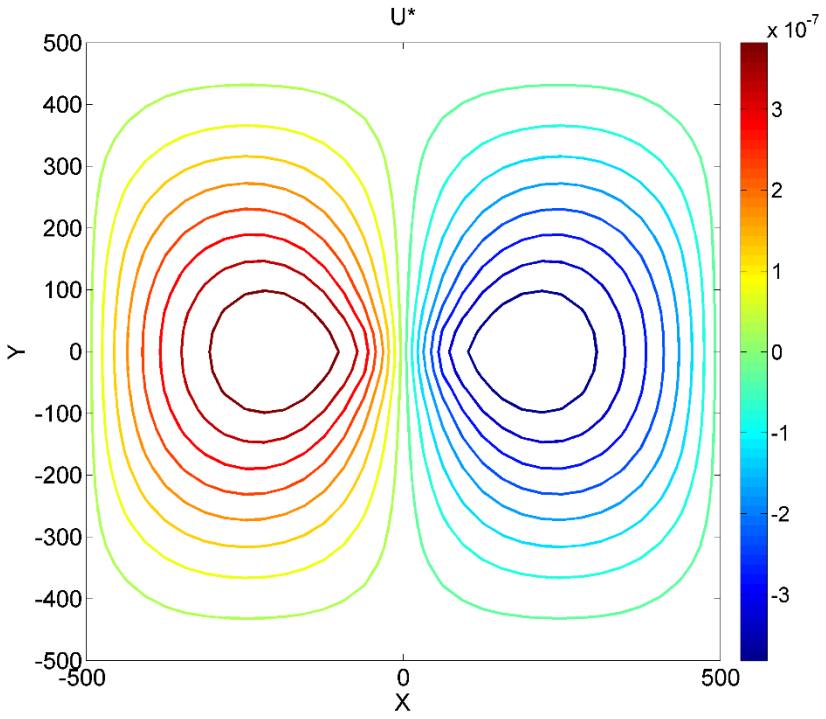

Figure 30. Normalized in-plane displacement "u" nodal values (Case I-LD333-16x16)

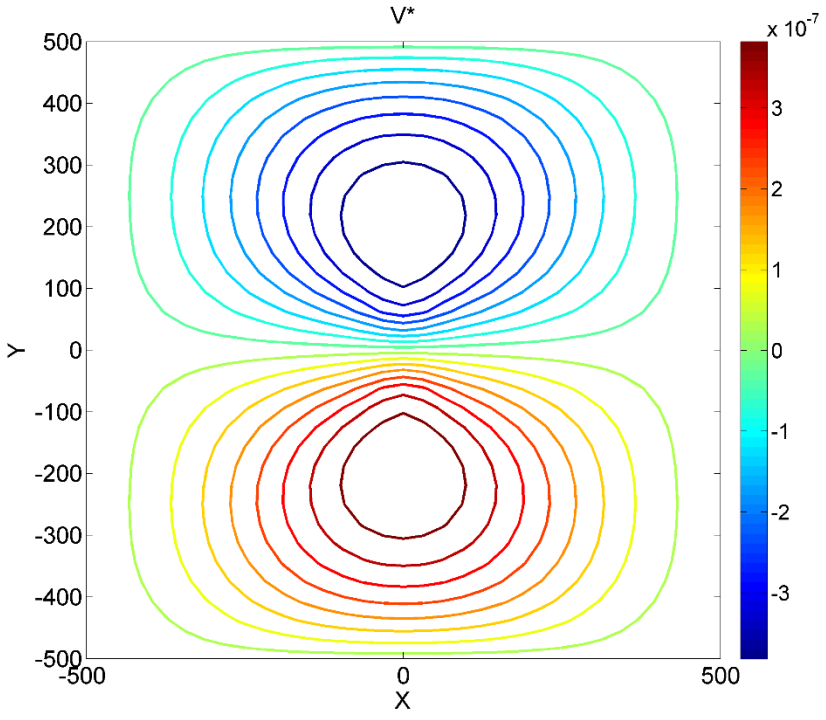

Figure 31. Normalized in-plane displacement "v" nodal values (Case I-LD333-16x16)

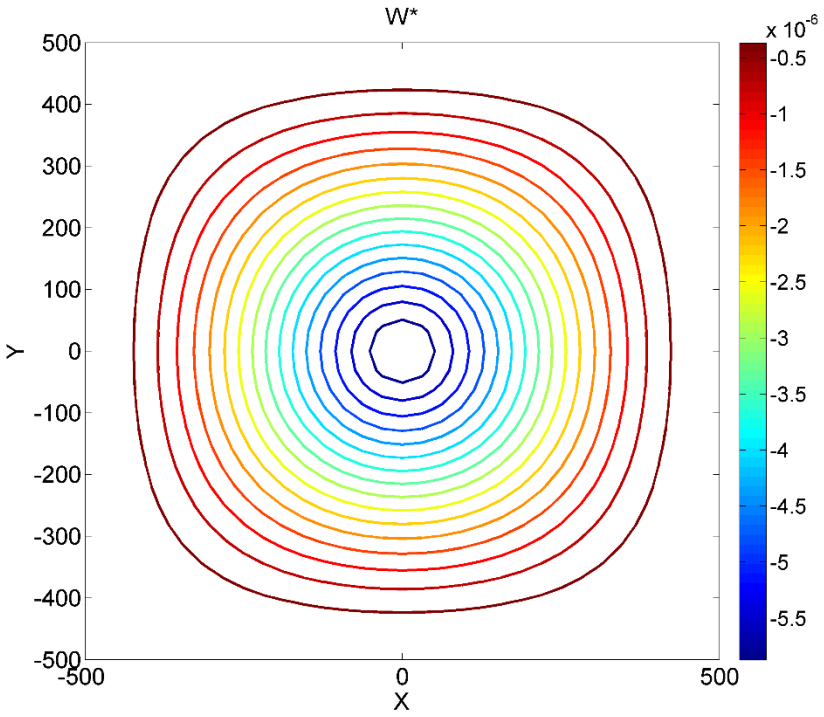

Figure 32. Normalized deflection "w" nodal values (Case I-LD333-16x16)

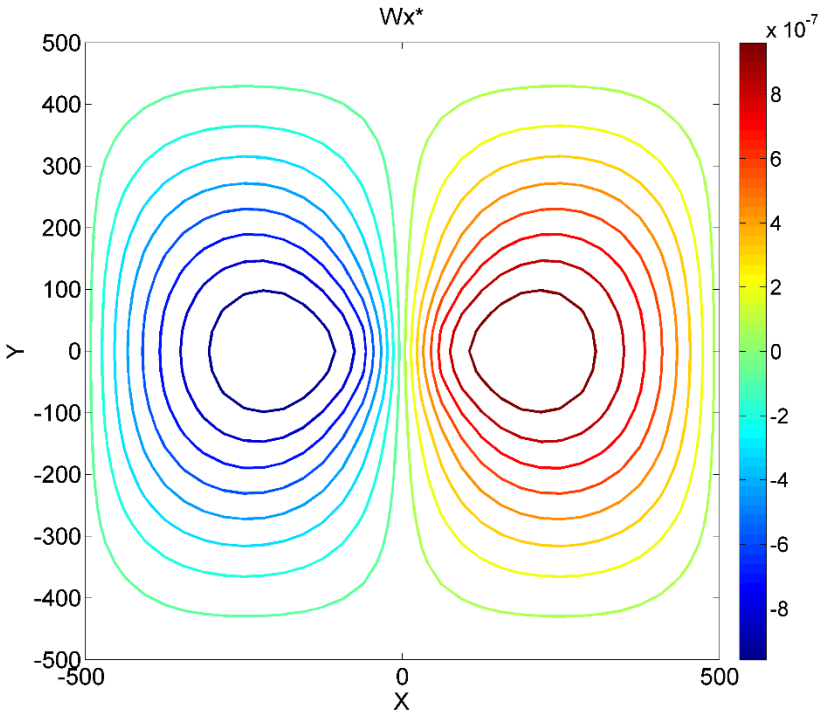

Figure 33. Normalized in-plane rotation "Wx" nodal values (Case I-LD333-16x16)

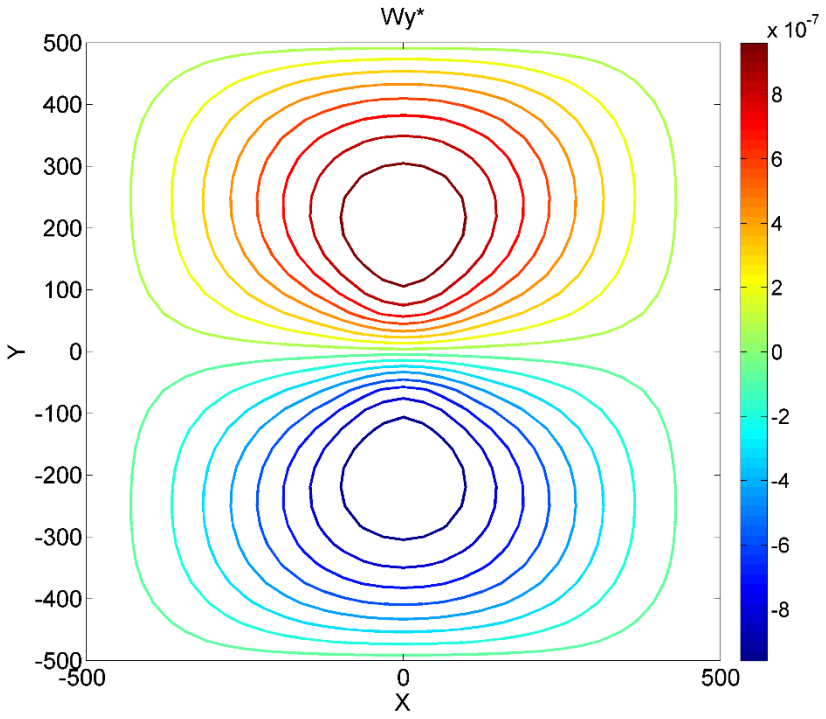

Figure 34. Normalized in-plane rotation "Wy" nodal values (Case I-LD333-16x16)

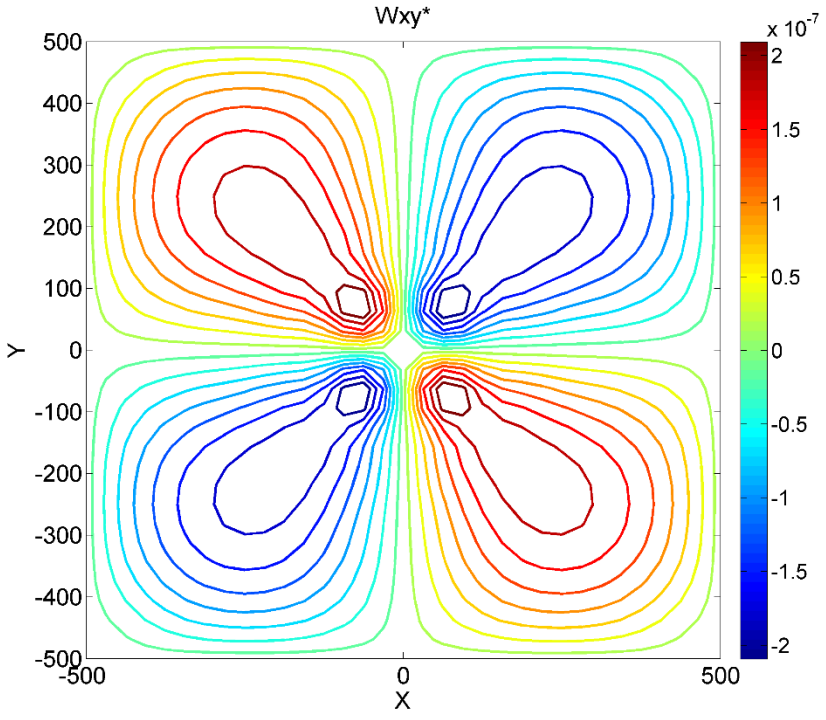

Figure 35. Normalized in-plane rotation "Wxy" nodal values (Case I-LD333-16x16)

The symmetry of the problem is quickly verified from the figures above. Also, the in-plane rotations and the twist can be seen directly. This is a straight output from CGF.

On the other hand, the stresses demand a minimal of post-processing effort, which is the application of the constitutive equations on the strain fields. From Figure 36 to Figure 41 the stress distribution on the top of the plate is given. Relative high local stresses are seen due to the concentrated load of Case I.

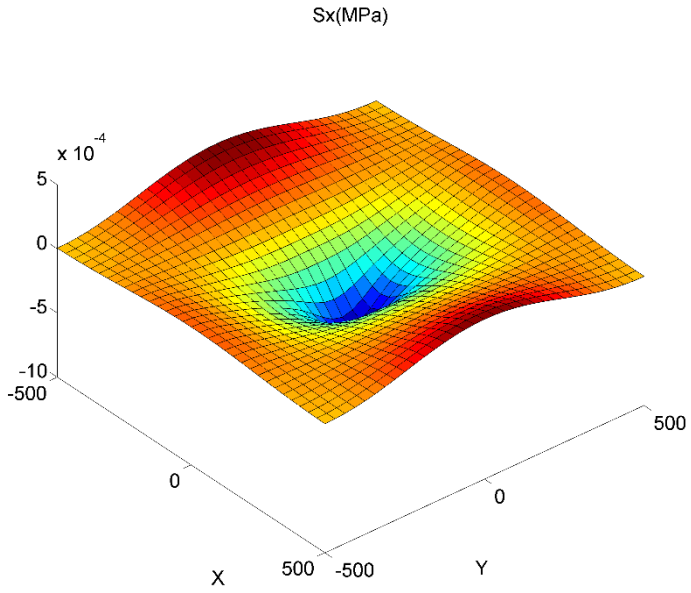

Figure 36. Isotropic plate: Sx stress distribution at the top of the plate (Case I-LD333-16x16)

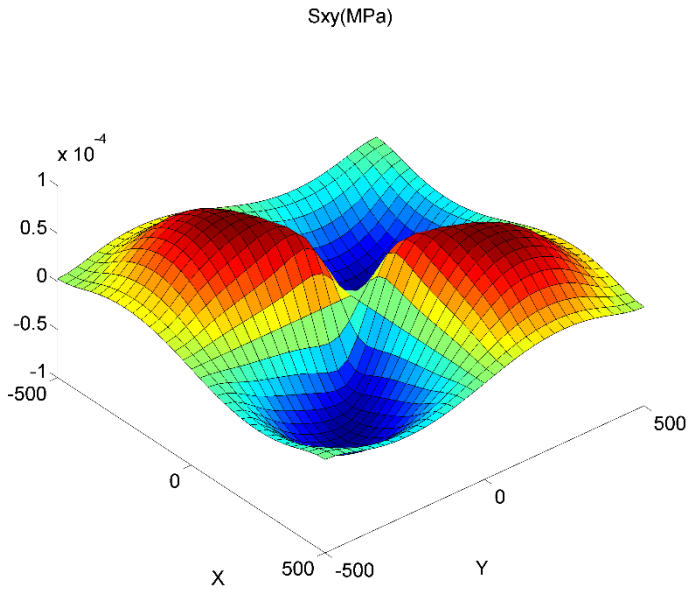

Figure 37 Isotropic plate: Sxy stress distribution at the top of the plate (Case I-LD333-16x16)

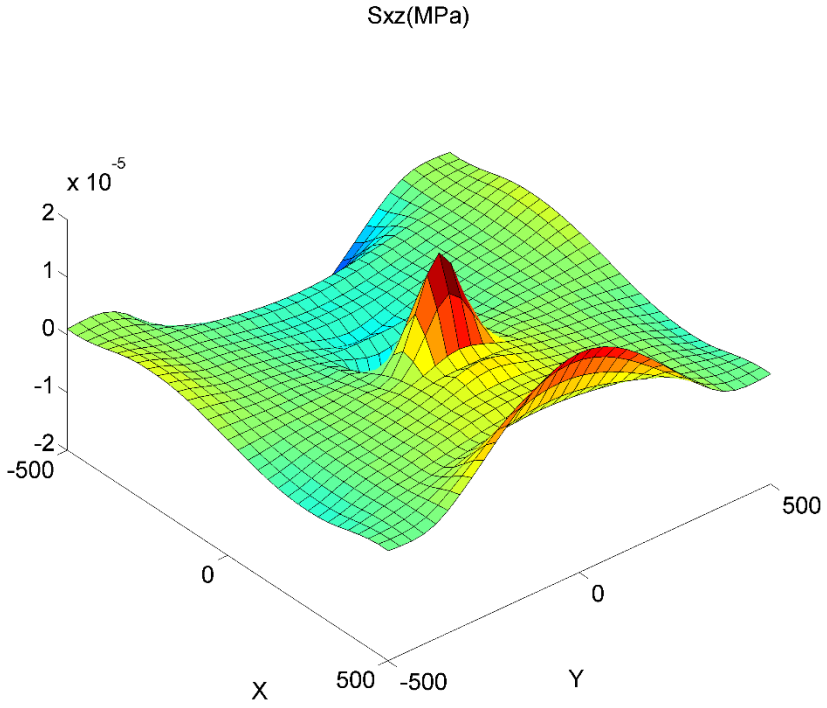

Figure 38. Isotropic plate: Sxz stress distribution at the top of the plate (Case I-LD333-16x16)

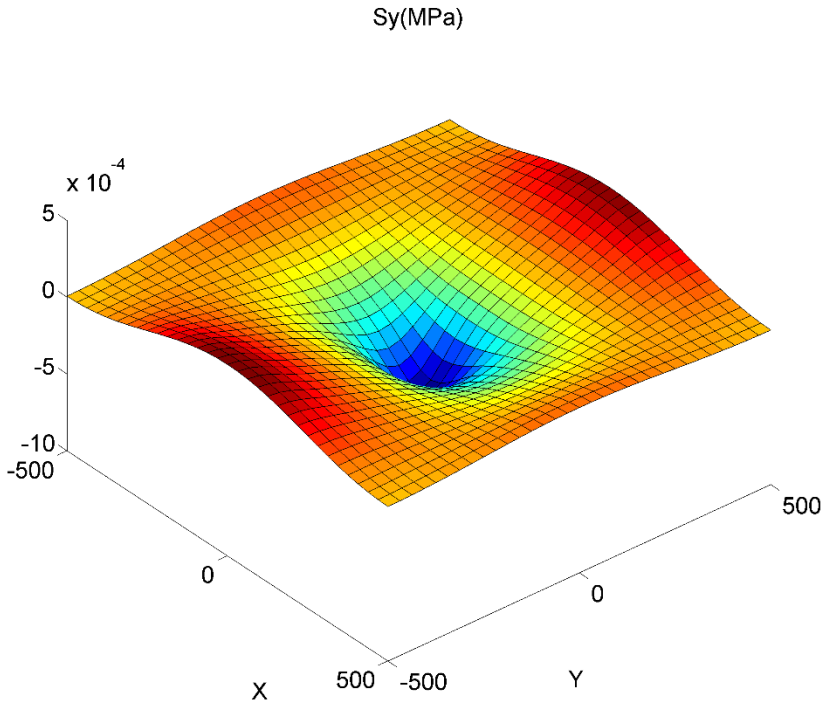

Figure 39. Isotropic plate: Sy stress distribution on the top of the plate (Case I-LD333-16x16)

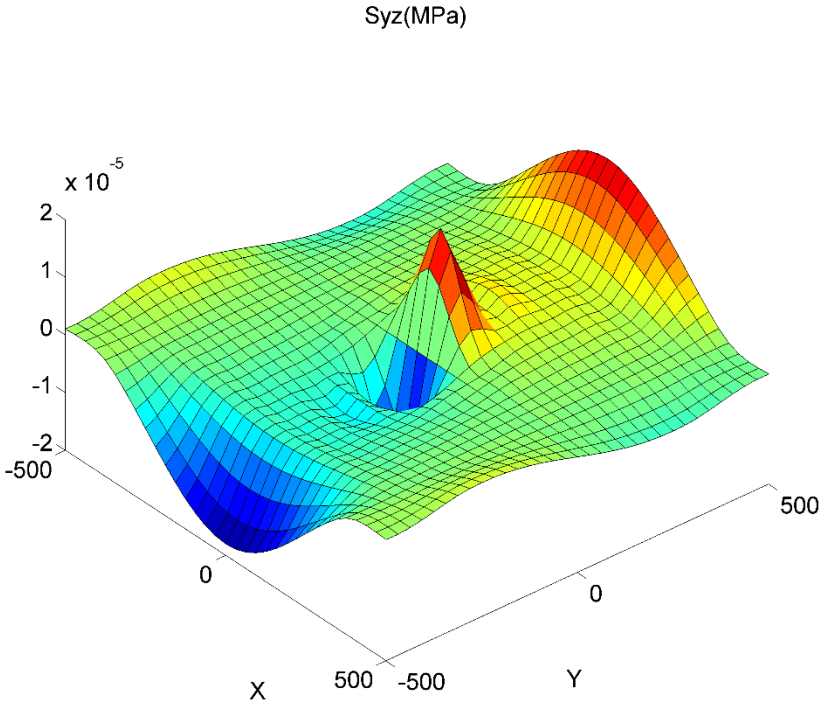

Figure 40. Isotropic plate: Syz stress distribution at the top of the plate (Case I-LD333-16x16)

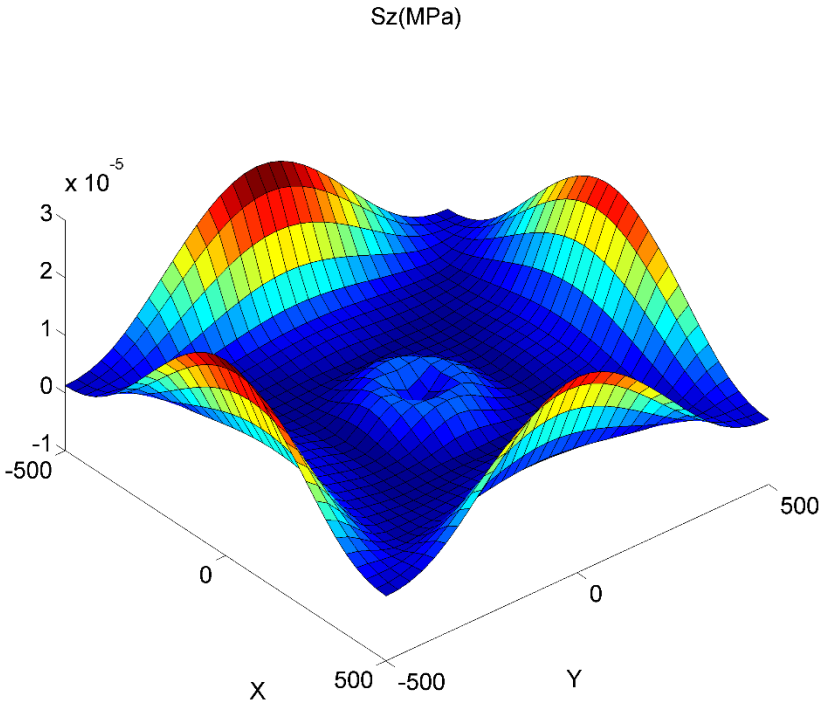

Figure 41 Isotropic plate: Sz stress distribution at the top of the plate (Case I-LD333-16x16)

After inspecting the stress surfaces, one can see that the number of elements is higher than 16x16. Such figures actually show twice a 32x32 mesh. However this is due to the spline

smoothing of data which required three nodal values corresponding to the double of actual elements. Also, please note that the values of the transverse shear stresses are half of the engineering values usually represented by the Greek letter "τ".

Next, some contour plots of the results obtained via Abaqus models are given for both Cases I and II. First, the boundary conditions and the loading are seen in Figure 42 for the 3D models built within Abaqus. The corresponding 2D figures are not necessary.

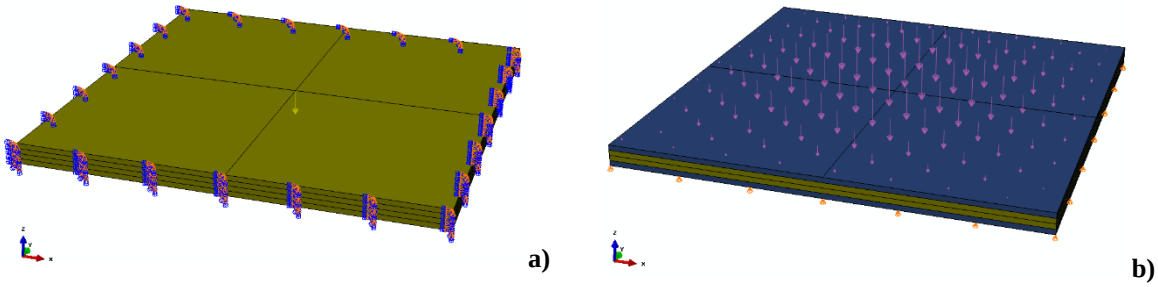

a) **b)**

Figure 42. 3D boundary conditions and applied load for Cases a) I and b) II

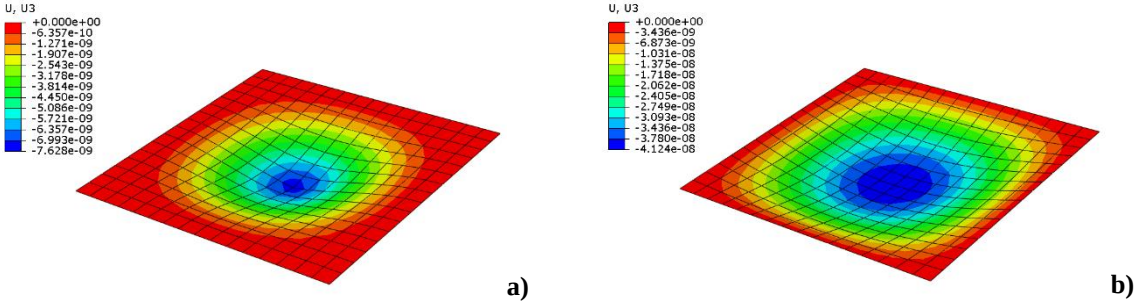

a) **b)**

Figure 43. Transversal displacement field (m) obtained with Abaqus 2D for Cases a) I and b) II

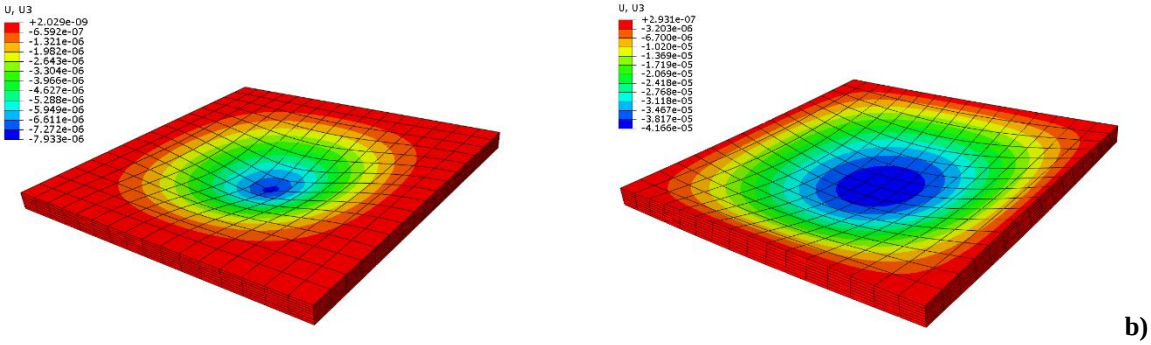

b)

a)

Figure 44. Transversal displacement field (mm) obtained with Abaqus 3D for Cases a) I and b) II

In Case I, the rate of convergence of the ESL models is inferior compared to the LW codes. It means that, since only one layer is being analyzed, the use of Legendre polynomials instead a regular Taylor polynomial expansion gives a better convergence rate. For ED111 the difference from LD111, considering the ESL result, is 14.3% (32x32). Also, the cubic theory converges much faster than the linear one. For instance, taking the difference between the LD111 and LD333 models, using the LD111 as a base result, is 19.4% (32x32).

Case I is a regular isotropic plate. No LW description is actually needed. However, if this approach is applied assuming more than one ply for the isotropic plate, the process is called *sub-lamination*, discussed earlier in this PhD thesis. This helps to increase the accuracy of the isotropic plate solution, if it is too thick for the implemented plate formulation. This does not need confirmation, and therefore it is not shown in this manuscript.

For Case II, the LW values also converge faster to the reference values in comparison to the ESL ones. For ESL111 and LD111, this difference is of 9% (32x32). This clearly shows that the LW formulation with Legendre polynomials is richer and better suited for laminated plates. However, in comparison to Case I, the convergence rate of Case II is higher. One of reasons is the use of the simply supported boundary condition, which is less restraining than the clamped one.

Regarding the reference results, the analytical ones are the stiffest ones for both cases. Nonetheless, it must be remembered that the reference formulation for Case I was derived for thin plies ($l/h > 100$) and this is not the case as for these evaluations, one has $l/h = 20$. Thus the results from Abaqus 3D are taken as a better reference. They (3D models) are also supposed to yield the most accurate results compared to the real/experimental values due to their 3D resolution. The numeric results from Abaqus show different qualitative behaviors for each case. For Case I, the 3D solution is stiffer than the 2D one, whereas in Case II, the opposite is observed. In this case, the 3D model shows a more flexible result, which can be partially explained by the orthotropic properties of the case. It is likely that, besides the error that the assemblage of the plate's stiffness in the thickness direction imposes, the calculation of the shear correction factor is responsible for part of this difference. A lower shear correction factor can provide larger deflections for the 2D solution from Abaqus.

Table 4 shows the trend of the converge rates, but it does not explicitly show the number of DOFs being solved in each case. Figure 45 exhibits how the transversal displacement of Case I converges to the 3D solution as the number of DOFs increases.

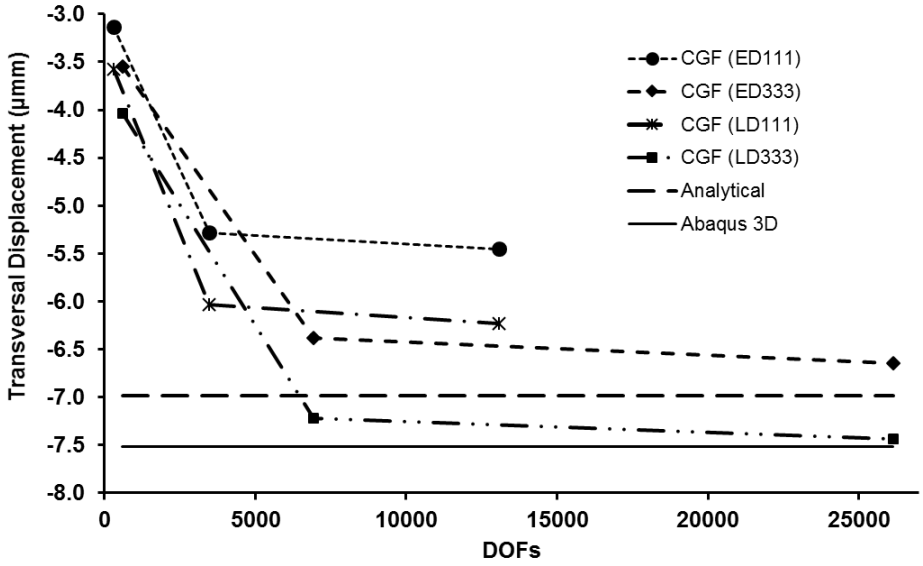

Figure 45. Convergence rate of Case I for both ESL theories

In Figure 45, one can easily see that the linear solution is far stiffer than the cubic one. Also, one can see once more that the LW approach provide a structure model softer than the ESL one. Case I results were chosen, because they are more sensitive to the use of non-linear theories, because the boundary layer effects are stronger in this case.

From this graph, it is seen that it is much more effective to increase the order of the solution or to go for a LW approach than to increase the mesh density to improve accuracy. This is mainly due to the fact that Case I is represents a moderately thin/thick plate. Thus, the need for more flexible elements is inexorable.

To decide which theory gives the best accuracy and performance, the ratio accuracy/DOFs, considering the 3D solution from Abaqus, can be investigated. For the 16x16 meshes, such ratio orders the theories as: LD111>ESL111>LD333>ESL333. This puts the LD111 as the best option, regarding precision and number of DOFs to be solved. Note that LD333>ESL333. This probably because the Case 1 has only one ply and such results once more reflects the use of the Legendre polynomials.

6.2 Theory Evaluations

Once again, the unit bi-sinusoidal pressure problem is chosen. Here, Case II is solved for difference ESL and LW theories. However, now, the plate is thicker since the length-to-

thickness ratio is smaller, l/h = 4. Solutions via Abaqus are also given. In Figure 46, the geometry, loading and boundary conditions of this case modeled within Abaqus is shown.

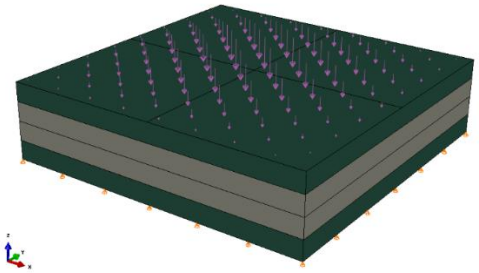

Figure 46. Thick laminate modeled in Abaqus under bi-sinusoidal pressure and simply supported

This section evaluates the accuracy of CGF as a whole, meaning that not only the transversal displacement will be checked, but the stress distributions as well. A fixed mesh density of 100 elements (10x10) is used to compare the accuracy of CGF to all the theories listed in Table 2. The 3D models in Abaqus have 10x10x8 elements and the 2D ones have 10x10 elements, just as in Table 2.

Several combinations of theories are chosen to evaluate the precision of the solution method compared to the reference data available. Since the problem presents in-plane loading symmetry, the expansion terms for the in-plane displacement fields are kept equal. Then, for each additional term in the in-plane expansions, from constant to cubic behavior, the transversal displacement field is evaluated. Once again, the LW implementation does not allow for a constant transversal displacement field and thereby it is not computed. Table 5 shows the normal transversal normal displacement at the center of the plate: x = y = l/2; z = 0. It is important to highlight that results are not normalized.

In Table 5, one can see that the ESL results converge to the analytical one, which carries more errors due to the wrong thin-plate assumption; but the LW one approaches Abaqus', which is closer to reality. Actually, the LD333 result is higher than Abaqus'. This was already seen in the previous section for LD333 and Abaqus 3D results for the 16x16 mesh density. This indicates that CGF can provide more flexible structural model than a 3D solution. An experimental test must be performed to check which solution method is more accurate for a particular in-plane mesh density.

Table 5 - Transversal normal displacement (μmm) at the mid-plane: x = y = l/2; z = 0

Theory	ESL	LW
110	-0.9731	n/a
111	-0.9731	-1.6858
112	-0.9981	-1.7470
113	-0.9981	-1.7603
220	-0.9731	n/a
221	-0.9731	-1.7846
222	-0.9981	-1.8522
223	-0.9981	-1.8608
330	-1.2235	n/a
331	-1.2235	-1.7957
332	-1.2418	-1.8737
333	-1.2418	-1.8826
Abaqus 2D	-1.3506	
Abaqus 3D	-1.7534	
Analytical*	-1.2395	

* Pagano and Hatfield (1972)

Next, the values of stresses at particular locations are compared. These spots are supposed to exhibit the respective highest stress values within the plate. Equations 6.3 to 6.5 respectively indicate the scale factor for the in-plane normal stresses, transversal normal stress and the shear stresses.

The locations chosen for point comparisons can be seen in Table 6. Still, the global coordinate system is located at the mid-plane of the lower corner of the plate. Different references set the coordinate system at either the bottom corner or center of the plate, regarding the in-plane coordinates. Nevertheless, the thickness coordinate axis is hardly off the mid-plane in the literature.

$$sf_{normal\_p} = (1\ /P_0\ ) * (h\ /l\ )^2 \tag{6.3}$$

$$sf_{normal\_t} = 1\ /P_0 \tag{6.4}$$

$$sf_{shear} = (1\ /P_0\ ) * (h\ /l\ ) \tag{6.5}$$

Table 6 - Maximum point stress locations for comparisons

S_x	S_y	S_z	S_{xy}	S_{xz}	S_{yz}
x = y = l/2; z = -h/2	x = y = l/2; z = -h/4	x = y = l/2; z = +h/2	x = l; y = 0; z = -h/2	x = 0; y = l/2; z = 0	x = l/2; y = 0; z = 0

Based on the definitions above, the stresses evaluated at these locations are grouped in Tables 7 and 8

It is important to say that the stress values at the top and bottom faces of the laminate have the same magnitude for equivalent single layer models, because all plies share the same

displacement fields and the laminate symmetric, as well. In LW cases, even for symmetric laminates, this cannot stated because the displacement fields are not symmetric, regarding the mid-plane, as in ESL models.

For brevity, only the *bottom values* are compared in Tables 7 and 8. However this is usually implicit in the references. In the original reference (PAGANO; HATFIELD, 1972), one can confirm these values at the bottom and at the top of the plate. For S_y, the highest value is taken at the interface of the $1^{st}/2^{nd}$ ply and at the side of the second ply.

Table 7 - Dimensionless normal stresses for Case II

	S_x		S_y		S_z	
Theory	ESL	LW	ESL	LW	ESL	LW
110	-0.4101	n/a	-0.5379	n/a	0.2690	n/a
111	-0.4101	-0.6450	-0.5379	-0.5960	0.2690	0.9941
112	-0.4124	-0.6371	-0.5517	-0.6039	-0.2548	0.8512
113	-0.4124	-0.6360	-0.5517	-0.6062	-0.2548	0.8302
220	-0.4101	n/a	-0.5379	n/a	0.2690	n/a
221	-0.4101	-0.7033	-0.5379	-0.6459	0.2690	1.0361
222	-0.4124	-0.6948	-0.5517	-0.6546	-0.2548	0.8872
223	-0.4124	-0.6935	-0.5517	-0.6559	-0.2548	0.8297
330	-0.6941	n/a	-0.6152	n/a	0.4159	n/a
331	-0.6941	-0.7043	-0.6152	-0.6509	0.4159	1.0384
332	-0.6929	-0.6926	-0.6260	-0.6610	-0.0270	0.8974
333	-0.6929	-0.6913	-0.6260	-0.6623	-0.0270	0.8400
Abaqus 2D	-0.3530		-0.6132		n/a	
Abaqus 3D	-0.7054		-0.6795		0.9721	
Analytical*	-0.720		-0.663		1	

* Pagano and Hatfield (1972)

Table 8 - Dimensionless shear stresses for Case II

	$2S_{yz}$*		$2S_{xz}$*		$2S_{yx}$	
Theory	ESL	LW	ESL	LW	ESL	LW
110	0.1623	n/a	0.1202	n/a	-0.0090	n/a
111	0.1623	0.1888	0.1202	0.1815	-0.0090	-0.0304
112	0.1647	0.2008	0.1262	0.1855	-0.0094	-0.0310
113	0.1647	0.2032	0.1262	0.1854	-0.0094	-0.0317
220	0.1623	n/a	0.1202	n/a	-0.0090	n/a
221	0.1623	0.2817	0.1202	0.1913	-0.0090	-0.0490
222	0.1647	0.2948	0.1262	0.1955	-0.0094	-0.0515
223	0.1647	0.2974	0.1262	0.1959	-0.0094	-0.0525
330	0.2496	n/a	0.2130	n/a	-0.0196	n/a
331	0.2496	0.2571	0.2130	0.1915	-0.0196	-0.0525
332	0.2504	0.2652	0.2177	0.1940	-0.0194	-0.0565
333	0.2504	0.2680	0.2177	0.1946	-0.0194	-0.0576
Abaqus 2D	0.0044		-0.0008		-0.0073	
Abaqus 3D	0.1134		0.0747		-0.0326	
Analytical**	0.2920		0.2190 (0.222)***		-0.0467	

*2^{nd} ply; ** Pagano and Hatfield (1972);*** Maximum stress at z/H = -0.27

In Table 5, the mid-plane displacement at the center of the plate is shown. One can see that among the reference results, the analytical one provides the stiffest structural model, followed by the 2D and 3D Abaqus solutions. This is because the analytical value and the 2D model are less sensitive to the singularities of the boundary conditions. Taking the 3D solutions as the target solution, both ESL and LW formulations approach the reference value as the number of terms in the thickness expansions increase. However, different performances are seen from both approaches.

From the Tables 5, 7 and 8, the layer-wise formulations are sensitive to every change in number of expansion terms. This means that regardless of the displacement field and the maximum order of the expansion chosen. However, in the ESL solution this is not seen. If the ESL results are analyzed, one sees that accuracy of the solution increases when the in-plane displacement fields are enhanced, as expected. But, if the transversal displacement is enhanced, improvement is only obtained when the theory changes from linear to quadratic (EDxx1to EDxx2). From constant to linear or from quadratic to cubic, no improvement is seen for this test case. This means that the quadratic term represents a physical degree of freedom in the solution. Both the transversal displacement and shear stresses have non-constant profiles through-the-thickness of the plate for moderately thick and thick plates. Nevertheless, even though such DOF added flexibility to this solution, depending on the problem and plate geometries, such term might not contribute substantially again.

Table 7 and 8 show the same trend for stresses. Apart from the in-plane shear stress, all the other variable show a very good agreement with the analytical reference. The layer-wise model with cubic expansions (LD333), as the most complex one, gives the highest agreement with the references. For instance, only 8% of deviation is found for the transversal shear stress S_{yz} and 0.1% for normal stress S_y.

The fact that the in-plane shear stress (S_{xy}) is more poorly resolved (difference of 23%) is due to the fact that CGF is calculating the stresses at the centroid of the elements and averaging these values at the nodes. Thus, the respective stress profile taken at the corner node is plotting the results a little far from the actual spot. The best option would be to calculate the stresses at the integration points closest to this node and through bilinear mapping of the results, find and extrapolation of this stress. However, as mentioned earlier, this work does not attempt such post-processing techniques. Even though this can provide a more accurate evaluation, it does not change the qualitative trends that this PhD thesis is exposing. This is also true for the transversal shear stresses. However, for S_{xz} and S_{xz}, the influence of this method is less

pronounced, because these values are taken at the mid of the edges. Thus, only one coordinate is influenced.

These edge or boundary effects are also present in Abaqus solutions. The 2D result provides a stiffer structural model than the 3D one regarding displacements. The 3D results for normal stresses are close the analytical reference but, on the other hand, the shear results do not agree as well as the normal ones. This is probably because, Abaqus 3D always solves for singularities and tries to achieve the free shear stress condition at the outer unloaded surfaces of the plate.

To better see this behavior, one can take a look at the thickness profiles in Figures 47 to 53. There, the ESL, LW and Abaqus results are grouped along with the additional results for the linear solid element C3D8. The author includes the 3D linear rectangular element C3D8 in order to evaluate the effect of the boundary conditions/layer.

Figure 47a shows the LW results for S_x. One can see that all three theories displayed agree quite well. However, in Figure 47b, the ESL results show some different. The linear and the quadratic solution have nearly linear transversal response and at the interface one sees a pronounced step. This is also seen in the 2D Abaqus solution in Figure 47c. However, the 3D results agree better with the LW solutions. The mid-node within the C3D20 did not influence the qualitative behavior of S_x when compared to C3D8.

Figure 48 exhibits the in-plane shear results. The different LW theories have similar qualitative behaviors. This behavior is asymmetric regarding the mid-plane of the plate. The same is seen at the plot for the ESL results, but in this case the pattern is symmetric. Still in Figure 48, the results from Abaqus show the influence of a corner node with boundary conditions applied. Both linear and quadratic elements feel this boundary layer effect, which is not seen in the 2D results. The 2D models are less sensitive to these singularities, because the transversal reactions are computed in an uncoupled fashion. This does not happen to 3D elements. Hence the difference is increased with the increase of the transversal anisotropy. The sandwich structure construction is an example and it will be explored later.

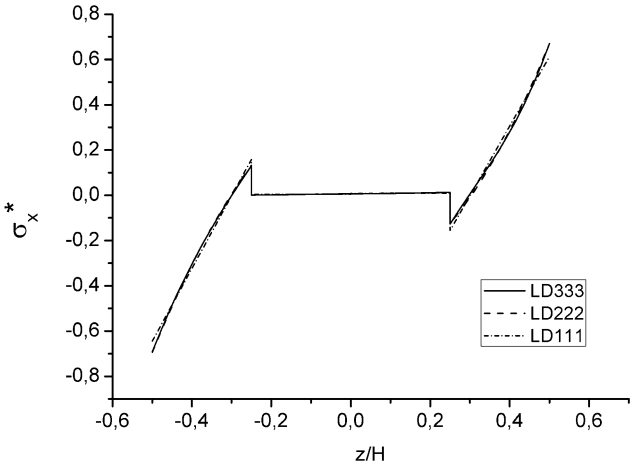

a)

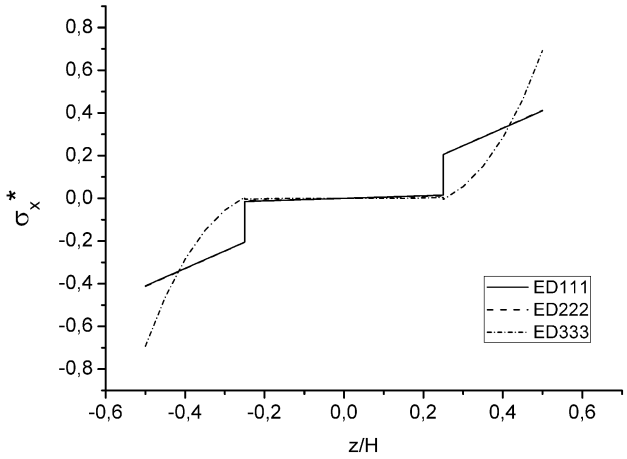

b)

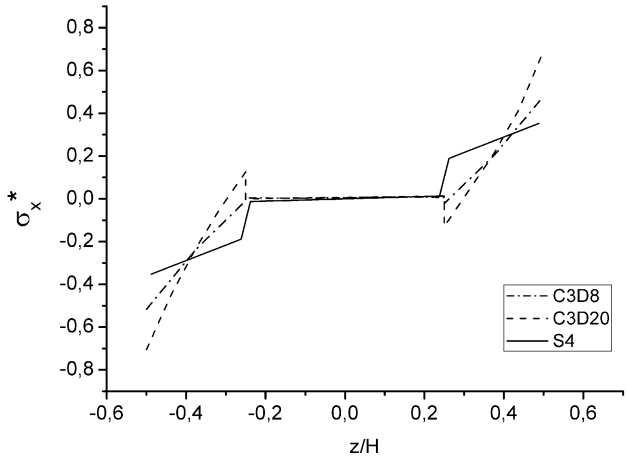

c)

Figure 47. Through-the-thickness Sx dimensionless stress (x = y = l/2). a) LW; b) ESL; c) Abaqus

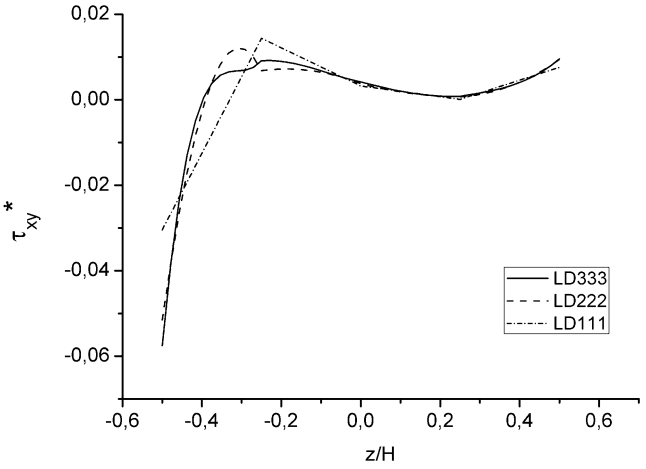

a)

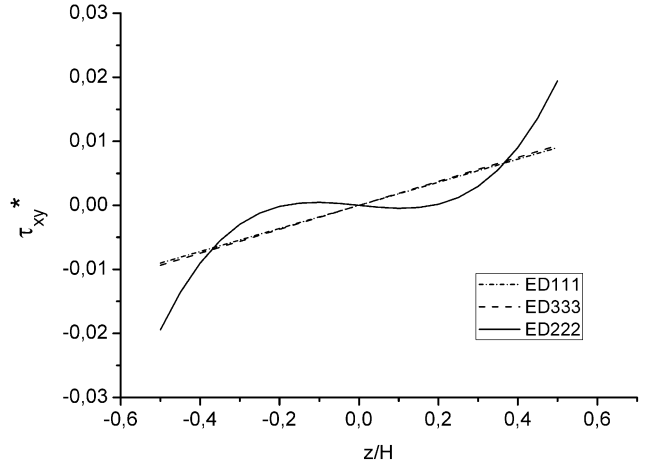

b)

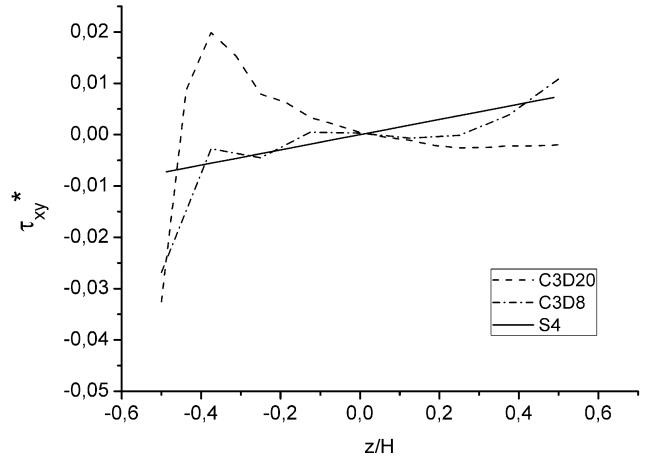

c)

Figure 48. Through-the-thickness Sxy dimensionless stress (x = y = l/2). a) LW; b) ESL; c) Abaqus

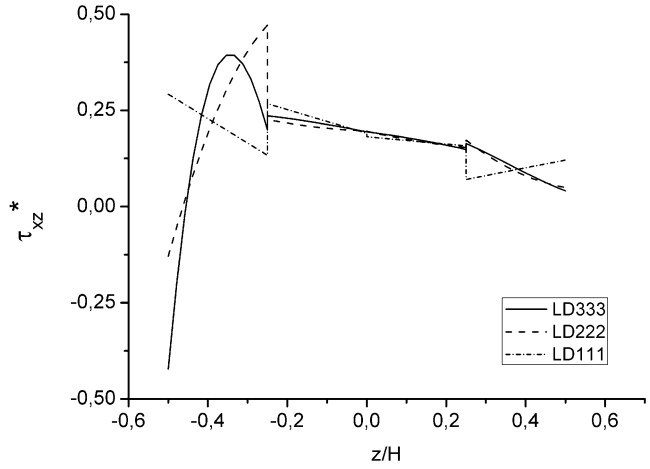

a)

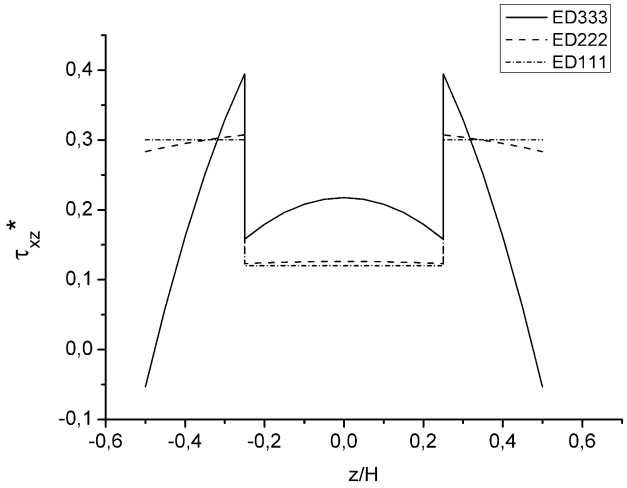

b)

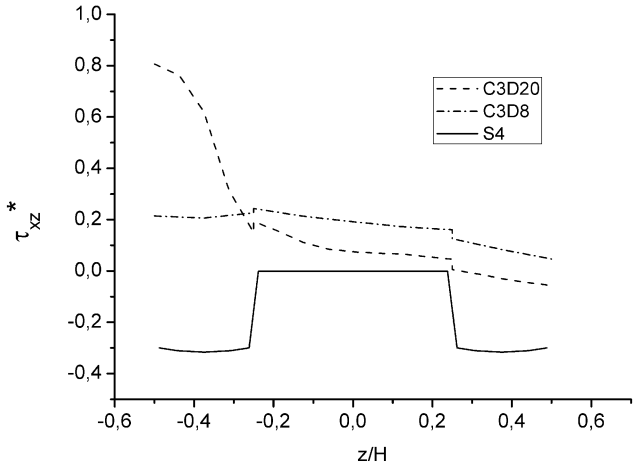

c)

Figure 49. Through-the-thickness Sxz dimensionless stress (x = 0, y = l/2). a) LW; b) ESL; c) Abaqus

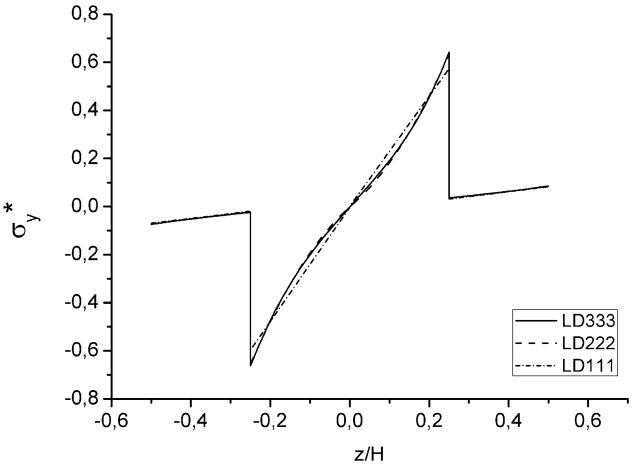

a)

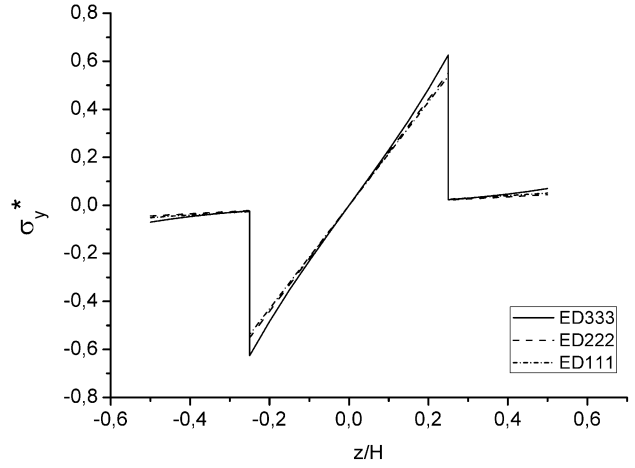

b)

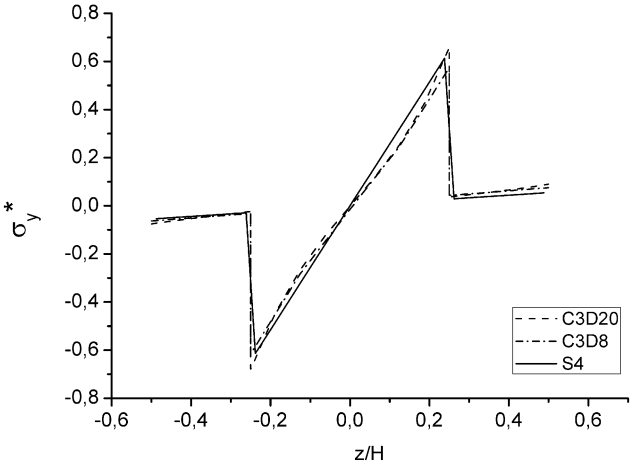

c)

Figure 50. Through-the-thickness Sy dimensionless stress (x = y = l/2). a) LW; b) ESL; c) Abaqus

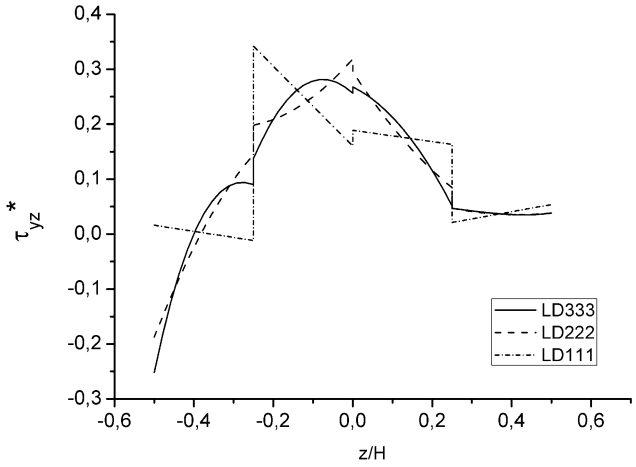

a)

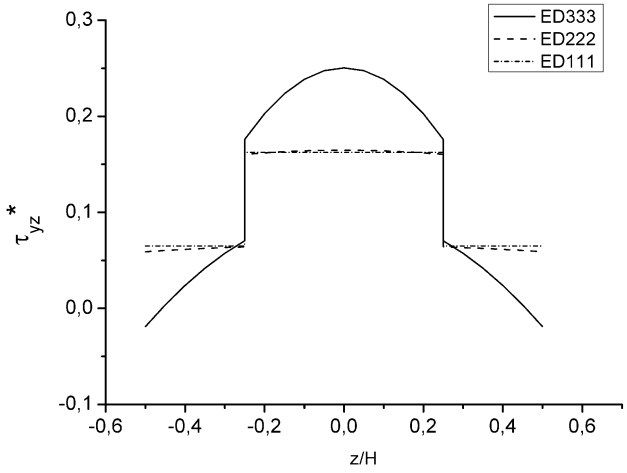

b)

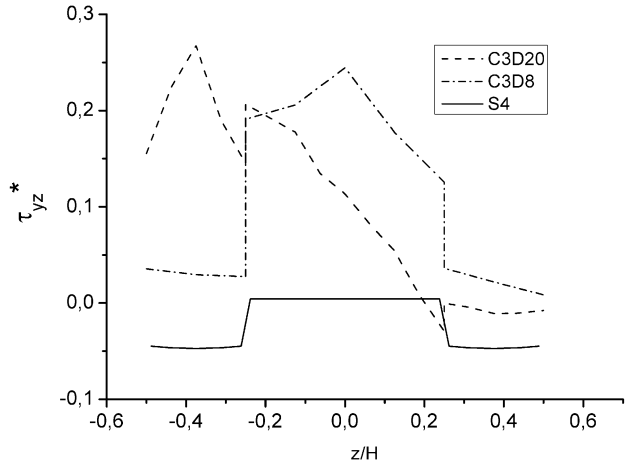

c)

Figure 51. Through-the-thickness Syz dimensionless stress (x = l/2 y = 0). a) LW; b) ESL; c) Abaqus

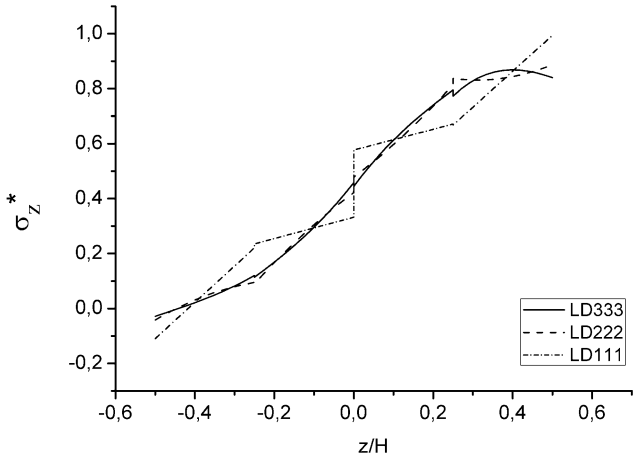

a)

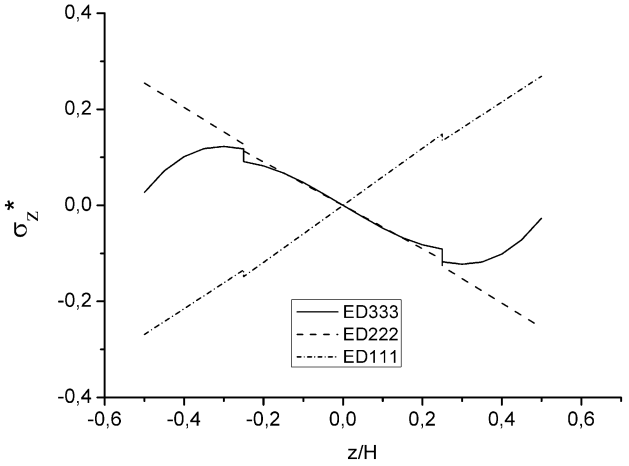

b)

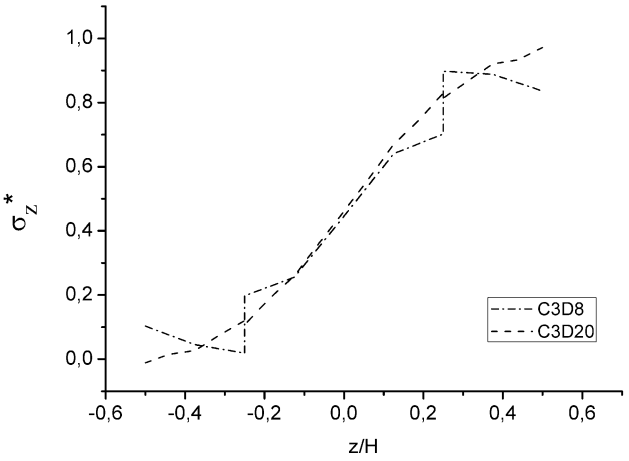

c)

Figure 52. Through-the-thickness Sz dimensionless stress (x = y = l/2). a) LW; b) ESL; c) Abaqus

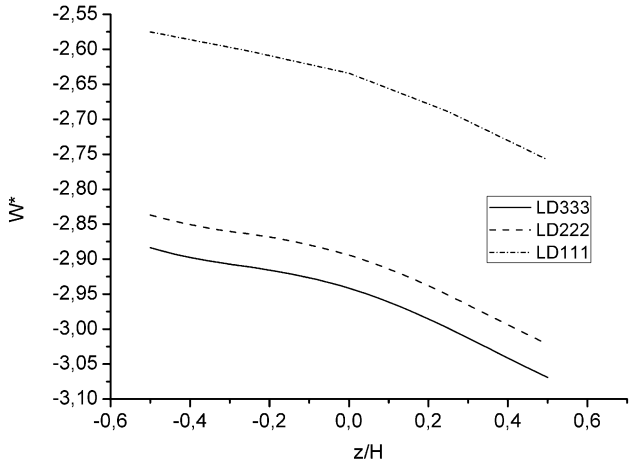

a)

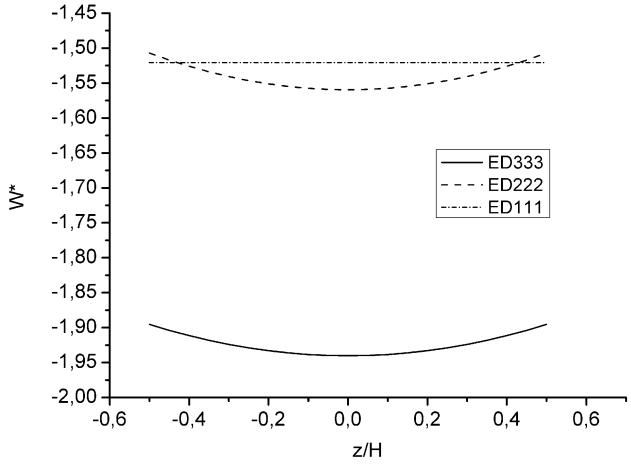

b)

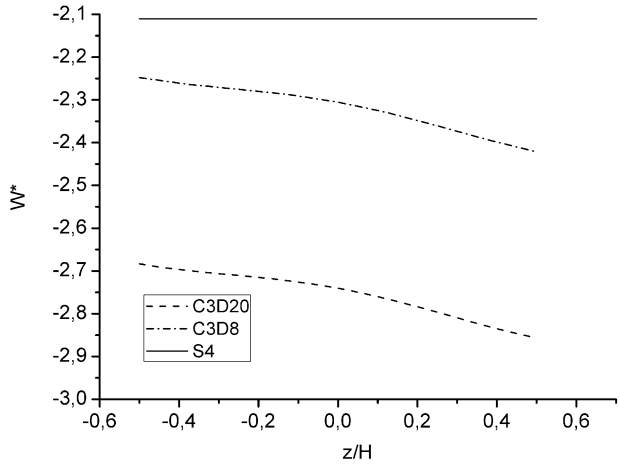

c)

Figure 53. Through-the-thickness normalized deflection (x = y = l/2). a) LW; b) ESL; c) Abaqus

Figure 49 shows the transversal shear stress S_{xz}. Once again, the ESL models are symmetric regarding the mid-plane of the plate. This includes the results from Abaqus obtained

with the S4 element. The LW implementation and the 3D models show a trend which attempts to satisfy the free shear stress at the top of the plate. Also, the LW models show that the respective maximum stress does not occur at the mid-plane of the center, but at a lower position, as indicated in Pagano and Hatfield (1972). The normalized position and the maximum value can be seen at the bottom of Table 7. In Figure 50, the curves of S_y in all three plots are very close.

The S_{yz} shear stress is shown in Figure 51. The ESL are symmetric as usual. The LW ones are not symmetric and, just like the C3D8 result, indicate that the respective maximum stress does not occur at the mid-plane of the plate either, but at a slightly lower position. This is not seen in Pagano and Hatfield (1972). In Figure 51c, the boundary conditions exert a substantial influence on the results C3D20 results.

Lastly, the transversal normal stress is given in Figure 52. The results from S4 element are not available. One can see that the 3D results from Abaqus scale from “zero” to “1” at the top face where the pressure is applied with considerable accuracy. This level of accuracy is only achieved with the LW formulations. The ESL formulation cannot represent this field for thick plates. From Figure 52b different qualitative behaviors can be obtained depending on the plate theory used. Therefore, only thin and very thin plate can be modeled using the ESL approach. This will be seen in the next section.

Back to the LW solutions, one can find discontinuities in the transversal field at Figure 52a. These jumps are not physically consistent and should not be present regardless of the material properties of two neighboring plies. In fact, though not explicitly show in this PhD thesis, it was noticed that if a sufficient number of terms is chosen for the LW formulation, these gaps tend to vanish. However, there is no general rule for this as it is a problem dependent assumption. This is an obvious outcome of unified formulations since high order polynomials have the flexibility to conform complex solutions.

In Figure 53, the transversal displacements are given. The LW solutions have the ability to properly represent the displacement profile regardless of the order of the theory. The ESL models cannot do this. The same value is taken through-the-thickness for the S4 element. The results obtained with CGF are actually of parabolic shape if sufficient resolution is applied to the plots. In addition, the LW results are closer to the 3D Abaqus profiles. One can see that the assumption of a constant transversal displacement field is not valid for thick plates. The next section will exhibit some thickness evaluations, which may or may not endorse the use simplified displacement fields.

Before evaluation of the thickness influence, the shear correction factor is briefly studied. The results are grouped into Table 9. In this study the value for laminated plates is not calculated as in Abaqus 2D. Rather, the two most common values for isotropic shells are chosen. Both ED111 and LD111 formulations are evaluated. The purpose is to see how such factor influence on the overall transversal results. This influence was incorporated in the formulation by weighting the two transversal shear moduli by this factor.

Table 9 - Shear correction factor impact on linear formulations (ED/LD111)

SCF	w (μmm)		$2S_{yz}$		$2S_{xz}$	
	ESL	LW	ESL	LW	ESL	LW
1	-0.9731	-1.6858	0.1623	0.1888	0.1202	0.1815
5/6	-1.1001	-1.8720	0.1685	0.1986	0.1202	0.1792
2/3	-1.2873	-2.1381	0.1758	0.2098	0.1176	0.1755

From inspection of Table 9, the magnitude of the transversal center displacement increases, indicating a more flexible structural model, in the macroscopic sense. The transversal shear stresses are affected by the extra transversal strain and their magnitude vary proportionally. This is a good option if one is seeking macroscopic results, which would be underestimated without these factors. However, caution is advised when microscopic results, such as stresses, are needed. The increase of flexibly also changes the stress levels and this may mask the true material response. Depending on whether the LD or the ESL approach is used, the value of the transversal stresses may become lower or higher. In this sense, it is preferable the use of a high order theory, which can provide a more real flexibility for the structural model.

The SCFs can be applied to high order theories too, but their use become meaningless as one begins to stack flexibility from different sources. Additionally, this is why it is rare to see a high order formulation with SCFs. The idea is to always seek a best solution method for the problem to be analyzed. Linear layer-wise formulations can provide structural models as flexible as or more, than a high order built on the ESL approach. This PhD thesis attempts to provide as much information as possible to the reader to help with the decision of which formulation to adopt.

6.3 Thickness Evaluations

The material properties and the loading conditions of Case II are chosen due to the available literature. However, in this section, different length to thickness ratios are studied to better understand how the non-linearity contributions vanish as the thickness decreases and the solution is sufficiently well represented by the ESL approach.

Table 10 shows the results calculated via CGF. The LD332 and the ED332 theories are investigated once more. Four length-to-thickness ratios are seen: 4, 10, 20 and 100. The same mesh densities from Table 4 are used. However, since this section focus on thickness trends, only the 3D solution for the thinned case is presented. To indicate the ratios, each theory is tagged with a letter "R", standing for "ratio", followed by the ratio itself (ER4, means ESL with ratio 4 and LR10 stands for LW with ratio 10). To ease further comparisons, the results from Pagano and Hatfield (1972) are displayed once more in Tables 10 to 13.

Table 10 - Transversal normal displacement (mm) at the mid-plane

l/h	ESL	LW	Analytical*\C3D20
4	-1.2418e-06	-1.8738e-06	-1.2395e-06 \ -1.7534e-06
10	-7.2593e-06	-8.0820e-06	-7.3700e-06 \ n/a
20	-4.0583e-05	-4.1442e-05	-4.1024e-05 \ n/a
100	-0.004294	-0.004296	-0.004347 \ -0.004305

* Pagano and Hatfield (1972)

Table 11 - Dimensionless normal stresses. Comparison for different thicknesses

	S_x			S_y		
l/h	ESL	LW	Analytical*\C3D20	ESL	LW	Analytical*\C3D20
4	-0.6929	-0.6926	-0.720 \ -0.7054	-0.6260	-0.6610	-0.663 \ -0.6795
10	-0.5482	-0.5370	-0.5590 \ n/a	-0.3827	-0.4082	0.4030 \ n/a
20	-0.5284	-0.5272	-0.5430 \ n/a	-0.2964	-0.3021	0.3090 \ n/a
100	-0.5195	-0.5195	-0.5390 \ -0.5389	-0.2610	-0.2612	-0.2710 \ -0.2680

* Pagano and Hatfield (1972)

Table 12 - Dimensionless transversal and shear stresses. Comparison for different thicknesses

	S_z			S_{xy}		
l/h	ESL	LW	Analytical*\C3D20	ESL	LW	Analytical*\C3D20
4	-0.0270	0.8974	n/a \ 0.9721	-0.0194	-0.0565	0.0467 \ -0.0362
10	-0.0124	0.8504	n/a	-0.0163	-0.0172	0.0275 \ n/a
20	-0.0766	0.7762	n/a	-0.0177	-0.0169	0.0230 \ n/a
100	-2.3560	-1.4949	n/a \ 1.572	-0.0203	-0.0202	-0.0214 \ -0.0197

* Pagano and Hatfield (1972)

In Table 10, the transversal displacements are given. It is easy to see, and this also happens to Tables 11, 12 and 13, that the precision of the results increase with the decrease of the thickness of the plate. This is true for both ESL and LW approaches. In addition, the ESL and LW deflection values are very close to the reference ones for the ratio l/h = 100. Such trend is expected because in the limit as h → 0 all plate theories collapse into a membrane theory, which possesses no transversal reactions.

Table 13 - Dimensionless transversal shear stresses. Comparison for different thicknesses

	S_{yz}			S_{xz}		
l/h	ESL	LW	Analytical*\C3D20	ESL	LW	Analytical*\C3D20
4	0.2504	0.25645	0.2920 \ 0.1134	0.2177	0.1946	0.2190 \ 0.0747
10	0.1667	0.2235	0.1960 \ n/a	0.2835	0.3192	0.3010 \ n/a
20	0.14306	0.1789	0.1560 \ n/a	0.3057	0.3400	0.3280 \ n/a
100	0.39337	0.4175	0.1390 \ 0.4512	0.4173	0.4410	0.3390 \ 0.5785

* Pagano and Hatfield (1972); Mendonça (2005)

From Figure 54 to 67, the through-the-thickness profile of each variable can be seen for different formulations and thicknesses. The main conclusion from these plots is the verification of the convergence of the ESL and LW theories as the plate gets thinner. For the normal stresses, the change in the behavior of the solution is clearly seen when the plate passes from ratio 20 to 100.

It is interesting to look into the 3D results from Abaqus for the transversal normal stress and those from CGF in Figures 64 and 65. Both ESL and LW results show a symmetrical behavior with top and bottom values which are approximately 2-3 times the normalized expected unit value. Abaqus gives approximately 1.6 for the transversal normal stress (S_z) value at the top of the laminate. This means that for (very) thin plates, and using 100 elements, CGF fails to represent the transversal normal stress (S_z) of this Case, even with high order LW formulations. Abaqus 3D (10x10x8) also fails, but the error is about ~57%, not ~249% (LW). This error can be minimized in Abaqus with finer meshes. This alleviates the error in CGF too, but there are other issues in place.

CGF weak solution method automatically defines every term of the expansion and calculates the transversal stiffness separately from the in-plane one. By these means, there is an error from not coupling the thickness direction terms with the in-plane ones, like the 3D solutions do. This is more pronounced with coarser meshes. However, these errors greatly affect the transversal normal stress for thin laminates as mentioned. That is because the actual normal strain is nearly null and the overall stacked absolute error for a particular theory is of the same

magnitude of the strain. Hence the large errors. ESL models and linear theories give the worst results for this variable.

In Figures 59 and 63, the coupling of the transversal reaction, which is present in the C3D20 element formulation with the results of the can be easily observed thinnest plate. As one gets away from the center towards the top or bottom face of the plate, the profiles obtained from Abaqus predict better the free shear stress conditions in comparison to CGF.

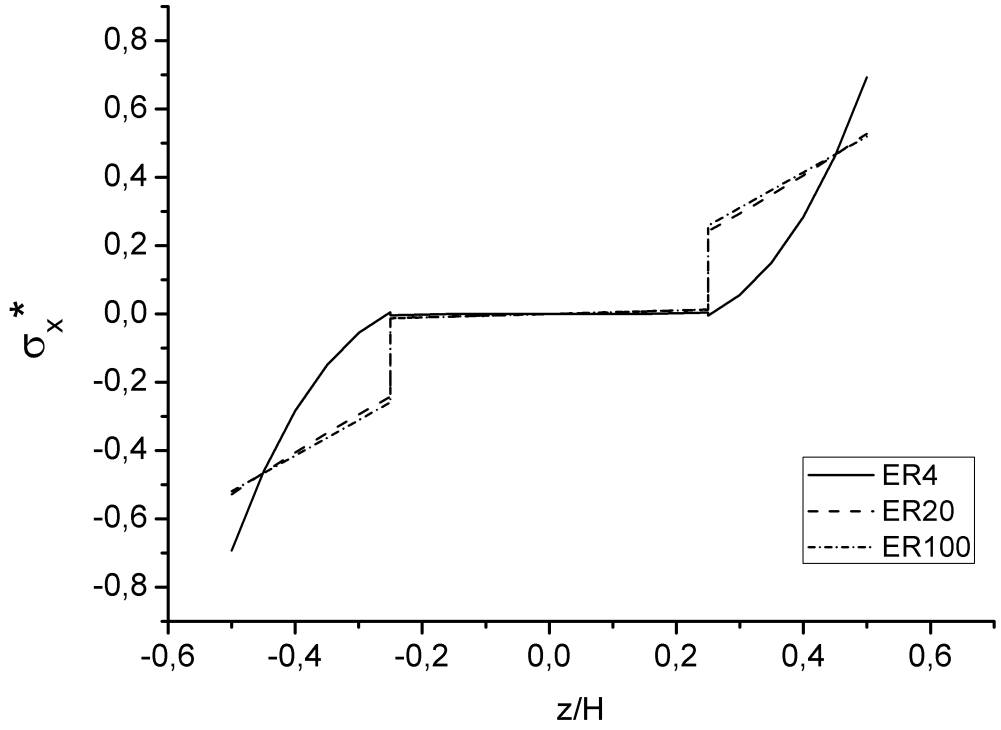

Figure 54. Through-the-thickness Sx stress via CGF (x = y = l/2). ESL formulation

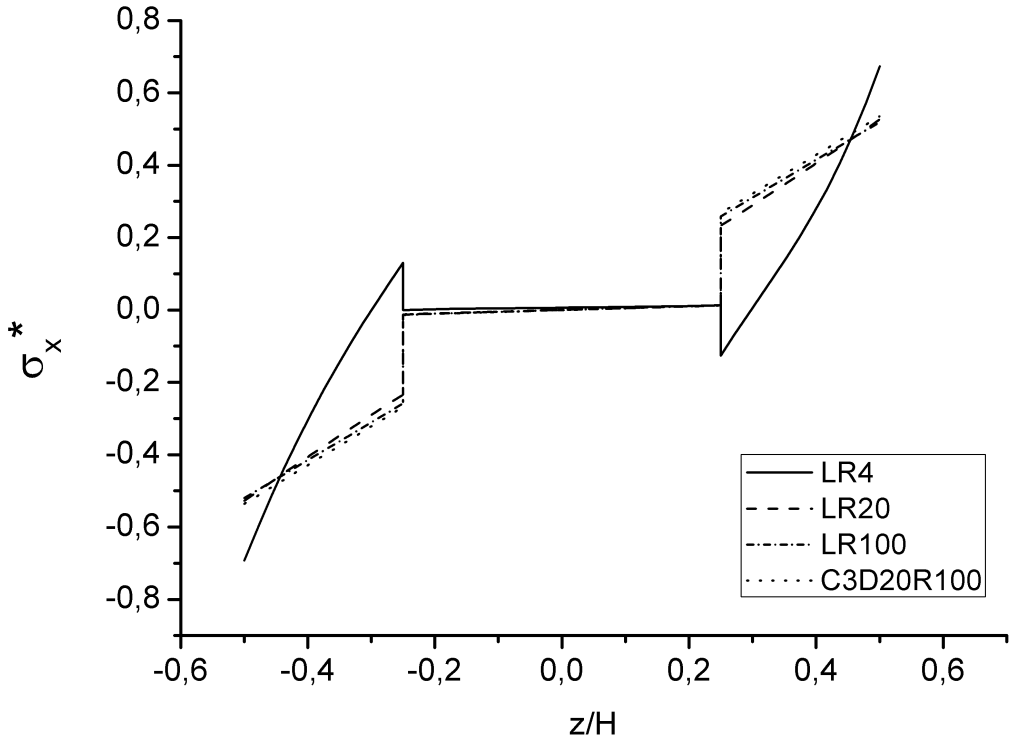

Figure 55. Through-the-thickness Sx stress via CGF (x = y = l/2). LW formulation

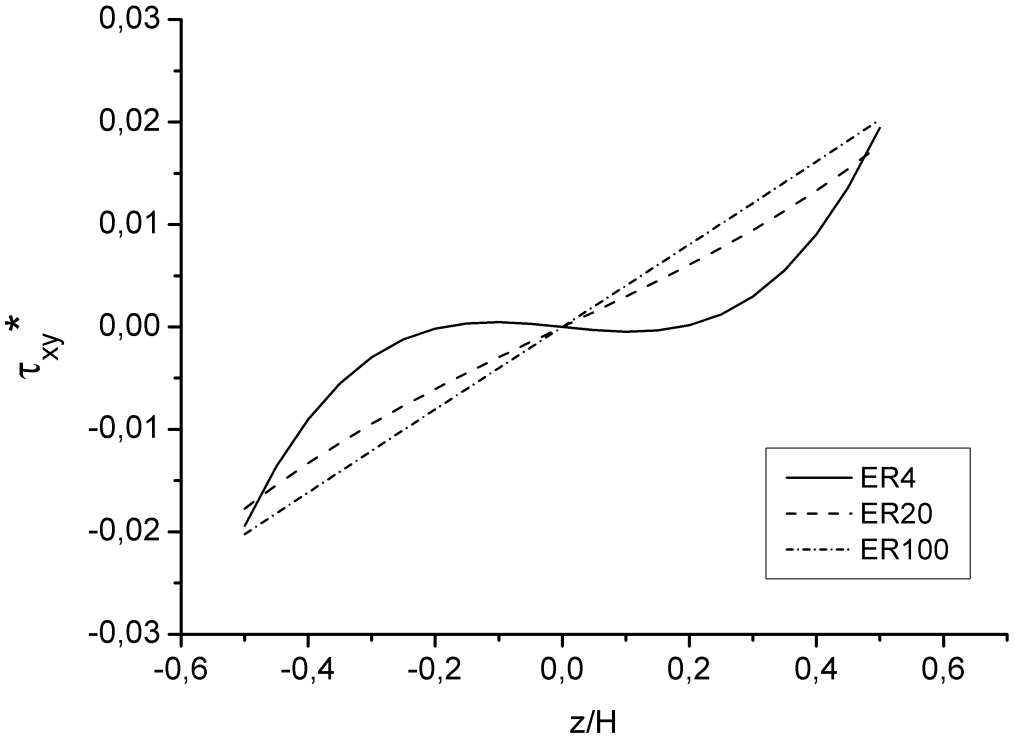

Figure 56. Through-the-thickness Sxy stress via CGF (x = y = 0). ESL formulation

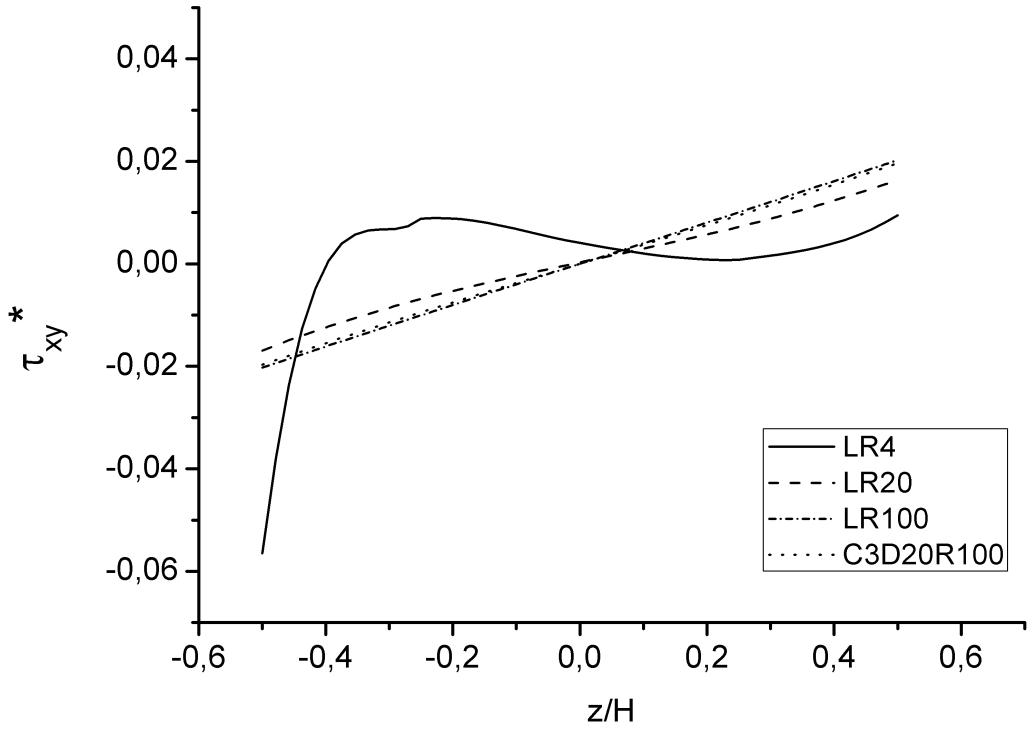

Figure 57. Through-the-thickness Sx stress via CGF (x = y = 0). LW formulation

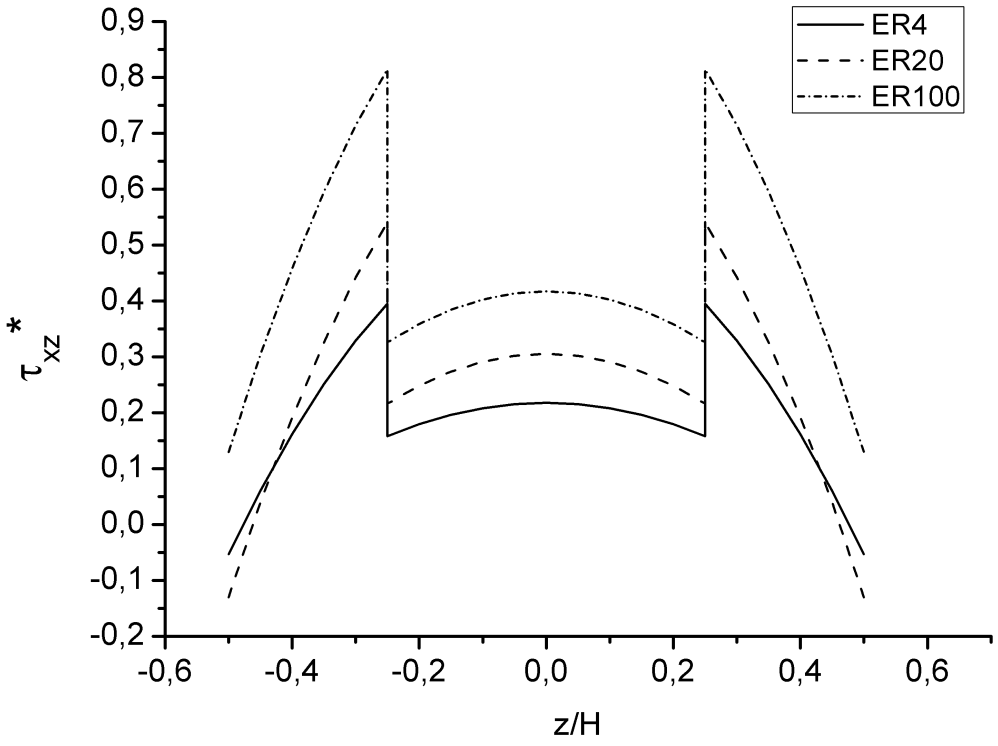

Figure 58. Through-the-thickness Sxz stress via CGF (x = 0, y = l/2). ESL formulation

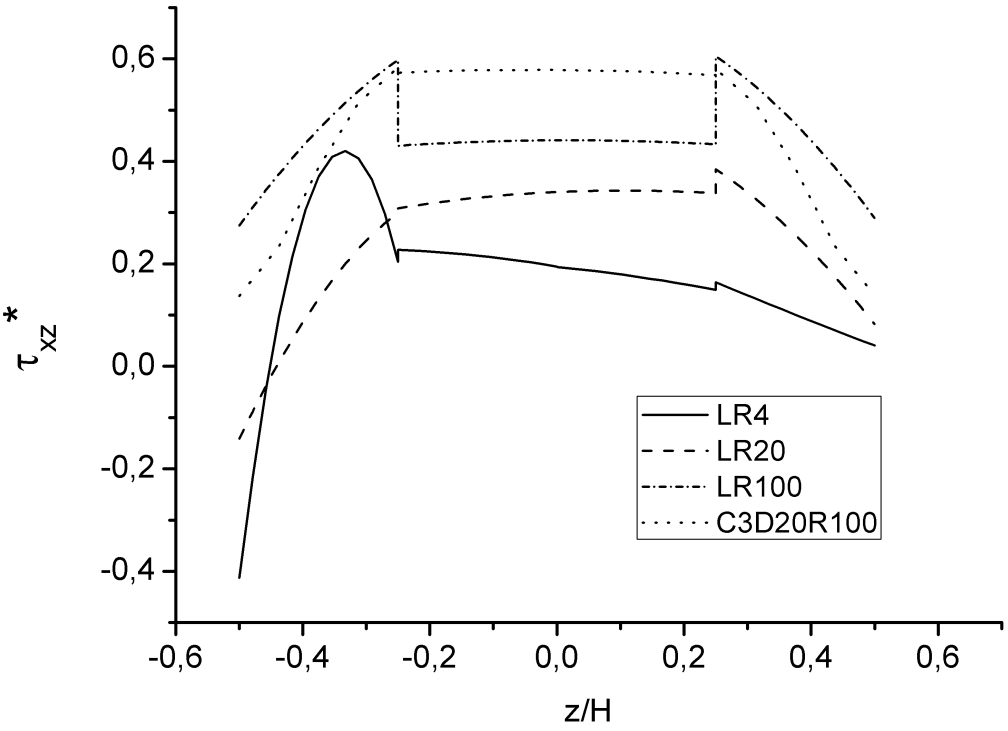

Figure 59. Through-the-thickness Sxz stress via CGF (x =0, y = l/2). LW formulation

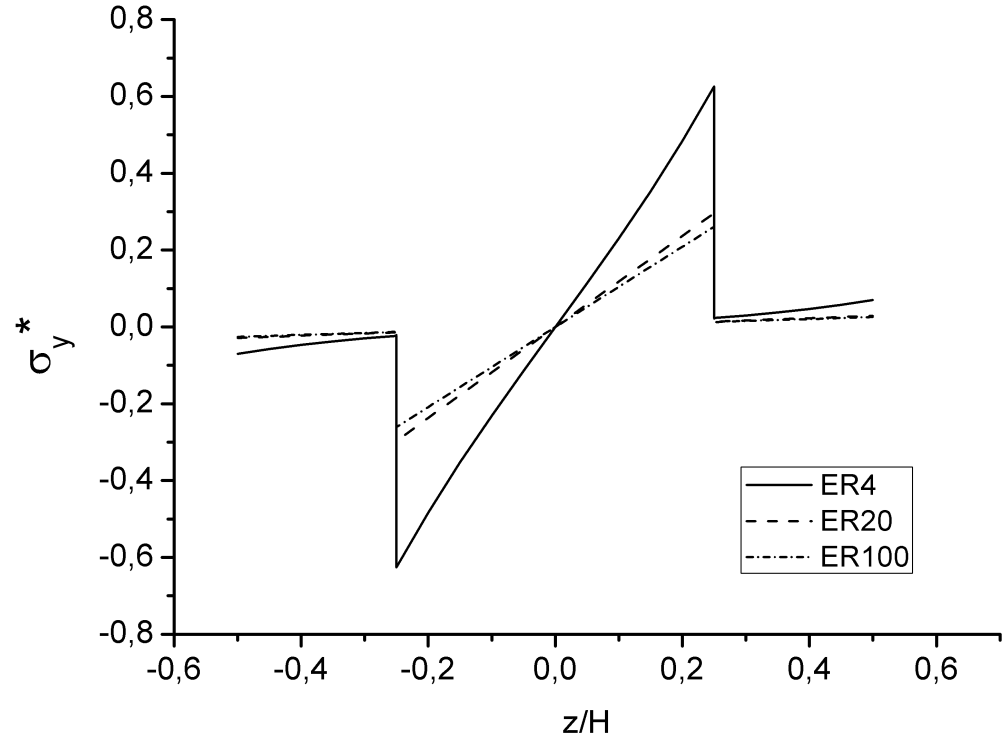

Figure 60. Through-the-thickness Sy stress via CGF (x = y = l/2). ESL formulation

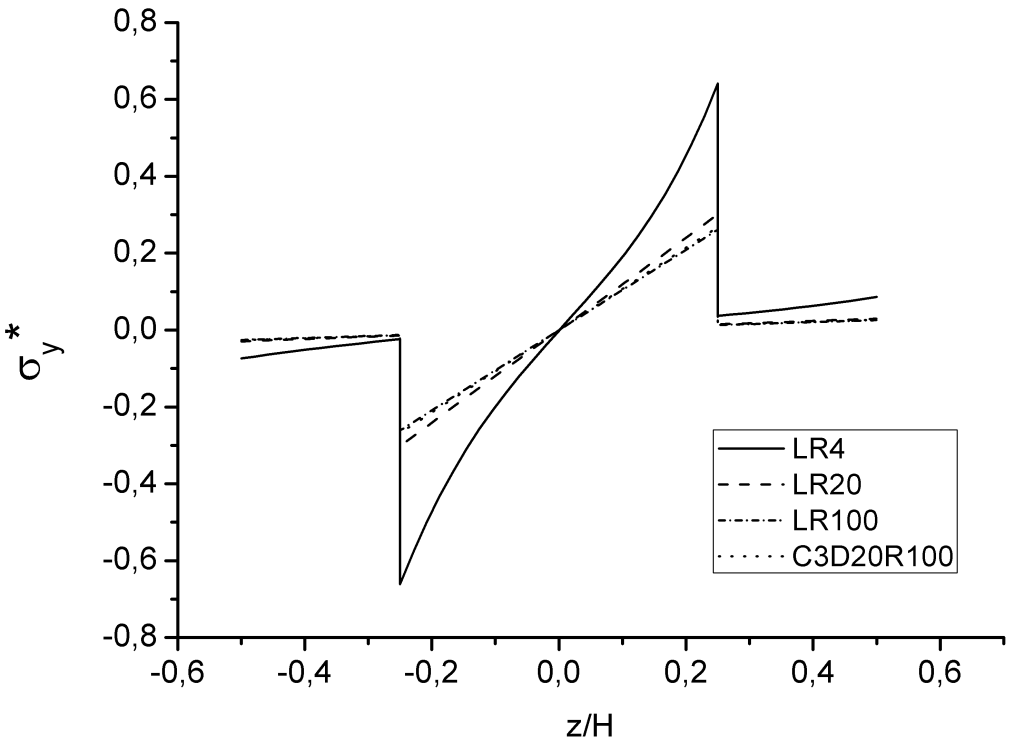

Figure 61. Through-the-thickness Sy stress via CGF (x = y = l/2). LW formulation

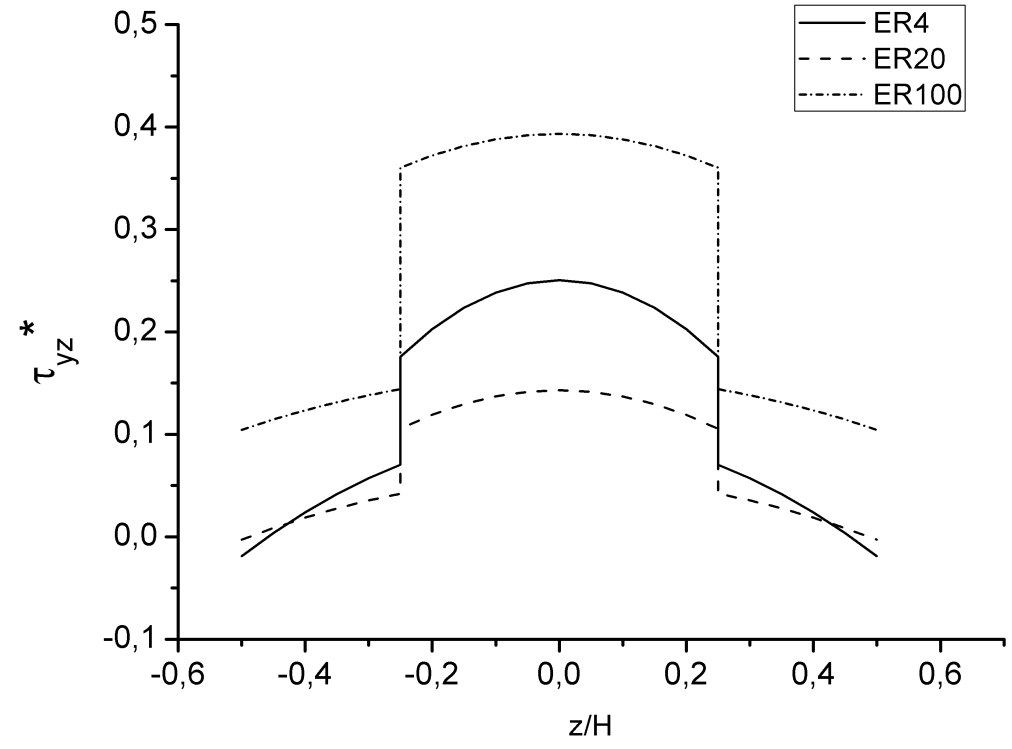

Figure 62. Through-the-thickness Syz stress via CGF (x =l/2, y = 0). ESL formulation

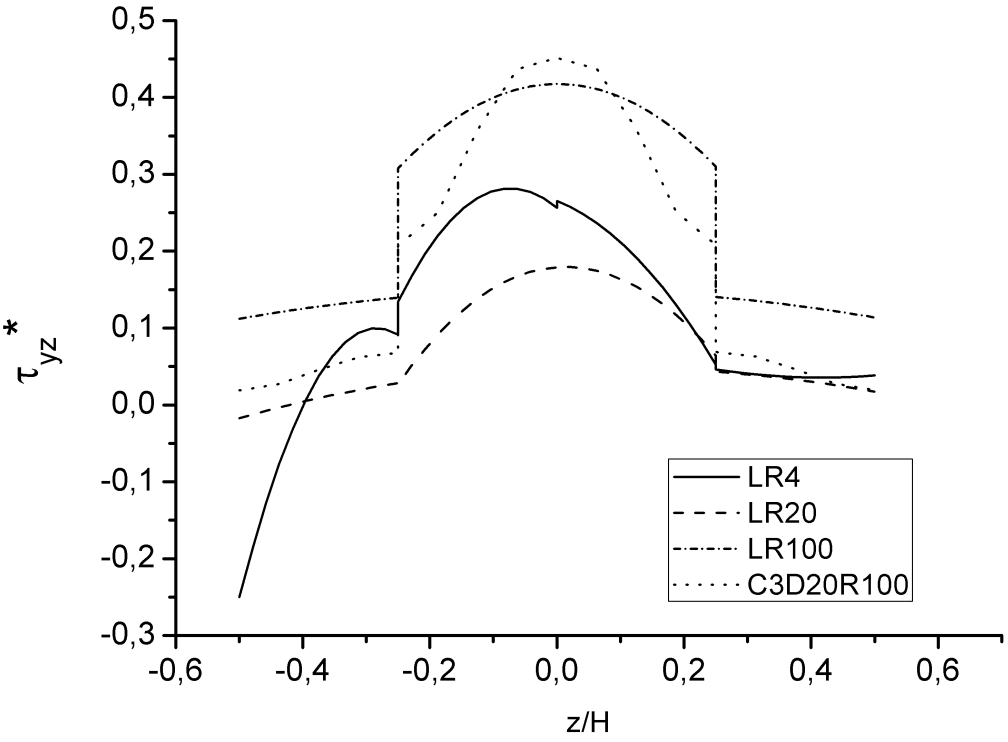

Figure 63. Through-the-thickness Syz stress via CGF (x = l/2, y = 0). ESL formulation

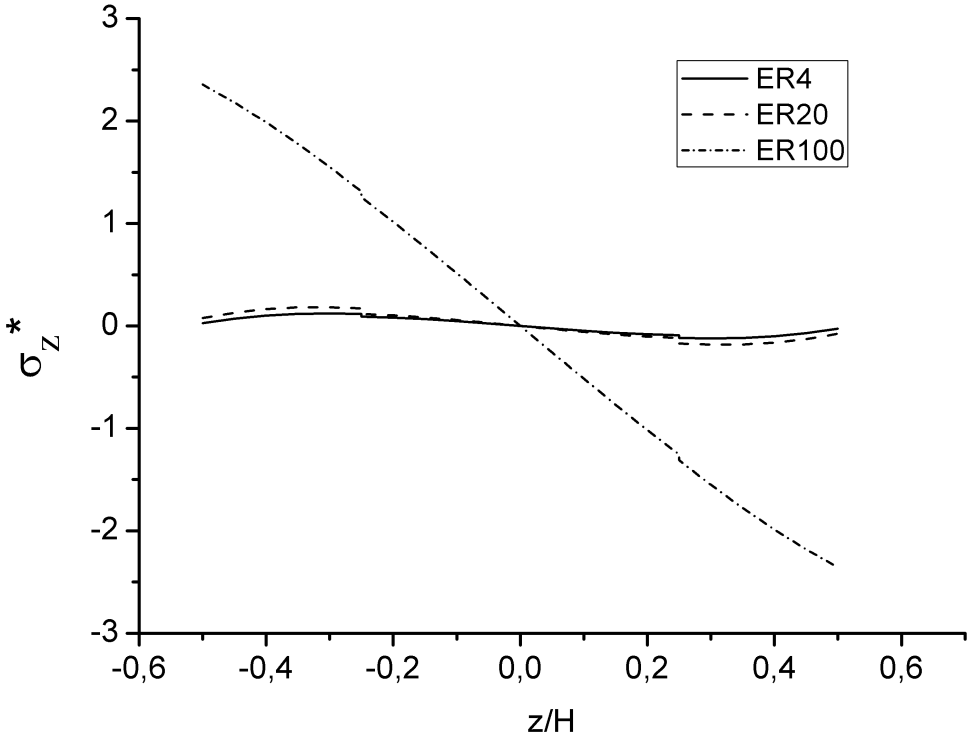

Figure 64. Through-the-thickness Sz stress via CGF (x = y = l/2). ESL formulation

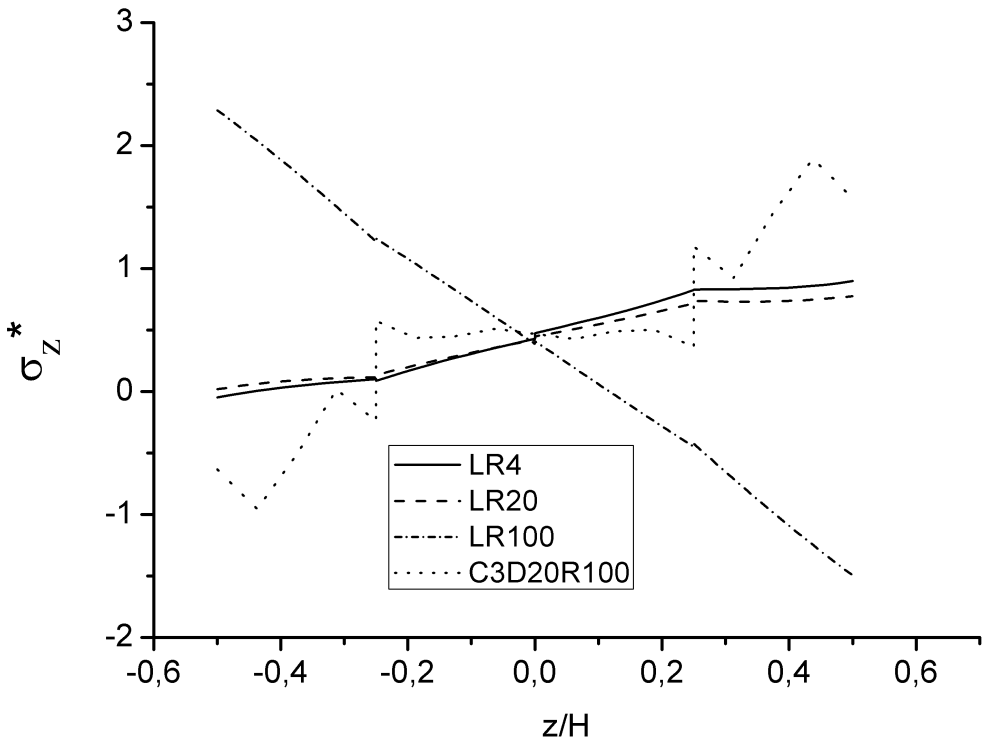

Figure 65. Through-the-thickness Sz stress via CGF (x = y = l/2). LW formulation

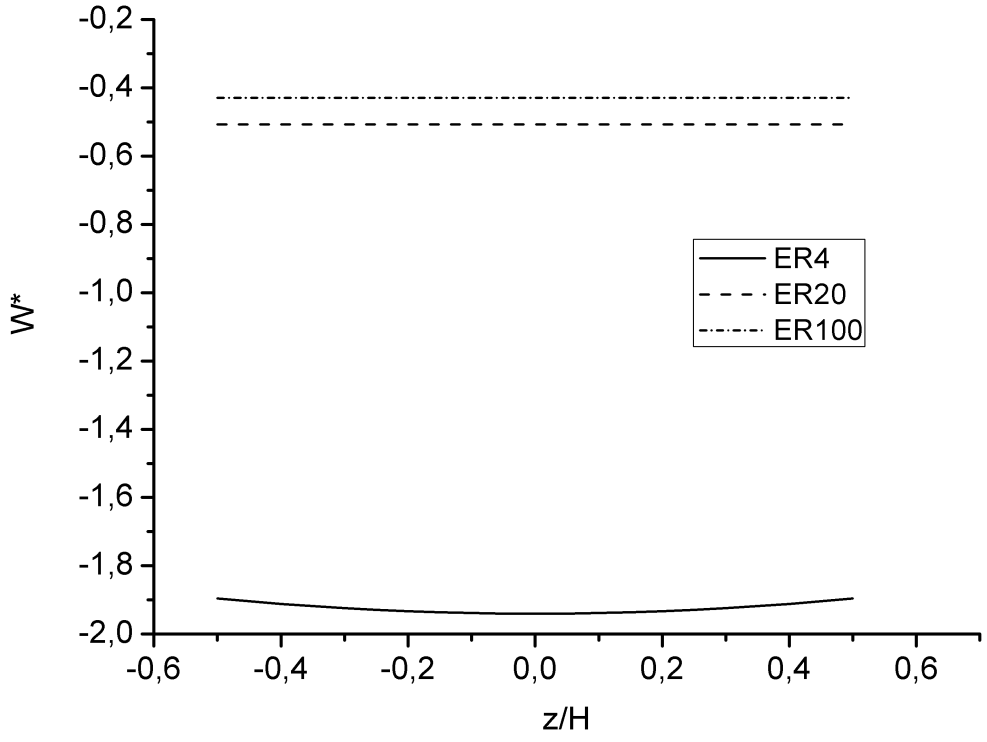

Figure 66. Through-the-thickness dimensionless deflection via CGF (x = y = l/2). ESL formulation

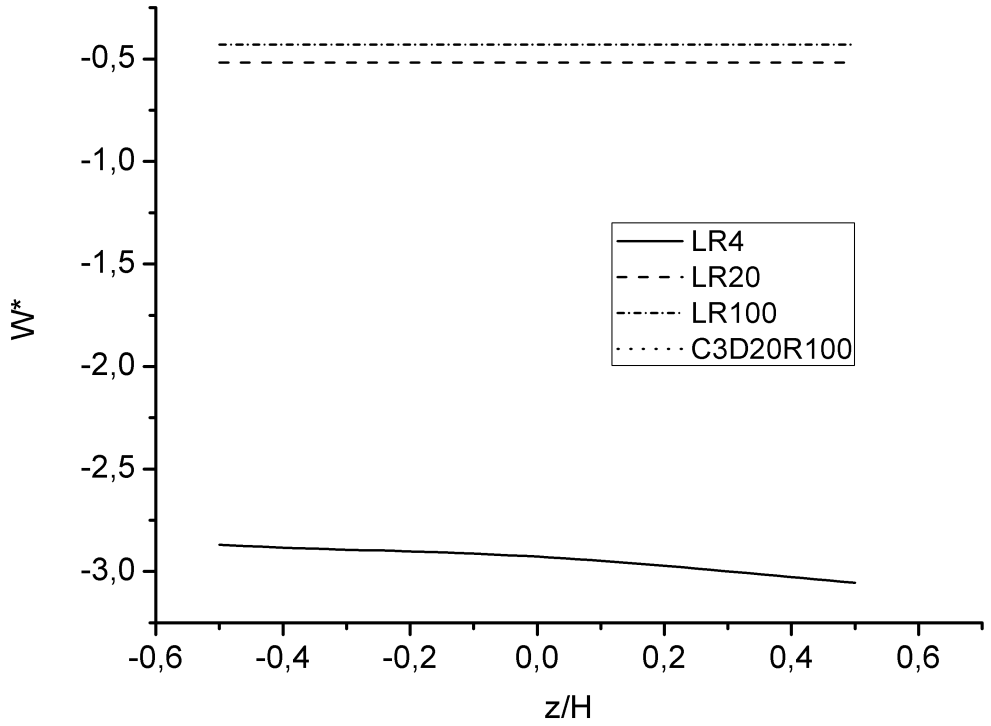

Figure 67. Through-the-thickness dimensionless deflection via CGF (x = y = l/2). LW formulation

At this point, it is possible to verify that thin plate formulations hold when the thickness of the laminated plate is at most "1" per cent of the shortest in-plane dimension. If this is the case, ESL are well suited for most applications. Even though only one theory was involved in this section, the same qualitative conclusion holds for other theories (See section 6.2). However, it is clear from this and from the previous section that non-linear contributions are needed for moderately thick and thick plates.

6.4 Modal Analyses Evaluations

To assess the inertial influence on CGF, two modal cases are proposed. The first is a variation from Case II, which was investigated in the other sections. This variation carries an asterisk.

Case II* is a clamped laminated plate. The geometry and aspect ratios are the same as Case II. These properties, along with those of the following Case III are shown in Table 14.

Case III is a simply-supported laminated plate. The geometry and aspect ratios are the same as Case II. However the material properties change.

Table 14 - Material properties and plate dimensions for dynamic analyses

Case / Material	**l** (mm)	**h** (mm)	$\mathbf{E_1}$ (MPa)	$\mathbf{E_2 = E_3}$ (MPa)	$\mathbf{G_{12} = G_{13}}$ (MPa)	$\mathbf{G_{23}}$ (MPa)	$\boldsymbol{\upsilon_{12} = \upsilon_{13} = \upsilon_2}$	**ρ** (ton/mm²)
II* – Orthotropic	1000	50	$25E_2$	1000	$0.5E_2$	$0.2E_2$	0.25	7e-9
III -Orthotropic	1000	500; 250; 100	$40E_2$	1000	$0.5E_2$	$0.6E_2$	0.25	7e-9

Regarding Case II*, the first 10 natural frequencies are compared to those obtained via Abaqus 2D and 3D. Later, an asymmetric and a symmetric laminate are studied and the results compared to values from Carrera (2003b). Abaqus results are also given with the same mesh densities of 10x10x8 and 10x10 for the 3D and 2D models respectively.

The 8x8 mesh is kept for CGF assessments. Different theories are evaluated as well as the use of a shear correction factor. This first 10 bending modes of this evaluation with the ED332 theory are shown in Figures 68 to 72 and in Table 15.

Table 15 - First 10 vibration frequencies for Case II*

Theory\ Mode	ED111 (k = 1)	ED111 (k = 2/3)	LD111 (k = 1)	LD111 (k = 2/3)	ED332 (k = 1)	LD332 (k = 1)	Abaqus 2D	Abaqus 3D
1	83.8	77.5	77.2	70.6	77.7	76.7	74.4	74.1
2	129.5	121.0	123.1	114.2	122.9	121.6	117.9	113.9
3	177.4	156.6	156.9	137.5	158.4	155.5	146.7	146.1
4	207.5	185.8	188.0	167.7	188.9	186.0	173.5	171.3
5	214.1	197.2	205.5	188.0	204.0	201.5	195.5	180.7
6	273.8	246.6	254.8	223.7	254.4	250.8	233.6	222.8
7	297.0	256.0	259.9	228.6	262.2	257.3	238.3	234.5
8	320.3	278.4	284.0	247.0	286.0	281.1	255.5	251.9
9	329.2	296.5	315.8	283.1	312.6	308.3	298.6	264.2
10	372.6	326.7	337.9	296.5	338.8	333.5	300.2	290.5

From inspection of Table 15, the softest solutions obtained by CGF are the LD332 and the LD111 (with k = 2/3) ones. Moreover, the latter one better matches the results from Abaqus. Abaqus 2D model provides softer structural model than the 3D model. By constraining all rotations along with the displacements, CGF provides stiffer and the deviation of the 10^{th} mode reached ~28% for ED111 & k = 1 compared to the 3D results of Abaqus.

The LD111 & k = 2/3 model gives the lowest frequency for the 10^{th} mode and it deviates only 2% from Abaqus 3D solution. Nonetheless, not every mode from this model has a corresponding higher frequency in Abaqus 3D. Abaqus 2D model, on the other hand, shows higher frequencies for every mode compared to the 3D solution. This may be due to the fact

that a constant shear correction fact was used in CGF and a factor for each ply was used in Abaqus.

However, these results are for the same 10x10 in plane meshes. A convergence study on higher order theories may give different patterns. Also, an experimental result should be used to evaluate which approach is best at representing a true laminate.

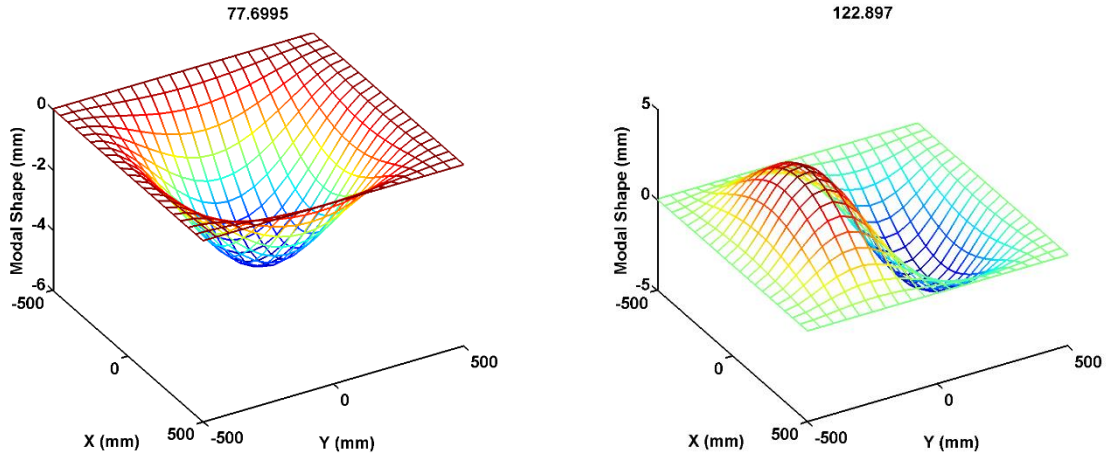

a) b)

Figure 68. ED332: Modal Shape and Natural Frequency (Hz) of a)1st mode; b)2nd mode

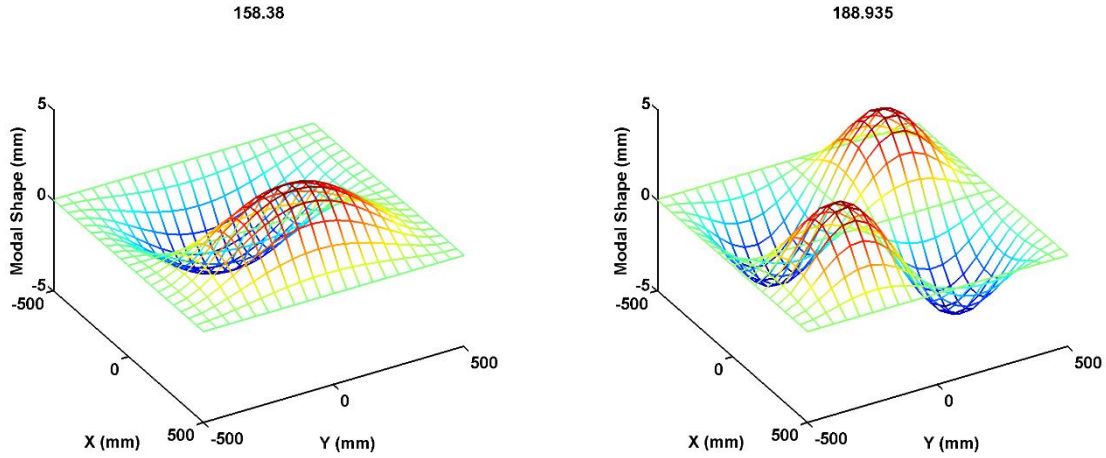

a) b)

Figure 69. ED332: Modal Shape and Natural Frequency (Hz) of a)3rd mode; b)4th mode

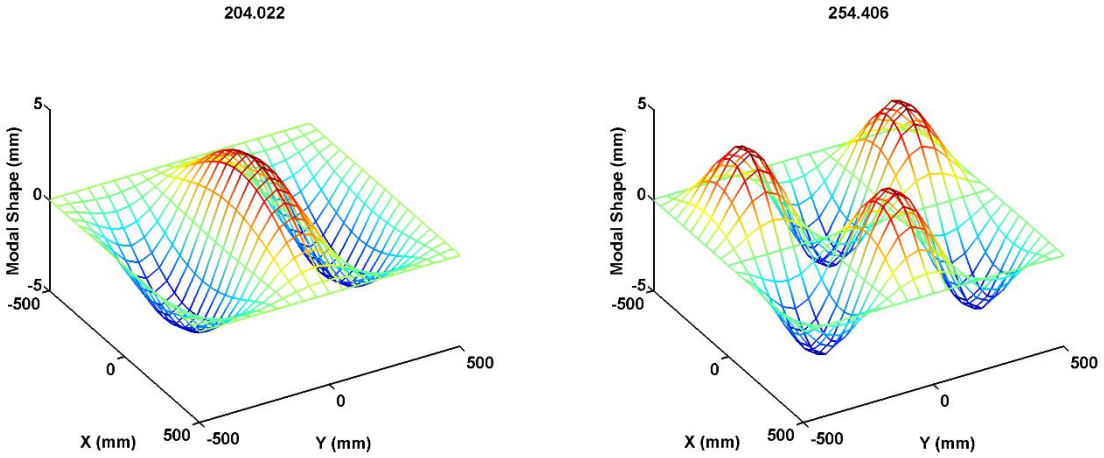

a) b)

Figure 70. ED332: Modal Shape and Natural Frequency (Hz) of a)5th mode; b)6th mode

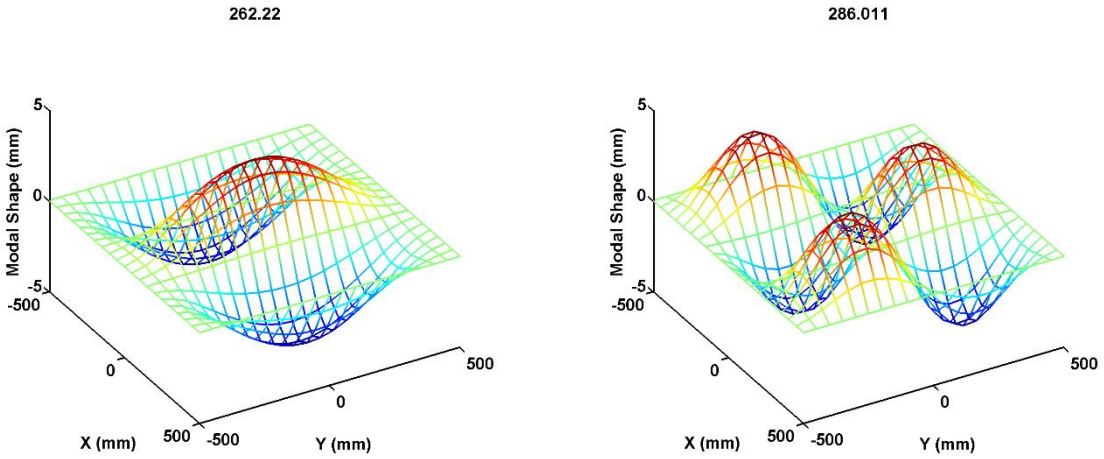

a) b)

Figure 71. ED332: Modal Shape and Natural Frequency (Hz) of a)7th mode; b)8th mode

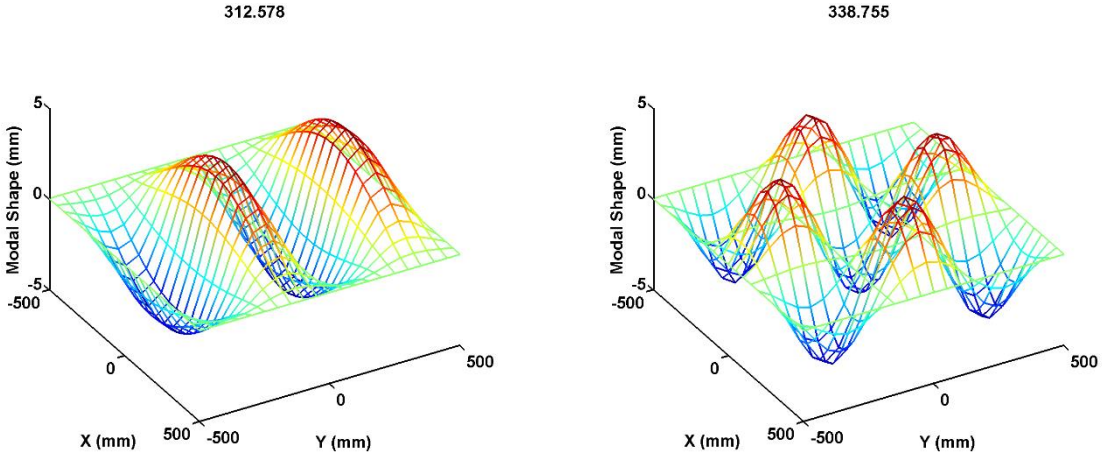

a) b)

Figure 72. ED332: Modal Shape and Natural Frequency (Hz) of a)9th mode; b)10th mode

Here, one must be reminded that both solutions are numeric and without damping properties. This is a topic of much concern, especially in dynamic applications of sandwich structures. Whenever possible, damping properties should be included in the formulations. However, due to the different types of damping and damping implementations, the inclusion of damping in the formulations is only advised if it is calibrated by experimental data.

Next, the evaluation of thick symmetric and non-symmetric plates is performed, i.e. Case III. Carrera (2003b) shows some closed form solutions for a normalized natural frequency. These values are compared to those solved via CGF in Table 16. The normalization is:

$$\bar{\omega} = \omega\sqrt{l^4\rho/E_T h^2} \tag{6.6}$$

Table 16 - Comparison of the first dimensionless natural frequency solved via closed-form solutions and CGF

Laminate	l/h	LM4*	LD3*	LD333	LD1*	LD111	ED3*	ED333	ED1*	ED111
0/90 2-plies	2	4.703	4.710	4.595	4.848	4.742	4.883	4.814	5.544	5.549
	4	7.345	7.346	7.275	7.562	7.509	7.647	7.601	8.314	8.311
	10	10.088	10.088	10.141	10.215	10.280	10.235	10.293	10.545	10.621
$0/90_s$ 4-plies	2	5.260	5.262	5.275	5.414	5.437	5.392	5.421	5.927	5.750
	4	9.224	9.224	9.285	9.473	9.541	9.389	9.458	9.960	10.034
	10	15.148	15.148	15.318	15.335	15.509	15.232	15.405	15.573	15.753

* Carrera (2003b)

Carrera (2003b) sets the mixed formulation of the 4th order (LM4) as the reference solution, because it approaches the values obtained by analytical closed form solutions. The respective cubic and linear solutions obtained analytically via PVD by Carrera (2003b) are compared to the solutions of CGF for the same expansions in Table 16. Three thickness-to-length ratios are studied for the symmetric and non-symmetric laminates. From Table 16, on can assert that CGF is comparable to CUF. Some results are slightly higher or lower.

Table 17 - Comparison of the first dimensionless natural frequency obtained by CGF and Abaqus

Laminate	l/h	Abaqus 2D	Abaqus 3D	LD3*	LD333
0/90 2-plies	2	4.63	5.74	4.710	4.595
	4	8.80	9.89	7.346	7.275
	10	17.02	17.36	10.088	10.141
$0/90_s$ 4-plies	2	5.34	5.83	5.262	5.275
	4	10.38	10.83	9.224	9.285
	10	22.37	22.43	15.148	15.318

* Carrera (2003b)

In Table 17, some results from Table 16 are compared to the results from Abaqus. When compared, the 3D results from Abaqus (as well as the 2D results excluding the ratios 2 and 4

of the non-symmetric case) show a structural model stiffer for higher natural frequency values. This means that the UFs provide more flexible structural models and inertia is considered.

After the comparisons in Tables 16 and 17, it is safe to say that CGF is at least as good as Carrera's solution concerning the solution of eigenvalues problem. This is a good trend of CGF which, as a FE solution method, carries more deviations than closed form solutions.

6.5 Performance Evaluations

It is of little use to develop a sophisticated theory if it takes forever to run. Thereby, a performance evaluation was carried out considering different theories, mesh densities and the problem loading and boundary conditions.

All of these evaluation were run on a Desktop computer running Windows 7.0. The processor was an Intel Core2Quad Q9550 @2.83GHz along with 8Gb of memory DDR2 DRAM @800MHz. The period for benchmarking was measured from the beginning of the code, step (i), until the end of the solver, which is step (viii) of the in-house FE code. See section 5.2 of this thesis.

First, analysis of the processing time of Case II is shown in Figure 73. Both LW and ESL formulations are plotted against the complexity of the theory being investigated. An 8x8 mesh is considered.

Figure 73 shows that the LW approach is always more expansive than the ESL. That is due to the larger number of DOFs to be solved in the LW case. One can say that, for this particular case, the ESL solution is 10 times faster than the LW one. Second, increasing the number of expansion terms of the out-of-plane displacement field (deflection) rapidly increases the computational time in a non-linear fashion.

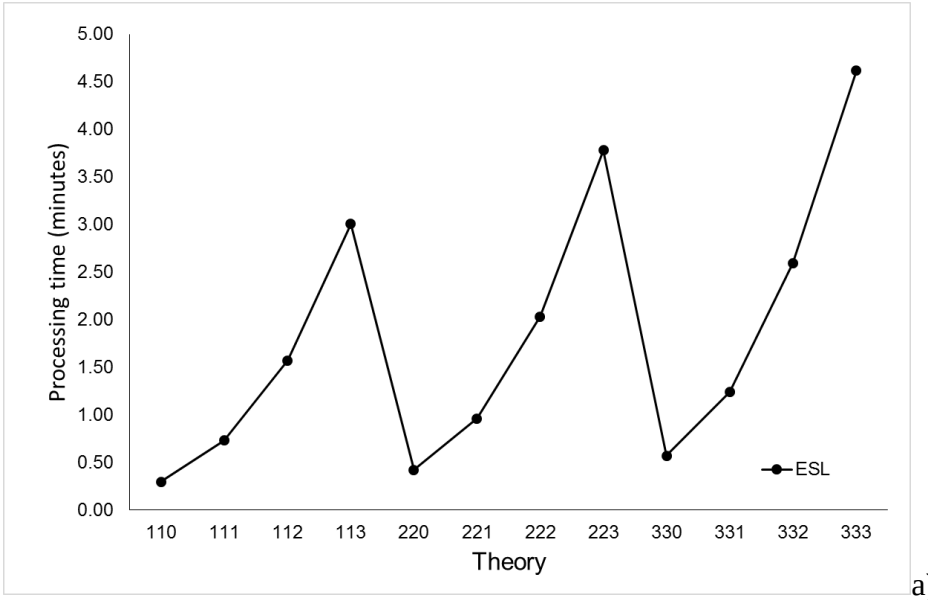

a)

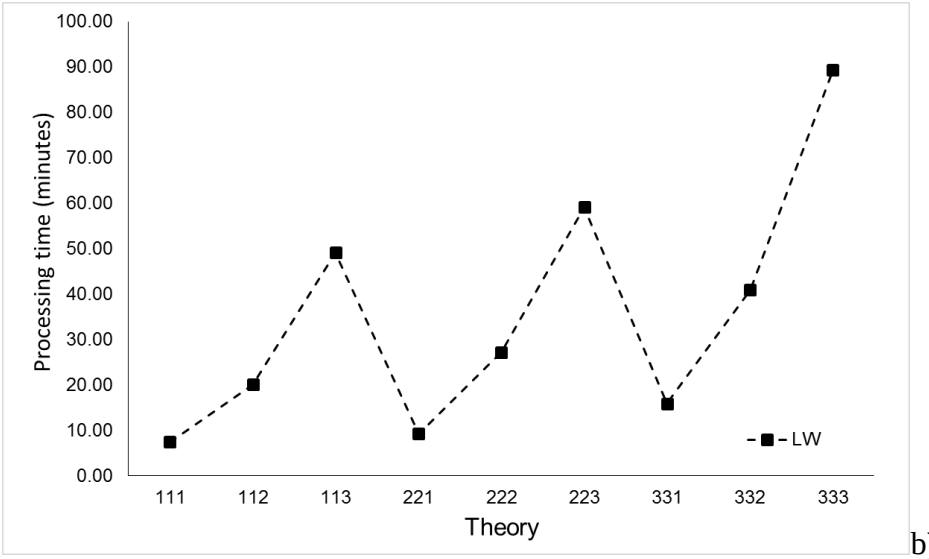

b)

Figure 73. Processing time as a function of the theory: a) ESL models; b) LW models

This is because the number of DOFs increases with a multiplier of "4x" because of the C-1 implementation. Recalling the number of nodal variables "Mt":

$$M_t = M_u + M_v + 4 * M_w \tag{6.7}$$
$$M_a = (nl - 1) * (N_u - 1) + N_u$$
$$M_b = (nl - 1) * (N_v - 1) + N_v$$
$$M_c = (nl - 1) * (N_w - 1) + N_w$$

Depending on the combination of "N_u" "N_v" and "N_w", both thickness and in-plane integration times will vary. Hence, the conclusions on the performance are somewhat clouded

because the code, as previously state, is not optimized because full integration is enforced as discusses in section 5.2 of this manuscript.

Next, the evaluation of Case I (concentrated force) and II (bi-sinusoidal pressure) for ED111/333 and LD111/333 theories is given in Figures 74 and 75, respectively.

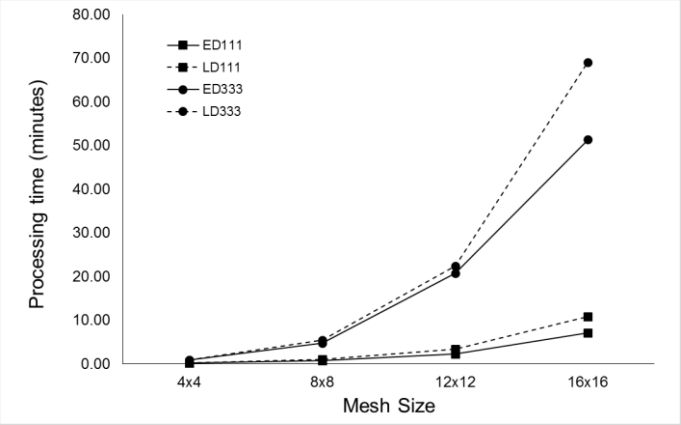

Figure 74. Processing time as a function of the mesh size for different theories (Case I)

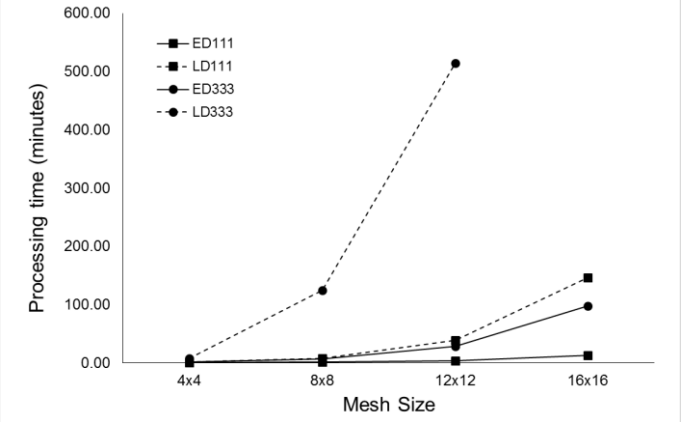

Figure 75. Processing time as a function of the mesh size for different theories (Case II)

Considering Figures 74 and 75, the processing time for both cases increases with the number of expansion terms. Moreover, as expected, the LW approaches are more time consuming than the ESL. In addition, since Case II is a laminated structure, the processing time for the LW solution greatly increases in comparison with the ESL one. This is not the case for Case I, because there only one layer is considered. Nonetheless the LW code is still slower. This is probably, because the code has the additional “ply-loops” to go over.

As explained in Chapter 5, the code needs optimization, reason why no performance comparisons are made by Abaqus solutions, as well. Therefore, in order to evaluate the actual processing time of the formulation, an optimization is required. For instance, an UEL (user-element sub-routine) can be built and run within Abaqus. However, the coupling of DOFs may

pose additional technical issues and perhaps errors. And, this is another issue for the future works.

6.6 Sandwich Structure Evaluations

Sandwich structures are one of main motivations of this work. Therefore two different cases, Case IV and Case V, are chosen for evaluations of CGF.

Case IV is a simply-supported 5-ply laminated sandwich structure under a bi-sinusoidal pressure (Figure 76). The laminate is symmetric and the plate is square-shaped. The stacking sequence is [0°/90°/core/90°/0°]. These properties can be found in Table 18. Details of this case can be found in Pandit, Sheikh and Singh (2010). According to the knowledge of the present author, the transversal Poisson's ratio for the core was assumed to be equal 0.1.

Case V is a simply-supported 3-ply sandwich structure under a bi-sinusoidal pressure (Figure 77). The laminate is non-symmetric and the plate has an aspect ratio of 3. All three plies are of isotropic materials. These properties can be found in Table 19. This Case is taken from the Demasi's work (2009a).

Both cases have the same unit bi-sinusoidal pressure from Equation (6.1).

Table 18 - Dimensions and material properties of the sandwich structure of Case IV

Layer	**l** (mm)	**h** (mm)	E_1 (MPa)	E_2 (MPa)	E_3 (MPa)	G_{23} (MPa)	G_{13} (MPa)	G_{12} (MPa)	υ_{12}=	υ_{13}= υ_{23}	**ρ** (ton/mm²)
Skins [0/90] (0.05h+0.05h)	1000	100	$25E_2$	1000	E_2	$0.2E_2$	$0.5E_2$		0.25	0.25	1e-9
Core (0.8h)			$0.04E_2$		$0.5E_2$	$0.06E_2$		$0.016E_2$		0.1	1e-11

Table 19 - Dimensions and material properties of the sandwich structure of Case V

Layer	**l** (mm)	**a** (mm)	**h** (mm)	**E** (MPa)	**υ**	**ρ** (ton/mm²)
Upper Skin	900	300	15	8000	0.34	1e-9
Core			52.5	1000; 0.1		1e-11
Lower Skin			7.5	10000		1e-9

For Case IV, the comparisons comprise the results obtained from the TE from Pagano (1970, apud PANDIT; SHEIKH; SINGH 2010, p. 316). For Case V, the comparisons are taken from Demasi (2009a). In this case, a comparison of solution methods is possible because the same theory for the displacement fields are evaluated. More test cases with sandwich structures

can be found in Ferreira et al. (1991). Results obtained by 2D and 3D models via Abaqus are also given for both cases.

In Figures 76 and 77, the discretization of the 3D models built in Abaqus are shown.

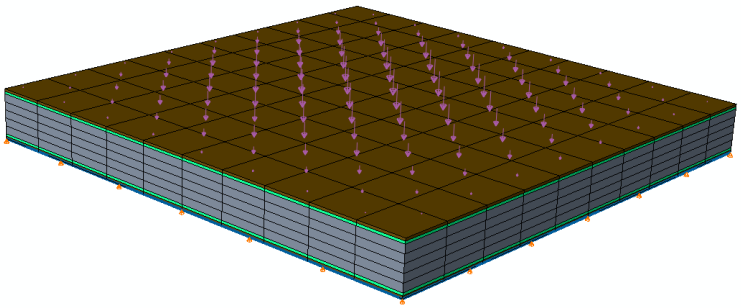

Figure 76. Case IV: Mesh, load and boundary conditions

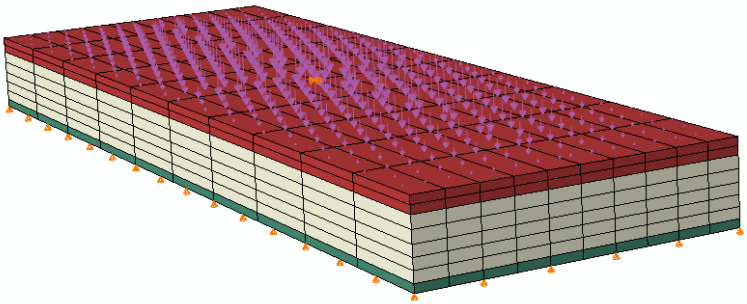

Figure 77. Case V: Mesh, load and boundary conditions

Both models built within Abaqus and CGF models have a 10x10 in-plane mesh density.

6.6.1 Results and Discussion of Case IV

To evaluate the potential of the new solution method in simulating sandwich structures, the analytical solution of a few particular points (Table 6) are compared with the corresponding values from CGF and Abaqus solutions. Two theories were chosen. The linear one (LD/ED111) as it represents Mindlin's theory and a quadratic/cubic one (LD/ED333), which is more physically consistent. The comparison of the magnitudes extracted with all methods are shown in Table 20. Note that the engineering shear stresses (e.g. $\tau_{xz} = 2S_{xz}$) are evaluated in this table.

Table 20 - Comparison of results from Case IV

Theory		W*	S_x	S_y	S_z	S_{xy}	S_{yz}	S_{xz}
ESL	111	-1.3040	-1.0347	-0.0599	2.5313	-0.0208	0.0773	0.0875
	333	-1.6709	-1.1050	-0.0611	0.6658	-0.0236	0.2006	0.2142
LW	111	-1.7773	-1.1155	-0.0602	1.0473	-0.0228	0.1689	0.1835
	333	-1.7912	-1.1155	-0.0596	0.7804	-0.0233	0.1812	0.1965
Abaqus 2D		-1.7344	-1.0486	-0.0523	n/a	-0.0130	0.1660	0.1789
Abaqus 3D		-1.7721	-1.1542	-0.0615	0.9403	-0.0045	0.1545	0.1649
Analytical*		1.7240	-1.1417	-0.0632	n/a	-0.0471	0.1694	0.1839

*Pagano (1970, apud PANDIT; SHEIKH; SINGH 2010, p. 316)

For theory ED111, the displacement is underestimated along with the in-plane stresses if compared to the analytical and Abaqus results (ED333 deviates ~5.7% from Abaqus 3D). The LD333,on the other hand, provides more flexible structural model, but it deviates only 1% from Abaqus 3D. Considering the S_x normal stresses, the LW results are very close to the reference values, but the ED111 result is closer to Abaqus 2D (deviation of 1.3%). The S_y results show an inferior agreement (LD333 96.9%). Next, from Table 20, one can see that none of the results of the transversal normal stress achieves the unit value. The best result is from LD333 with 4.7% of error.

Regarding the shear stresses, the transversal ones show a better accuracy than the in-plane shear stress S_{xy}. They is probably due to the proximity of the restrained nodes. The best result of S_{yz} comes from LD111 with 90.7% of accuracy and the best result for S_{xz} is also from LD111 with 88.7% of accuracy.

The comparisons were performed considering the results from Abaqus 3D which better simulates the boundary layer/conditions effect. If the analytical reference are taken, the error for the displacement results and normal stresses are of the same magnitude. The biggest difference is on the shear stresses. Considering the analytical reference, the results show an even greater accuracy. S_{xy} shows an error of 49.5% (LD333), while S_{xz} shows an error of 0.2% (LD111) and S_{yz} present an also small error of 0.3% (LD111). Once more, the proximity to the free-edge of the plate increased the error of the in-plane shear stress S_{xy}.

In sum, for this particular case, the LW solutions should be used. Both LD111/333have good accuracy, but considering the processing time, the LD111 is the best one. However, another qualitative aspect through-the-thickness of the laminate might be important before choosing a theory. To investigate this fact, such profiles for the variables in Table 20 are plotted in Figures 78 to 91.

The main aspect to be looked into in these figures is the effect of the singularities of boundary conditions on the models and the non-linearity of the results.

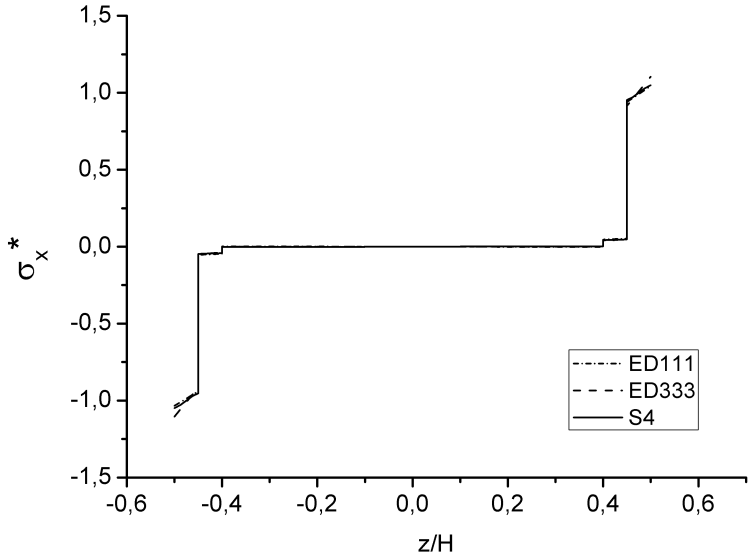

Figure 78. Through-the-thickness Sx stress via CGF (x = y = l/2)

It is seen from the transversal results, that the linear ESL theories cannot represent the behavior of the core properly considering the transversal stress results. Actually, even the LW results do not agree very well with Abaqus results for these variables. However, the results from LW models are better than those from ESL models. Once more, the 2D integration characteristic of CGF hinders the possibility of better transversal results of sandwich structures.

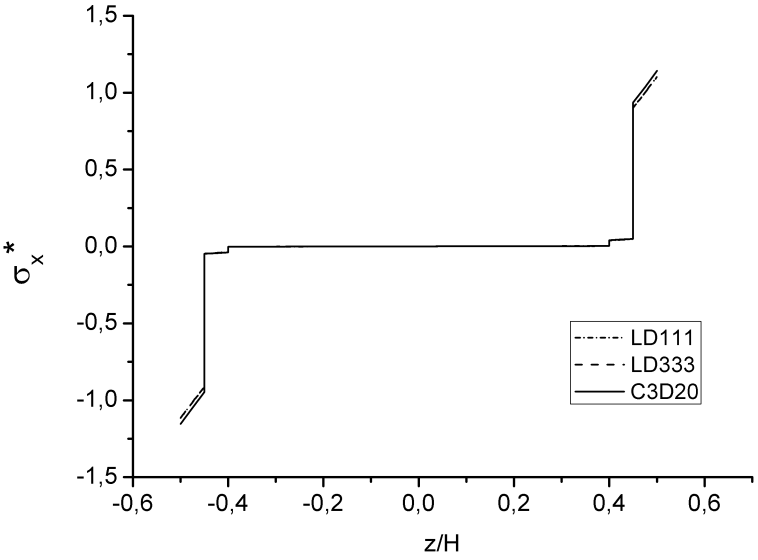

Figure 79. Through-the-thickness Sx stress via CGF (x = y = l/2)

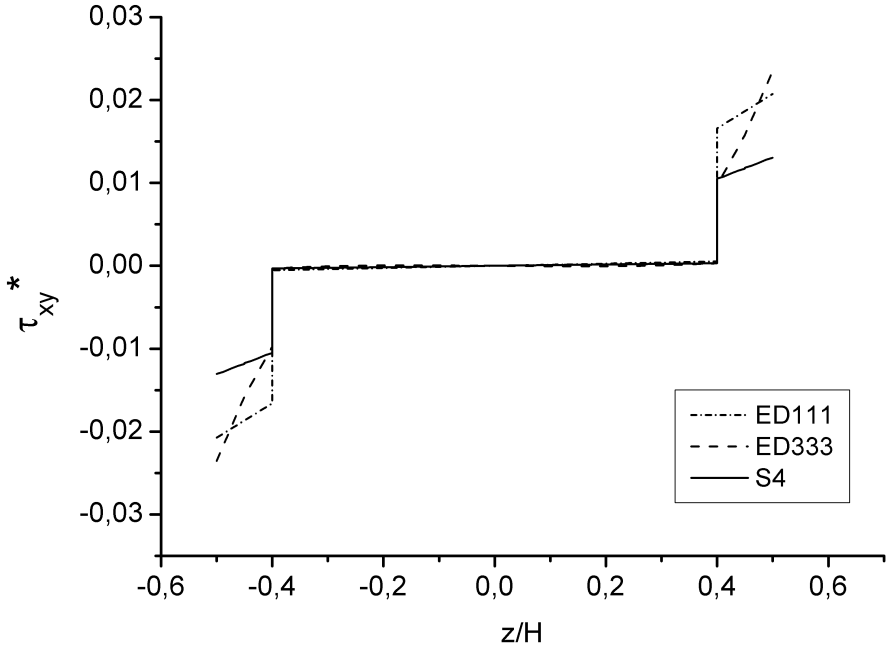

Figure 80. Through-the-thickness Sxy stress via CGF (x = y = 0)

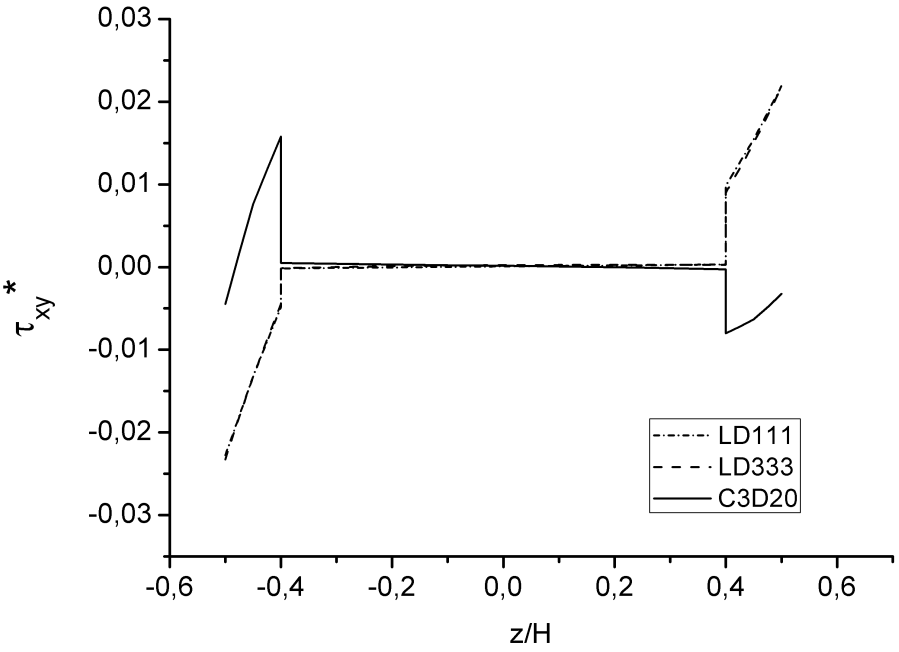

Figure 81. Through-the-thickness Sxy stress via CGF (x = y = 0)

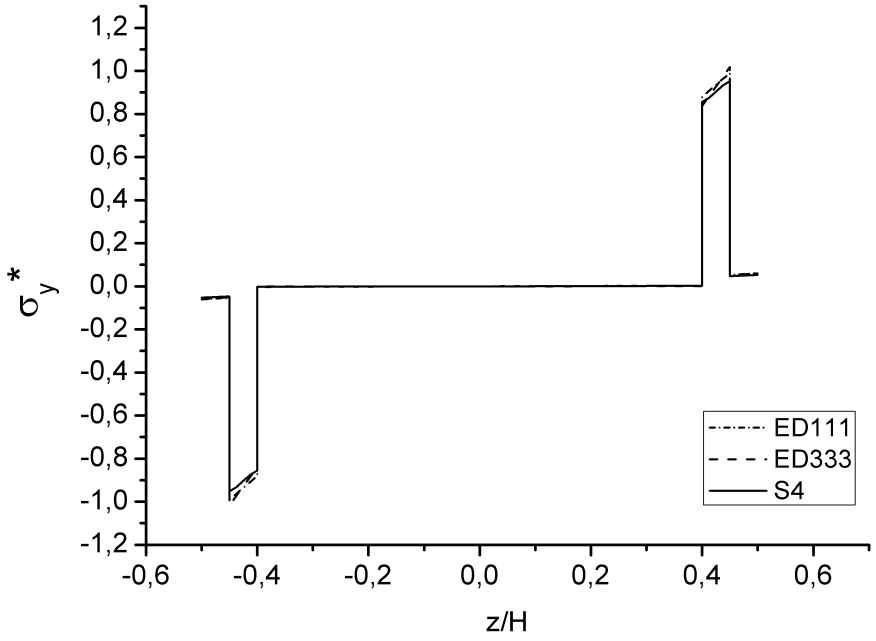

Figure 82. Through-the-thickness Sy stress via CGF (x = y = l/2)

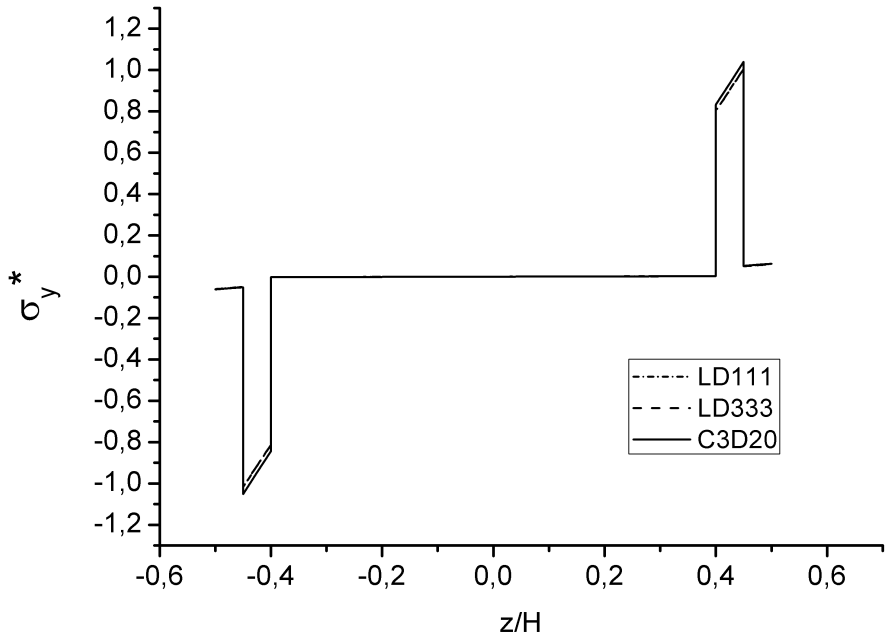

Figure 83. Through-the-thickness Sy stress via CGF (x = y = l/2)

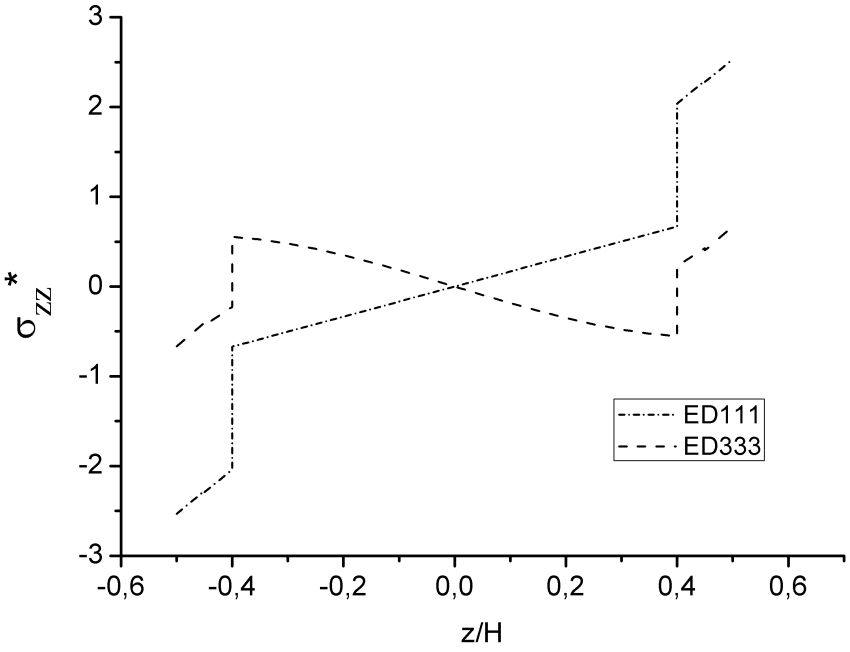

Figure 84. Through-the-thickness Sz stress via CGF (x = y = l/2)

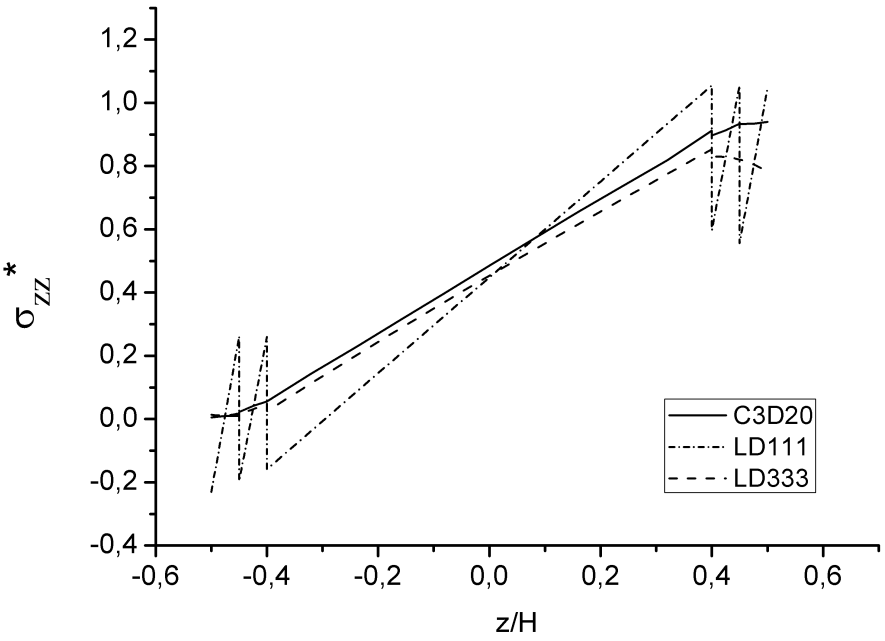

Figure 85. Through-the-thickness Sz stress via CGF (x = y = l/2)

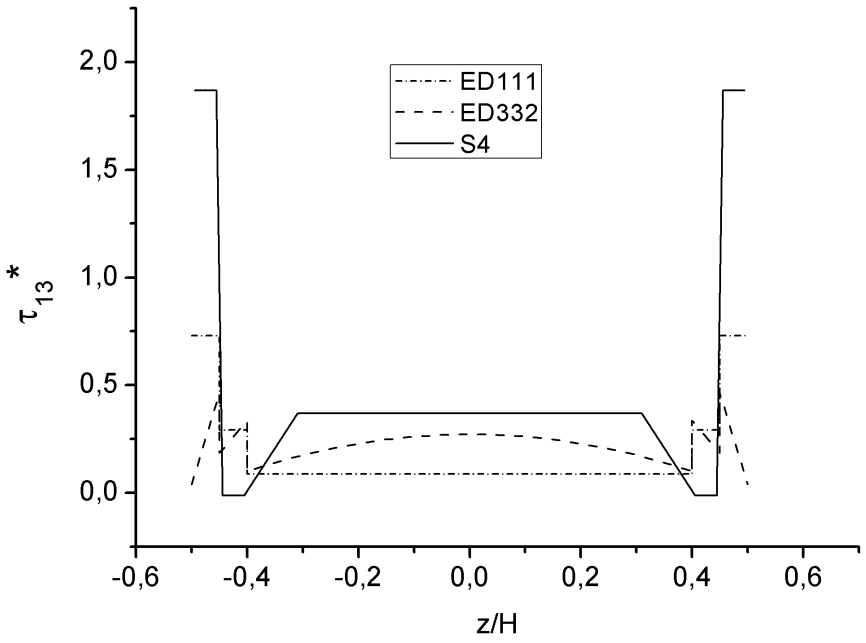

Figure 86. Through-the-thickness Szx stress via CGF (x = 0, y = l/2)

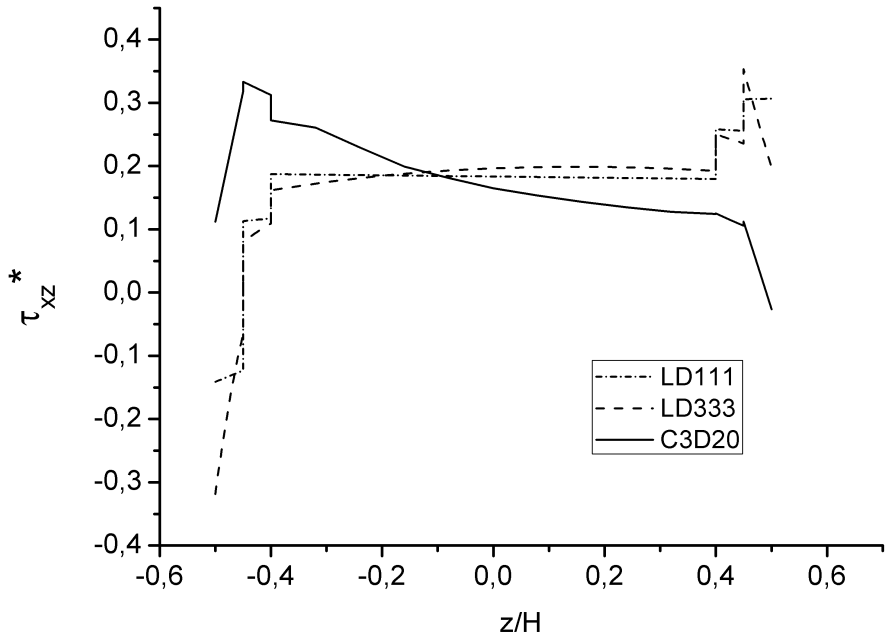

Figure 87. Through-the-thickness Szx stress via CGF (x = 0, y = l/2)

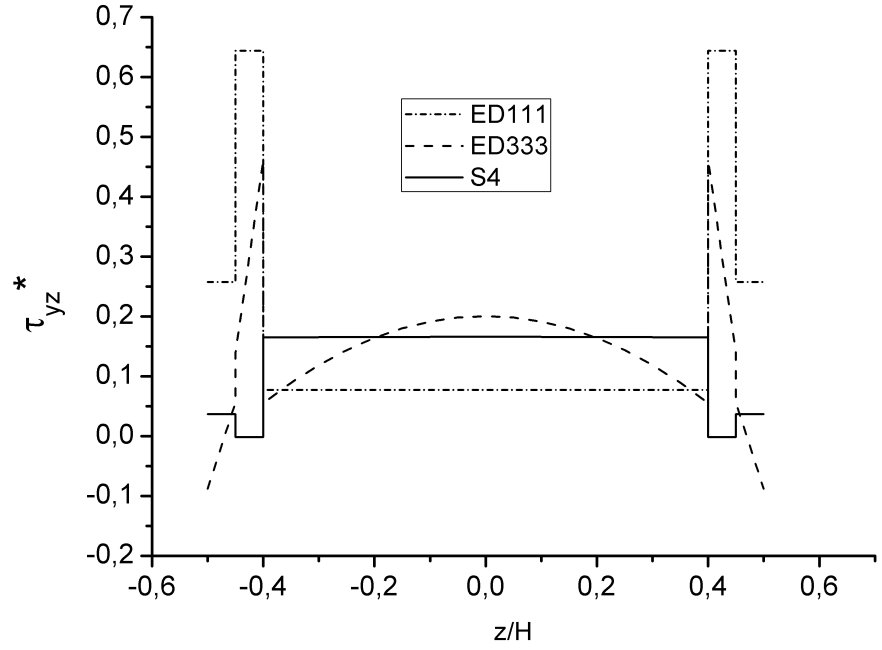

Figure 88. Through-the-thickness Syz stress via CGF (x = l/2, y = 0)

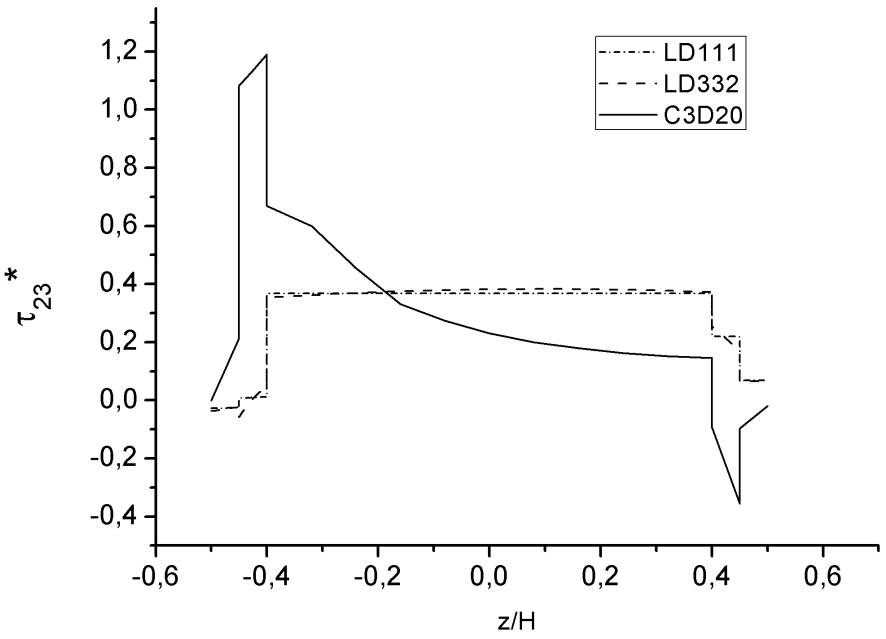

Figure 89. Through-the-thickness Syz stress via CGF (x = l/2, y = 0)

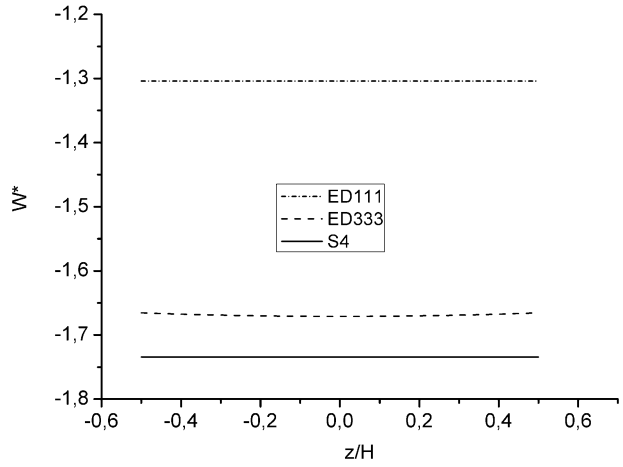

Figure 90. Through-the-thickness dimensionless deflection via CGF (x = y = l/2)

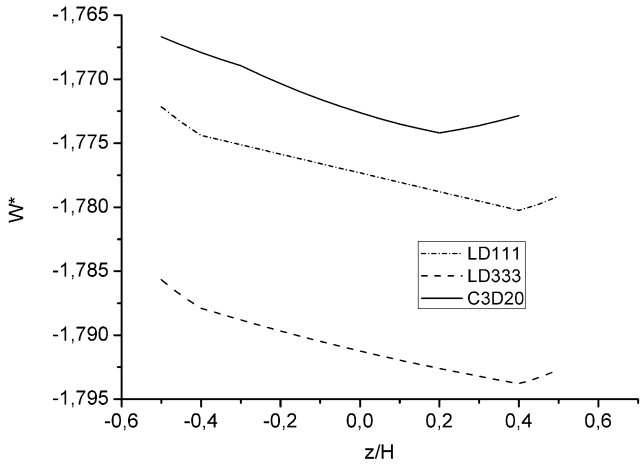

Figure 91. Through-the-thickness dimensionless deflection via CGF (x = y = l/2)

On the other hand, if only the macroscopic behavior of sandwich structures is sought, an ESL theory with high-order terms or a linear LW theory may suffice as seen in Figures 90 and 91. This is maybe the case of dynamic analyses. Many problems demand only the displacement fields.

In Figure 92, the first two bending modes and the respective frequency values are shown for both Abaqus 2D and 3D models along with CGF/LD333. In addition, Table 21 compares the first bending mode obtained by all the theories of this section.

The LW formulations are softer than the ESL, as expected. Comparing the ESL results with the ones from the S4 element and the LW results with the results from the C3D20 model,

the non-linear theories show the best agreement. LD333 shows an error of 0.7% and ED333 shows an error of 2.8%. This is a very good result.

Table 21 - Comparison of first natural frequency of the sandwich plate

Theory		Frequency (Hz)
ESL	111	306.3
	333	272.0
LW	111	261.1
	333	259.5
Abaqus 2D		264.5
Abaqus 3D		257.6

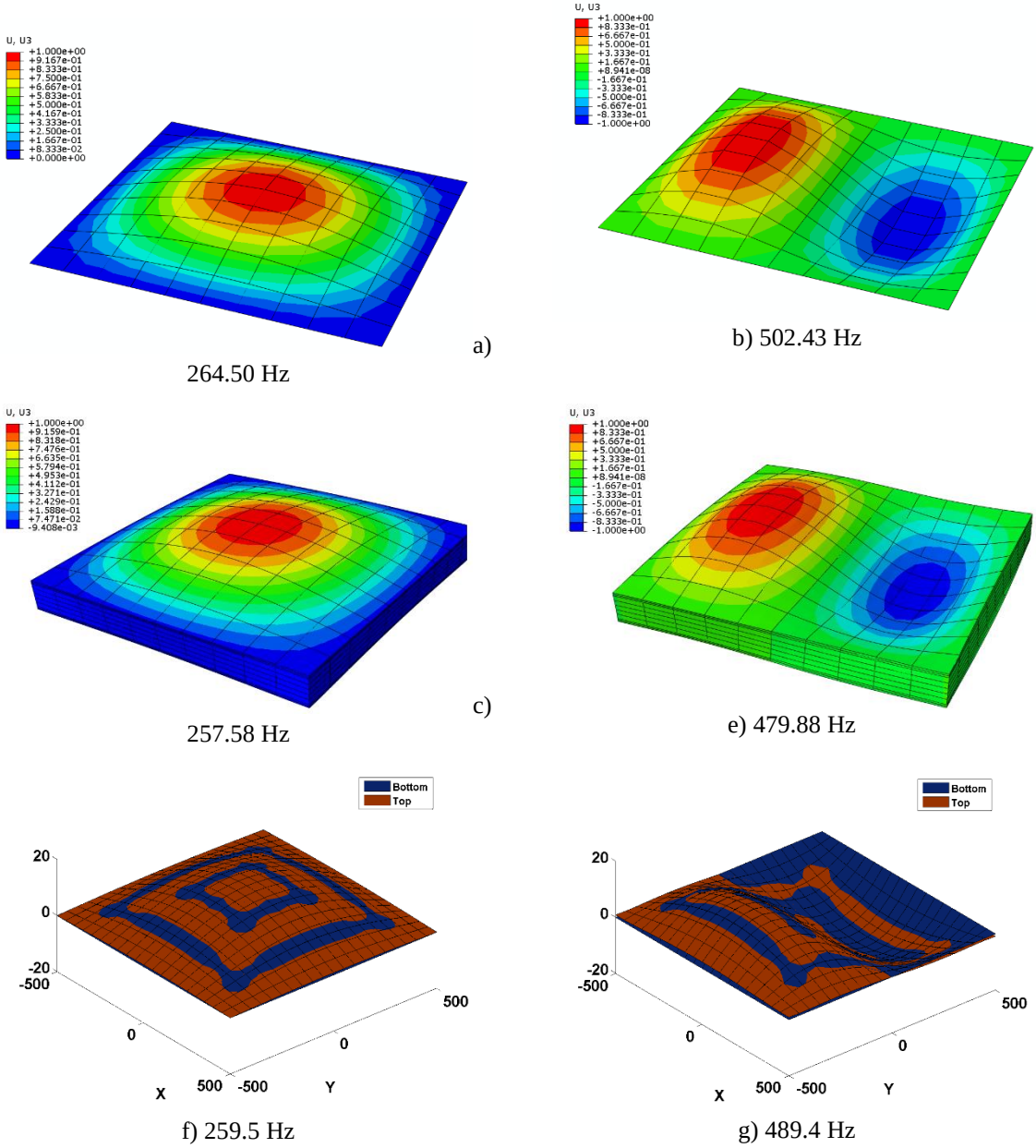

a) 264.50 Hz

b) 502.43 Hz

c) 257.58 Hz

e) 479.88 Hz

f) 259.5 Hz

g) 489.4 Hz

Figure 92. First two bending modes of vibration via Abaqus 2D, 3D and CGF/LD333

In Figures 92f and 92g, both bottom and top plies are shown to exhibit the ability of the formulation to capture not only the regular plate bending modes, but also the sandwich structure modes. This is seen in Figure 93 where the 5th and the 10th modes are shown. It is clear that these are sandwich modes, which cannot be achieved with ESL models. At most, the natural frequency values of the regular plate bending modes can be better calculated, as seen in Table 21 for the ED333 theory.

Through this sandwich structure case, it was possible to demonstrate the ability of the current formulation to simulate thick sandwich structures with orthotropic plies. In the following section, a non-symmetric thick laminate with isotropic plies is chosen to assess the accuracy of CGF with non-square plates with FCSR as high as 1E5.

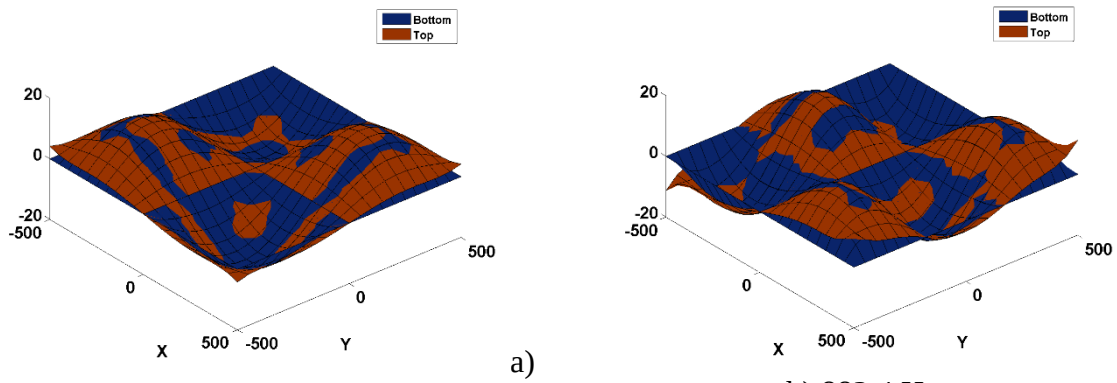

a) 666.4 Hz b) 882.4 Hz

Figure 93. 5th and 10th sandwich modes - LD333

6.6.2 Results and Discussion of Case V

In this case, the analytical solution for a particular point is selected to compare the transversal shear stress "S_{xz}" and the transversal displacement "W". However, in Equation (6.2), the elasticity modulus is that of the core. Also, the selected point is not the one from Table 6 as in Case IV, but rather at: x = 0; y = b/2; z = 3h/10. This height corresponds to the bottom face of the upper skin. This sandwich is made of three different isotropic plies. Both the aspect ratio of b/a = 3 and the length-to-thickness ratio of a/h = 4 makes this plate an anisotropic case, geometrically speaking. Also, two values of the FCSR (E_{bot_skin}/E_{core}) are investigated. The results are in Table 22. Note again that it is the engineering shear stress ($\tau_{xz} = 2S_{xz}$) in this table.

Moreover, Demasi's (2009a) solution for this sandwich plate problem will be directly compared to CGF for the same ED225 and LD225 theories. All meshes have 10x10 elements in plane and the 3D model has 5 elements in the core, one in the lower skin and two at the upper skin (see Figure 77).

Table 22 - Comparison of dimensionless transversal shear stress and displacement

Variable	$\bar{W}$				$2\bar{S}_{xz}$ (core/upper skin values)***			
FCSR	1E1		1E5		1E1		1E5	
Theory	ED225	LD225	ED225	LD225	ED225	LD225	ED225	LD225
GUF**	-2.0330	-3.0098	-4.098E-4	-0.0132	0.3250	0.3214	0.3317	5.400E-4
CGF	-2.1154	-3.8819	-2.664E-4	-0.1337	0.0801	0.317/0.256	1.147E-5	-0.039/0.056
Abaqus 2D	-3.1032		-1.4457		0.3961		0.3584	
Abaqus 3D	-3.8885		-0.1352		0.0512/-0.0055		-0.0763/-0.0035	
Analytical*	-3.0112		-0.0132		0.3217		5.408E-4	

*Pagano (1970, apud PANDIT; SHEIKH; SINGH 2010, p. 316); **Demasi (2009a); *** when available

Considering the displacement results, CGF gives a much closer results to Abaqus 3D than GUF. For FCSR = 10, CGF LD225 model has 99.8% of agreement whereas GUF has only 77.4% of accuracy. For FCSR = 1E5, the same model yields 98.9% of accuracy and GUF gives only 9.8% of agreement. If the Analytical result is considered, CUF shows a better results. However, it is believed that the C3D20 element in Abaqus gives a better resolution of the displacement fields when compared to analytical solution of such anisotropic problem.

The accuracy of stresses is a more delicate matter. First, there are two values to be considered at the location of study. They correspond to either the core or the upper skin. The model built within Abaqus shows both values for the 3D model. However, both values for both FSCR values show errors higher than 100%. Nevertheless, for FCSR = 10 and at the core side, the 2D results from the S4 element match quite well the results from GUF (81% of accuracy), CGF(80%) and the analytical reference (81%).

Thus, from Table 22, it is possible to see that CGF provides softer structural models than GUF. It may be due to the weakness of the finite element method and/or the C-1 implementation.

The overall qualitative analyses of the through-the-thickness profiles are provided in Figures 94 to 107.

These figures show that even though this sandwich structure is composed of isotropic plies, the geometrical difference in thickness and material properties can provide a set of results with profound differences for both core and skins layers. Compared to the 3D results from Abaqus, the LW and high order theories can better simulate the 3D microscopic behavior of the

bulk material. These profiles are of great importance when the transversal response of the sandwich is needed to either design intelligent structures or to perform FSI simulations.

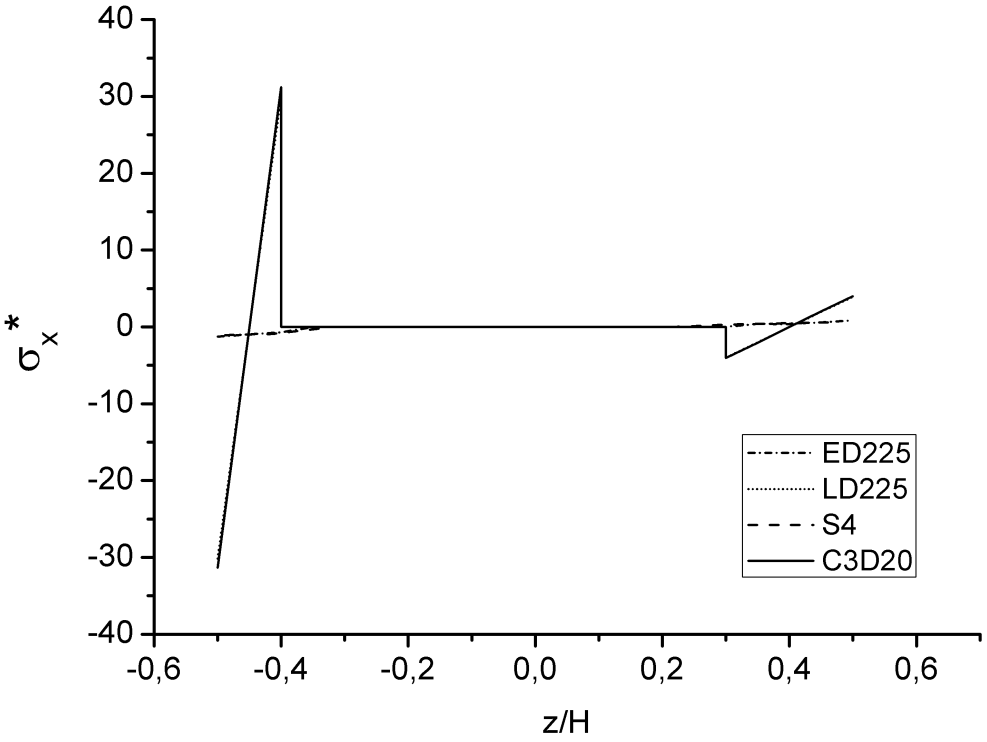

Figure 94. Through-the-thickness Sx stress via CGF (x = y = l/2): FCSR=1E5

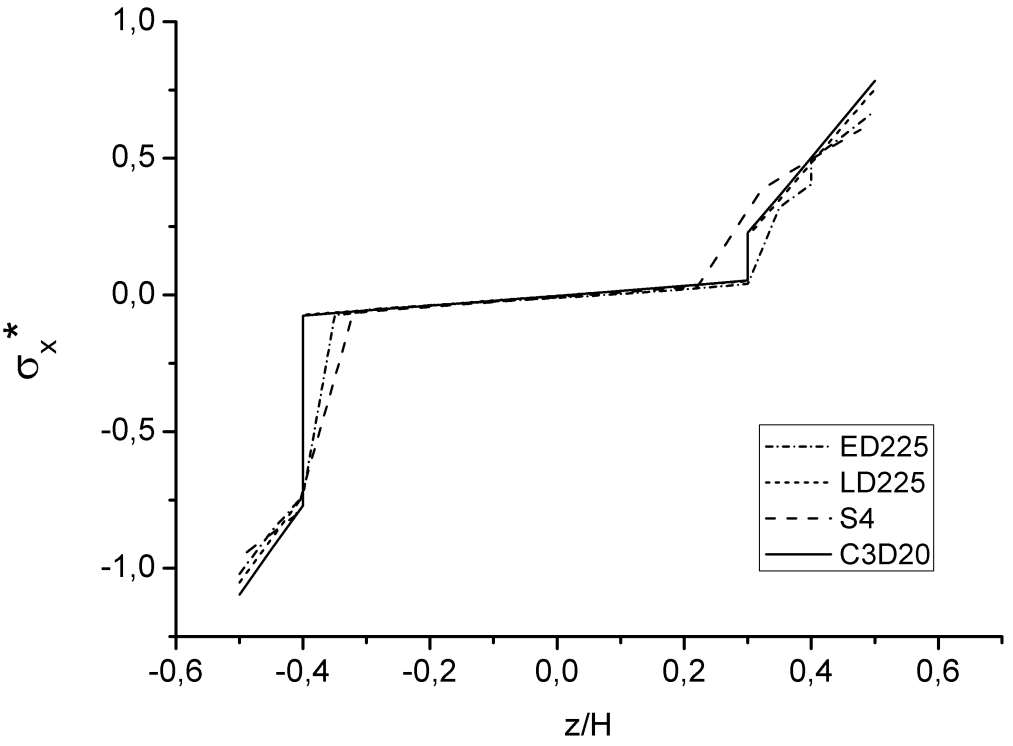

Figure 95. Through-the-thickness Sx stress via CGF (x = y = l/2) : FCSR=1E1

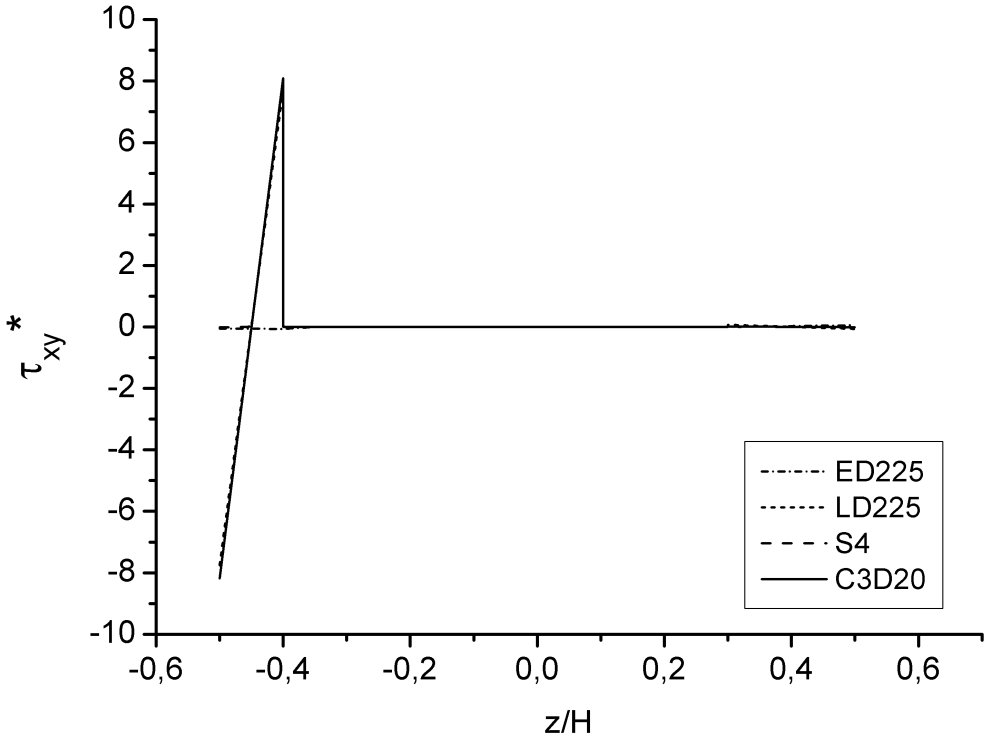

Figure 96. Through-the-thickness Sxy stress via CGF (x = y = 0) : FCSR=1E5

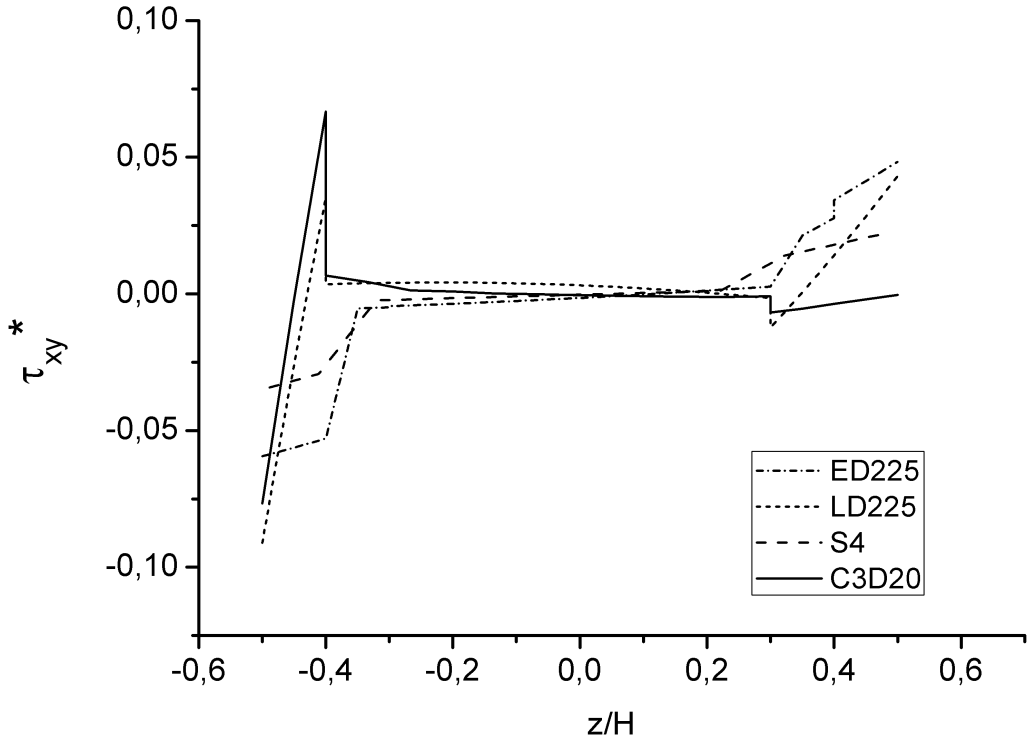

Figure 97. Through-the-thickness Sxy stress via CGF (x = y = 0) : FCSR=1E1

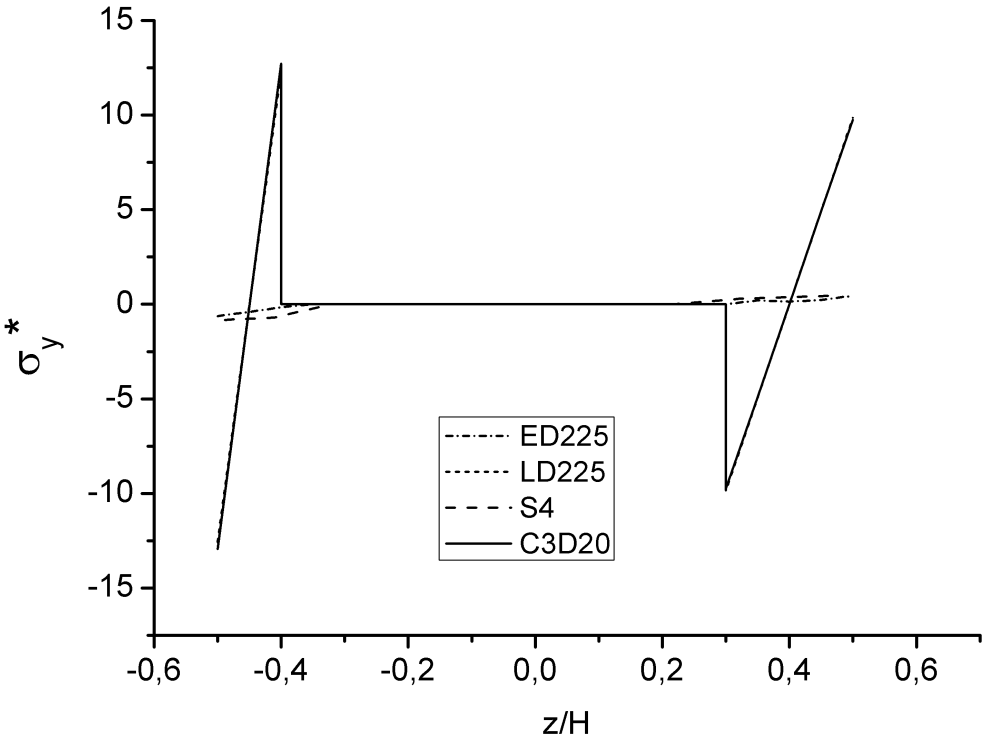

Figure 98. Through-the-thickness Sy stress via CGF (x = y = l/2) : FCSR=1E5

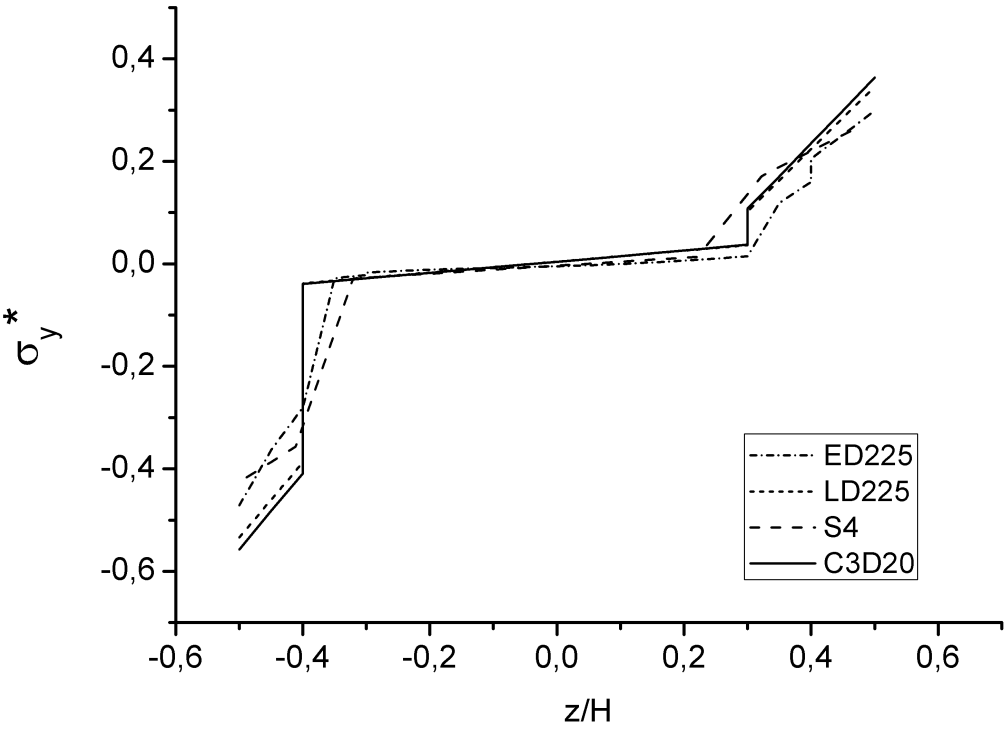

Figure 99. Through-the-thickness Sy stress via CGF (x = y = l/2) : FCSR=1E1

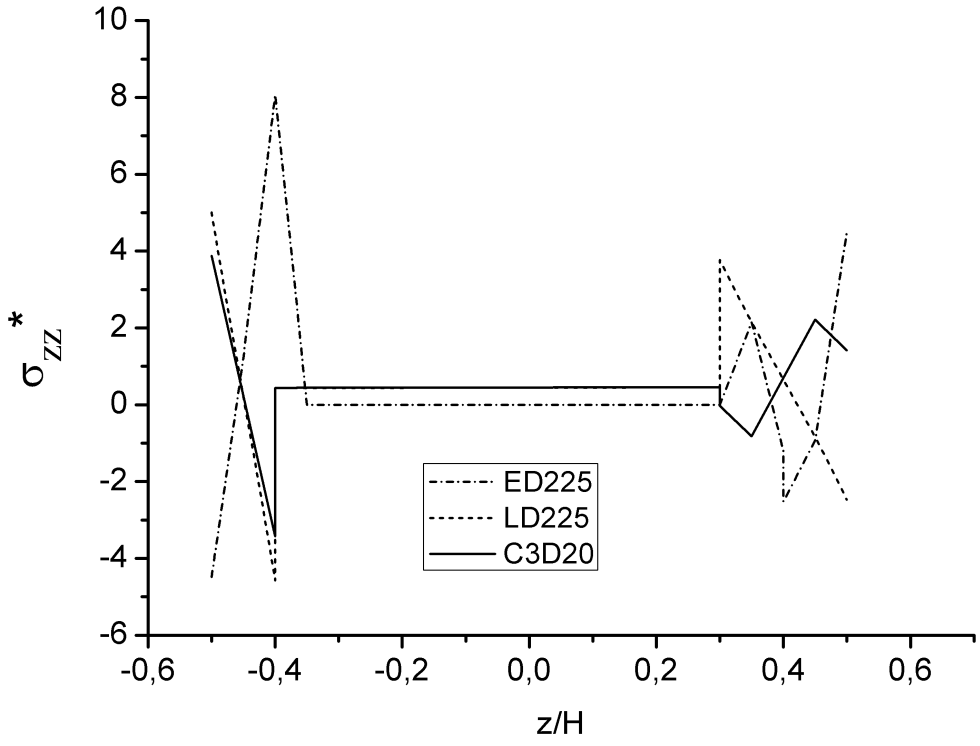

Figure 100. Through-the-thickness Sz stress via CGF (x = y = l/2) : FCSR=1E5

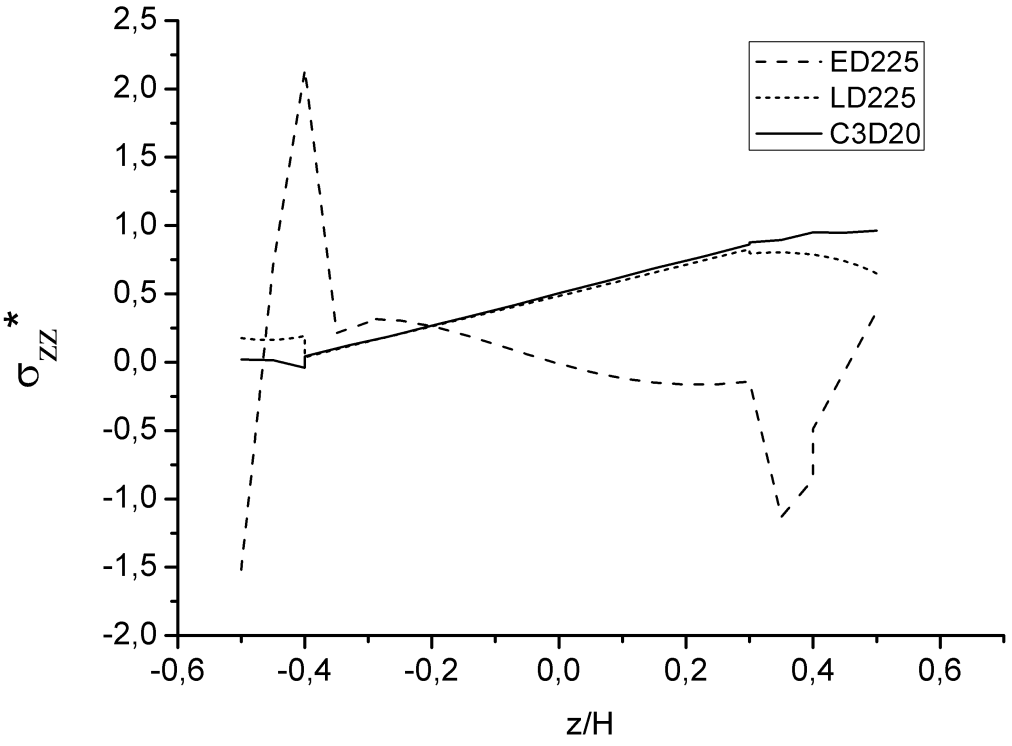

Figure 101. Through-the-thickness Sz stress via CGF (x = y = l/2) : FCSR=1E1

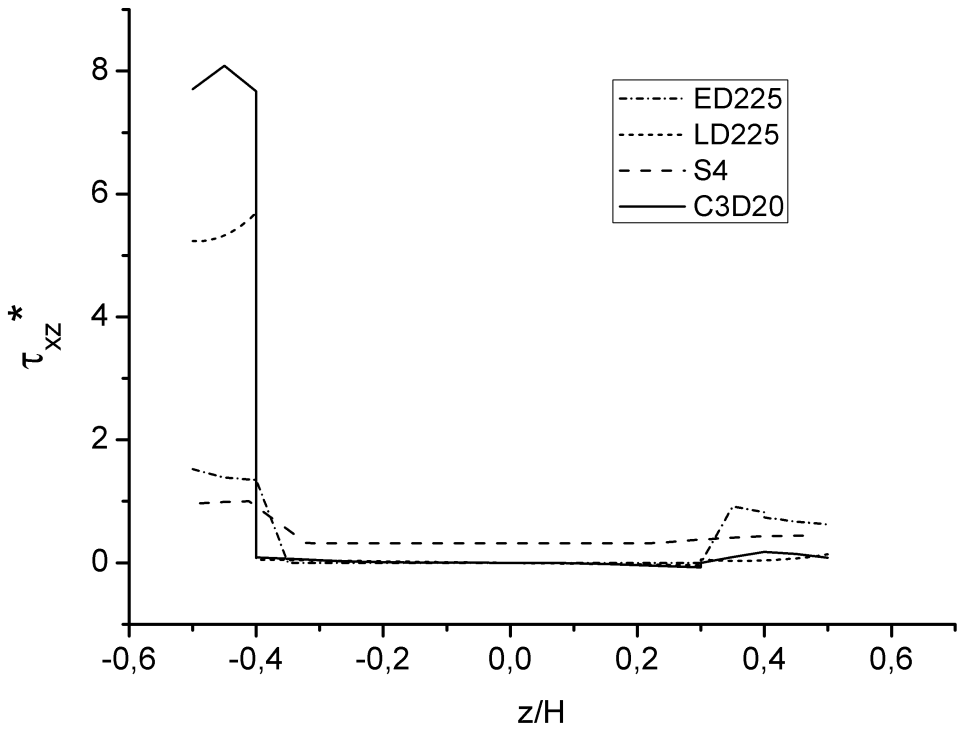

Figure 102. Through-the-thickness Szx stress via CGF (x = 0, y = l/2) : FCSR=1E5

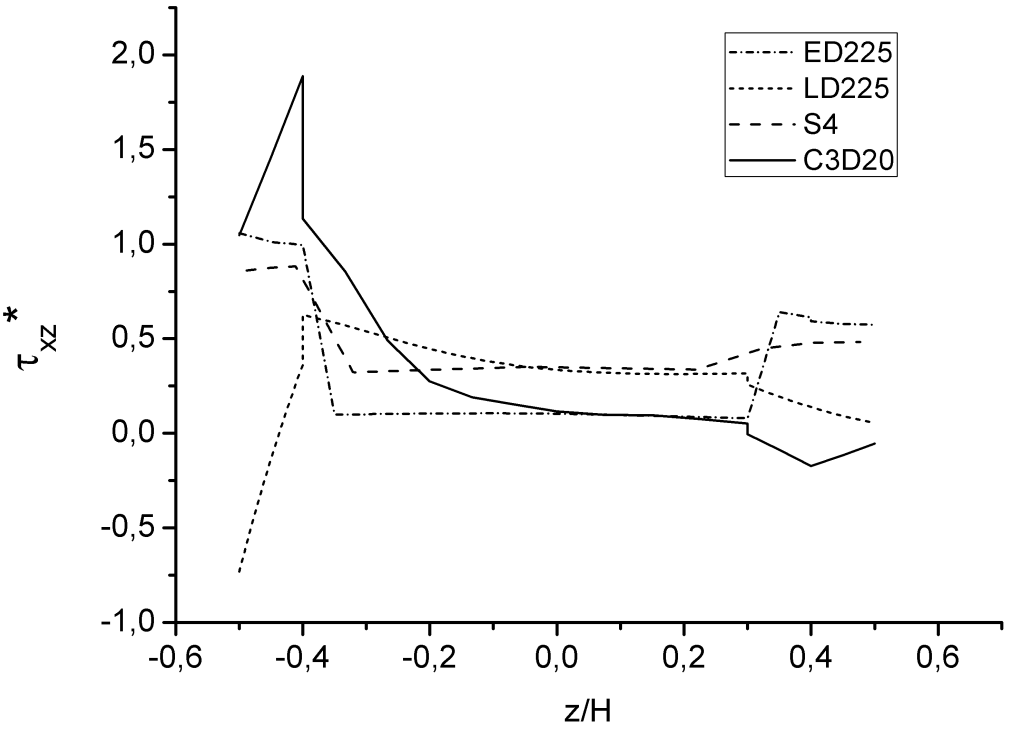

Figure 103. Through-the-thickness Szx stress via CGF (x = 0, y = l/2) : FCSR=1E1

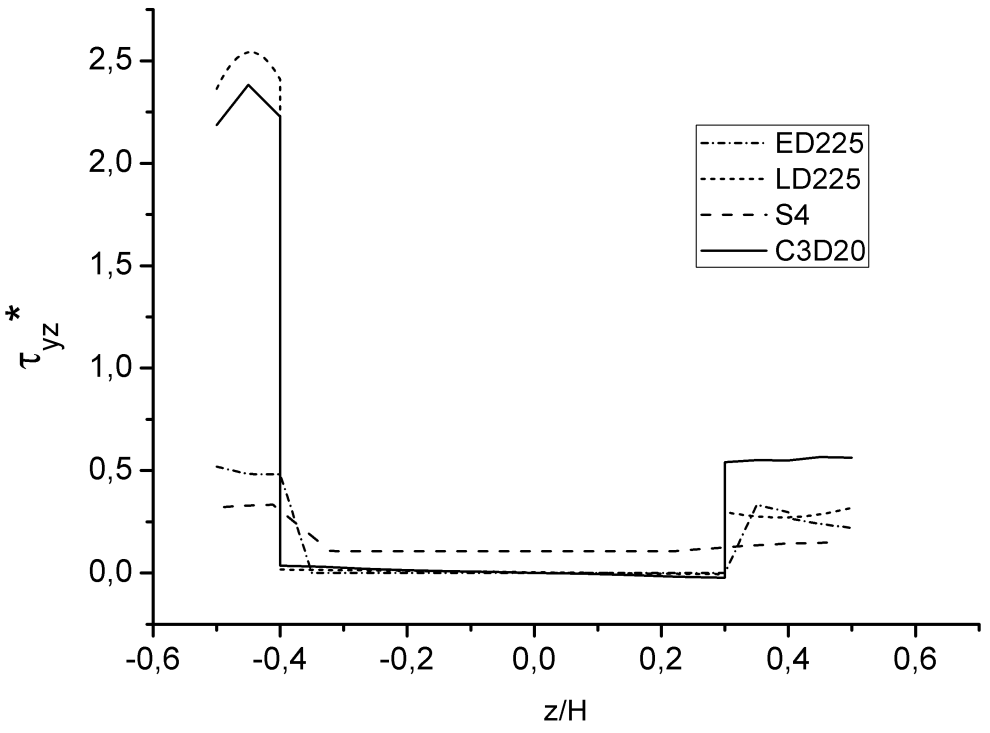

Figure 104. Through-the-thickness Syz stress via CGF (x = l/2, y = 0) : FCSR=1E5

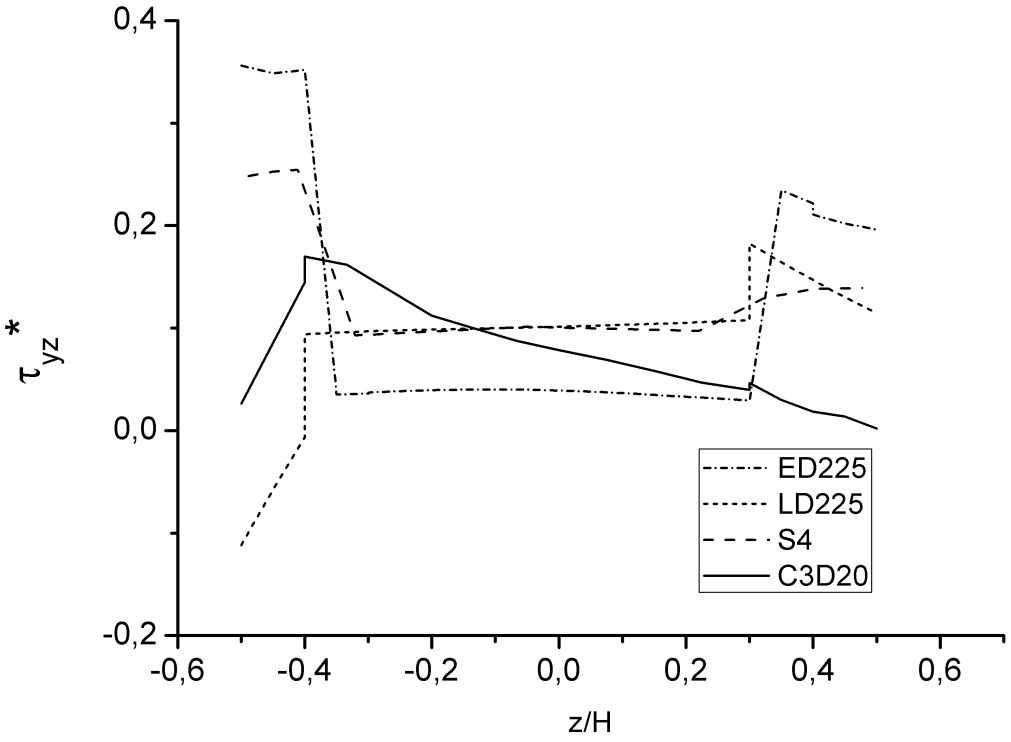

Figure 105. Through-the-thickness Syz stress via CGF (x = l/2, y = 0) : FCSR=1E1

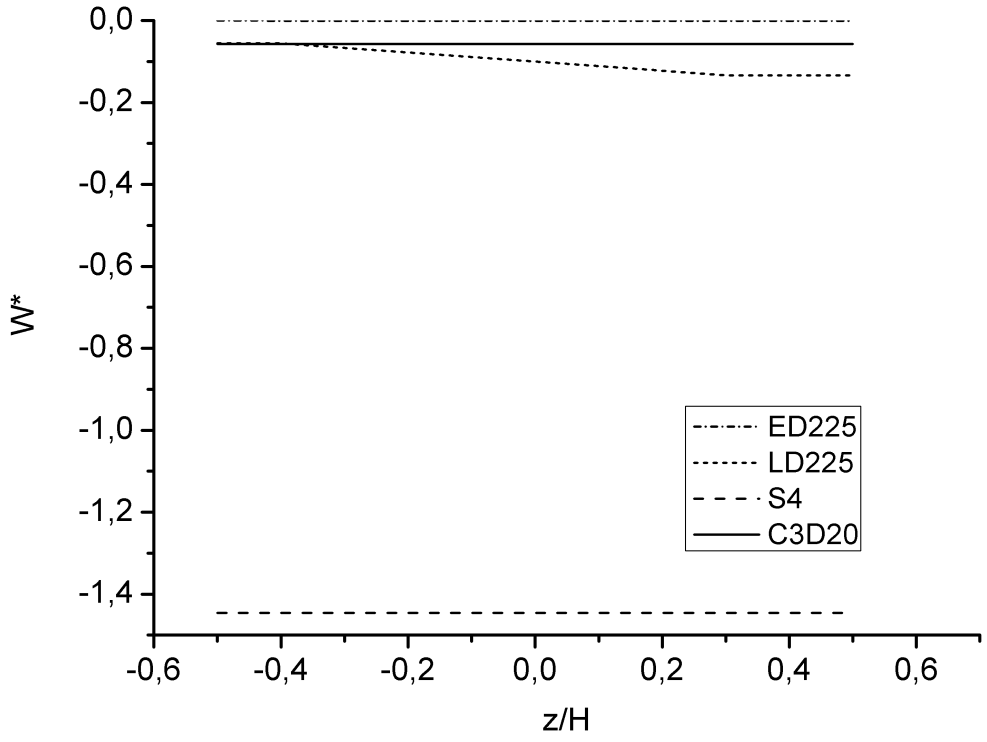

Figure 106. Through-the-thickness dimensionless deflection via CGF (x = y = l/2) : FCSR=1E5

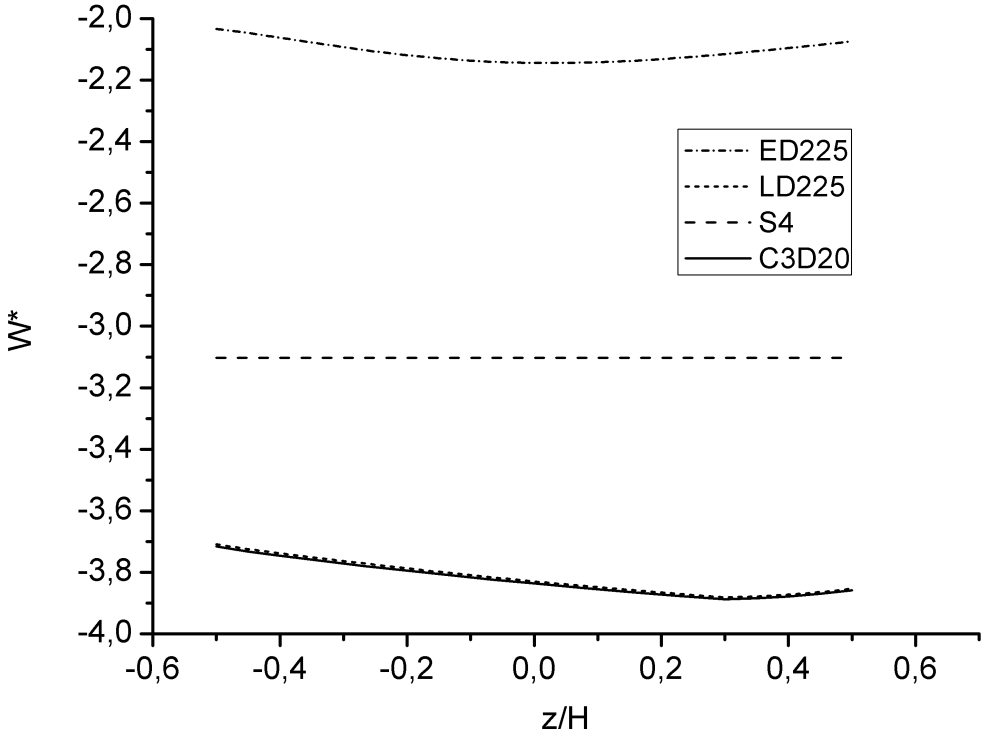

Figure 107. Through-the-thickness dimensionless deflection via CGF (x = y = l/2) : FCSR=1E1

The dynamic evaluation for this section a rather interesting once one of the FSCRs is very high. For this configuration, the sandwich structure modes of vibration are expect to dominate in the low natural frequencies. To confirm this, the first two bending mode for both FCSRs are calculated via Abaqus solutions. The mode shapes and natural frequency levels are seen in Figure 108.

Considering the low value of FCSR, both 2D and 3D approaches via Abaqus give similar modes and the respective natural frequencies are close too. The first 2D frequency for FCSR = 10, deviates 19% from the 3D values. However these modes are not the actual first and second mode. Here, only the “bending modes”, meaning the modes which excite mainly the thickness coordinate, are shown.

Next, inspecting the modes with the highest FCSR, for both 3D and 2D models, one sees that not only the frequency levels are different, but the mode shapes themselves.

The ESL model of Abaqus with the S4 elements gives the first bending modes with shapes similar to the results with the FCSR = 10. Nevertheless, sandwich modes should be observed instead, as in the 3D case.

Sandwich modes can be identified by the relative motion among of the main components of the plate. In other words, the plies move in respect to the core and one another. Figures 108g and 108h show two of these sandwich modes. Such modes cannot be seen with the ESL formulations. Thus, in Figure 109, the first four modes obtained via LD332 are shown.

It is clear from Figure 109 that ESL formulations cannot be used for dynamic analysis of soft-core sandwich structures. In this Figure 109, the natural frequencies of each mode is given along with the frequency of the corresponding modes obtained via Abaqus 3D. This figure shows that the LD225 theory can reproduce the macroscopic response of the 3D models with considerable accuracy. The forth mode, which can be seen in Figure 108g has a small deviation of 0.7%.

The bending mode from Figure 108h is compared with that from LD225 model is given in Figure 110. The error for this mode is no more than 0.5%. These values for the dynamic results are more precise than those from Case IV due to the high FCSR. Such high ratio (FCSR = 1E5) yields a macroscopic behavior, which is easier to capture than the one from a more homogenous plate (low FCSRs).

Therefore, it was seen that sandwich structures are sophisticated structures, which usually demand a 3D approach to be properly solved. The sandwich structure in this section endorses this assertion. It was seen that the equivalent single layer results and the layer-wise results can provide good representativeness of the transversal displacement and shear stresses.

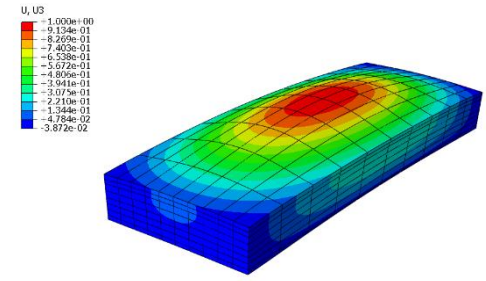

a) 1338.1 Hz (FCSR=1E1)

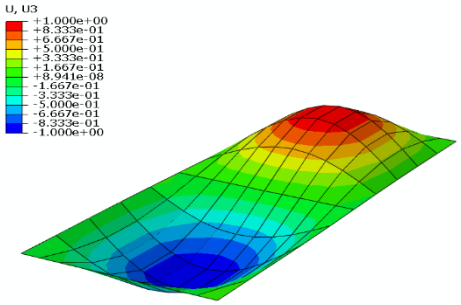

b) 1592.6 Hz (FCSR=1E1)

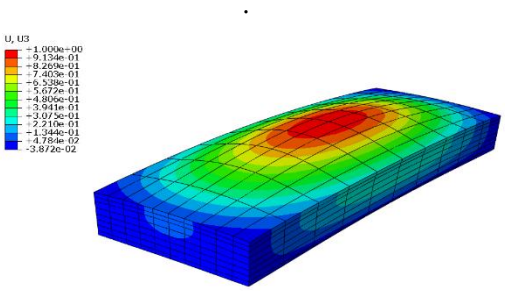

c) 1157.6 Hz (FCSR=1E1)

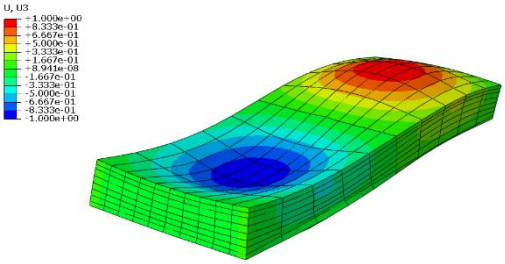

d) 1385.4 Hz (FCSR=1E1)

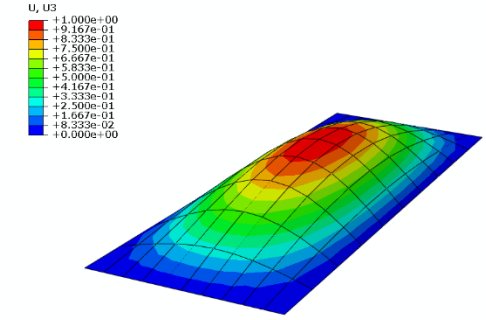

e) 19.989 Hz (FCSR=1E5)

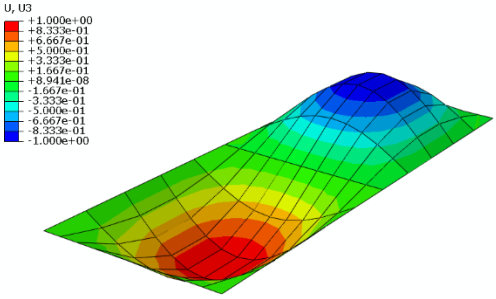

f) 22.777 Hz (FCSR=1E5)

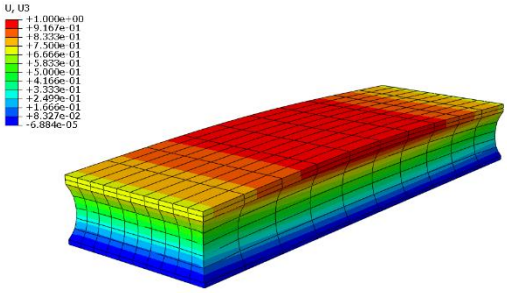

g) 58.005 Hz (FCSR=1E5)

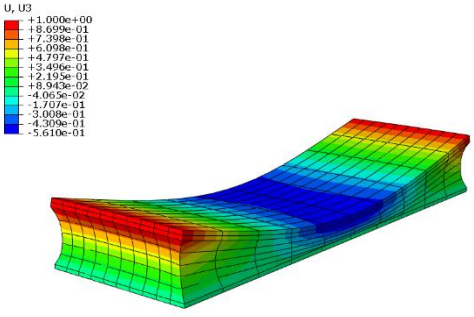

h) 83.090 Hz (FCSR=1E5)

Figure 108. First and second "bending modes" obtained by Abaqus

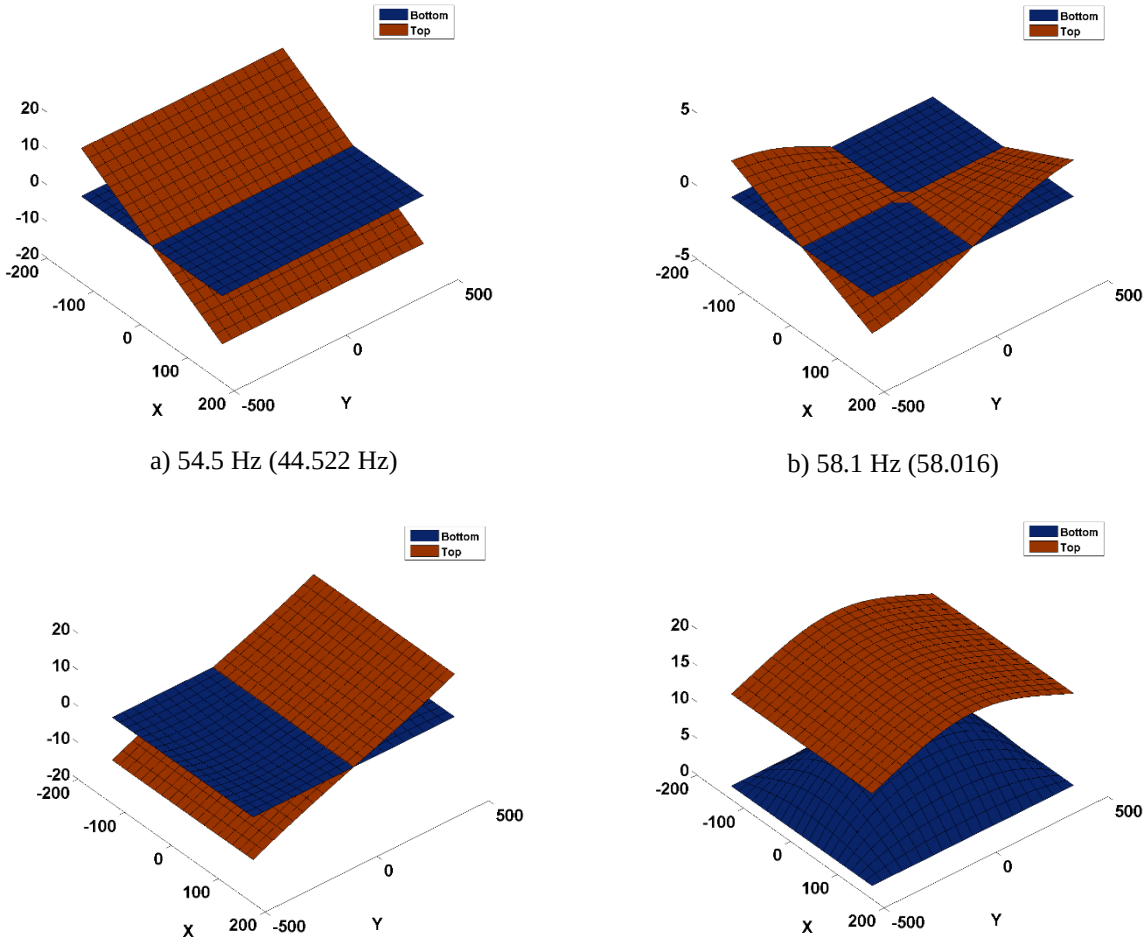

a) 54.5 Hz (44.522 Hz)

b) 58.1 Hz (58.016)

c) 58.2 Hz (47.655 Hz)

d) 58.4 Hz (58.005Hz)

Figure 109. First 4 modes of vibration of Case V via LD225. The Abaqus 3D counter values are shown in parenthesis

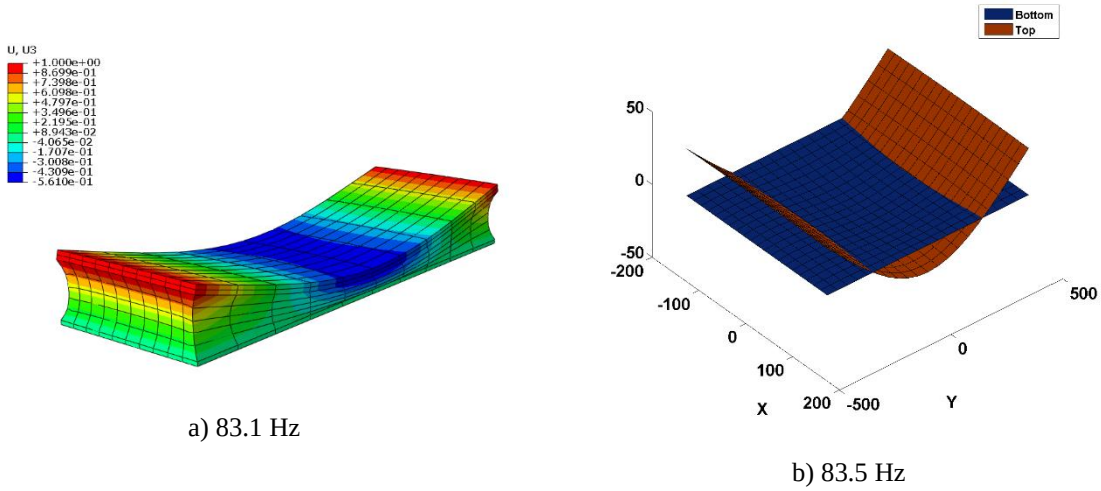

a) 83.1 Hz

b) 83.5 Hz

Figure 110. Comparison of the 7th sandwich mode obtained by Abaqus 3D and LD225 via CGF

The magnitude of the deviations seen in the stress values is not as low as desired but this outcome was expected though. The laminated problem is an orthotropic/anisotropic 3D case and for a plate formulation to simulate such complex through-the-thickness behavior is an

outstanding task. However, CGF performs considerably well recalling that a four node, with linear interpolation of the in-plane displacements is being used. It was seen from the theory evaluation section that the in-plane displacement fields need to be accurately represented in order to increase the precision of the solution. Thus, the author believes that an eight node plate element would perform considerably better and increase the convergence rate. However, first, a more elaborated post-processing is recommended. The additional effort, which should extrapolate the stresses at the integration points, should increase the accuracy of the solution without having to implement an element with twice the number of DOFs to solve for.

It is unfortunate that the present PhD thesis does not comprise its own experimental results for comparisons. The goal is always to better simulate reality and not to reproduce the results from other approximate solution methods. Probably, the error in the current formulation, when compared to analytical ones, is just a theoretical error, meaning that, actually, the reference formulation can be worse formulated than CGF.

Also, regarding the dynamics of the structure, the dissipation of energy via damping was not investigated. For sandwich plates this is very important, because the assemblage of different materials and dimensions may give birth to different magnitudes of damping. And, this is one more topic for the future works.

Chapter 7 - Conclusion

7.1 Conclusion

This PhD thesis worked on plate theories to study and/or develop different ways to solve laminated composite plate problems. More specifically, this work was motivated by sandwich structures and their current applications in the aeronautical industry, wind turbine blades for wind farms and smart structures.

It was seen that the laminated plate problem is very intricate and the dimensions of the problem give guidelines to properly choose the best approach to simulate these laminated structures. Also, the anisotropic (or orthotropic) characteristics of the material properties along with the (non-) symmetrical stacking sequence of the laminated composite may greatly impact the results. This is intensified in the case of sandwich structures where the mid layer, which is the core, is usually much weaker and softer than the skins and, therefore, steep gradients can be found for the field variables through the thickness of the plate.

CGF is a method, which was proposed in an attempt to provide a solution method via FE, to predict the behavior of complex plate structures. Not only so, but also to provide a systematic way to evaluate the through-the-thickness profile of displacement and stresses according to the plate theory, which was used. Such result is very important in multi-physics problems such as FSI and smart structures.

CGF was based on a Generalized Unified Formulation, whose analytical closed form solutions can be found in the literature. Numerical solutions of Unified Formulations (CUF) via FE are also given in the references. However, these FE numerical solutions are based on the C-0 continuity type. This means that plate formulations such as Reddy's (1990) could not be generalized with CUF, nor GUF. Due to the C-1 aspects of CGF, the derivatives of the deflections are coupled with the in-plane expansion terms and thereby the solution is much richer.

Regarding the use of a 4-node quadrilateral element

It was seen, mainly during the recovery of stresses at the integration points/centroid coordinates, that the results from the use of linear interpolations for the in-plane displacements can be improved with the use of an eight node Serendipity element or a nine node Lagrangian one. This is motivated by the deviations of the stress values calculated at corner/edge elements. Probably, a parabolic field within the element maybe diminish the need for too high order theories such as LD444 and above. Nonetheless, as suggested in Chapter 6, a more elaborated post-processing of the results, including the calculation of stresses at the integration points, can already suffice to improve the current results of CGF.

Regarding Equivalent Single Layer Assemblage

ESL assemblages are, without a doubt, useful for thin isotropic plates. The symmetrical through the thickness deflections seen in Chapter 6, endorses this statement. Also, for symmetric laminates plates and sandwich structures, it can be of useful too. In the first case, symmetric stacking is required for symmetrical responses. For sandwich structures, if the core is not too soft transversally (FCSR < 100) and thick ($H/h_{core} > 2$), the mechanical responses can be obtained with a considerably accuracy at the center of the plate, but this is not recommended. This is true for static analyses, but, for dynamic modeling of highly anisotropic and/or non-symmetrical structures, the use of ESL assemblages gives high errors not only in the mode shapes, but in natural frequencies, as well.

Regarding Layer-Wise Assemblage

For accurate 3D like resolution of the structural responses of complex laminates structures, the LW assemblage is needed. It surely increases the computational costs, but they pay off in the end. However, even in this case, the LW solution is not a 3D solution, but only an approximation. To get a 3D result, the through the thickness integration must be coupled with the in-plane integration, which is done in 3D continuum finite elements.

This approach is accurate in the time domain as well. The eigenvalue problems solved in Chapter 6 proved this. The LW solutions were able to represent both shape and frequency models of the evaluated sandwich structures and their 3D sandwich modes. Even for a high

FCSR, the results of CGF matched those of the 3D simulations performed by Abaqus with small deviations as low as 0.5%.

Regarding the in-plane displacement Expansions

Both in-plane axiomatic displacement fields showed that the accuracy of the in-plane solution depends on the order of the expansion of the thickness variable. Third order (cubic) solutions are accounted as physically consistent, because the cubic term allows for either an odd or an even non-linear response through the thickness of the plate for the displacement and/or stress variables. If more terms are used, the accuracy increases. The trigonometric terms, such as sine and co-sine, proposed in the literature, along with the mathematics characteristics of the polynomials expansions can confirm this. Nonetheless, the trigonometric functions do not have the flexibility of the polynomial solutions in shaping different responses through-the-thickness of the laminate.

Regarding the transversal displacement expansions

It was seen that for ESL solutions, the use of non-linear terms for the deflection field does render a non-linear solution, yet symmetrical. However, for thick plates, the LW approach is preferred, even in its linear form. Depending on the structure, higher order terms may be needed, especially for sandwich structures where inflection points are often seen in the through-the-thickness profiles.

Regarding transversal stresses

When thin plates were evaluated by CGF, for both LW and ESL models, the through-the-thickness profile of the transversal normal stress S_z showed physical inconsistency. This is due to the fact that the absolute errors from the FE implementation is of the same magnitude of the respective transversal normal deformation. Thus, when the constitutive equations are applied to the strain fields, the S_z results deviates considerably from the actual values and therefore, for thin plates, such variable should be disregarded.

For the ESL approach, due to the symmetric characteristic of its displacement fields, it is not possible in CGF, through the ESL method, to obtain the transversal normal stress profile

varying from “0” (bottom face) to “1” (top face). However, for LW approaches of moderately thin/thick and thick plates, such profile can be simulated.

As for the transversal shear stresses, CGF cannot fulfill the free shear stress at the top and bottom of the plate and sandwich structures. Nevertheless, for a particular theory applied to a specific problem, CGF can approach this condition, especially with LW assemblages.

CGF weak solution method automatically defines every term of the expansion and calculates the transversal stiffness separately from the in-plane one. By these means, there is an error from not coupling the thickness direction terms with the in-plane ones, like the 3D solutions do. This is more pronounced with coarser meshes. However, these errors greatly affect the transversal normal stress for thin laminates as mentioned.

Regarding CGF and the C-1 implementation

CGF is a powerful tool to study and simulate laminated composites, such as sandwich structures. The accuracy of the results, however, are curbed by the limitations of a 2D theory. In fact, by considering all stress (strain) components to be non-zero, this formulation is a quasi-3D solution method. An advantage is the fact that it can used to understand the use of plate and laminated plate elements in FE codes.

For the sake of brevity, this text does not evaluate the other variables derived from the FE C-1 kernel: the rotations and moments. Such evaluation is left for future publications, also, because this requires specific test cases and comparison with the respective references.

The C-1 implementation, when compared to the analytical solution of GUF in Case V along with the convergence results showed that this solution provides more “flexible” structural models and, thus, this is able to better represent both gradients of macroscopic and microscopic variables. For a better conclusion of the C-1 implementation, a C-0 one should be implemented within the same in-house FE code. However, based on some FE results of a C-0 implementation of 9 node element (CARRERA, 2003b), even the LW theories developed via PVD usually provides stiffer structural models than both analytical solutions via the 3D Theory of Elasticity and closed form solutions with double sine/co-sine series. Hence, it is believed that the current formulation, at least matches the overall flexibility provided by the analytical solutions. But it has the versatility of being a FE solution.

The sandwich structures models via CGF showed very good qualitative results and for particular cases, the quantitative results are better than the analytical ones, assuming that the 3D solution from Abaqus is the most accurate among the references.

Even so, the author is aware that experimental tests are needed to accurately access the performance of this solution method.

7.2 Recommendations

After studying the results of different plate problems for laminated and/or sandwich structures, this author leaves some recommendations for working with plate theories.

- First, decide on the solution method. Sometimes, analytical/closed form solution are available and numeric errors can be skipped and a lot of computational time can be saved.
- Analyze the resources. It is important to know how much computing power is available. In these days, only large scale problems demand the use of massive clusters of computing power. This means, a full aircraft structural analyses, transient responses of 3D CFD and/or FSI simulations of airplanes, racing boats or wind blade turbine farms. Thus, if possible, for complex 3D mechanical behavior, 3D solutions should be used, followed by LW and then ESL models.
- Identify the problem. Check on the anisotropy and symmetry of the structure as well as the expected/known loading conditions. Sometimes it takes both before a full 3D solution is chosen.
- Quantify the anisotropy and symmetry of the problem. More generally, thick plates can be assumed for the span-to thickness ratios large than 20. Soft cores can be taken for transversal FCSR larger than 100. Thick soft cores can be assumed when the core covers at least half the total thickness of the structure ($H/h_{core} > 2$). These are only recommendations which praise for accuracy and robustness. They are no rules nor based on specific calculation as can be seen in the books of Gibson and Ashby (1985) or Mendonça (2005).
- Define outputs. This is crucial. If one needs a very accuracy description of the transversal fields, the LW solution may be the only option. However, depending on the problem and the location of the desired outputs, an ESL may suffice. The dynamic response of Case IV is an example.

- Choose between shell and plate theory. Even though this PhD thesis does not evaluate shell formulations, some guidelines are given. First one must decide between shallow or deep shells. The limit a/R > 5 is a good threshold (where "R" is the radius of the shell and "a" its shortest in-plane dimension). But this threshold is important when the shell is also thick (a/h < 20). Because when using the FEM, if the shell is shallow, it can be represented as an assembly of a few flat elements. Deep shells can be modeled with flat elements too, but a much finer mesh is needed.
- Define the theory. If the plate of the plies of a laminated plate are thick, a shear deformable theory is needed, meaning that Kirchhoff one does not fit. The order of the theory is problem dependent, but for LW static solutions, the linear one is already good (LD111). For ESL static solutions, the ED332 is recommended as it attempts to be physically consistent. For dynamic analyses, if the structure is not too anisotropic in the thickness direction, the ESL can predict the structure behavior. However, if the anisotropy points to the existence of sandwich modes of vibration, the LW solution is only option. Another option for highly anisotropic sandwich plates is to couple ESL assemblages into a LW one. This configures the High order SAndwich Plate Theories (HSAPT) mentioned in the references. Such assemblage can be implemented in a UF if desired.

The bottom line of modeling 2D structures is the current and constant need for modeling complex plate structures in a fast and accurate fashion. Without experience, this is nearly impossible. Most of the recent research and publications on plate and shell theories does not actually provide an answer in this direction. The use and implementation of Unified Formulations in FE, even though most of the times, they are not physically based, but it is a way to group all of the plate theories so, with experience, one can "pick" the desired theory for a particular problem. Or, if the user is not that experienced, this solution method allows for quick tests of different theories while keeping the same numeric errors. Thereby, any actual improvement from a plate/shell theory to another is not masked by the element formulation. In this direction, CGF, as a FE C-1 implementation in bending based on GUF, incorporates plate theories which involve the first derivations of the transversal displacement field with in-plane directions. Such derivatives can be found coupled with the displacement fields. Reddy's plate theory falls into this category and is one of the most successful plate theories as it satisfies the free transversal shear stress at the bottom and top faces of the plate with a parabolic distribution of transversal shear stress.

7.3 Future works

Throughout the PhD thesis, some suggestions for future works were given and they comprise:

Development of continuum plate theories (Cosserat)

This is a very appealing topic. Cosserat surface and similar formulations comprise a different way to model the 3D continuum. Normally the media is taken as a bundle of points, spheres or ellipses, depending on the microscopic characteristics of the media. This is why this approach is found in all engineering areas, such as fluid mechanics. For sandwich structures with a core made of a foam, the influence of its cell's shape can be accounted for in this plate formulation, not on the material model. Actually, the material model is usually dependent on the theory developed with this method. These are called the Cosserat parameters, which demands different tests to calibrate the model.

Implementation of CGF on an 8(9) node element

This is a straightforward task, which can be achieved with a little more effort to derive the interpolation functions. Mainly, the Hermite functions will need more attention to due to the C-1 continuity requirements. However, as mentioned, a more detailed post-processing of the current element results is suggested prior to this implementation.

Implementation of CGF into a commercial FE code (Abaqus-UEL)

This is another technical suggestion. If a unified formulation such (CUF, GUF or CGF) is coded into Abaqus, the computational cost of this element will be evaluated with other 2D and 3D elements. Also, more complex problems can be solved without having to implement non-linear solvers, material models and load cases in a manual pin-point manner.

Upgrade of the plate theory into a shell formulation

To see the full usefulness of CGF, a shell element is needed. So far very few geometrical problems can be solved with a plate formulation. Either a curved element or degenerated shell element will suffice. Also, this particular formulation may no longer be C-1, because the element edges will no longer be aligned with the global coordinate axes. Nonetheless it is a worthy method to be implemented in FEM due to reported success of incompatible elements. Spherical and conical problems can be addressed. Then, the formulation will be ready for, say, commercial and engineering use.

Development of the damping kernel

Unfortunately, the damping response was not considered in this PhD thesis. It is a straightforward task though, apart from the calibration process. If a FE kernel is desired, then different options to insert the damping properties are available: Micro, meso or macro. The first is the constitutive microscopic dissipation behavior of the material. The last is the damping which results from the structure. Different structures with different dimensions and material can show a structural damping, which is a phenomenological response of that particular structure. Lastly, the meso approach is left for last, because it is attractive in the context of FE. Experimental tests can be used to find damping parameters, which can be used at the element level and it eases the calibration process and naturally increases the accuracy of the solution. Nonetheless either approach is valid.

Multi-Physics problems – FSI/Smart Structures

Multi-physics problems are inexorably more difficult because of the presence of the additional DOFs to the mechanical ones and the coupling of all these terms. Thus, 2D approaches are preferred in these problems, but the accuracy of the mechanical problem needs to be optimal. Depending on the problem, a particular in-plane or through-the-thickness profile is needed. CGF allows one to quickly pick/chose the theory, which is best for the problem at hands.

For instance, if the optimal structural solution theory is found and solved accurately with the minimum computational cost, the proposed structural solution can be coupled with a CFD solution to investigate a static or dynamic FSI of a laminated structure. It is really useless to proceed with a FSI simulation, if one begins to stack errors from several different sources. This is why this PhD thesis contributes for this review on plate theories and solution methods.

Also, most of FSI problems focus on the structure side of the problem, the fluid usually represents the loading in aeronautical problems. Moreover, such loadings can be estimated experimentally. But such tests can be extremely costly when performed in true scale. Moreover, the experimental tests may not consider local measures and the outcome of the structural solution will be limited. Thus, to optimize the structural simulation, a 3D FSI solution is needed.

If the structural side of the problem has already been mastered, the remaining uncontrolled sources of numeric/theory error would then come from the 3D CFD code and/or the coupling method, i. e., the FSI interface. However, these two comprise areas of study with their own particularities and is surely an area for the future of this author.

References

ABAQUS/CAE User's Manual. **ABAQUS version 6.10 - documentation.** © Dassault Systèmes, 2010.

ABBADI, A.; KOUTSAWA, Y.; CARMASOL, A.; BELOUETTAR, S.; AZARI, Z. Experimental and numerical characterization of honeycomb sandwich composite panels. **Simulation Modelling Practice and Theory**, v. 17, p. 1533-1547, 2009.

ALTENBACH, J.; ALTENBACH, H.; EREMEYEV, V. A. On generalized Cosserat-type theories of plates and shells: a short review and bibliography. **Archive of Applied Mechanics**, v. 80, p73-92, 2010

AMBARTSUMIAN, S. A. On theory of bending plates. Isz Otd Tech Nauk AN SSSR n.5, p.69–77, 1958.

ARFKEN, G. B.; WEBER, H. J. **Mathematical Methods for Physicists**. Elsevier Academic Press, New York, NY, USA, 6th edition, 2005.

ARGYRIS, J.; TENEK, L. A practicable and locking-free laminated shallow shell triangular element of varying and adaptable curvature. **Computer Methods in Applied Mechanics and Engineering**, v. 119, p. 215-282, 1994c.

ARGYRIS, J.; TENEK, L. An efficient and locking-free flat anisotropic plate and shell triangular element. **Computer Methods in Applied Mechanics and Engineering**, v. 118, p. 63-119, 1994b.

ARGYRIS, J.; TENEK, L. Linear and geometrically non-linear bending of isotropic and multilayered composite plates by the natural mode method. **Computer Methods in Applied Mechanics and Engineering**, v. 113, p. 207-251, 1994a.

ASADI, E.; WANG, W.; QATU, M. S. Static and vibration of thick deep laminated cylindrical shells using 3D and various shear deformation theories. **Composite Structures**, v. 94, p. 494-500, 2012.

ASHORY, M. R. **High Quality Modal Testing Methods.** Thesis (Phd). Department of Mechanical Engineering, Imperial College of Science, Technology and Medicine London, 1999.

AVERILL, R. C. Static and dynamic response of moderately thick laminated beams with damage. **Composites Engineering**, v. 4, p. 381-395, 1994.

BABUSKA, I.; BANERJEE, U. Stable generalized finite element method (SGFEM). **Computer Methods in Applied Mechanics and Engineering**, v. 201-204, p. 91-111, 2012.

BABUSKA, I.; BANERJEE, U.; OSBORN, J. E. Survey of meshless and generalized finite element methods: A unified approach. **Acta Numerica**, v. 12, p 1-125, 2003.

BARBOSA, F. S.; FARAGE, M. C. R. A finite element model for sandwich viscoelastic beams: Experimental and numerical assessment. **Journal of Sound and Vibration**, v. 317, p. 91-111, 2008.

BATHE, K. J.; DVORKIN, E. N. A continuum mechanics based four-node shell element for general non-linear analysis. **Engineering Computations**, v.1, p. 77-88, 1984.

BATHE, K. J.; DVORKIN, E. N. Short communication. A Four-node plate bending element based on Mindlin/Reissner plate theory and a mixed interpolation. **International Journal for Numerical Methods in Engineering**, v. 21, p. 267-283, 1985.

BEARDS, **C. F. Structural Vibration**: Analysis and Damping. New York: John Wiley & Sons Inc, 1996

BELYTSCHKO, T.; ONG, J. S.-J.; LIU, W. K.; KENNEDY, J. M. Hourglass control in linear and nonlinear problems. **Computer Methods in Applied Mechanics and Engineering**, v. 43, p. 251-276, 1984.

BERDICHEVSKII, V. L. Variational-asymptotic method of constructing a theory of shells. **Journal of Applied Mathematics and Mechanics**, v. 43, n. 4, p. 664-687, 1979.

BHARDWAJ, M. K. - **A CFD/CSD Interaction Methodology for Aircraft Wings**. Doctor thesis (Phd). Blacksburg, Virginia, 1997.

BIRSAN, M. On Saint-Venant's principle in the theory of Cosserat elastic shells. **International Journal of Engineering Science**, v. 45 p. 187–198, 2007.

BISPLINGHOFF, R. L.; ASHLEY, H.; HALFMAN, R. L. **Aeroelasticity.** Dover Publications, Inc. Mineola: New York, 1996.

BOTELLO, S.; ONATE, E.; CANET, J. M. A layer-wise triangle for analysis of laminated composite plates and shells. **Computers & Structures**, v. 70, p. 635-646, 1999.

BOUAYED, K.; HAMDI, M. -A. Finite element analysis of the dynamic behavior of a laminated windscreen with frequency dependent viscoelastic core. **Journal of the Acoustical Society of America**, v. 132, n. 2, p. 757-766, 2012.

BOUDAOUD, H.; BELOUETTAR, S.; DAYA, E. M.; FERRY, M. P. A numerical method for nonlinear complex modes with application to active-passive sandwich structures. **Engineering Structures**, v. 31, p. 284-291, 2009.

BRIASSOULIS, D. The performance of a reformulated four-node plate bending element in moderately thick to very thin plate applications. **Computers & Structures**, v. 47, n. 1, p. 125-141, 1993.

BURTON, W. S.; NOOR, A. K. Assessment of computational models for sandwich panels and shells. **Computer Methods in Applied Mechanics and Engineering**, v. 124, p. 125-151, 1995.

CALIRI JR, M. F. **Material models for polymeric foams applied to aircraft structures in sandwich composite materials**. 2010. 168 p**.** Dissertation (Master of Science) – Escola de Engenharia de São Carlos, Universidade de São Paulo, São Paulo, 2010.

CARRERA, E. A study of transverse normal stress effect on vibration of multilayered plates and shells. **Journal of Sound and Vibration**, v. 225, n. 5, p. 803-829, 1999.

CARRERA, E. Historical review of Zig-Zag theories for multilayered plates and shells. **Applied Mechanics Reviews**, v. 56, n. 3, p. 287-308, 2003a.

CARRERA, E. On the use of the Murakami's Zig-Zag function in the modeling of layered plates and shells. **Computers & Structures**, v. 82, p. 541-554, 2004.

CARRERA, E. Theories and finite elements for multilayered anisotropic, composite plates and shells. **Archives of Computational Methods in Engineering**, v. 9, n. 2, p. 87-140, 2002.

CARRERA, E. Theories and finite elements for multilayered anisotropic, composite plates and shells: A unified compact formulation with numerical assessment and benchmarking. **Archives of Computational Methods in Engineering**, v. 10, n. 3, p. 215-296, 2003b.

CARRERA, E.; CINEFRA, M.; NALI, P. MITC technique extended to variable kinematic multilayered plate elements. **Composite Structures**, v. 92, p. 1888-1895, 2010.

CARRERA, E.; CIUFFREDA, A. A unified formulation to assess theories of multilayered plates for various bending problems. **Composite Structures**, v. 69, p. 271-293, 2005.

CARRERA, E.; DEMASI, L. Classical and advanced multilayered plate elements based upon PVD and RMVT. Part1: Derivation of finite element matrices. **International Journal for Numeric Methods in Engineering**, v. 55, pp. 191-231, 2002a.

CARRERA, E.; DEMASI, L. Classical and advanced multilayered plate elements based upon PVD and RMVT. Part 2: Numerical implementations. **International Journal for Numeric Methods in Engineering**, v. 55, pp. 253-291, 2002b.

CARRERA, E.; MIGLIORETTI, F.; PETROLO, M. Accuracy of refined finite elements for laminated plate analysis. **Composite Structures**, v. 93, p. 1311-1327, 2011a.

CARRERA, E.; MIGLIORETTI, F.; PETROLO, M. Guidelines and recommendations on the use of higher order finite elements for bending analysis of plates. **International Journal for Computational Methods in Engineering Science and Mechanics**, v. 12, p. 303-324, 2011b.

CHAKRABARTI, A.; CHALAK, H. D.; IQBAL, M. A.; SHEIKH, A. H. A new FE model based on higher order zigzag theory for the analysis of laminated sandwich beam with soft core. **Composite Structures**, v. 93, p. 271-279, 2011.

CHALAK, H. D.; CHAKRABARTI, A.; IQBAL, M. A.; SHEIKH, A. H. An improved C0 FE model for the analysis of laminated sandwich plate with soft care. **Finite Elements in Analysis and Design**, v. 56, p. 20-31, 2012.

CHEN, W.F.; HAN, D.J. **Plasticity for structural engineers**. New York: Springer-Verlag, 1988.

CHINOSI, C.; CINEFRA, M.; CROCE, L. D.; CARRERA, E. Reissner's mixed variational theorem toward MITC finite elements for multilayered plates. **Composites: Structures**, v. 99, p. 443-452, 2013.

CRISFIELD, M. A. **Non-linear finite element analyses of solids and structures**: Essentials. Chichester, England: John Wiley & Sons, 1991. v. 1.

CRISFIELD, M. A. **Non-linear finite element analyses of solids and structures**: Advanced topics. Chichester, England: John Wiley & Sons, 1997. v. 2.

D'OTTAVIO, M.; BALLHAUSE, D.; WALLMERSPERGER, T.; KROPLIN, B. Considerations on higher-order finite elements for multilayered plates based on a Unified Formulation. **Computers & Structures**, v. 84, p. 1222-1235, 2006.

DAU, F.; POLIT, O.; TOURATIER, M. C1 plate and shell finite elements for geometrically nonlinear analysis of multilayered structures. **Computers & Structures**, v. 84, p. 1264-1274, 2006.

DEMASI, L. 2D, quasi 3D and 3D exact solutions for bending of thick and thin sandwich plates. **Journal of Sandwich Structures and Materials**, v. 10, p. 271-310, 2008.

DEMASI, L. ∞-3 Hierarchy plate theories for thick and thin composite plates: The generalized unified formulation. **Composite Structures**, v. 84, p. 256-270, 2008.

DEMASI, L. ∞-6 Mixed plate theories based on the Generalized Unified Formulation. Part I: Governing equations. **Composite Structures**, v. 87, p. 1-11, 2009b.

DEMASI, L. ∞-6 Mixed plate theories based on the Generalized Unified Formulation. Part II: Layerwise theories. **Composite Structures**, v. 87, p. 12-22, 2009c.

DEMASI, L. ∞-6 Mixed plate theories based on the Generalized Unified Formulation. Part III: Advanced mixed high order shear deformation theories. **Composite Structures**, v. 87, p. 183-194, 2009d.

DEMASI, L. ∞-6 Mixed plate theories based on the Generalized Unified Formulation. Part IV: Zig-zag theories. **Composite Structures**, v. 87, p. 195-205, 2009e.

DEMASI, L. ∞-6 Mixed plate theories based on the Generalized Unified Formulation. Part V: Results. **Composite Structures**, v. 88, p. 1-16, 2009f.

DEMASI, L. An invariant model for any composite plate theory and FEM applications: the generalized unified formulation. In: 50th AIAA/ASME/ASCE/AHS/ASC STRUCTURES, STRUCTURAL DYNAMICS & MATERIALS CONFERENCE, May, 4-9, **Proceedings**… Palm Springs, California, United States of America, 2009a.

DEMASI, L. Partially Zig-Zag advanced higher order shear deformation theories based on the generalized unified formulation. **Composite Structures**, v. 94, p. 363-375, 2012.

DEMASI, L. Three-dimensional closed form solutions and exact thin plate theories for isotropic plates. **Composite Structures**, v. 80, p. 183-195, 2007.

DEMASI, L. Treatment of stress variables in advanced multilayered plate elements based upon Reissner's mixed variational theorem. **Computers & Structures**, v. 84, p. 1215-1221, 2006.

DI SCIUVA, M. A general quadrilateral multilayered plate element with continuous interlaminar stresses. **Computers & Structures**, v. 47, n. 1, p. 91-105, 1993.

DI SCIUVA, M. Development of an anisotropic, multilayered, shear-deformable rectangular plate element. **Computers & Structures**, v. 21, n. 4, p. 789-796, 1985.

DI SCIUVA, M. Evaluation of some multilayered, shear-deformable plate elements. **Computers & Structures**, v. 24, n. 6, p. 845-854, 1986.

DIEBELS, S.; STEEB, H. The size effect in foams and its theoretical and numerical investigation. **Proceedings of the Royal Society of London. Series A: Mathematical, Physical and Engineering Sciences – RSPA**, v. 458, n. 2028, p. 2869-2883, 2002.

DVORKIN, E. N. Nonlinear analysis of shells using MITC formulation. **Archives of Computational Methods in Engineering**, v. 2, n. 2, p. 1-50, 1995.

DVORKIN, E.N. **On Nonlinear Finite Element Analysis of Shell Structures**. 1984. 157 p. Thesis (Doctor of Philosophy) - Department of Mechanical Engineering, M.I.T., Cambridge, Massachusetts.

ELMALICH, D.; RABINOVITCH, O. A high-order finite element for dynamic analysis of soft-core sandwich plates. **Journal of Sandwich Structures & Materials**, v. 14, p. 525-555, 2012.

EWINS, D. J. **Modal Analysis:** Theory and Practice. London: Research Studies Press, 1985.

FARSAKH, G. A.; QATU, M. S. A triangular conforming element for laminated shells. **Thin-Walled Structures**, v. 21, p. 31-42, 1995.

FELIPPA, C. A.; HAUGEN, B. A unified formulation of small-strain corotational finite elements: I. Theory. **Computer Methods in Applied Mechanics and Engineering**, v. 194, p. 2285–2335, 2005.

FERREIRA, A. J. M.; ARAUJO, A. L; NEVES, A. M .A.; RODRIGUES, J. D., E.; CARRERA, E.; CINEFRA, M.; SOARES, C. M. M. A finite element model using a unified formulation for the analysis of viscoelastic sandwich laminates. **Composites: Part B**, v. 45, p. 1258-1264, 2013.

FERREIRA, A. J. M.; BARROS, J. A. O.; MARQUES A. T. Finite Element Analysis of Sandwich Structures. **Composite Structures,** pp. 105-118, 1991.

FERREIRA, A. J. M.; CARRERA, E.; CINEFRA, M.; ROQUE, C. M. C.; POLIT, O. Analysis of laminated shells by a sinusoidal shear deformation theory and radial basis functions collocation, accounting for through-the-thickness deformations. **Composites: Part B**, v. 42, p. 1276-1284, 2011a.

FERREIRA, A. J. M.; ROQUE, C. M. C.; CARRERA, E.; CINEFRA, M.; POLIT, O. Two higher order Zig-Zag theories for the accurate analysis of bending, vibration and buckling response of laminated plates by radial basis functions collocation and a unified formulation. **Journal of Composite Materials**, v. 45, p. 2523-2536, 2011.

FERREIRA, A. J. M.; ROQUE, C. M. C.; CARRERA, E.; CINEFRA, M.; POLIT, O. Radial basis functions collocation and a unified formulation for bending, vibration and buckling analysis of laminated plates, according to a variation of Murakami's Zig-Zag theory. **European Journal of Mechanics A/Solids**, v. 30, p. 559-570, 2011b.

FERREIRA, A. J. M.; ROQUE, C. M. C.; JORGE, R. M. N. Analysis of composite plates by trigonometric shear deformation theory and multiquadrics. **Computers & Structures**, v. 83, p. 2225-2237, 2005.

FERZIGER, J. H.; PERIC, M. **Computational Methods for Fluid Dynamics.** Germany: Springer, 2002.

FRIED, I.; JOHNSON, A.; TESSLER, A. Minimal-degree thin triangular plate and shell bending finite elements of order two and four. **Computer Methods in Applied Mechanics and Engineering**, v. 56, p. 283-307, 1986.

FROSTIG, Y. Hygrothermal (environmental) effects in high-order bending of sandwich beams with a flexible core and a discontinuous skin. **Composites Structures**, v. 37, p 205-221, 1997.

FROSTIG, Y.; THOMSEN, O. T. Non-linear thermal response of sandwich panels with a flexible core and temperature dependent mechanical properties. **Composites Part B**, v. 39, p 165-184, 2008.

GHINET, S.; ATALLA, N. Modeling thick composite laminate and sandwich structures with linear viscoelastic damping. **Computers and Structures**, v. 89, p. 1547-1561, 2011.

GHUGAL, Y. M.; SHIMPI, R. P. A review of refined shear deformation theories of isotropic and anisotropic laminated plates. **Journal of Reinforced Plastics and Composites**, v. 21, p. 775-813, 2002

GIBSON, L. J.; ASHBY, M. **Cellular solids**: structures & properties. England: Pergamon Press-Headington Hill Hall, 1988.

GILEWSKI, W.; RADWANSKA, M. A survey of finite element model for the analysis of moderately thick shells. **Finite Elements in Analysis and Design**, v. 9, p. 1-21, 1991.

GOL'DENVEIZER, A. L. Methods for justifying and refining the theory of shells (Survey of recent results). **Journal of Applied Mathematics and Mechanics**, v. 32, n. 4, p. 684-695,1968.

GREEN, A. E.; NAGHDI, P. M.; WAINWRIGHT, W. L. A general theory of a Cosserat surface. **Archive for Rational Mechanics and Analysis**, v. 20, n. 4, p. 287-308, 1965

HANSEN, M.O.L.; J.N. SØRENSEN, J.N.; VOUTSINAS, S.; SØRENSEN, N.; MADSEN, H. AA. State of the art in wind turbine aerodynamics and aeroelasticity. **Progress in Aerospace Sciences**, vol. 42, pp. 285–330, 2006.

HINTON, E.; ROCK, T.; ZIENKIEWICZ, O. C. A note on mass lumping and related processes in the finite element method. **Earthquake Engineering & Structural Dynamics**, vol. 4, n. 3, pp. 245–249, 1976.

HU, H.; BELOUETTAR, S.; POTIER-FERRY, M.; DAYA, EL-M. Review and assessment of various theories for modeling sandwich composites. **Composite Structures**, v. 84, p. 282-292, 2008.

HUEBNER, K. H.; THORNTON, E. A. **The finite element method for engineers**. Chichester, England: John Wiley & Sons,1982.

ICARDI, U. A three-dimensional Zig-Zag theory for analysis of thick laminated beams. **Composite Structures**, v. 52, p. 123-135, 2001.

ICARDI, U. Applications of Zig-Zag theories to sandwich beams. **Mechanics of Advanced Materials and Structures**, v. 10, p. 77-97, 2003.

ICARDI, U. C0 plate element for global/local analysis of multilayered composites, based on a 3D Zig-Zag model and strain energy updating. **International Journal of Mechanical Sciences**, v. 47, p. 1561-1594, 2005.

IURA, M.; ATLURI, S. N. Formulation of a finite element with drilling degrees of freedom. **Computational Mechanics**, v. 9, p. 417-428, 1992.

IVANELL S. S. A. **Numerical computations of wind turbine wakes**. Doctor Thesis (Phd), KTH, Royal Institute of Technology, Stokholm, 2005.

JOHNSON, C. D.; KIENHOLZ, D. A. Finite Element Predictions of Damping in Structures with constrained Viscoelastic Layers. **AIAA Journal**, vol. 20, No. 9, 1982.

KANSA, E. J. Multiquadrics – A scattered data approximation scheme with applications to computational fluid-dynamics – I Surface approximations and partial derivatives estimates. **Computers Math Applications**, v. 19, n. 8, p. 127-145, 1990a.

KANSA, E. J. Multiquadrics – A scattered data approximation scheme with applications to computational fluid-dynamics – II Solutions to parabolic, hyperbolic and elliptic partial differential equations. **Computers Math Applications**, v. 19, n. 9, p. 147-161, 1990b.

KANT, T.; KOMMINENI, J. R. Geometrically non-linear transient analysis of laminated composite and sandwich shells with a refined theory and C-0 finite elements. **Computers & Structures**, v. 52, n. 6, p. 1243-1259, 1994.

KANT, T.; OWEN, D. R. J.; ZIENKIEWICZ, O. C. A refined higher-order C0 plate bending element. **Computers & Structures**, v. 15, n. 2, p. 177-183, 1982.

KANT, T.; PANDYA, B. N. A simple finite element formulation of a higher-order theory for unsymmetrically laminated composite plates. **Composite Structures**, v. 9, p. 215-246, 1988.

KARAMA, M.; HARB, B. A.; MISTOU, S.; CAPERAA, S. Bending, buckling and free vibration of laminated composite with transverse shear stress continuity model. **Composite Part B**, v. 29B, p. 223-234, 1998.

KARGER, L.; WETZEL, A; ROLFES, R.; ROHWER, K. A three-layered sandwich element with improved transverse shear stiffness and stresses based on FSDT. **Computers & Structures**, v. 84, p. 843-854, 2006.

KERWIN JR., E. M. Damping of flexural waves by a constrained viscoelastic layer. **The Journal of the Acoustical Society of America**, v. 31, n. 7, p. 952-962, 1959.

KHALILI, S. M. R.; SHARIYAT, M.; RAJABI, I. A finite element based global-local theory for static analysis of rectangular sandwich and laminated composite plates. **Composites: Structures**, v. 107, p. 177-189, 2014.

KIM, D. -J.; DUARTE, C. A.; PROENÇA, S. P. A generalized finite element method with global-local enrichment functions for confined plasticity problems. **Computational Mechanics**, v. 50, n. 5, p. 563-578, 2012.

KOH, B. C.; KIKUCHI, N. New improved hourglass control for bilinear and trilinear elements in anisotropic linear elasticity. **Computer Methods in Applied Mechanics and Engineering**, v. 65, p. 1-46, 1987.

KOLMAN, R.; PLESEK, J.; GABRIEL, D.; OKROUHLIK, M. Optimization of lumping schemes for plane square quadratic finite element in elastodynamics. **Applied and Computational Mechanics**, v. 1, p. 105-114, 2007.

KULKARNI, S. V.; PAGANO, N. J. Dynamic characteristics of composite laminates. **Journal of Sound and Vibration**, v. 23(1), p. 127-143, 1972.

LEKHNITSKII, S. G. **Anisotropic plates**. New York, NY: Gordon and Breach, Science Publishers, 1968.

LI, X.; LIU, D. Generalized laminate theories based on double superposition hypothesis. **International Journal for Numerical Methods in Engineering**, v. 40, p. 1197-1212, 1997.

LI, Z. **Vibration And Acoustical Properties Of Sandwich Composite Materials.** Tese (Doutorado). Auburn, Alabama, 2006.

LIBRESCU, L.; HAUSE, T. Recent developments in the modeling and behavior of advanced sandwich constructions: a survey. **Composite Structures**, v. 48, p. 1-17, 2000.

LIMA, A. M. G.; FARIA, A. W.; RADE, D. A. Sensitivity analysis of frequency response functions of composite sandwich plates containing viscoelastic layers. **Composite Structures**, vol. 92, pp 364-376, 2010.

LIU, W. **Experimental and Analytical Estimation of Damping In Beams and Plates with Damping Treatments.** Tese (Doutorado). Faculty of the University of Kansas School of Engineering, 2008.

LO, K., H.; CHRISTENSEN, R. M.; WU, E. M. A high-order theory of plate deformation-part 2: laminated plates**. Journal of applied Mechanics**, v. 44 p. 669-676, 1977.

MANTARI, J. L.; OKTEM, A. S.; SOARES, C. G. A new higher order shear deformation theory for sandwich and composite laminated plates. **Composites: Part B**, v. 43, p. 1489-1499, 2012a.

MANTARI, J. L.; OKTEM, A. S.; SOARES, C. G. A new trigonometric layerwise shear deformation theory for the finite element analysis of laminated composite and sandwich plates. **Computers and Structures**, v. 94-95, p. 45-53, 2012b.

MARINKOVIC, D; KOPPE, H.; GABBERT, U. Numerically Efficient Finite Element Formulation for Modeling Active Composite Laminates. **Mechanics of Advanced Materials and Structures**, v. 13, p. 379–392, 2006.

MATTER, M.; GMUR, T.; CUGNONI, J.; SCHORDERET, A. Identification of the elastic and damping properties in sandwich structures with a low core-to-skin stiffness ratio. **Composite Structures**, v. 93, p. 331-341, 2011.

MELENK, J. M.; BABUSKA, I. The partition of unity finite element method: Basic theory and applications. **Computer Methods in Applied Mechanics and Engineering**, v. 39, p. 289-314, 1996.

MENDONÇA, P. T. R. **Materiais compostos e estruturas sanduíche:** projeto e análise**.** Barueri: Manole, 2005.

MEUNIR, M.; SHENOI, R. A. Dynamic analysis of composite sandwich plates with damping modelled using high-order shear deformation theory. **Composite Structures**, v. 54, p. 243-254, 2001.

MINDLIN, R. D. Influence of the rotary inertia and shear on flexural motion of isotropic elastic plates. **Journal of Applied Mechanics**, v. 18, p. 336-343, 1951.

MOITA, J. S.; ARAÚJO, A. L.; MARTINS, P.; MOTA SOARES, C. M.; MOTA SOARES, C. A. A finite element model for the analysis of viscoelastic sandwich structures. **Computers and Structures**, v. 89, p. 1874-1881, 2011.

MOREIRA, R. A. S.; DIAS RODRIGUES, J.; FERREIRA, A. J. M. A generalized layerwise finite element for multi-layer damping treatments. **Computational Mechanics**, v. 37, p. 426-444, 2006.

MORENO, M.; TITA, V.; MARQUES, F. D. Influence of boundary conditions on the determination of effective material properties for active fiber composites. In: 11th PACAM, Pan-American Congress of Applied Mechanics, January, 4-8, **Proceedings**… Foz do Iguaçu, Paraná, Brazil, 2010.

MOULIN, B.; KARPEL, M. Static condensation in modal-based structural optimization. **Structural Optimization**, v. 15, p. 275-283, 1998.

MURAKAMI, H. A laminated composite plate theory with improved in-plane responses. **Proceedings of the 1985 PVP Conference, ASME, PVP**, v. 98-2, p. 257-263, 1985. Also **ASME Journal of Applied Mechanics**, v. 53, p. 661, 1986.

NATIONAL RENEWABLE ENERGY LABORATORY. **Advanced Wind Turbine Program Next Generation Turbine Development Project.** California: 2006. 87 p. NREL/SR-500-38752 Report.

NAYAK, A. K.; SHENOI, R. A.; MOY, S. S. J. Transient response of composite sandwich plates. **Composite Structures**, v. 64, p. 249-267, 2004.

NEFF, P.; CHELMINSKI, K. Well-Posedness of Dynamic Cosserat Plasticity. **Applied Mathematics & Optimization**, v. 56, p. 19–35, 2007.

NEVES, A. M .A.; FERREIRA, A. J. M.; CARRERA, E.; CINEFRA, M.; ROQUE, C. M. C.; JORGE, R. M. N.; SOARES, C. .M . M. A quasi-3D hyperbolic shear deformation theory for the static and free vibration analysis of functionally graded plates. **Composite Structures**, v. 94, p. 1814-1825, 2012a.

NEVES, A. M .A.; FERREIRA, A. J. M.; CARRERA, E.; CINEFRA, M.; ROQUE, C. M. C.; JORGE, R. M. N.; SOARES, C. .M . M. Static analysis of functionally graded plates according to a hyperbolic theory considering Zig-Zag and warping effects. **Advances in Engineering Software**, v. 52, p. 30-43, 2012b.

NEVES, A. M .A.; FERREIRA, A. J. M.; CARRERA, E.; CINEFRA, M.; ROQUE, C. M. C.; JORGE, R. M. N.; SOARES, C. .M . M. Static, free vibration and buckling analysis of isotropic and sandwich functionally graded plates using a wausi-3D higher-order shear deformation theory and a meshless technique. **Composites: Part B**, v. 44, p. 657-674, 2013.

NOOR, A. K.; BURTON, W. S.; PETERS, J. M. Predictor-corrector procedures for stress and free vibration analyses of multilayered composite plates and shells. **Computer Methods in Applied mechanics and Engineering**, v. 82, p. 341-363, 1990.

NOOR, A. K.; MATHERS, M. D. Shear-flexible finite element models of laminated composite plates and shells. **NASA Technical Note**, TN D-8044, 1975.

OWEN, D. R. J.; LI, Z. H. A refined analysis of laminated plates by finite element displacement methods - I. Fundamentals and static analysis. **Computers & Structures**, v. 26, n. 6, p. 907-914, 1987a.

OWEN, D. R. J.; LI, Z. H. A refined analysis of laminated plates by finite element displacement methods - II. Vibration and stability. **Computers & Structures**, v. 26, n. 6, p. 915-923, 1987b.

PAGANO, N. J; HATFIELD, S. J. Elastic behavior of multilayered bidirectional composites. AIAA Journal, v. 10, p. 931 – 933, 1972.

PANDIT, M. K.; SHEIKH, A. H.; SINGH, B. N. Analysis of Laminated Sandwich Plates Based on an Improved Higher Order Zigzag Theory. **Journal of Sandwich Structures and Materials**, v. 12, pp. 307-326, 2010.

PANDYA, B. N.; KANT, T. A refined higher-order generally orthotropic C0 plate bending element. **Computers & Structures**, v. 28, n. 2, p. 119-133, 1988.

PANDYA, B. N.; KANT, T. Higher-order shear deformable theories for flexure of sandwich plates - finite element evaluations. **International Journal of Solids and Structures**, v. 24, n. 12, p. 1267-1286, 1988.

PERVEZ, T.; ZABARAS, N. Transient Dynamic and Damping analysis of Laminated Anisotropic Plates using a Refined Plate Theory. **International Journal for Numerical Methods in Engineering,** vol. 33, pp 1059-1080, 1992.

POLAT, C. Co-rotational formulation of a solid-shell element utilizing the ANS and EAS methods. **Journal of Theoretical and Applied Mechanics,** v. 48, n. 3, p. 771-788, 2010.

POLIT, O.; TOURATIER, M. A multilayered/sandwich triangular finite element applied to linear and non-linear analyses. **Composite Structures**, v. 58, p. 121-128, 2002.

POLIT, O.; TOURATIER, M. Higher-order triangular sandwich plate finite element for linear and non-linear analyses. **Computer Methods in Applied Mechanics and Engineering**, vol. 185, p. 305-324, 2000.

QATU, M. S. On the validity of nonlinear shear deformation theories for laminated plates and shells. **Composite Structures**, v. 27, p. 395-401, 1994.

QATU, M. S.; ALGOTHANI, A. Bending analysis of laminated plates and shells by different methods. **Computers & Structures**, v. 52, n. 3, p. 529-539, 1994.

RASTGAAR, A. M.; MAHINFALAH M.; MAHMOUDIAN, N.;NAKHAIE, J. G. Modal Analysis of Laminated Composite Plates Using Third Order Shear Deformation Theory. In: International Congress and Exposition on Experimental and Applied Mechanics - SEM X 2008, June 7 – 10, **Proceedings**...Costa Mesa, C.A., 2004.

REDDY, J. N. A general non-linear third-order theory of plates with moderate thickness. **International Journal of Non-Linear Mechanics**, v. 25, n. 6, p. 667-686, 1990.

REISSNER, E. On a mixed variational theorem and on shear deformable plate theory. **International Journal for Numeric Methods in Engineering**, v. 23, p.193-198, 1986.

REISSNER, E. The effect of transverse shear deformation on the bending of elastic plates. **Journal of Applied Mechanics**, v. 12, p. 69-77, 1945.

ROGOVOY, A. A. The stress recovery procedure for the finite element method. **Computers & Structures**, v. 63, n. 6, pp. 1121-1137, 1997.

ROMBERG, O.; TAUSCHE, M.; PEREIRA, C.; PANNING, L. Passive Damping Of Spacecraft Sandwich Panels. In: 10TH EUROPEAN CONFERENCE ON SPACECRAFT STRUCTURES, MATERIALS & MECHANICAL TESTING, September, 10 – 13, **Proceedings**... Berlin, 2007.

SALAM, M. A.; BONDOK. N. E. Free Vibration Characteristics for Different Configurations of Sandwich Beams. **International Journal of Mechanical & Mechatronics**, vol. 10, No: 03, 2010.

SAMPAIO, M. S. M.; PACCOLA, R. R.; CODA, H. B. A geometrically nonlinear FEM formulation for the analysis of fiber reinforced laminated plates and shells. **Composite Structures**, v. 119, p. 799-814, 2015.

SANSOUR, C.; BEDNARCZYK, H. The Cosserat surface as a shell model, theory and finite-element formulation. **Computational Methods in Applied Mechanics and Engineering**, v. 120, p. 1-32, 1995.

SANTIUSTE, C.; THOMSEN, O. T.; FROSTIG, Y. Thermo-mechanical load interactions in foam cored axi-symmetric sandwich circular plates - High-order and FE models. **Composite structures**, v. 93, p. 369-376, 2011.

SARTORATO, M. ; TITA, V. . A finite element for composite laminated beams with a shear correction factor model. In: 21th International Congress of Mechanical Engineering - COBEM 2011, Natal, RN, October 24-28, 2011. **Proceedings...** Natal, RN, ICME, 21, 2011**.**

SARTORATO, M.; MEDEIROS, R.; RIBEIRO, M. L; TITA, V. Transversal Shear Caracterization of Thick laminated Composite using a Representative Volume Element (RVE). In: 1st BRAZILIAN CONFERENCE ON COMPOSITE MATERIALS - BCCM1, 2012, Natal-RN, July 16-19, 2012. **Proceedings**... Natal, RN, BCCM, 1, 2012.

SCHULZ, J. C. Global mode hourglassing control. **Computer Methods in Applied Mechanics and Engineering**, v. 64, p. 553-566, 1987.

SHANEL, V.; KOLMAN, R.; PLESEK, J. Mass lumping methods for the semi-loof shell element. In: INTERNATIONAL CONFERENCE. ENGINEERING MECHANICS - ICEM. 18., May, 2012, Svratka, Czech Republic. **Proceedings**… Czech Republic: ICEM, 2012.

SKATULLA, S.; SANSOUR, C. A formulation of a Cosserat-like continuum with multiple scale effects. **Computational Material Science**, v. 67, p. 113–122, 2013.

SOLDATOS, K. P. A transverse shear deformation theory for homogeneous monoclinic plates. **Acta Mechanica**, v. 94, p. 195-220, 1992.

SRINIVAS, S.; RAO, A. K. Bending, vibration and buckling of simply supported thick orthotropic rectangular plates and laminates. **International Journal of Solids and Structures**, v. 6, p. 1463-1481, 1970.

TANNEHILL, J. C.; ANDERSON, D. A.; PLETCHER, R. H. **Computational Fluid Mechanics and Heat Transfer** (Second Edition). Philadelphia, PA: Taylor & Francis, 1997.

TAYLOR, M. W.; VASILIEV, V. V.; DILLARD, D. A. On the problem of shear-locking in finite elements based on shear deformable plate theory. **International Journal of Solids and Structures**, v. 34, n. 7, p. 859-875, 1997.

TESSLER, A.; DI SCIUVA, M.; GHERLONE, M. A refined zigzag beam theory for composite and sandwich beams. **Journal of Composite Materials**, v. 43, p. 1051-1081, 2009.

THOMSEN, O. T. Sandwich Materials for Wind Turbine Blades – Present and Future. **Journal of Sanwich Structures and Materials**, v. 11, 2009.

TIMOSHENKO, S.; KRIEGER, S. W-. **Theories of plates and shells**. 2nd ed. New York: McGraw-Hill Book Company, 1959.

TITA, V. **Análise dinâmica teórica e experimental de vigas fabricadas a partir de materiais compósitos poliméricos reforçados**. 125 f. Dissertação (Mestrado) - Escola de Engenharia de São Carlos, Universidade de São Paulo, São Carlos, 1999.

TITA, V.; CARVALHO, J.; LIRANI, J. A procedure to estimate the dynamic damped behavior of fiber reinforced composite beams submitted to flexural vibrations. Materials Research (São Carlos. Impresso), v.4, p. 315 - 321, 2001.

TITA, V., CARVALHO, J., LIRANI, J. Theoretical and experimental dynamic analysis of fiber reinforced composite beams. Journal of the Brazilian Society of Mechanical Sciences and Engineering (Impresso), v.25, p. 306 - 310, 2003.

TOLEDANO, A.; MURAKAMI, H. A high-order laminated plate theory with improved in-plane responses. **International Journal of Solids and Structures**, v. 23, n. 1, p. 111-131, 1987.

TOURATIER, M. A refined theory for thick composite plates. **Mechanics Research Communications**, v. 15, n. 4, p. 229-236, 1988.

TOURATIER, M. A refined theory of laminated shallow shells. **International Journal of Solids and Structures**, v. 29, n. 11, p. 1401-1415, 1992.

TOURATIER, M. An efficient standard plate theory. **International Journal of Engineering Science**, v. 29, n. 8, p. 901-916, 1991.

TU, T. M.; THACH, L. N.; QUOC, T. H. Finite element modeling for bending and vibration of laminated and sandwich composite plates based on higher-order theory. **Computational Materials Science**, v. 49, p. 5390-5394, 2010.

PIEFORT, V. **Finite element modelling of piezoelectric active structures**. 154p. Thesis (Phd). Department of Mechanical Engineering and Robotics, Universite Libre de Bruxelles, 2001.

VOS, J. B.; RIZZI, A.; DARRACQ, D.; E.H. HIRSCHEL, E. H. Navier–Stokes solvers in European aircraft design. **Progress in Aerospace Sciences**, vol. 38, pp. 601–697, 2002

WHITNEY, J.M. The effects of transverse shear deformation on the bending of laminated plates, **Journal of Composite Materials**, v. 3, p. 534–547, 1969.

YANG, H. T. Y.; SAIGAL, S.; MASUD, A.; KAPANIA, R. K. A survey of recent shell finite elements. **International Journal for Numerical Methods in Engineering**, v. 47, p. 101-127, 2000.

YU, W.; HODGES, D. H.; VOLOVOI, V. V. Asymptotic generalization of Reissner-Mindlin theory: accurate three-dimensional recovery for composite shells. **Computer Methods Applied in Mechanics and Engineering**, v. 191, p. 5087-5109, 2002.

ZHEN, W.; WANJI, C. A C0-type higher-order theory for bending analysis of laminated composite sandwich plates. **Composite Structures**, v. 92, p. 653-661, 2010.

ZHEN, W.; WANJI, C. A quadrilateral element based on refined global-local higher-order theory for coupling bending and extension thermo-elastic multilayered plates. **International Journal of Solids and Structures**, v. 44, p. 3187-3217, 2007.

ZHEN, W.; WANJI, C.; XIAOHUI, R. An accurate higher-order theory and C0 finite element for vibration analysis of laminated composite sandwich plates. **Composite Structures**, v. 92, p. 1299-1307, 2010.

ZIENKIEWICZ, O. C.; TAYLOR, R. L. **The finite element method**: Solid Mechanics. 5th ed. Jordan Hill, Oxford, England: Butterworth-Heienemann, 2000b. v. 2.

ZIENKIEWICZ, O. C.; TAYLOR, R. L. **The finite element method**: The basis. 5th ed. Jordan Hill, Oxford, England: Butterworth-Heienemann, 2000a. v. 1.

ZWAAN, R. J.; PRANANTA, B. B. Fluid/structure interaction in numerical aeroelastic simulation. **International Journal of Non-Linear Mechanics**, vol. 37, pp. 987–1002, 2002.

Appendix A

From equations (A.1) to (A.4), the Serendipity and Hermite functions which were implemented in the developed FE code are explicitly shown:

Serendipity: (A. 1)

$$^{1}Ns = \left(\frac{1}{4}\right) * (1-e) * (1-n);$$
$$^{1}Ns_{,e} = \left(\frac{1}{4}\right) * (-1) * (1-n);$$
$$^{1}Ns_{,n} = \left(\frac{1}{4}\right) * (-1) * (1-e);$$

Hermite:

$$^{1}N^{1} = \left(1-3*\left(\frac{e+1}{2}\right)^{2}+2*\left(\frac{e+1}{2}\right)^{3}\right)*\left(1-3*\left(\frac{n+1}{2}\right)^{2}+2*\left(\frac{n+1}{2}\right)^{3}\right);$$
$$^{1}N^{1}_{,e} = \left(\frac{1}{2}\right)*\left(-6*\left(\frac{e+1}{2}\right)+6*\left(\frac{e+1}{2}\right)^{2}\right)*\left(1-3*\left(\frac{n+1}{2}\right)^{2}+2*\left(\frac{n+1}{2}\right)^{3}\right);$$
$$^{1}N^{1}_{,n} = \left(\frac{1}{2}\right)*\left(1-3*\left(\frac{e+1}{2}\right)^{2}+2*\left(\frac{e+1}{2}\right)^{3}\right)*\left(-6*\left(\frac{n+1}{2}\right)+6*\left(\frac{n+1}{2}\right)^{2}\right);$$

$$^{1}N^{2} = \left(\left(\frac{e+1}{2}\right)-2*\left(\frac{e+1}{2}\right)^{2}+\left(\frac{e+1}{2}\right)^{3}\right)*\left(1-3*\left(\frac{n+1}{2}\right)^{2}+2*\left(\frac{n+1}{2}\right)^{3}\right);$$
$$^{1}N^{2}_{,e} = \left(\frac{1}{2}\right)*\left(3*\left(\frac{e+1}{2}\right)^{2}-4*\left(\frac{e+1}{2}\right)+1\right)*\left(1-3*\left(\frac{n+1}{2}\right)^{2}+2*\left(\frac{n+1}{2}\right)^{3}\right);$$
$$^{1}N^{2}_{,n} = \left(\frac{1}{2}\right)*\left(\left(\frac{e+1}{2}\right)-2*\left(\frac{e+1}{2}\right)^{2}+\left(\frac{e+1}{2}\right)^{3}\right)*\left(-6*\left(\frac{n+1}{2}\right)+6*\left(\frac{n+1}{2}\right)^{2}\right);$$

$$^{1}N^{3} = \left(1-3*\left(\frac{e+1}{2}\right)^{2}+2*\left(\frac{e+1}{2}\right)^{3}\right)*\left(\left(\frac{n+1}{2}\right)-2*\left(\frac{n+1}{2}\right)^{2}+\left(\frac{n+1}{2}\right)^{3}\right);$$
$$^{1}N^{3}_{,e} = \left(\frac{1}{2}\right)*\left(-6*\left(\frac{e+1}{2}\right)+6*\left(\frac{e+1}{2}\right)^{2}\right)*\left(\left(\frac{n+1}{2}\right)-2*\left(\frac{n+1}{2}\right)^{2}+\left(\frac{n+1}{2}\right)^{3}\right);$$
$$^{1}N^{3}_{,n} = \left(\frac{1}{2}\right)*\left(1-3*\left(\frac{e+1}{2}\right)^{2}+2*\left(\frac{e+1}{2}\right)^{3}\right)*\left(3*\left(\frac{n+1}{2}\right)^{2}-4*\left(\frac{n+1}{2}\right)+1\right);$$

$$^{1}N^{4} = \left(\left(\frac{e+1}{2}\right)-2*\left(\frac{e+1}{2}\right)^{2}+\left(\frac{e+1}{2}\right)^{3}\right)*\left(\left(\frac{n+1}{2}\right)-2*\left(\frac{n+1}{2}\right)^{2}+\left(\frac{n+1}{2}\right)^{3}\right);$$
$$^{1}N^{4}_{,e} = \left(\frac{1}{2}\right)*\left(3*\left(\frac{e+1}{2}\right)^{2}-4*\left(\frac{e+1}{2}\right)+1\right)*\left(\left(\frac{n+1}{2}\right)-2*\left(\frac{n+1}{2}\right)^{2}+\left(\frac{n+1}{2}\right)^{3}\right);$$
$$^{1}N^{4}_{,n} = \left(\frac{1}{2}\right)*\left(\left(\frac{e+1}{2}\right)-2*\left(\frac{e+1}{2}\right)^{2}+\left(\frac{e+1}{2}\right)^{3}\right)*\left(3*\left(\frac{n+1}{2}\right)^{2}-4*\left(\frac{n+1}{2}\right)+1\right);$$

$Node\ 1:\ e=-1; n=-1$

Serendipity: (A. 2)

$$^{2}Ns = \left(\frac{1}{4}\right) * (1+e) * (1-n);$$
$$^{2}Ns_{,e} = \left(\frac{1}{4}\right) * (1-n);$$
$$^{2}Ns_{,n} = \left(\frac{1}{4}\right) * (-1) * (1+e);$$

Hermite:

$$^{2}N^{1} = \left(3 * \left(\frac{e+1}{2}\right)^{2} - 2 * \left(\frac{e+1}{2}\right)^{3}\right) * \left(1 - 3 * \left(\frac{n+1}{2}\right)^{2} + 2 * \left(\frac{n+1}{2}\right)^{3}\right);$$
$$^{2}N^{1}_{,e} = \left(\frac{1}{2}\right) * \left(6 * \left(\frac{e+1}{2}\right) - 6 * \left(\frac{e+1}{2}\right)^{2}\right) * \left(1 - 3 * \left(\frac{n+1}{2}\right)^{2} + 2 * \left(\frac{n+1}{2}\right)^{3}\right);$$
$$^{2}N^{1}_{,n} = \left(\frac{1}{2}\right) * \left(3 * \left(\frac{e+1}{2}\right)^{2} - 2 * \left(\frac{e+1}{2}\right)^{3}\right) * \left(-6 * \left(\frac{n+1}{2}\right) + 6 * \left(\frac{n+1}{2}\right)^{2}\right);$$

$$^{2}N^{2} = \left(\left(\frac{e+1}{2}\right)^{3} - \left(\frac{e+1}{2}\right)^{2}\right) * \left(1 - 3 * \left(\frac{n+1}{2}\right)^{2} + 2 * \left(\frac{n+1}{2}\right)^{3}\right);$$
$$^{2}N^{2}_{,e} = \left(\frac{1}{2}\right) * \left(3 * \left(\frac{e+1}{2}\right)^{2} - 2 * \left(\frac{e+1}{2}\right)\right) * \left(1 - 3 * \left(\frac{n+1}{2}\right)^{2} + 2 * \left(\frac{n+1}{2}\right)^{3}\right);$$
$$^{2}N^{2}_{,n} = \left(\frac{1}{2}\right) * \left(\left(\frac{e+1}{2}\right)^{3} - \left(\frac{e+1}{2}\right)^{2}\right) * \left(-6 * \left(\frac{n+1}{2}\right) + 6 * \left(\frac{n+1}{2}\right)^{2}\right);$$

$$^{2}N^{3} = \left(3 * \left(\frac{e+1}{2}\right)^{2} - 2 * \left(\frac{e+1}{2}\right)^{3}\right) * \left(\left(\frac{n+1}{2}\right) - 2 * \left(\frac{n+1}{2}\right)^{2} + \left(\frac{n+1}{2}\right)^{3}\right);$$
$$^{2}N^{3}_{,e} = \left(\frac{1}{2}\right) * \left(6 * \left(\frac{e+1}{2}\right) - 6 * \left(\frac{e+1}{2}\right)^{2}\right) * \left(\left(\frac{n+1}{2}\right) - 2 * \left(\frac{n+1}{2}\right)^{2} + \left(\frac{n+1}{2}\right)^{3}\right);$$
$$^{2}N^{3}_{,n} = \left(\frac{1}{2}\right) * \left(3 * \left(\frac{e+1}{2}\right)^{2} - 2 * \left(\frac{e+1}{2}\right)^{3}\right) * \left(3 * \left(\frac{n+1}{2}\right)^{2} - 4 * \left(\frac{n+1}{2}\right) + 1\right);$$

$$^{2}N^{4} = \left(\left(\frac{e+1}{2}\right)^{3} - \left(\frac{e+1}{2}\right)^{2}\right) * \left(\left(\frac{n+1}{2}\right) - 2 * \left(\frac{n+1}{2}\right)^{2} + \left(\frac{n+1}{2}\right)^{3}\right);$$
$$^{2}N^{4}_{,e} = \left(\frac{1}{2}\right) * \left(3 * \left(\frac{e+1}{2}\right)^{2} - 2 * \left(\frac{e+1}{2}\right)\right) * \left(\left(\frac{n+1}{2}\right) - 2 * \left(\frac{n+1}{2}\right)^{2} + \left(\frac{n+1}{2}\right)^{3}\right);$$
$$^{2}N^{4}_{,n} = \left(\frac{1}{2}\right) * \left(\left(\frac{e+1}{2}\right)^{3} - \left(\frac{e+1}{2}\right)^{2}\right) * \left(3 * \left(\frac{n+1}{2}\right)^{2} - 4 * \left(\frac{n+1}{2}\right) + 1\right);$$

$Node\ 2\colon\ e = 1; n = -1$

Serendipity: (A. 3)

$$^{3}Ns = \left(\frac{1}{4}\right) * (1+e) * (1+n);$$
$$^{3}Ns_{,e} = \left(\frac{1}{4}\right) * (1+n);$$
$$^{3}Ns_{,n} = \left(\frac{1}{4}\right) * (1+e);$$

Hermite:

$$^{3}N^{1} = \left(3 * \left(\frac{e+1}{2}\right)^{2} - 2 * \left(\frac{e+1}{2}\right)^{3}\right) * \left(3 * \left(\frac{n+1}{2}\right)^{2} - 2 * \left(\frac{n+1}{2}\right)^{3}\right);$$
$$^{3}N^{1}_{,e} = \left(\frac{1}{2}\right) * \left(6 * \left(\frac{e+1}{2}\right) - 6 * \left(\frac{e+1}{2}\right)^{2}\right) * \left(3 * \left(\frac{n+1}{2}\right)^{2} - 2 * \left(\frac{n+1}{2}\right)^{3}\right);$$
$$^{3}N^{1}_{,n} = \left(\frac{1}{2}\right) * \left(3 * \left(\frac{e+1}{2}\right)^{2} - 2 * \left(\frac{e+1}{2}\right)^{3}\right) * \left(6 * \left(\frac{n+1}{2}\right) - 6 * \left(\frac{n+1}{2}\right)^{2}\right);$$

$$^{3}N^{2} = \left(\left(\frac{e+1}{2}\right)^{3} - \left(\frac{e+1}{2}\right)^{2}\right) * \left(3 * \left(\frac{n+1}{2}\right)^{2} - 2 * \left(\frac{n+1}{2}\right)^{3}\right);$$
$$^{3}N^{2}_{,e} = \left(\frac{1}{2}\right) * \left(3 * \left(\frac{e+1}{2}\right)^{2} - 2 * \left(\frac{e+1}{2}\right)\right) * \left(3 * \left(\frac{n+1}{2}\right)^{2} - 2 * \left(\frac{n+1}{2}\right)^{3}\right);$$
$$^{3}N^{2}_{,n} = \left(\frac{1}{2}\right) * \left(\left(\frac{e+1}{2}\right)^{3} - \left(\frac{e+1}{2}\right)^{2}\right) * \left(6 * \left(\frac{n+1}{2}\right) - 6 * \left(\frac{n+1}{2}\right)^{2}\right);$$

$$^{3}N^{3} = \left(3 * \left(\frac{e+1}{2}\right)^{2} - 2 * \left(\frac{e+1}{2}\right)^{3}\right) * \left(\left(\frac{n+1}{2}\right)^{3} - \left(\frac{n+1}{2}\right)^{2}\right);$$
$$^{3}N^{3}_{,e} = \left(\frac{1}{2}\right) * \left(6 * \left(\frac{e+1}{2}\right) - 6 * \left(\frac{e+1}{2}\right)^{2}\right) * \left(\left(\frac{n+1}{2}\right)^{3} - \left(\frac{n+1}{2}\right)^{2}\right);$$
$$^{3}N^{3}_{,n} = \left(\frac{1}{2}\right) * \left(3 * \left(\frac{e+1}{2}\right)^{2} - 2 * \left(\frac{e+1}{2}\right)^{3}\right) * \left(3 * \left(\frac{n+1}{2}\right)^{2} - 2 * \left(\frac{n+1}{2}\right)\right);$$

$$^{3}N^{4} = \left(\left(\frac{e+1}{2}\right)^{3} - \left(\frac{e+1}{2}\right)^{2}\right) * \left(\left(\frac{n+1}{2}\right)^{3} - \left(\frac{n+1}{2}\right)^{2}\right);$$
$$^{3}N^{4}_{,e} = \left(\frac{1}{2}\right) * \left(3 * \left(\frac{e+1}{2}\right)^{2} - 2 * \left(\frac{e+1}{2}\right)\right) * \left(\left(\frac{n+1}{2}\right)^{3} - \left(\frac{n+1}{2}\right)^{2}\right);$$
$$^{3}N^{4}_{,n} = \left(\frac{1}{2}\right) * \left(\left(\frac{e+1}{2}\right)^{3} - \left(\frac{e+1}{2}\right)^{2}\right) * \left(3 * \left(\frac{n+1}{2}\right)^{2} - 2 * \left(\frac{n+1}{2}\right)\right);$$

$Node\ 3\colon\ e = 1; n = 1$

Serendipity: (A. 4)

$$^4Ns = \left(\frac{1}{4}\right) * (1-e) * (1+n);$$
$$^4Ns_{,e} = \left(\frac{1}{4}\right) * (-1) * (1+n);$$
$$^4Ns_{,n} = \left(\frac{1}{4}\right) * (1-e);$$

Hermite:

$$^4N^1 = \left(1 - 3 * \left(\frac{e+1}{2}\right)^2 + 2 * \left(\frac{e+1}{2}\right)^3\right) * \left(3 * \left(\frac{n+1}{2}\right)^2 - 2 * \left(\frac{n+1}{2}\right)^3\right);$$
$$^4N^1_{,e} = \left(\frac{1}{2}\right) * \left(-6 * \left(\frac{e+1}{2}\right) + 6 * \left(\frac{e+1}{2}\right)^2\right) * \left(3 * \left(\frac{n+1}{2}\right)^2 - 2 * \left(\frac{n+1}{2}\right)^3\right);$$
$$^4N^1_{,n} = \left(\frac{1}{2}\right) * \left(1 - 3 * \left(\frac{e+1}{2}\right)^2 + 2 * \left(\frac{e+1}{2}\right)^3\right) * \left(6 * \left(\frac{n+1}{2}\right) - 6 * \left(\frac{n+1}{2}\right)^2\right);$$

$$^4N^2 = \left(\left(\frac{e+1}{2}\right) - 2 * \left(\frac{e+1}{2}\right)^2 + \left(\frac{e+1}{2}\right)^3\right) * \left(3 * \left(\frac{n+1}{2}\right)^2 - 2 * \left(\frac{n+1}{2}\right)^3\right);$$
$$^4N^2_{,e} = \left(\frac{1}{2}\right) * \left(3 * \left(\frac{e+1}{2}\right)^2 - 4 * \left(\frac{e+1}{2}\right) + 1\right) * \left(3 * \left(\frac{n+1}{2}\right)^2 - 2 * \left(\frac{n+1}{2}\right)^3\right);$$
$$^4N^2_{,n} = \left(\frac{1}{2}\right) * \left(\left(\frac{e+1}{2}\right) - 2 * \left(\frac{e+1}{2}\right)^2 + \left(\frac{e+1}{2}\right)^3\right) * \left(6 * \left(\frac{n+1}{2}\right) - 6 * \left(\frac{n+1}{2}\right)^2\right);$$

$$^4N^3 = \left(1 - 3 * \left(\frac{e+1}{2}\right)^2 + 2 * \left(\frac{e+1}{2}\right)^3\right) * \left(\left(\frac{n+1}{2}\right)^3 - \left(\frac{n+1}{2}\right)^2\right);$$
$$^4N^3_{,e} = \left(\frac{1}{2}\right) * \left(-6 * \left(\frac{e+1}{2}\right) + 6 * \left(\frac{e+1}{2}\right)^2\right) * \left(\left(\frac{n+1}{2}\right)^3 - \left(\frac{n+1}{2}\right)^2\right);$$
$$^4N^3_{,n} = \left(\frac{1}{2}\right) * \left(1 - 3 * \left(\frac{e+1}{2}\right)^2 + 2 * \left(\frac{e+1}{2}\right)^3\right) * \left(3 * \left(\frac{n+1}{2}\right)^2 - 2 * \left(\frac{n+1}{2}\right)\right);$$

$$^4N^4 = \left(\left(\frac{e+1}{2}\right) - 2 * \left(\frac{e+1}{2}\right)^2 + \left(\frac{e+1}{2}\right)^3\right) * \left(\left(\frac{n+1}{2}\right)^3 - \left(\frac{n+1}{2}\right)^2\right);$$
$$^4N^4_{,e} = \left(\frac{1}{2}\right) * \left(3 * \left(\frac{e+1}{2}\right)^2 - 4 * \left(\frac{e+1}{2}\right) + 1\right) * \left(\left(\frac{n+1}{2}\right)^3 - \left(\frac{n+1}{2}\right)^2\right);$$
$$^4N^4_{,n} = \left(\frac{1}{2}\right) * \left(\left(\frac{e+1}{2}\right) - 2 * \left(\frac{e+1}{2}\right)^2 + \left(\frac{e+1}{2}\right)^3\right) * \left(3 * \left(\frac{n+1}{2}\right)^2 - 2 * \left(\frac{n+1}{2}\right)\right);$$

Node 4: $e = -1; n = 1$